

POLITECNICO DI MILANO

School of Civil, Environmental and Land Management Engineering
Master of Science in Civil Engineering for Risk Mitigation



POLITECNICO
MILANO 1863

**Effect of the climate change on the snow regime
in the Alps of Lombardy**

Supervisor: Dr. Daniele Bocchiola

Co-Supervisor: Ing. Giovanni Martino Bombelli

Master Thesis of:
Mariani Alberto – ID. 946273

Academic year 2021-2022

Acknowledgments:

First, I would like to acknowledge and give my warmest thanks to my supervisor Giovanni Bombelli and the Professor Daniele Bocchiola, who gave me the possibility to study a topic so important for my valley and the place where I live. When you dive in an ocean of number it's easy to get lost, and here my supervisor came into the game, with availability and advice.

Other huge thanks go to my family, my girlfriend Giulia and my friends in my village "Castiun!", because they've always believed in me, even when I was self-doubt!

Snow and mountains are my life, and I dedicated the last two years focusing on the study of this cold magic! This gave me the chance to live 5 months in Sisimiut, on the Greenland west coast, studying the snow to put the basis for an avalanche forecasting system as the ones that we have in the Alps.

There, I spent 5 months in a "snowball", surrounded by the arctic magic, the infinite Greenlandic freedom, a completely different society and really amazing new friends from all over the world, sharing the same passion for the wild.

Part of my thesis was written there, in the cozy Arctic DTU office, when the snowstorms outside prevented freeride skiing or getting out with the snowmobile to patrol the snow. So, every time that I will read this thesis again, I will always remember those times and friends.

Among them, a special thanks goes to Tom and Anton, since they taught me the power of *ctrl+F* and other fancy informatic tricks!

Last, but not least, I wanna thanks the nature to always be so unpredictable and charming, as well as my home mountains for let themselves be studied!

Apuserineq inuuneruvoq !

22/06/2022

Alberto Mariani

Abstract (Original version):

Snow, in addition to be a complex meteorological phenomenon, is one of the main resources of the mountain environment and is proved that more than one-sixth of the Earth's population relying on glaciers and seasonal snowpack for their water supply. Evidence from present knowledge indicates European Alps are undergoing noticeable and measurable transient climate change and their hydrological cycle is impacted. The aim of this thesis is to investigate the effects of Global Climate Change (GCC) on the snowy regimes of the Lombard Alps, analyzing the current situation and proposing a series of possible future scenarios. Based on the results obtained, the main effects of this phenomenon on the natural environment are then analyzed, focusing on the possible hazards induced at the hydrological and avalanche levels.

After a series of introductory theoretical notions and a detailed description of the available database, the study is divided in three parts. In the first part a trend analysis of the historical series of some Snow Variables, representative of the snowiness regime of the area, is presented. In this analysis the effect of some parameters, such as the elevation, the mountain area, and the season, is evaluated, also analyzing the influence of large-scale atmospheric circulation patterns through a correlation with the NAO teleconnection index. Temperature and total precipitation trends are studied as well.

The second part of the thesis concerns the analysis of possible future regimes. The proposed trend analysis is therefore applied to the Snow Variable's future projections until the end of the XXI century. Temperature and total precipitation variables are projected with 6 different Global Circulation Models (GCM) based on the future radiative forcing values, obtained with IAM models for 4 different scenarios (SSP) descriptive of the possible future society's development. The shift from resolution of the models to the local scale is provided thanks to a downscaling procedure, and the snow depth future projections are computed with a snowpack evolution model starting from temperature and precipitation ones.

Both the past and the future years trend assessments seems to confirm a general snow decreasing in the studied areas, with a significant temperature increment and a generally steady precipitations regime. The phenomenon has different entities, mainly due to elevations and the social development scenario considered. After a discussion of the obtained results, in the third part of the thesis work, the importance of snow is resumed, focusing attention on the effects that the described change may have, both in the hydrological and avalanche field. Furthermore, is shown how this phenomenon, induced by GCC, constitutes a real hazard which modern society must face.

Abstract (Italian version):

La neve, oltre che un complesso fenomeno meteorologico, è una delle principali risorse dell'ambiente montano ed è dimostrato come più di 1/6 della popolazione terrestre dipenda dai ghiacciai e dalla copertura nevosa stagionale per l'approvvigionamento idrico. Le attuali conoscenze indicano che le Alpi europee sono soggette ad un cambiamento climatico evidente e quantificabile, e che il loro ciclo idrologico ne è fortemente influenzato. Lo scopo del presente lavoro di tesi è quello di investigare gli effetti del GCC (Cambiamento climatico globale) sul regime di nevosità delle Alpi lombarde, analizzando la situazione corrente e proponendo una serie di scenari futuri. Sulla base dei risultati ottenuti, vengono poi analizzati i principali effetti di questo fenomeno sull'ambiente naturale, focalizzandosi sui possibili pericoli, indotti a livello idrologico e valanghivo.

Dopo una serie di nozioni teoriche introduttive, nonché una dettagliata descrizione del database disponibile, lo studio può essere diviso in tre parti. Nella prima parte viene presentata un'analisi delle tendenze sulle serie storiche di alcune variabili nivologiche, considerate rappresentative della nevosità dell'area. Nell'analisi vengono inoltre valutati gli effetti di alcuni parametri, come la quota, l'area montuosa o la stagione dell'anno, analizzando poi l'influenza dei patterns di circolazione atmosferica a larga scala attraverso la correlazione delle variabili nivologiche con l'indice di tele-connessione NAO. L'analisi delle tendenze viene eseguita anche per le variabili di temperatura e precipitazione.

La seconda parte della tesi riguarda l'analisi dei possibili sviluppi futuri. L'analisi delle tendenze viene qui applicata alle proiezioni future delle variabili nivologiche fino alla fine del XXI secolo. La temperatura e la precipitazione totale vengono proiettate con 6 diversi GCM (modelli di circolazione globale) basati sui valori futuri di forzante radiativa ottenuti con i modelli IAM per 4 diversi scenari SSP, descrittivi dei possibili sviluppi futuri della società. Il passaggio dalle scale risolutive dei modelli alla scala locale viene effettuato con una procedura di downscaling, ricavando poi le proiezioni delle variabili nivologiche grazie ad un modello di evoluzione del manto nevoso a partire dalle proiezioni di temperatura e precipitazione totale.

Sia l'analisi delle tendenze storica che quella futura sembrano confermare una generale diminuzione della nevosità nell'area, con un incremento significativo delle temperature e un regime precipitativo sostanzialmente stazionario. Il fenomeno è caratterizzato da diversa entità principalmente sulla base della quota e dello scenario di sviluppo sociale considerato. Dopo aver discusso i risultati ottenuti, nella terza parte della tesi viene ripresa l'importanza della neve, focalizzandosi sugli effetti che i cambiamenti descritti possono avere sia in campo idrologico che valanghivo. In conclusione, viene mostrato come questo fenomeno, indotto dal GCC, costituisca un vero e proprio pericolo con il quale la società moderna dovrà confrontarsi.

Table of contents:

Abstract (Original version):	2
Abstract (Italian version):	3
List of figures:	7
1. INTRODUCTION:	10
1.1. Snow is life	11
1.2. Climate change in the Alps	13
2. THEORETICAL HINTS OF SNOW SCIENCE.....	16
2.1 Snow properties:.....	16
2.2 Snow formation in atmosphere:.....	18
2.3 Snowpack evolution on the ground:	21
2.4 Snowpack evolution model.....	27
3. SPATIAL FRAMEWORK AND CLIMATIC FEATURE.....	28
3.1 Study area introduction:.....	28
3.2 General climatic features.....	29
3.3 Teleconnections and NAO index	32
4. TERRITORY SUBDIVISION IN HOMOGENEOUS AREAS:.....	35
4.1 Mountain sides characterization:.....	35
4.2 Vertical subdivision of the territory based on altitude belts:	36
4.3 Spatial subdivision of the territory based on mountain areas:.....	38
5. DATASET AND DATASOURCE OVERVIEW.....	48
5.1 Data sources and variables involved:	48
5.2 Used measurement stations:	51
6. PROPOSED TECNIQUE FOR THE TREND ANALYSIS:	56
6.1 Statistical tools for trend assessment:.....	56
6.2 Single sites analysis vs homogeneous group analysis:.....	58
6.3 Annual vs seasonal analysis:	59
6.4 Correlation between SV and NAO winter index:	60
7. PAST YEAR TREND ASSESSMENT:.....	61
7.1 Snow variable results:.....	62
7.2 Precipitation and temperature results:	72
7.3 Correlation between SV and NAO index:	73
7.4 Comments of the results:.....	77
8. METHODS AND MODELS TO PROJECT CLIMATE CHANGE	81

8.1	Shared Socioeconomic Pathways (SSPs).....	81
8.2	Effects of the SSPs scenarios on the earth climate:	84
8.3	Global circulation model	86
8.4	Downscaling procedure:	91
9.	MODEL IMPLEMENTATION FOR HS PROJECTIONS	93
9.1	Database resizing:.....	93
9.2	Models' calibration:	95
10.	FUTURE PROJECTIONS AND TREND ANALYSIS.....	98
10.1	Proposed elaborations	98
10.2	Snow variable results:.....	99
10.3	Temperature and precipitation results:	109
10.4	Comments of the results.....	112
11.	ANALYSIS OF THE PRINCIPAL HAZARDS INVOLVED.....	115
11.1	Hydrological hazard	116
11.2	Avalanche hazard.....	119
12.	CONCLUSIONS	126
12.1	Main results obtained in the study.....	126
12.2	Main limitation encountered in the study.....	127
12.3	Possible future development of the study	128
12.4	A warning from the season 2021-2022	128
13.	Bibliography	130
	ANNEX 1: Past year trend assessment results	134
	Single stations annual analysis:	134
	Single stations seasonal analysis:.....	135
	Homogeneous groups analysis:.....	136
	ANNEX 2: Future years trend assessment results	138

List of figures:

FIGURE 1.1: CHANGES IN T AND CO ₂ CONCENTRATIONS OVER THE PAST 422000 YEARS. -----	10
FIGURE 1.2: FACTORS AFFECTED BY SNOW COVER EXTENT, DURATION, AND DYNAMICS. -----	11
FIGURE 1.3: WATER CYCLE IN A MOUNTAIN ENVIRONMENT. -----	12
FIGURE 1.4: CHANGES IN RUNOFF IN THE CENTRAL ALPS - HIRHAM RCM (BENISTON M., 2006). ---	14
FIGURE 1.5: CHANGE IN THE FELLARIA GLACIER (RHAETIAN ALPS - VALTELLINA) FROM EARLY '900 TO 2020. -----	15
FIGURE 2.1: TRANSFER OF MOLECULES FROM WATER DROPS. -----	19
FIGURE 2.2: EFFECT OF T AND P COMBINATION IN THE SNOW CRYSTAL FORMATION. -----	19
FIGURE 2.3: PICTURE REPRESENTING THE SURFACE HOAR.-----	20
FIGURE 2.4: ENERGY BALANCE OF THE SNOWPACK. -----	22
FIGURE 2.5: EXAMPLE OF A VERTICAL THERMAL PROFILE IN THE SNOWPACK. -----	24
FIGURE 2.6: DEPTH HOAR CRYSTAL. -----	25
FIGURE 2.7: SKETCH OF THE KINETIC GROWTH PROCESS.-----	25
FIGURE 2.8: SCHEMATIC MECHANISM OF THE WIND EFFECT ON THE SNOW. -----	26
FIGURE 3.1: SPATIAL FRAMEWORK OF THE STUDY AREAS WITH SOIUSA SUBDIVISION. -----	28
FIGURE 3.2: MACRO-CLIMATIC REGIONS IN THE ALPS-----	30
FIGURE 3.3: SKETCH EXPLAINING THE BARRIER EFFECT. -----	30
FIGURE 3.4: DIFFERENCE IN THE CONDITIONS OF SUN AND SNOW COVER BETWEEN RHAETIAN AND OROBIC FACE IN DECEMBER 2021, SOURCE SENTYNEL-2 L2A HUB. -----	31
FIGURE 3.5: AVERAGE ANNUAL PRECIPITATIONS IN THE LOMBARD ALPS. -----	32
FIGURE 3.6: REPRESENTATION OF THE TWO NAO PHASES.-----	33
FIGURE 3.7: INFLUENCE ON EUROPEAN WINTER CLIMATE OF NAO ATMOSPHERIC PATTERN. -----	34
FIGURE 4.1: ALTITUDE BELTS AND HORIZONS IN A GENERIC ALPINE MOUNTAIN WITH PHOTOGRAPHIC EXAMPLE FROM VALTELLINA ENVIRONMENT. -----	36
FIGURE 4.2: HOMOGENEOUS SUBDIVISION BASED ON MOUNTAIN AREAS.-----	39
FIGURE 5.1: SPATIAL FRAMEWORK OF THE AVAILABLE MEASUREMENT STATIONS WITH THE AVAILABLE MEASUREMENTS YEARS. -----	51
FIGURE 5.2: THIESSEN POLYGONS OF HS AT 2000 M ASL. -----	53
FIGURE 7.1: LEGEND FOR THE HOMOGENEOUS GROUP RESULTS:-----	61
FIGURE 7.2: EXAMPLE OF A STATION WITH POSITIVE SIGNIFICANT TREND. -----	62
FIGURE 7.3: EXAMPLE OF A STATION WITH NEGATIVE TREND (NON-SIGNIFICANT). -----	62
FIGURE 7.4: HS_AV ALTITUDE BELTS RESULTS. -----	62
FIGURE 7.5: HS_AV MOUNTAIN AREAS RESULT. -----	63
FIGURE 7.6: ANNUAL VS SEASONAL ANALYSIS.-----	63
FIGURE 7.7: EXAMPLE OF A STATION WITH NEGATIVE SIGNIFICANT TREND. -----	64
FIGURE 7.8: EXAMPLE OF STATION WITH POSITIVE NON-SIGNIFICANT TREND. -----	64
FIGURE 7.9: SCD5 ALTITUDE BELTS RESULTS -----	65
FIGURE 7.10: SCD5 MOUNTAIN AREAS RESULTS. -----	65
FIGURE 7.11: EXAMPLE OF A STATION WITH POSITIVE TREND. -----	66
FIGURE 7.12: EXAMPLE OF A STATION WITH NEGATIVE TREND.-----	66
FIGURE 7.13: SD SEASONAL ANALYSIS.-----	66
FIGURE 7.14: SD ALTITUDE BELT RESULTS. -----	67
FIGURE 7.15: SD MOUNTAIN AREAS RESULTS. -----	67
FIGURE 7.16: COMPARISON AMONG H(N)D TREND [WITH N=1,2,3] -----	68
FIGURE 7.17: EXAMPLE OF A STATION WITH POSITIVE SIGNIFICATIVE TREND. -----	68
FIGURE 7.18: HN MOUNTAIN AREAS RESULTS. -----	68
FIGURE 7.19: H ₃ D AND HN HOMOGENEOUS AREAS RESULTS.-----	69
FIGURE 7.20: H ₂ D HOMOGENEOUS AREAS RESULTS. -----	69
FIGURE 7.21: EXAMPLE OF A STATION WITH SIGNIFICATIVE NEGATIVE TREND IN AUTUMN. -----	70

FIGURE 7.22: H3D SEASONAL ANALYSIS-----	70
FIGURE 7.23: STATION WITH SIGNIFICATIVE NEGATIVE TREND. -----	71
FIGURE 7.24: HN_AV ALTITUDE BELTS RESULTS. -----	71
FIGURE 7.25: HN_AV HOMOGENEOUS AREAS RESULTS. -----	71
FIGURE 7.26: HN_AV SEASONAL ANALYSIS RESULTS. -----	72
FIGURE 7.27: POSITIVE SIGNIFICANT T MEAN TREND IN LIVIGNO LA VALLACCIA. -----	72
FIGURE 7.28: EXAMPLE OF STATION WITH POSITIVE SIGNIFICANT TREND ON PTOT. -----	73
FIGURE 7.29: VARIABILITY OF THE NAO WINTER INDEX SINCE 1980. -----	73
FIGURE 7.30: LINEAR REGRESSION BETWEEN HS AVERAGE AND NAO WINTER. -----	74
FIGURE 7.31: LINEAR REGRESSION BETWEEN SCD5 AND NAO WINTER INDEX. -----	74
FIGURE 7.32: LINEAR REGRESSION BETWEEN SD AND NAO WINTER INDEX. -----	75
FIGURE 7.33: LINEAR REGRESSION BETWEEN HN AVERAGE AND NAO WINTER INDEX. -----	76
FIGURE 7.34: LINEAR REGRESSION BETWEEN H3D AND NAO WINTER INDEX. -----	76
FIGURE 7.35: MAIN RESULTS OBTAINED FROM THE ANALYSIS BY ALTITUDE BELTS. -----	79
FIGURE 8.1: FRAMEWORK OF THE SHARED SOCIOECONOMIC PATHWAYS SCENARIOS. -----	82
FIGURE 8.2: APPROXIMATE TRENDS IN POPULATION OUTCOMES AND EMISSIONS PER CAPITA OUTCOMES SUPERIMPOSED TO THE SSPs CONCEPTUAL MAP. -----	84
FIGURE 8.3: FLOW CHART CONCERNING THE FUNCTIONING OF IAMs MODELS. -----	85
FIGURE 8.4: RCP - SSP SCENARIO MATRIX ILLUSTRATING THE SCENARIO MIP SIMULATIONS. -----	86
FIGURE 8.5: EXCHANGE RELATIONS BETWEEN OGCM AND AGCM. -----	87
FIGURE 8.6: SCHEMATIC STRUCTURE OF A GLOBAL CIRCULATION MODEL. -----	88
FIGURE 9.1: FLOW CHART REPRESENTING THE CASCADE PROCESS USED FOR THE ANALYSIS. -----	93
FIGURE 9.2: STATIONS USED FOR THE TREND ASSESSMENT ON FUTURE CLIMATIC PROJECTIONS. -----	94
FIGURE 9.3: SPATIAL DISTRIBUTION OF THE STATIONS USED FOR THE PROJECTIONS. -----	95
FIGURE 9.4: NSE INDEX COMPUTED AT THE STATION. -----	97
FIGURE 10.1: HS AVERAGE XXI CENTURY PROJECTIONS FOR EACH SSP SCENARIO. -----	100
FIGURE 10.2: AVERAGE HS AVERAGE VALUE AT MID-CENTURY AND END OF CENTURY -----	101
FIGURE 10.3: EXTREME HS AVERAGE VALUE AT MID-CENTURY AND END OF THE CENTURY. -----	101
FIGURE 10.4: SCD5 XXI CENTURY PROJECTIONS FOR EACH SSP SCENARIO. -----	102
FIGURE 10.5: SCD5 AVERAGE VALUE AT MID-CENTURY AND END OF CENTURY -----	102
FIGURE 10.6: EXTREME SCD5 AVERAGE VALUE AT MID-CENTURY AND END OF THE CENTURY. -----	102
FIGURE 10.7: SD XXI CENTURY PROJECTIONS FOR EACH SSP SCENARIO. -----	103
FIGURE 10.8: AVERAGE SD AVERAGE VALUE AT MID-CENTURY AND END OF CENTURY -----	103
FIGURE 10.9: EXTREME SD AVERAGE VALUE AT MID-CENTURY AND END OF THE CENTURY. -----	104
FIGURE 10.10: HN XXI CENTURY PROJECTIONS FOR EACH SSP SCENARIO. -----	104
FIGURE 10.11: AVERAGE SD AVERAGE VALUE AT MID-CENTURY AND END OF CENTURY. -----	105
FIGURE 10.12: EXTREME SD AVERAGE VALUE AT MID-CENTURY AND END OF THE CENTURY. -----	105
FIGURE 10.13: H2D XXI CENTURY PROJECTIONS FOR EACH SSP SCENARIO. -----	106
FIGURE 10.14: AVERAGE H2D AVERAGE VALUE AT MID-CENTURY AND END OF CENTURY -----	106
FIGURE 10.15: EXTREME H2D AVERAGE VALUE AT MID-CENTURY AND END OF THE CENTURY. -----	106
FIGURE 10.16: H3D XXI CENTURY PROJECTIONS FOR EACH SSP SCENARIO. -----	107
FIGURE 10.17: AVERAGE H3D AVERAGE VALUE AT MID-CENTURY AND END OF CENTURY -----	107
FIGURE 10.18: EXTREME H3D AVERAGE VALUE AT MID-CENTURY AND END OF THE CENTURY. -----	108
FIGURE 10.19: HN_AV XXI CENTURY PROJECTIONS FOR EACH SSP SCENARIO. -----	108
FIGURE 10.20: AVERAGE HN_AV AVERAGE VALUE AT MID-CENTURY AND END OF CENTURY -----	109
FIGURE 10.21: EXTREME HN_AV AVERAGE VALUE AT MID-CENTURY AND END OF THE CENTURY. ---	109
FIGURE 10.22: AVERAGE T_AV VALUE AT MID-CENTURY AND END OF CENTURY -----	110
FIGURE 10.23: EXTREME T_AV AVERAGE VALUE AT MID-CENTURY AND END OF THE CENTURY. -----	110
FIGURE 10.24: P_TOT XXI CENTURY PROJECTIONS FOR EACH SSP SCENARIO. -----	111
FIGURE 10.25: AVERAGE P_TOT VALUE AT MID-CENTURY AND END OF CENTURY. -----	111
FIGURE 10.26: EXTREME P_TOT VALUE AT MID-CENTURY AND END OF THE CENTURY. -----	111
FIGURE 10.27: % RESIDUAL REACHED AT MID-CENTURY (2060) IN THE VARIOUS SSP SCENARIOS. ---	113
FIGURE 10.28: % RESIDUAL REACHED AT THE END OF THE CENTURY (2099) IN THE VARIOUS SSP SCENARIOS. -----	113

FIGURE 10.29: SUMMARY OF THE SSP SCENARIOS EFFECT ON THE FUTURE SNOW CONDITIONS OF THE LOMBARD ALPS. -----	114
FIGURE 11.1: FACTORS AFFECTED BY SNOW COVER EXTENT, DURATION, AND DYNAMICS. -----	115
FIGURE 11.2: SPATIAL FRAMEWORK OF THE INVESTIGATED RIVER SECTIONS AND RELATIVE CATCHMENTS.-----	117
FIGURE 11.3: PORTION OF THE HISTORICAL FLOW RATE OF THE ADDA IN THE FUENTES SECTION.-----	117
FIGURE 11.4: PORTION OF THE HISTORICAL FLOW RATE OF THE MALLERO IN THE SONDRIO SECTION. -----	117
FIGURE 11.5: RELATIVE RUNOFF REGIME DURING THE YEAR FOR CATCHMENT ZONES AT DIFFERENT ALTITUDES. THE PARDE ´ COEFFICIENT IS THE QUOTIENT OF THE MEAN MONTHLY RUNOFF AND THE MAN ANNUAL RUNOFF (WSL INSTITUTE FOR SNOW AND AVALANCHE RESEARCH SLF, 2022). -----	118
FIGURE 11.6: LINEAR REGRESSION BETWEEN ADDA SPRING PEAK FLOW RATE AND HS AVERAGE. -----	118
FIGURE 11.7: LINEAR REGRESSION BETWEEN ADDA SPRING PEAK FLOW RATE AND HS AVERAGE. -----	118
FIGURE 11.8: HISTORICAL SERIES OF THE EUROPEAN AVALANCHE FATALITIES. -----	120
FIGURE 11.9: DRY SNOW SOFT SLAB AVALANCHE OBSERVED AND STUDIED PERSONALLY IN SISIMIUT - GREENLAND WEST COAST (15-03-2022). -----	122
FIGURE 11.10: AVALANCHE ACCIDENTS RECORDED IN THE LOMBARD ALPS AND AVERAGE ANNUAL SNOWPACK DEPTH. -----	123
FIGURE 11.11: LINEAR REGRESSION BETWEEN THE N. OF AVALANCHE FATALITIES AND HS_AV IN THE LOMBARD ALPS.-----	123
FIGURE 11.12: NUMBER OF AVALANCHE FATALITIES FOR EACH AVALANCHE PROBLEM. -----	125

1. INTRODUCTION:

The word “climate change” is more than ever part of the collective vocabulary and more and more people are becoming aware of this complex phenomenon. To this situation of growing awareness about the human effects on natural environments, unfortunately, often contrasts skepticism and dissemination of fake news. The phenomenon of climate change, however, is extremely complex. In the following paragraphs, as an introduction to the thesis, climate change will be introduced in a basic way, focusing on the effects that it can have on the alpine environment and the snow cycle.

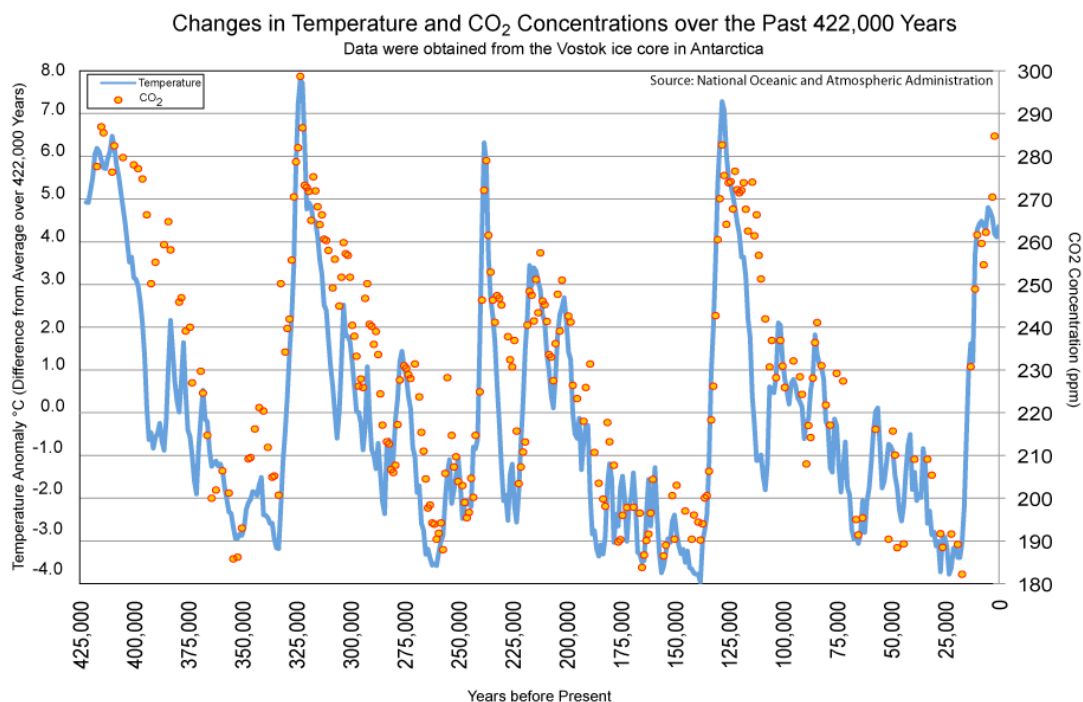


Figure 1.1: Changes in T and CO₂ concentrations over the past 422000 years.

Above all, one can distinguish between climate variability and global climate change (GCC). The first consists in the change of environmental and climatological parameters due to natural causes (natural cycles such as the variation of the terrestrial axis, the movement of the solar system in the galaxy etc.), while the second consists in change due to anthropogenic causes.

This distinction is extremely important, since it allows to correctly interpret the big variability of the global temperature historical series, with the alternation of cold period and warm periods (even more hot than today).

Paleoclimatology allowed to derive the course of the terrestrial temperatures and CO₂ concentrations up to about 2,5 billion of years ago, using the so-called proxy data. As one can see in Figure 1.1, there is an alternation of cold and warm periods, defined by scientists with the alternation of glacial ages (or ice ages), divided in

turn into glacial and interglacial periods (such as the current one), and interglacial ages. An ice age is an indefinite period of the Earth's history in which the globe presents a certain permanent amount of water in the solid phase, subdivided in turn into glacial periods, in which it increases (about 100000 years long) and interglacial periods, in which the amount of ice decreases (about 10-15000 years long). The last glacial period was Wurm, which lasted from 110000 to 12000 years ago.

The anthropic effect on climate change has been amply demonstrated by the world scientific community, thanks to the discovery of the concept of greenhouse gases (whose existence was demonstrated in the early '800), such as water vapor and CO₂. From a statistical point of view, it is also demonstrated that there is a strong correlation between the increase in CO₂ atmospheric concentrations and the rise in temperatures. In conclusion, starting from the industrial age, it is demonstrated that the rise in temperatures is happening at an extremely faster rate than history, allowing us to unequivocally affirm the anthropogenic effect on climate change (Bolin B., 2007).

The effect of GCC is already visible within natural and anthropized systems, with relevant impacts upon human health, water/food security, biodiversity, economy, migrations, natural hazard (Beniston M., 2006). Predictive models foresee a further increase of temperature until the end of XXI century. Henceforth, the need for mitigation, and adaptation to this complex phenomenon.

1.1. Snow is life

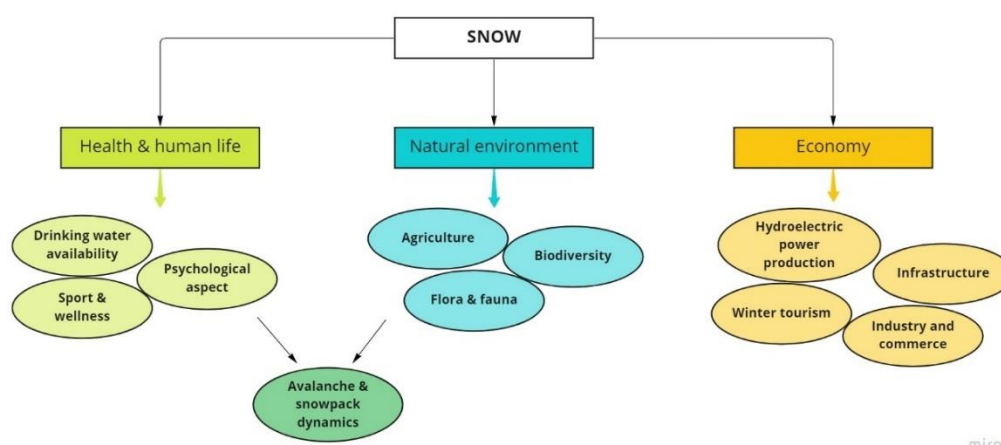


Figure 1.2: Factors affected by snow cover extent, duration, and dynamics.

Snow, in addition to a complex meteorological phenomenon, is one of the main resources of the mountain environment. Together with glaciers, it is a fundamental frozen water resource that is released gradually during the spring and summer season, filling rivers and lakes, allowing the production of

hydroelectric power (80% of Alpine waterways are exploited by hydroelectric power plant) but above all, renewing the groundwater reserves essential for drinking water supply and agriculture (Bocchiola D, 2007).

The Alpine hydrological cycle is composed of a chain of very delicate processes, in which solid precipitation plays a fundamental role, accumulating water on the mountains and releasing to the surrounding valley environment in a delayed and gradual way with respect to rainfall, satisfying the natural needs of the downstream regions.

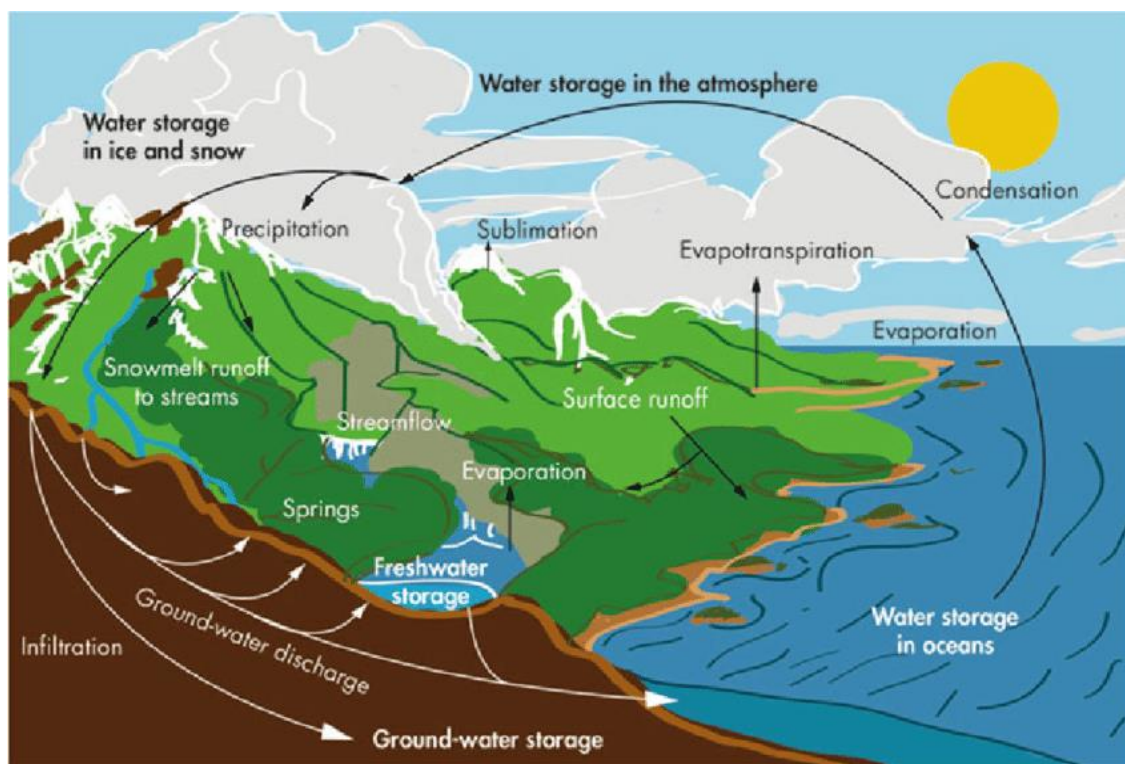


Figure 1.3: Water cycle in a mountain environment.

More than one-sixth of the Earth's population relying on glaciers and seasonal snowpack for their water supply (Barnett T., 2005), this means that the life of more than 1 billion of people around the world will be affected by a general snow decrement.

The snowpack, as a porous material containing air, is an excellent insulator especially for the soil of the alpine environments, allowing the life of numerous plant species that otherwise would not resist the freezing winter temperatures. The accumulated water reserve is then released to the environment during the melting phase, in the growing season of the vegetation, where they need it more. This is one of the main reasons for the high biodiversity of the alpine environment.

Snow cover extent, duration and dynamics influence vegetal and animal biota. In addition, even an extreme and potentially harmful phenomenon such as avalanches can have beneficial effects on the natural environment. It is known,

indeed, that the avalanche's depositions are often more fertile and richer in biodiversity than the surrounding areas. This because, especially gliding avalanches, erode soil in the flow area depositing then silty material, rich in organic substances, and because avalanche deposits constitute greater water reserve, released by irrigating the soil until summer. Avalanche activity can also cause the alpine flora to extent below the threeline (Freppaz M., 2010).

The high albedo effect of the snow allows a strong regulation of the climate, considerably cooling the temperatures and delaying the glacial melting during the summer.

Snow is also influential on the economic sector, both from the point of view of winter tourism and ski resorts and from the point of view of the manufacturing sector related to winter sports, technical equipment, infrastructures and transport. In addition, the possibility of playing sports in a natural and snowy environment can be linked to the well-being of people, especially those who live in the mountain (Zhang X., 2006).

It is also important to remember that the snowy features of an area have important consequences on avalanche activity, spontaneous and not. In the European mountains, in season 2020/2021 alone, 130 people died in avalanches, most of them in the Alps (EAWS, 2022). The study of snow, in all its aspects, allows scientific progress in the avalanche field with the aim to save human losses.

In summary, as one can see in Figure 1.2, snow has a strong influence on various aspects, particularly on the health and on the natural environment. It is important to remark that mountains act as huge 'water towers' storing and releasing water for about 1/6 of the global population and for this reason, the study of the phenomenon and the possible future developments due to climate change is of fundamental importance, constituting the loss of snowfall a real hazard.

1.2. Climate change in the Alps

Evidence from present knowledge indicates European Alps are undergoing noticeable and measurable transient climate change and their hydrological cycle is impacted. The thermal change in the Alps seems to follow a double trend compared to the global warming. During the 20th century, an increase of about 2°C in minimum temperatures is observed, with a substantial stationary precipitation regime but with a marked decrease in snowfall (Matiu M, 2021).

The temperature increase has important consequences on the hydrological cycle of areas in which water supply is mainly due to ice and snow melting (like the alpine region). In a warmer world there are less snowfalls and the snowpack melting is anticipated. Even if the total precipitation does not increase this change implies an anticipation of the river's peak runoff discharge from summer (where there is more need) to spring or late winter. Where the storage capacity is not

sufficient this anticipated runoff goes lost into the ocean, leaving the countryside dry during the most intense phase of the growing vegetable season (Beniston M., 2006).

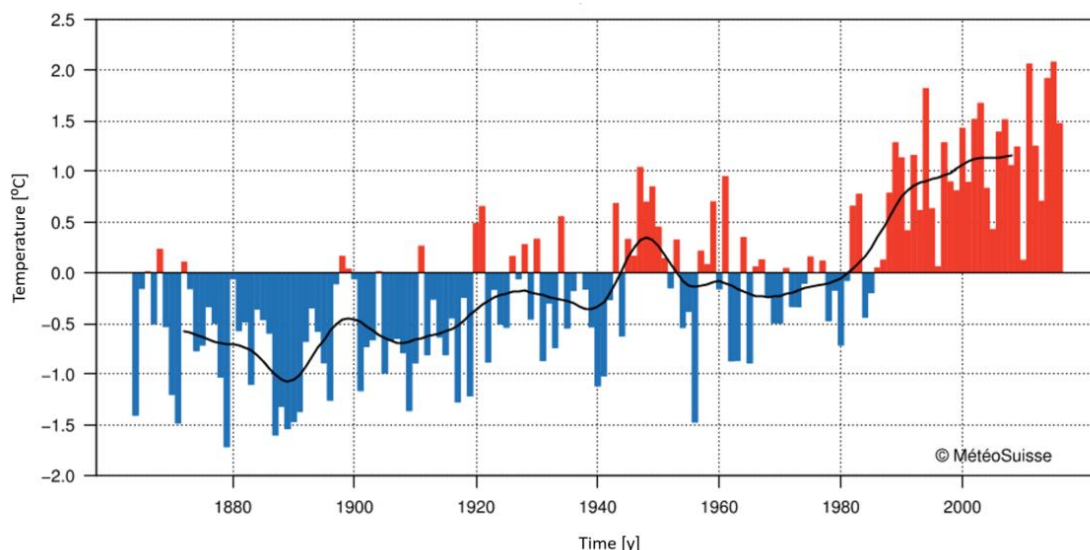


Figure 1.4: Average annual temperature in Switzerland based on 1961-1990 average (WSL Institute for Snow and Avalanche Research SLF, 2022).

In addition to the direct effects on snow cover, climate change has accelerated the phenomenon of the withdrawal of perennial ice. The glacier balance line is expected to rise from 60-70 m to 140 m with associated increased ablation and withdrawal. This process is already widely observable: from 1850 to 1980 glaciers in the Alps lost approximately 30-40 % of their area and half of their mass and since 1980 a further 10-20 % of remaining ice was lost. Only exceptionally hot summer like 2003 led to a loss of 10 % of the residual mass of the Alpine glaciers. In Italy, monitoring a sample of 335 glaciers in the period 1980-1999 was detected as the percentage of advanced glaciers drop from 66 % in 1980 to 4 % in 1999, while retreats rise from 12 % to 89 % (Bosello B., 2008).

Not only Alpine glaciers suffer from global warming, but also periglacial environments such as rock glaciers and permafrost. Their degradation leads to profound changes in the territorial morphology and to an increase in hydrogeological hazards such as rock avalanche or rockfall. Also, structures with foundations resting on icy terrain are subject to severe instability and deformation, like for example the ex. Desio hut, located on the Corna Rossa pass in the Raetian Alps (2880 m asl), abandoned for the structural deformation due to permafrost degradation.



Figure 1.5: Change in the Fellaria Glacier (Rhaetian Alps - Valtellina) from early '900 to 2020.

In response to changing climatic stresses both animal and plant species change their distribution in the Alpine territory. During the century there has already been a progressive shift to major altitudes of plant species, quantifiable in 0.5 - 4 m per decade, at which, together with human factors, climate change has certainly contributed (Bosello B., 2008).

As temperatures increase and glaciers retreat, invasive and colonizing species will do well, whereas alpine species will steadily lose habitat until they eventually disappear.

Alpine flora and fauna are called “glacial relics.” They evolved to survive in conditions from the last glacial period. When the glaciers began to retreat around 10,000 years ago, alpine species retreated with the glaciers to mountain regions.

Increasing temperatures and the rising elevation of snow cover mean that emblematic alpine species such as the ptarmigan and mountain hare are being forced higher and higher up the mountains. The ptarmigan is at risk of losing 60% of its habitat by 2050 and could be extinct by 2090. It's not only animals that are migrating upwards, though. Alpine flowers are also being forced to migrate and the question is whether they can keep pace with the rapid rate of change. Trees are taking advantage of the new habitat available to them, and observations show that the tree line is rising in the Alps (Stretton J., 2020).

2. THEORETICAL HINTS OF SNOW SCIENCE

In the present thesis work, as well as knowledge about the investigated territories, the knowledge and the experience acquired in the snow field proved to be decisive. Knowledge and physical study of climatic phenomena is as important as statistical analysis, which provides mathematical results that need to be understood and interpreted in the correct way.

In this chapter, some theoretical hints concerning the science of snow are reported by describing the main snowpack properties, its formation in the atmosphere and its evolution in the ground, paying particular attention to the physical process that needs to be modelled for study the snowiness characteristics of an area and its behavior through the year. This theoretical chapter also allow to understand how the climatic change described in scientific literature could affect snow and snowpack properties, that is a crucial aspect for well describing the past and future behavior of the snowiness condition.

2.1 Snow properties:

When the snow settles on the grounds forms the snowpack, a heterogeneous porous granular medium that could be composed by 2 phases (ice and air) or 3 phases (ice, air and liquid water) depending on its temperature.

The properties of the snowpack are crucial to well understand its formation and evolution. Some of these are listed below.

2.1.1 Liquid water content:

The liquid water content can be defined as the percentage of liquid water in the snow volume that forms once the temperature of the snow exceeds the 0°C and the grains melts. If the water content is null means that the snow is composed only by 2 phases and it is defined as dry . Snowpacks with higher water content are frequently at lower elevation or in the spring and summer seasons when the daytime temperature and the solar radiation can melt the surface.

2.1.2 Snow water equivalent (SWE):

This parameter, fundamental in the hydrological field can be interpreted as the volume per unit of area of water that would theoretically result if one melted the entire snowpack instantaneously. SWE is used to describe the amount of water contained within the snowpack, or in some cases to describe the amount of water deposited as snow during a storm.

Because in hydrology we are primarily interested in water supply during the spring and summer, snow water equivalent is used as the standard for summarizing individual site and basin snowpack conditions. Snowpack depth

can vary greatly from hour to hour, due to settlement or compaction but the amount of water contained within the snow remains consistent.

The SWE can be computed as (1):

$$SWE = HS * \frac{\rho_{HS}}{\rho_w} \quad (1)$$

Where HS is the snow depth, ρ_{HS} the density of the snow and ρ_w the density of water.

2.1.3 Density:

The density is defined as the ratio between the mass of snow and the volume of the sample itself, measured in kg/m³. It varies seasonally between 30 and 600 kg/m³: in dry snow between 50 and 100 kg/m³ in case of wet snow also reaches 600 kg/m³. The maximum density limit for dry snow is usually 550 kg/m³, a value close to that calculated for a set of ice balls compacted as possible. The density has minimum (rare) values of about 30 kg/m³ for very light fresh snow (porosity of 97 %) and maximum of about 600 kg/m³ for wet snow present in a spring snowpack (porosity of 35%). In case of firn higher values can be reached (Craig F. Boren, 1979).

2.1.4 Cohesion:

The cohesion of the snow is one of the main parameters studied for avalanche forecasting. It can be defined as the ability of ice grains (or crystals) to stick together thanks to the intermolecular attraction forces or the bonds created in the various evolutionary processes. It depends on the shape of the grains, density and water content in addition to temperature changes, the humidity, the degree of settling of the snowpack and the type of crystals present. The cohesion also affects the snow transport capacity by the wind and the transmission of the stresses inside the mantle.

In general, 4 types of cohesion can be detected:

- Felting cohesion: Typical of the recently precipitated fresh snow, which consists of a deposit of snowflakes which have numerous ramifications. This cohesion is due to the respective interweaving between the branches and is very unstable due to the metamorphisms that cause a loss of the branches themselves.
- Capillarity cohesion: The capillarity is the bond between the various crystals imposed on the moisture diffused in the snowpack that is arranged like a thin film around the grains creating ties among themselves. This cohesion is very unstable since the cohesion decreases as the water content increase.
- Sintering cohesion: Is due to the joints created between the grains under the action of temperature and pressure and is very stable. It grows with the rounding and shrinking of crystals.

- Refreezing cohesion: Is the most stable and strong cohesion type. If snow melts liquid water rises into the snowpack and around the individual grains, once it refreezes, becoming ice, creates strong connection between the grains.

2.2 Snow formation in atmosphere:

When solid or liquid water is present in the atmosphere clouds are formed, which can undergo transformations by evaporation, which determine their dissolution, or by saturation, which lead to precipitations.

Precipitation is formed in the air which has become saturated, due to the following phenomena: cooling of the humid air by rising of the masses (the increase of the altitude induces decrease of pressure and consequent expansion with loss of internal energy of the system and temperature); isobaric cooling (expansion of heat to higher altitudes at low pressures) and humidification of the air mass.

To achieve condensation even with high percentages of humidity, the simultaneous presence of condensation cores is essential. The latter are particles suspended in the air, consisting mainly of atmospheric dust (hygroscopic substances such as dust, industrial residues, salt particles derived from evaporation of the seas, pollen, fumes and ash) measuring 0.2-10 microns (millionth of a millimeters), which when temperatures are negative and come into contact with water droplets giving rise to tiny particles with hexagonal crystalline structure: the ice germs (or freezing cores).

In the absence of ice germs, water released into the atmosphere can remain liquid even at negative temperatures.

Precipitation phenomenon is still not very clear. There are two main theories: collision and coalescence process training and Bergeron-Findeisen process (McClung D., 2006).

The first process, which turns out to be a very slow process, includes an initial increase in the condensation of steam around the droplets present within the cloud. It is flanked by coalescence, a phenomenon in which the small droplets, during the ascending motion, collide and are incorporated by the larger ones. There is a cycle where the droplets rise up thanks to the vertical thrusts, diverge laterally where the forces are lower, go down and continue the circular motion until the weight force wins the force of the upward currents.

This process is characteristic especially in cumulus clouds on tropical seas, while on the continent it causes only drizzle.

The Bergeron-Findeisen process is based on the simultaneous presence of ice crystals and water within the clouds. At high altitudes and low temperatures, enough ice crystals are formed in the upper part of the clouds (stratiforms and/or cumuliform clouds) which are essential for the formation of precipitation.

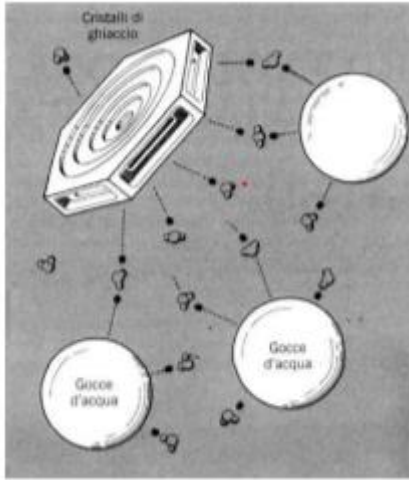


Figure 2.1: Transfer of molecules from water drops.

The formation of the crystal does not follow a predefined pattern but is almost a random aggregation of molecules that however always retain symmetry. It's generally known that:

- The temperature into the cloud drives the crystal shapes.
- The humidity into the cloud drives the crystal sizes.

Because of the high turbulence inside the clouds, the values of temperature and pressure change continuously, and no crystal is equal. However, the following scheme can be defined:

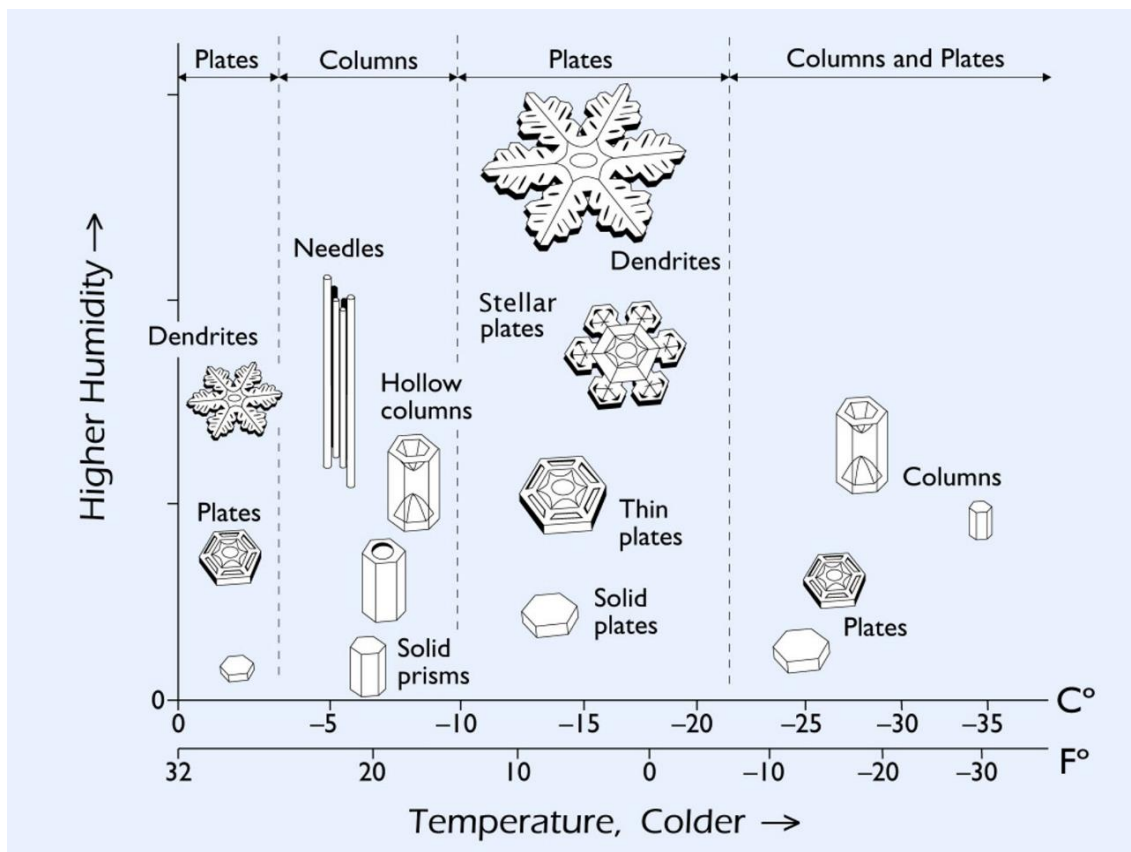


Figure 2.2: Effect of T and P combination in the snow crystal formation.

The newly formed crystals can precipitate to the ground individually or, as often happens, in crystalline clusters called snowflakes.

2.2.1 The bullet snow:

This type of snowfall formation is created when in the cloud there is a layer of drops of liquid water at negative temperatures (over-melted water) that the crystals in precipitation must cross. When this happens, they aggregate in small balls, and this is common in the early stages of snowfall or when it takes on thunderstorm characteristics.

2.2.2 Ice crystal that forms at the ground level:

- Hoarfrost:

Deposit of ice spherules formed by the solidification of the micro-drops of water in the fog in contact with surfaces at a negative temperature.

- Surface hoar:

It consists of feathery-shaped frost crystal that grow upward from the snow surface when the air just above is cooled to the hoar point (dew point at negative temperatures). Once buried, layers of surface hoar are slow to gain strength, sometimes persisting for a month or more as a weak layer into the snowpack. The surface hoar grows most easily on cold and relatively clear nights, when the wind is calm, though it can also grow during the day on shady slopes. It can be identified by the feathery, sparkly crystal that grow on the snow surface as it forms.



Figure 2.3: Picture representing the surface hoar.

2.2.3 The snowfall altitude threshold:

The snowfall altitude threshold is referred to the elevation above which more than 30 % of the precipitations are in the solid phase. This threshold depends on several factor, reported below:

- Initial elevation of the frost line:

As reported in (McClung D., 2006), generally, precipitations can be snowy up to about 300 m below the frost line.

- Intensity and duration of the meteorological event:

When snowflakes fall under the frost line, they pass through an environment at positive temperatures and melt, gaining heat from the surrounding environment. This process causes a significant cooling of the surrounding atmosphere that causes a lowering of the frost line. The greater the intensity and duration of precipitation, the greater the heat transfer from the atmosphere to the snowflakes, resulting in a more significant drop in temperatures.

- Geographical position and climate aspect:

The climatology of the area significantly affect the oscillation of the frost line during a meteorological event. An example is the South faces of the Alpine chain that receives more precipitations from the south-western quadrants. These meteorological events involve the recall of mild prefrontal currents, which lead to a rise in the frost line level first in the areas adjacent to the Po Valley and in the main valleys, and subsequently and less significantly in the more continental areas and in the secondary valleys.

2.3 Snowpack evolution on the ground:

Once the snow crystals reach the ground, finding a different environment compared to that of formation, is subject to a series of transformations in different ways and times that are called metamorphisms. The properties of snow, such as temperature, layer composition, liquid water content, density, hardness, the degree of bonding, etc., are constantly changing because of many external agents such as:

- Gravity
- Air temperature oscillations
- Radiative balance
- Phase shifts
- Mechanical stresses
- Vapor diffusion

The study of the physical and mechanical processes inside the snowpack is one of the main topics of snow science. The external agents described induce a series of metamorphisms in the snow, classified as follows:

- Melting and refreezing metamorphism
- Vapor diffusion metamorphism (with or without thermal gradient)
- Mechanical metamorphism

The following sub-chapters describe the main evolutionary processes that the snowpack undergoes at ground level, paying attention to the different metamorphisms induced. The theoretical notions described are intended to be an introduction to the world of snow science useful to understand some processes modeled in the present thesis work, the study of metamorphisms is much more complex, especially when aimed for avalanche forecasting purposes.

2.3.1 Melting and refreezing process:

As well as the rain, which involves a strong melting due to its penetrative capacity (dependent on the permeability of the layers), the external agents capable of melting snow are solar radiation and temperature and so, the snowpack energy balance is fundamental.

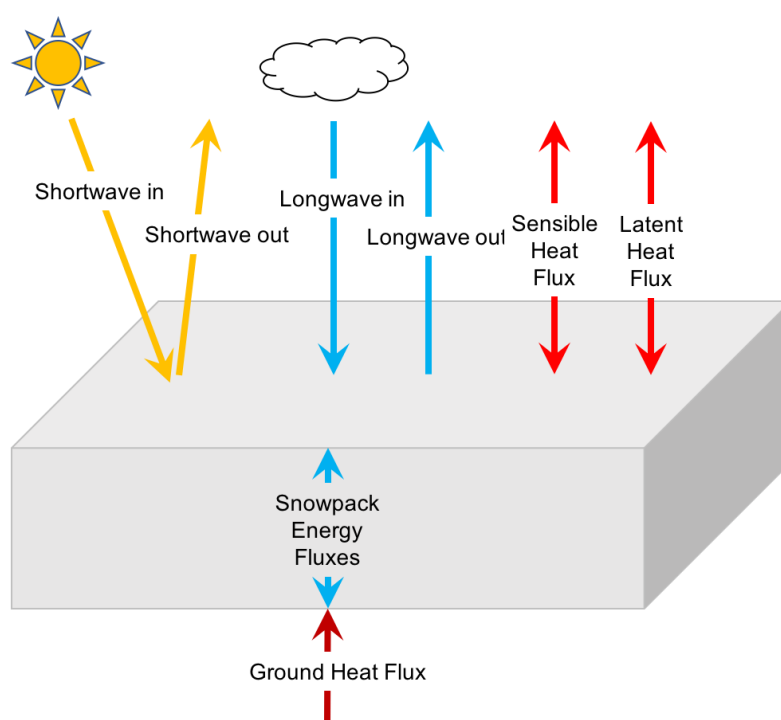


Figure 2.4: Energy balance of the snowpack.

As one can see in the image the snowpack is subject to two different energy exchanges, thermal and radiative.

- Outgoing longwave radiation:

All surface on the earth constantly emits longwave radiation (in the infrared spectrum portion) that constitutes a loss of energy for the snowpack. The amount of energy lost is mainly driven by the surface temperature and the presence of vegetation: the warmer and the more vegetation free the surface, the greater the rate of radiative loss.

This loss of energy cools the snowpack at the very top few millimeters and can be reflected from the clouds towards the mantle, resulting in an incoming longwave

radiation. It is for this reason that the cooling of the snowpack takes place more significantly in conditions of clear sky.

- Incoming shortwave radiation:

Is the solar energy that reach the snow surface, which is then absorbed, reflected and refracted. Snowpack is particularly reflective, due to its albedo effect that in general varies from 0,9 for the fresh new snow to 0,3 for very old snow transformed into firn or with the presence of visible impurities (even visible in a change of coloring). The albedo primarily depends on the age of snow and on the crystal size.

The high reflection rates means that only a little portion of the solar energy is absorbed within the snowpack, but if this portion exceeds the amount of energy lost with long wave radiation the melting process begins.

- Heat transfer:

Is the direct transfer of thermal energy from warmer to cooler substances that are in contact with each other. This phenomenon is present at the surface of the snowpack between snow and atmosphere, on the bottom between soil and snow and within the mantle itself between the various crystalline grains present. The melting process begins if the heat exchange is unbalanced towards the snow.

- Phase change:

The melting process mainly consist in a loss of cohesion of the snowpack itself, due to liquid water content increasing. This liquid water can penetrate within the snowpack lubricating the interface between permeable and non-permeable layers. If the temperature decreases or the radiative balance is favorable the snow can refreeze, resulting in a cohesion increase due to the ice bonds that forms among the grains. Numerous melting-refreezing cycles, typical in spring snow in alpine environments, lead to the formation of "firn" within a year, and subsequently, as the process continues, form glacial ice.

Sublimation can also take place, especially at the surface level in days with low air humidity and no wind. The sublimation of the snowpack involves a cooling of the surrounding atmosphere, which can create a sharp drop in temperatures in the thin layer of air that lies above the snow surface. In absence of solar radiation and wind, it's uncommon to observe snow melting also although the air temperature is a few degree above zero.

2.3.2 Vapor diffusion within the snowpack:

This phenomenon is responsible for the metamorphisms of the dry snow, a two-phase material formed by ice and air containing water vapor. The water vapor is present in the snowpack inside the spaces between the various grains and cannot exceed the saturated vapor pressure (P_v) at that temperature.

The saturated vapor pressure is not constant within the snowpack and one can observe that:

- Pv is greater in warmer areas than in colder ones.
- Pv is greater in the convex areas of the grains than in the concave ones.

According to this information it is possible to introduce three different metamorphisms, whose presence is driven by the thermal gradient inside the snowpack.

Snow is an excellent thermal insulating material and, in the absence of permafrost or glacial ice, the temperature at the soil – snow interface settles around 0 °C. During winter, then, it is common to have air temperatures lower than 0 °C even of many degrees and therefore a vertical thermal gradient is formed.

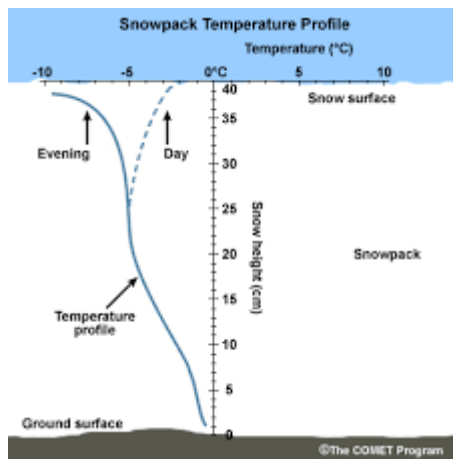


Figure 2.5: Example of a vertical thermal profile in the snowpack.

The isothermia of the snowpack is reached only in case of very thick snowpack or in spring, when the melting of the mantle and the percolation of free water inside it brings the whole vertical section to a temperature close to 0 °C.

Defined ΔH a generic vertical axis segment one can calculate the thermal gradient as (2):

$$\text{Gradient} = \Delta H / \Delta T \quad (2)$$

If the thermal gradient is low, the difference in vapor pressure between convex and concave areas is prevalent over that between warmer and colder areas. The fresh snow crystal has numerous ramifications from which vapor molecules will detach to travel towards the concavity, rounding the grain. This phenomenon (called destructive metamorphism) initially causes a loss of stability, because the cohesion by felting decreases, but then the snowpack regain a stable cohesion by the sintering of the little rounded particles. This type of metamorphism allows the snowpack to settle in a few days and is faster if the temperature is closer to zero degrees.

If the thermal gradient is medium (between 0,05 °C/cm and 0,2 °C/cm), and especially if it is high (> 0,2 °C/cm) the vapor pressure gradient is dominated by the difference in temperature (higher towards the bottom if not for few exceptions of inverted gradient). The vapor diffusion follows the same directions, with the molecules that sublimate at the lower layers and refreeze at the upper colder layers, leading to the phenomenon of kinetic growth which involves the faceting of the crystal. Faceted crystal has a very low cohesion and constitute weak layers inside the snowpack. If the gradient is medium and the process stops the

phenomenon is reversible, with the restoration of low gradient conditions and resulting destructive metamorphism.

If the gradient is high and the process continues the kinetic growth is exasperated, with the formation of the so-called depth hoar. This process is irreversible if not for the melting metamorphism and creates persistent weak layer within the snowpack, which can last until spring.

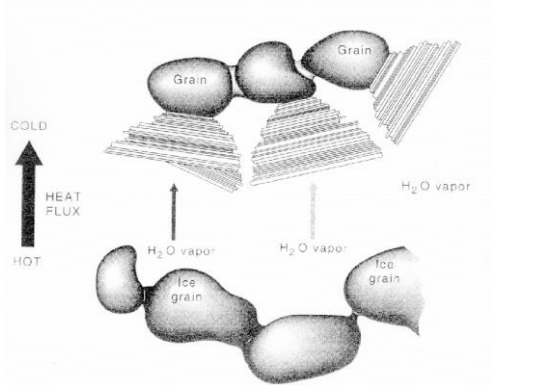


Figure 2.7: Sketch of the kinetic growth process.

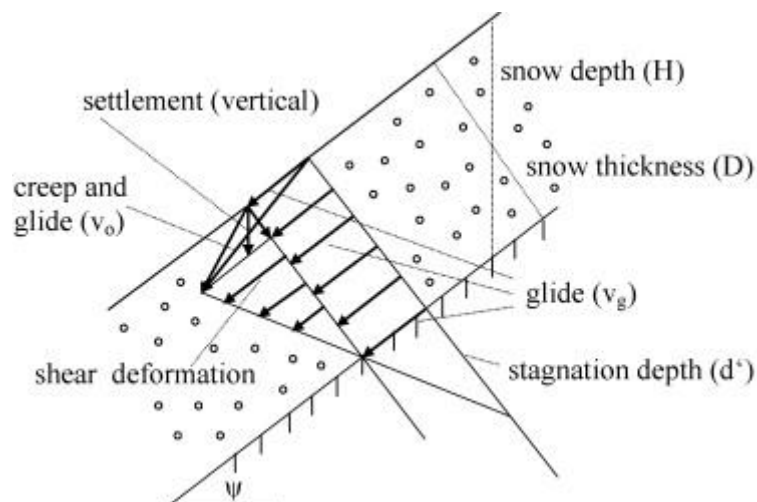


Figure 2.6: Depth hoar crystal.

2.3.3 Mechanical metamorphism:

The main agents of mechanical metamorphisms are the weight strength of the upper snow layers, any other overload, and the wind action.

The gravity force allows the snowpack to be compacted, resulting in a loss of thickness. If the mantle is placed on an inclined plane there is then a component of weight force parallel to the plane that involves a sliding of the same (reptation phenomenon), which causes internal tensions responsible for the gliding avalanches.



The wind acts on the snow redistributing it. The different phases of wind action are erosion, transport, and sedimentation.

The erosion of the snowpack by the wind is driven by wind velocity as well as snow surface characteristics. The wind erodes the surface if its kinetic energy can overcome the force of gravity, cohesion and friction acting on the snow particles. For each kind of snow, it is possible to define a critical velocity (v_c):

- Fresh snow with low cohesion: $v_c > 10$ m/s
- Compacted snow: 10 m/s $< v_c < 20$ m/s
- Very compacted snow, crust: $v_c > 20$ m/s

Once the snow is taken over by the wind, especially if there is a vertical velocity component, it is transported as long as the kinetic energy of the flow allows. The particles in this phase undergo strong mechanical stress (bumps and collisions) that determine the erosion creating a fine dust of ice crystals.

When the particles settle, being very small and angular, they acquire a strong cohesion by sintering forming the so-called 'wind slab'.

The wind slabs are very hard, have a density that can reach 350 kg/m³ and have a fragile mechanical behavior. The study of the mechanical characteristics of wind slabs is especially important for avalanche forecasting, since they are very dangerous when they lie on a weak layer.

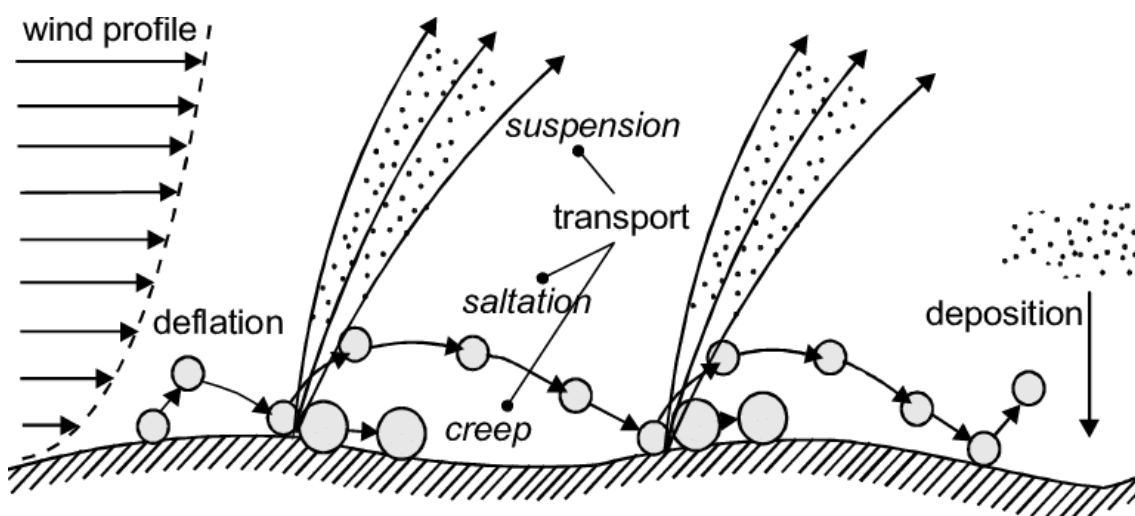


Figure 2.8: Schematic mechanism of the wind effect on the snow.

The snow redistribution due to wind load can significantly affect the amount of local snow, especially in seasons characterized by strong wind activity. Since the measuring stations used in this paper should be placed in neutral areas from the point of view of this phenomenon the effect of the wind should not affect the results that will be presented. For a more detailed analysis, it might be interesting to understand if (and how) the wind parameters have changed over time.

2.4 Snowpack evolution model

A snowpack evolution model will be used in the second part of this thesis works to compute the future series of daily snowpack height starting from temperature and rainfall projections.

In the last decades many snowpack evolutions models have been developed, such the ones by SLF called “Snowpack”, used worldwide for avalanche forecasting, hydrology, and research (Bartelt P., 2002).

In the present work a settling model according to the Martinec method is used (Martinec J., 1991). This instrument, mainly used in the hydrological field, models all the evolutionary process of the snowpack described in the chapter 2.3, taking the temperature, precipitation and solar radiation series as input, and providing the snowpack depth (HS) and snow water equivalent (SWE) series as output.

The final model is the combination of two different sub-model:

- Snow accumulation model
- Settling model
- Melting model

The accumulation of snow on the ground is evaluated in function of precipitation and air temperature, which allows to distinguish between precipitation in liquid or solid phase. The model uses two threshold temperatures, one upper ($T_{sup} = 0.5$ °C) and one lower ($T_{inf} = -0.5$ °C). If the air temperature is higher than T_{sup} the precipitation is totally in the liquid phase, and is added to the snowpack (possibly present on the ground) as a water supply to the SWE. If the air temperature is lower than T_{inf} the precipitation is totally in solid phase, while if falls inside the two thresholds you have a rain part and a snow part.

The settling model evaluate the compaction of snow and the evolution of the main parameters (such as SWE and density), relying on a finite element method for simulate with differential equations the physical and mechanical processes described above. Each finite element represents a different layer, with homogeneous characteristics, that compose the snowpack.

Finally, a degree day ablation model is used to simulate the melting of the snowpack, and the consequent loss of water such as surface or underground runoff. The degree day factors are parameters that describe how many mm of SWE melt as a result of a unit increase of an ablation factor (radiation and temperature) in the unit of time.

This settling model has been tested in several studies also for climate change assessment purposes (Martinec J., 2004).

3.SPATIAL FRAMEWORK AND CLIMATIC FEATURE

3.1 Study area introduction:

The study area corresponds to the portion of the Alps inside the Lombard regional borders, in northern Italy.

The Lombard territory is about 50% mountainous, with an extremely complex morphology engraved over the millennia by the action of glaciers and rivers. The main valleys are Val Chiavenna, Valtellina, Val Camonica, Val Seriana, Val Brembana and Valsassina. Their U-shapes is due to the work of glaciations that affect the area from the Quaternary period to the Wurm Ice Age and distinguishes them from the numerous lateral valleys with typical V-shapes due to the action of water streams. The main rivers are the Adda, the Serio, the Mera and the Brembo, all tributaries of the river Po'. The main lakes are Lake Maggiore, Lake Como, Lake Iseo and Lake Garda. Only two important rivers aren't tributaries of Po': Reno di Val di Lei (tributaries of the Rhine) and Spöl (tributaries of the Danube).

Referring to the SOIUSA subdivision (Marazzi, 2002) this portion of the alpine chain can be subdivided in different sections as reported in Figure 3.1.

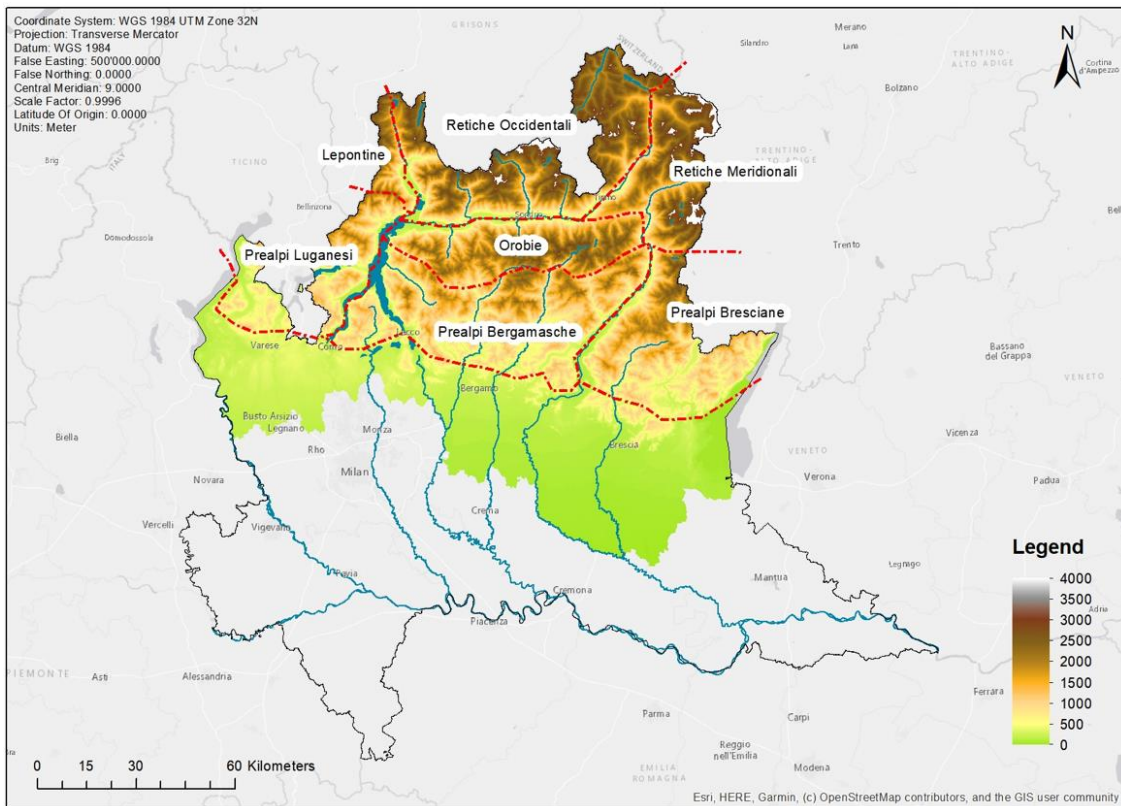


Figure 3.1: Spatial framework of the study areas with SOIUSA subdivision.

The first division could be made between the Alps, located further north on the border with Switzerland (Canton Ticino and Canton Graubünden), characterized by a higher height, and the Pre-alps, located further south in separation with the Po Valley.

Starting from the west there is a small strip of Lepontine Alps, which is then separated by the Chiavenna valley from the Western Rhaetian Alps. Valtellina then separates these from the Orobie Alps (located between Val Camonica and Lake Como) and from the Southern Rhaetian Alps (located to the east on the border with Trentino Alto Adige).

In the pre-alpine area, there are a portion of Prealpi Luganesi (located between the western regional border and Lake Como), the Prealpi Bergamasche (in the middle) and the Prealpi Bresciane, which extend up to Lake Garda.

In the mountainous area of Lombardy there are several towns, including Como, Lecco, and Sondrio (capitals of the respective provinces), with numerous smaller villages and many mountain resorts frequented throughout the year, particularly in winter. The frequenting of the mountain is very active in many, different single sites, leaving space to wild and uncontaminated areas frequented only by a few.

3.2 General climatic features

The Alpine region is characterized by a very complex orography with high elevation gradients and deep valleys forming different mountain massifs with different orientations. These characteristics drive the complexity of the climate in the region, which can be described by the superimposition of a large-scale and a small-scale effect (Matiu M, 2021).

The large-scale effects regard the climatic setting. The European Alps are located in a transitional area influenced by the intersection of three main climates:

- The zone impacted by the Atlantic Ocean (moderate wet climate)
- The zone linked to the Mediterranean Sea (dry summers and wet and mild winters)
- The zone characterized by European continental climate (dry and cold winters and warm summers)

The effect of the geographical location is then superimposed to the so-called small-scale effect (or elevation effect) due to the complex morphology of the territory and the high elevation gradients.

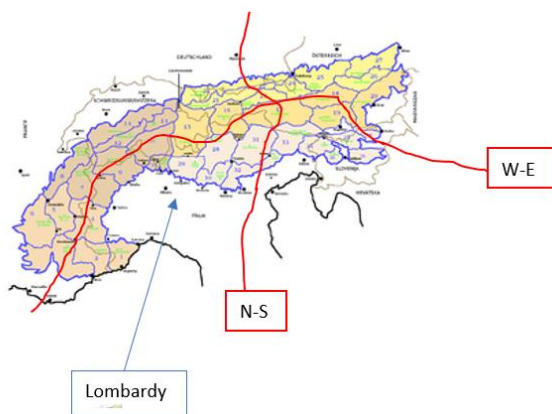


Figure 3.2: Macro-climatic regions in the alps

The interaction of the three climate forcing zones, together with the topography of the mountain chain, results in two climatic gradients along the north-south and west-east directions. The intersection of these two gradients can be characterized by four main climate regions. The first and sharpest climatic border is along the central main ridge separating the temperate westerly from the Mediterranean subtropical climate, the second climatic border,

instead, separates the western oceanic from the eastern continental influences.

As one can see in the figure the Lombard alps are in the areas characterized by western oceanic influences with a Mediterranean subtropical climate. This definition is valid only from a macroclimatic point of view because the portion of the Lombard Alps is in turn characterized by a very heterogeneous climate, always due to the complex morphology of the territory (Centro Meteorologico Lombardo, 2018).

Temperatures are milder in the lake areas, as the large lakes act as a thermal reservoir mitigating the climate and making it Mediterranean at low altitudes and Temperate Mountain at higher altitudes. The climate becomes more continental as you enter the large valleys, closed by high mountain ranges. In these zones in altitude there is a mountain climate of the temperate zones of continental type.

The greatest rainfall comes from the West due to the oceanic influence. They can bring great amounts of snow in the cold season, but they recall Mediterranean humid currents which are often accompanied by warm winds of Libeccio able to raise the frost line. The rainiest areas are those where the flows hit first, the most arid and continental are the innermost.

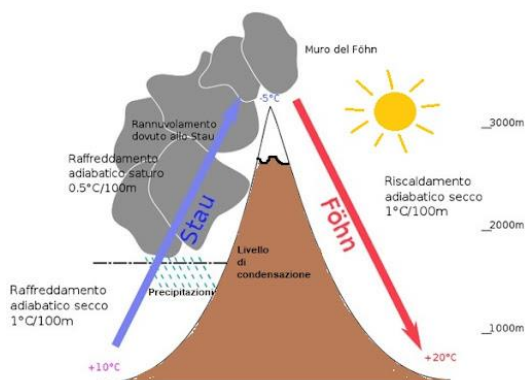


Figure 3.3: Sketch explaining the barrier effect.

Due to its proximity to other climatic macro-areas in the Alps, it is possible to have snowfall with flows from the North. These precipitations, intense on the border reliefs as the area of Livigno (which does not belong to the Mediterranean catchment area), are often little significant in the other areas, where the warm wind called Föhn (typical of the entire Alpine chain) flows due to the STAU barrier effect present in the opposite side of the ridge. As

seen the presence of a territory with a complex morphology involves a complex climatology, especially in the large valleys.

As example in the Valtellina valley is very strong the shadow effect imposed by the reliefs (see Figure 3.4), which determines a deep diversification of the sun conditions between the two sides of the valley axis. With the same quota, especially in the winter months, it is possible to have a gradient in the maximum order of twenty degree between the valley bottom of the Rhaetian slope, exposed to the South, and that of the Orobic slope, that for several months is in the shade of the mountain range.

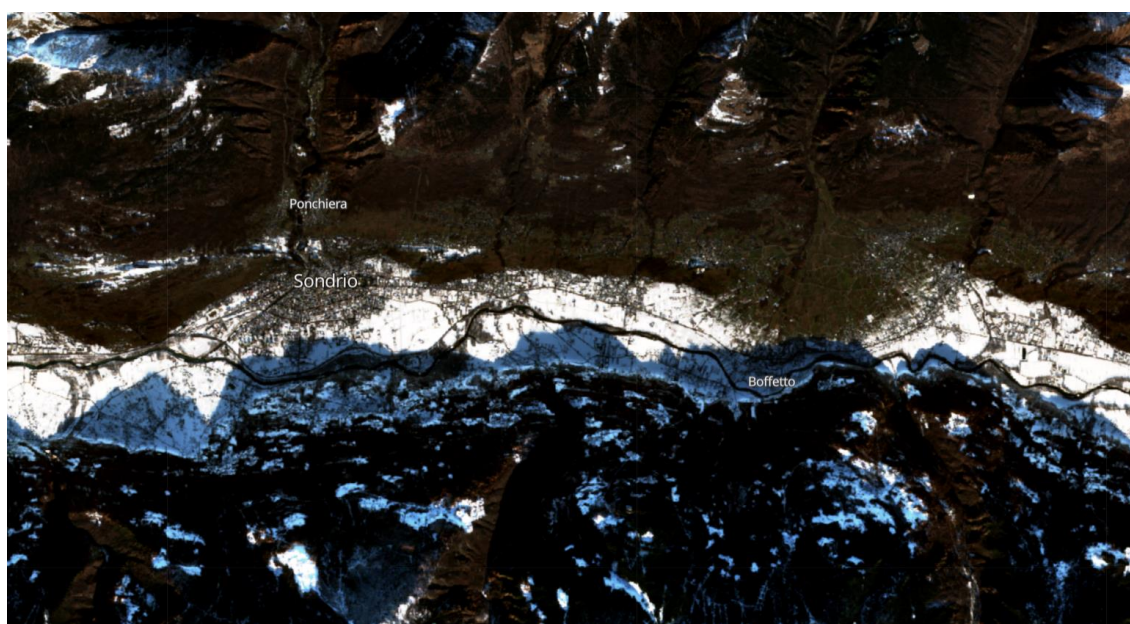


Figure 3.4: Difference in the conditions of sun and snow cover between Rhaetian and Orobic face in December 2021, source Sentynel-2 L2A hub.

During the winter period, in (often frequent) high pressure conditions, low temperatures of the bottom of the valley determine a lowering of the mixing layer resulting in thermal inversion. Because of this phenomenon it is not rare to observe more snow on the shady bottom of the valley (where the cold air stagnates) than at the medium mountain altitude. This phenomenon has been observed personally in a particular way during the current winter season (2021-2022), characterized by a consistent snowfall in December followed by a long dry period in December and January.

The rainfall distribution during each rainfall event is very high variable even at few kilometers, as well as the average annual rainfall of a given area (Figure 3.5). In addition to the above-mentioned STAU effect this is due to convection effect (very difficult to model and depending on the interaction of elevations with the flux directions). The rainiest areas of the Lombardy Alps are the Lake Como and the pre-alpine ones (where the western flows impact first), while the rainfall decreases as the territory continental increases, with the area of Livigno among the driest of the entire Lombard territory.

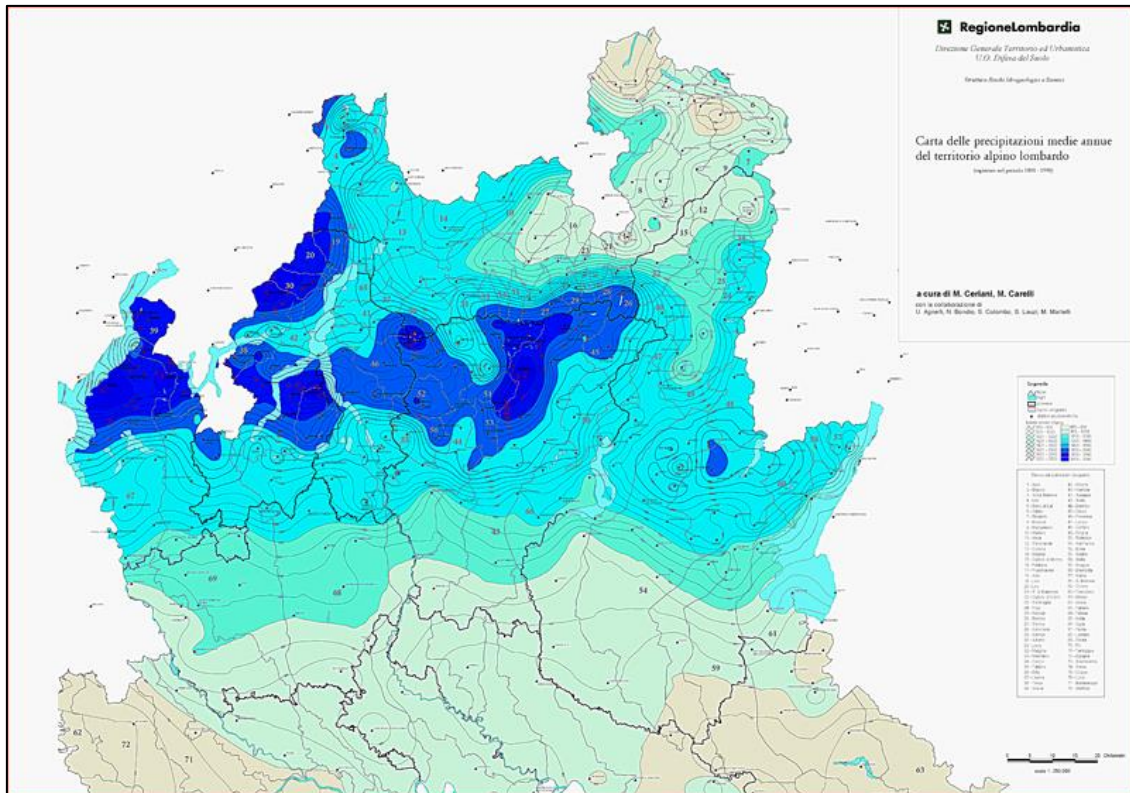


Figure 3.5: Average annual precipitations in the Lombard Alps.

3.3 Teleconnections and NAO index

As explained in the previous chapter, the Lombard Alps are influenced by western oceanic flux, which bring the most consistent precipitation. To better understand the climatic characteristics of the studied region, especially in relation to the snowiness, it is possible to briefly introduce the teleconnections, a fundamental chapter of the earth's climate study and of the world's meteorology. The study of atmospheric and oceanic teleconnections constitutes a relatively new and interesting type of approach to the study of medium-large scale atmospheric and oceanic circulation, different from the use of global physical-mathematical models (GCM and AOGCM) that generally fail to highlight circulation patterns (Yoojin Kim, 2012). The existence of typical and recurrent circulation patterns is undoubtedly an element of order in the face of the apparent, absolute, and intrinsic "chaotic" of atmospheric circulation.

Teleconnections are synoptic-scale (thousands of kilometers) patterns of atmospheric circulation and two points in the atmosphere are teleconnected if the associated physical-meteorological parameters (like pressure or temperature) are correlated over time (i.e. they vary synchronously or inversely proportionally so as to show a statistical correlation). Teleconnections can be purely atmospheric or due to thermal anomalies on surface oceanic water.

The main teleconnections include NAO (North Atlantic Oscillation), AO (Arctic Oscillation), El Nino and La Nina, AMO (Atlantic Multidecadal Oscillation) etc.

3.3.1 The North Atlantic Oscillation and its influence on Lombard Alps:

The NAO is a teleconnection located in the North Atlantic Ocean and characterized by the cyclical fluctuation of the sea-level pressure difference between the anticyclone of the Azores and the Iceland depression. The intensity of the teleconnection is measured by the NAO index, which represents the normalized difference in sea-level pressure abnormalities between Iceland and the Azores.

When the Iceland cyclone is intense (low pressure) and the Azores anticyclones is strong it has a positive phase (NAO+ with $NAO > 0,5$), vice versa it has the negative phase (NAO- with $NAO < 0,5$).

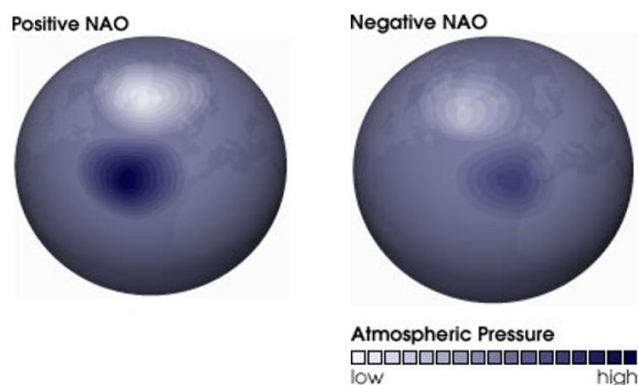


Figure 3.6: Representation of the two NAO phases.

Thanks to the information acquired in (National-weather-service, 2018) it is possible to states that NAO oscillation has the main influences on European circulation in winter (NAO winter) because in this period the dipole is more pronounced. The effect on the European continent of the two cyclic phases are:

- NAO +: It defines an unbalanced trajectory of disturbed flows towards Northern Europe, where a more humid and milder climate is observed. In southern Europe there are drier and colder winters but the persistence of the anticyclone at the low latitudes of the continent leads to a general increase of temperature and frequently thermal inversion conditions.
- NAO -: It results in a more mild, humid and perturbed climate in southern Europe and the Mediterranean. Temperatures in this area are not necessarily rigid, especially at lower altitudes due to the recall of prefrontal currents. Northern Europe is experiencing cold, dry winters.

As examined in several scientific studies, the cyclical fluctuation of the winter NAO, calculated as the average monthly NAO (dec-feb or dec-mar), greatly

influences the characteristics of European winters, especially in those areas (such as Lombardy) directly subject to perturbed flows of western matrix.

In the article (Yoojin Kim, 2012) the general increase in temporal snow cover (SCD) in southern Europe is shown in the case of winters with NAO- phases, and vice versa. The study also shows the general increase in snowfall (average snowpack thickness, snow cover, snowfall) during this phase. In the study (Bocchiola D, 2007) it is shown, for an area inside the ones studied in the present work, as a general increase of the NAO index corresponds to a decrease of HS and SCD.

The influence of a negative winter NAO peak on snowfall is also demonstrated for winter 2009, characterized by intense and continuous snowfall on the southern side of the Alps, which have caused a high number of avalanche accidents and catastrophic avalanches with centennial return period due to frequent thermal rises following the extreme snowfall (AINEVA, 2010).

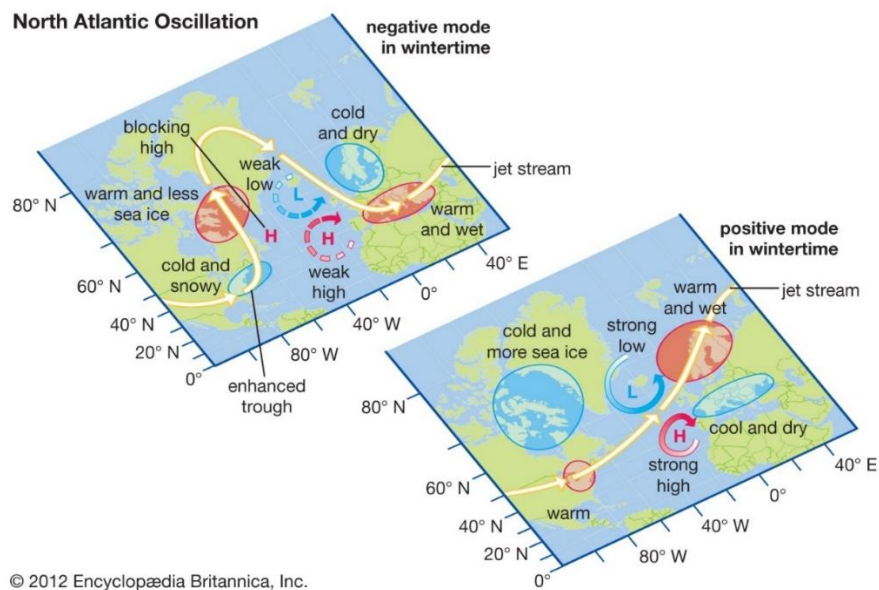


Figure 3.7: Influence on European winter climate of NAO atmospheric pattern.

4. TERRITORY SUBDIVISION IN HOMOGENEOUS AREAS:

To detect common variability path of the snow parameters a classic trend assessment is complemented with a trend analysis applied on grouped stations, homogenous from the point of view of one geomorphological characteristics of the site where the station is located (called '*homogeneous group*'). This technique allows to investigate the influence that some parameters could have on SV trends.

The proposed geomorphological characteristics of the single sites, deemed based on the experience most influential on the snowfall regimes and snowpack evolution are (Cresta R., 2014):

- Mountain area
- Elevation range
- Slope aspect

In the following subchapter, an explanation of the discriminant parameters together with all the grouping choice done are reported.

4.1 Mountain sides characterization:

The aspect of the mountain slope where stations are located mainly influence the evolution of the snowpack. It must be noticed that ARPA and AINEVA snow measurements stations are built in neutral aspect site (flat), and therefore the aspect is intended has the ones that characterizes the environment surrounding the stations.

In general, North-facing sides are the coldest due to the shadow cast by the mountains above and South-facing sides the mildest, due to the higher solar radiation recovered. The sides to the north frequently, during winter, are totally deprived of the sun's rays and temperatures drop considerably, often leading to dry snow metamorphism. At the opposite, the south-faced slope snowpack is frequently exposed to freeze-thaw cycles, which often allow a faster stabilization of the snowpack, but also predispose this slope to wet snow and gliding avalanches.

The Est-faced sides and the West-faced ones receive intermediate sunny conditions. Despite this, the slopes exposed to the east are generally colder, since the sun's rays must heat the air cooled in the night and then leave the slopes in the afternoon, while those exposed to the West receive the direct radiation in the afternoon, when the air temperature is milder (Cresta R., 2014).

4.2 Vertical subdivision of the territory based on altitude belts:

It is known that average air temperature decreases with altitude and other meteorological phenomena, such as wind, tend to be more extreme at higher elevations (Cresta R., 2014). Therefore, the altitude at which the stations are located is considered an important influencing factor on snowy conditions, due to the vertical tropospheric thermal gradient.

In this work a vertical subdivision of the mountain territory is proposed according to the theoretical altitude belts of vegetations, which are altimetric ranges characterized by formally homogenous flora and vegetation attributable to the similar climatic conditions typical of the entire belt (Pignatti, 1979).

In the following sketch it is possible to see the subdivision valid for the alpine chain with the borders of the various bands traced according to the so-called altitude horizons.

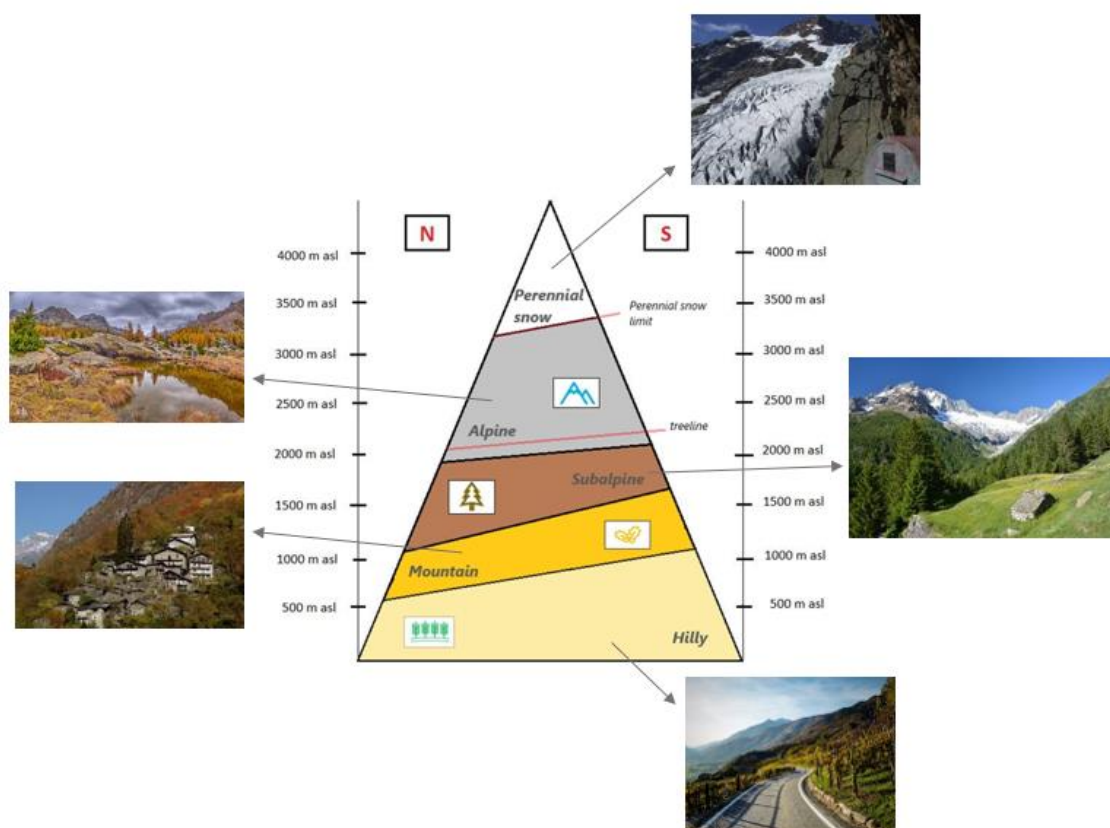


Figure 4.1: Altitude belts and horizons in a generic alpine mountain with photographic example from Valtellina environment.

As one can notice, because of the different heating conditions explained in the previous chapter, the altitude horizons are at lower elevation in the north face (colder) than in the south face (milder), instead East and West side can be in intermediate conditions.

For what concern the different belts, one can distinguish:

- Hilly belt:

It originates between the low level and 500-1000 m asl and is characterized by mixed woods of broad-leaved trees (such as oaks or hornbeams) and agricultural crops. The growing season is more than 250 days per year and the climate is generally mild and strongly influenced by the alpine geographical area (proximity to the Mediterranean Sea, presence of large lakes exc.). It's the most anthropized belt.

- Mountain belt:

This belt extends up to 1200 - 1800 m asl and is characterized in the most exposed mountains to the south and to the damp currents coming from the sea by the presence of beech. In the drier areas of the Alps, white fir is widespread, while red fir almost always grows there. The average annual temperature is between 5°C and 10°C and the growing period exceeds 200 days.

- Subalpine belt:

Its upper floor extends between 1800 m and 2200 asl and is mainly characterized by coniferous woods (such as spruce, larch and stone pine) or other plants capable of resisting frost phases during the vegetative period (such as birch). At these altitudes the days of strong wind are not rare, and the snow cover can be present even for six months per year. The average annual temperature slightly exceeds the zero degrees, and the vegetative period is between 150 and 200 days per year.

- Alpine belt:

In the lower part there is the presence of dwarf bushes, which resist thanks to the protection by the snowy coat towards the intense atmospheric agents and end with the upper limit of the trees. From this limit up to the limit of the perennial snow (coinciding with the upper limit of this band, just above the 3000 m) they resist mountain prairies thanks to the thermal insulation due to the continuous presence of the snowpack for many months. In the upper part this belt is often characterized by morainic debris, rock glaciers and rocks. The solar radiation is very intense due to the lower humidity in the air, and the vegetative period is less than 100 days.

- Perennial snow belt:

This belt is not really an altitude belt based on vegetation, which is unable to resist the extreme environmental conditions that characterize its nature but is however reported for continuity. It originates from the limit of the perennial snow, that is

the limit above which the accumulated snow never melts completely during the year and is characterized by the presence of glaciers and snowfields. In the present work this altitude belt is not considered, since there aren't stations with enough measurement's years in the Lombard territory.

4.3 Spatial subdivision of the territory based on mountain areas:

The mountain climate gives to this region a heterogeneity such as to justify the interest of a trend analysis for individual spatial areas.

In the avalanche field, a subdivision of the Lombardy Alps into 9 hazard zones is proposed by the Nivometeorological centre of AINEVA (AINEVA, 2020) for the dissemination of avalanche bulletins. However, this subdivision, useful at a practical level for the authorities, omits some natural boundaries that often act as a climatic watershed, delimiting two zones with different nivologic feature and therefore worthy of subdivision.

The subdivision proposed in Figure 4.2 is based, in addition to the experience due to the frequentation and the direct knowledge of the area on the following geographical and morphological parameters descriptive of the alpine climate (Beniston M., 2006):

- Mountain range or mountain subgroup (i.e., Retiche range, Orobie range, Bernina subgroup ...)
- Mountainside (i.e., Orobie northface, Orobie Southface ...)
- Proximity to a great lake.
- Catchment
- Precipitation's regime

All the geographical informations are recovered on the DTM with 20 m sampling pitch, that is considered a good resolution for the aim of this work. The used DTM comes from Geoportale Service of the Lombardy Region (Regione Lombardia, 2014) and calculations are carried out in ArcMap 10.7.1 (ESRI, 2019). As regards the nomenclature used in the description of zones, reference is made to the names of the official SOIUSA subdivision (Marazzi, 2002).

A description of the proposed areas, together with the choices made for the subdivision, is given in the following subchapters. A total number of 8 areas is proposed, namely:

- Valchiavenna
- Prealpi Lariane
- Retiche Occidentali
- Orobie Nord
- Orobie Sud
- Livigno

- Alta Valtellina
- Adamello

Notice that the Prealpi Varesine and Comasche as well as the Prealpi del Lago D'Iseo are not reported, since no useful snow measuring stations are founded in the area.

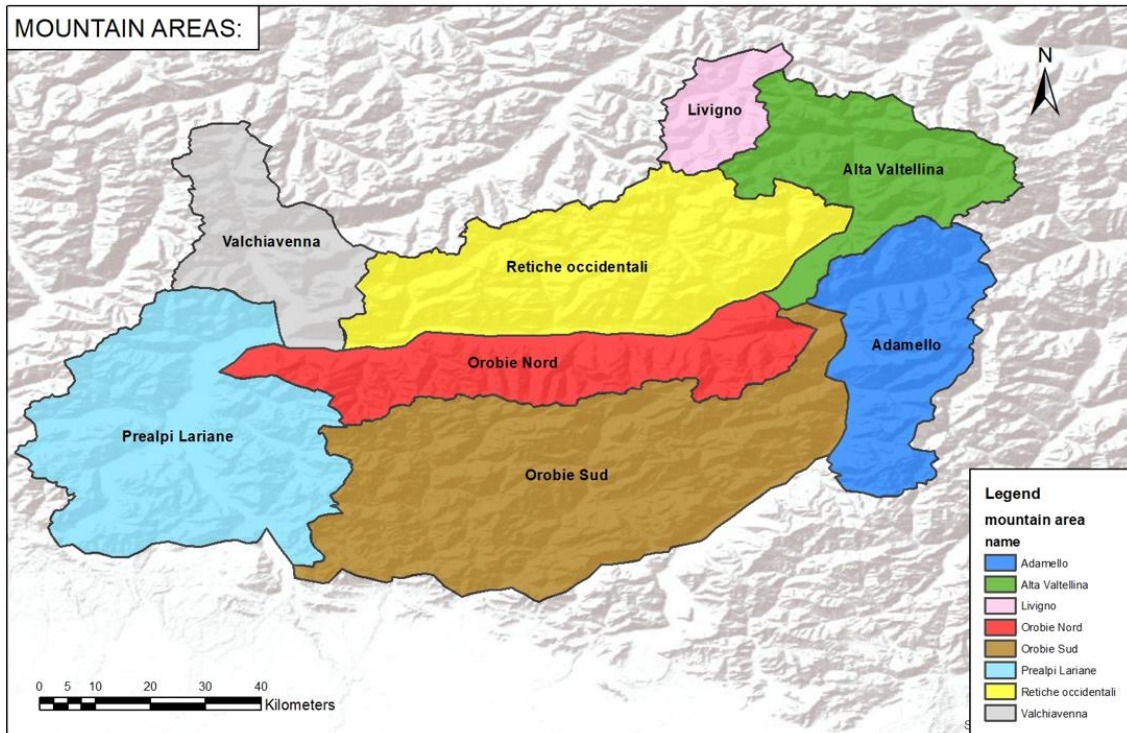


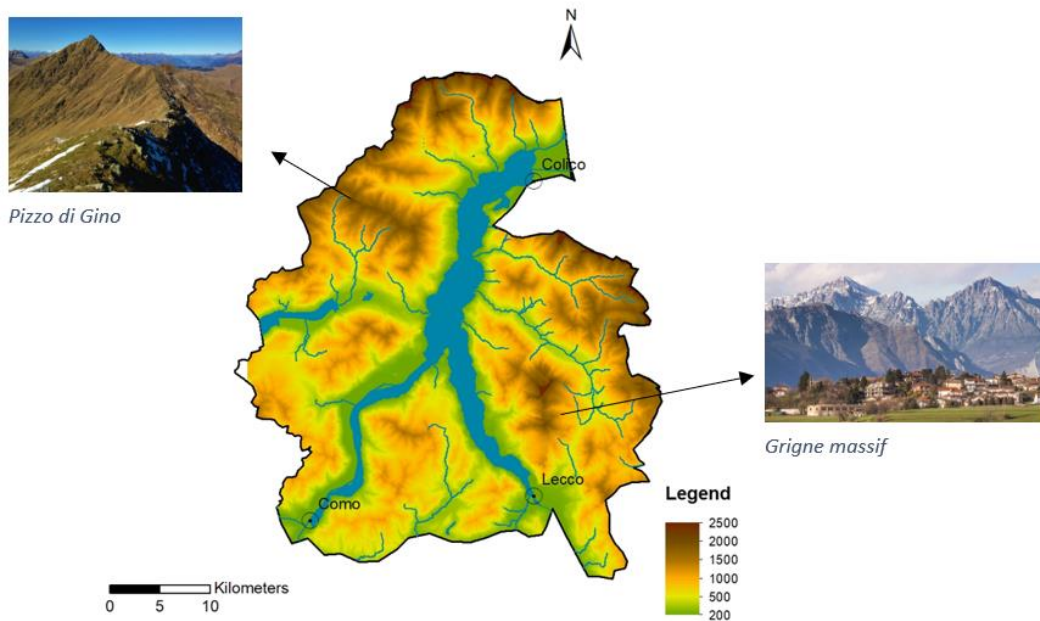
Figure 4.2: Homogeneous subdivision based on mountain areas.

4.3.1 Prealpi Lariane:

This area corresponds roughly to the western portion of the Lombardy pre-alps, including part of the Lugano pre-alps, Como Prealps and Bergamo Prealps subsection, as well as a small portion of Orobic alps facing the Como Lake. The main massifs are those of Pizzo di Gino (2245 m), the Grigne Group (2410 m) and the mountains of the Triangolo Lariano. The highest point is the Monte Legnone (2609 m), which falls within this area only in its southern slope and, from a purely morphological point of view, it is important the presence of marked valleys such as Val Sassina, Val Varrone and Val Cavargna.

The average elevation is 896 m asl, which is in the upper portion of the Hilly belt and is indicative of the low altitude of the pre-alpine mountains. There is no predefined orientation of the slopes while from the climate point of view, as well as the moderate altitude, is influential the presence of Lake Como in the center of the area, which exerts a certain thermoregulatory function. Only one ski resort is present in the area.

The average annual precipitation is among the largest in the region and is around 1800 - 2200 mm/y.

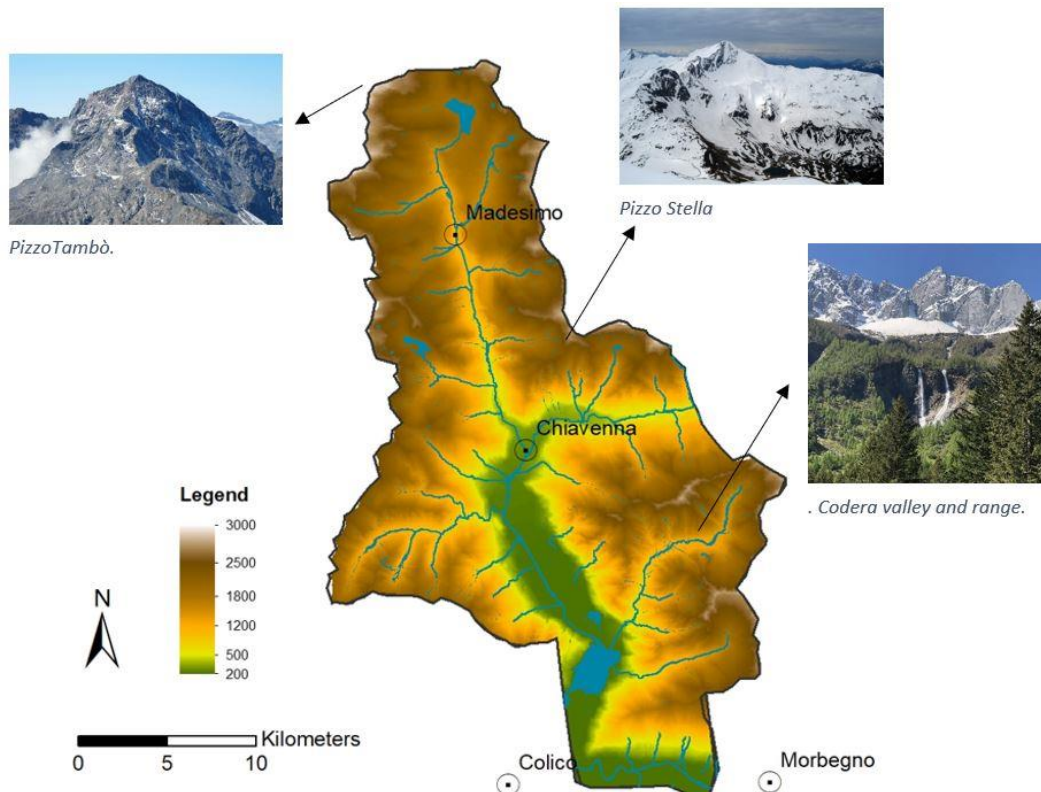


4.3.2 Valchiavenna:

This area mainly corresponds to the valley defined by the course of river Mera, which flows with North-South axis separating the western Rhaetian Alps (right side) from the easternmost portion of Lepontine Alps (West side). Several lateral valleys are included, of which the main are Valle Spluga (famous for winter tourism), Val Bodengo, Val Codera, Valle dei Ratti and Val Bregaglia (only the Italian portion is considered). Excluded from this territory is the Val di Lei, as it does not belong to the Valchiavenna's and Mediterranean watershed area.

The glaciers of Val San Giacomo and Val Bregaglia, in the last glacial period, joined together in the place where Chiavenna now stands, forming a single large mass that reached as far as Valtellina. The action of the glaciers has forged the valley sides giving the typical "U" shape, then modelled by the river.

The main reliefs include Mount Tambò (3279 m), Pizzo Stella (3163 m), Pizzo di Prata (2727 m) and Pizzo Ligoncio (3032 m). The average altitude of the area is about 1500 m asl, the main orientation of the slopes is South and the most important lake, located in the lower part of the valley adjacent to Lake Como, is the ones of Novate. The average annual precipitation is 1200/1600 mm/y.



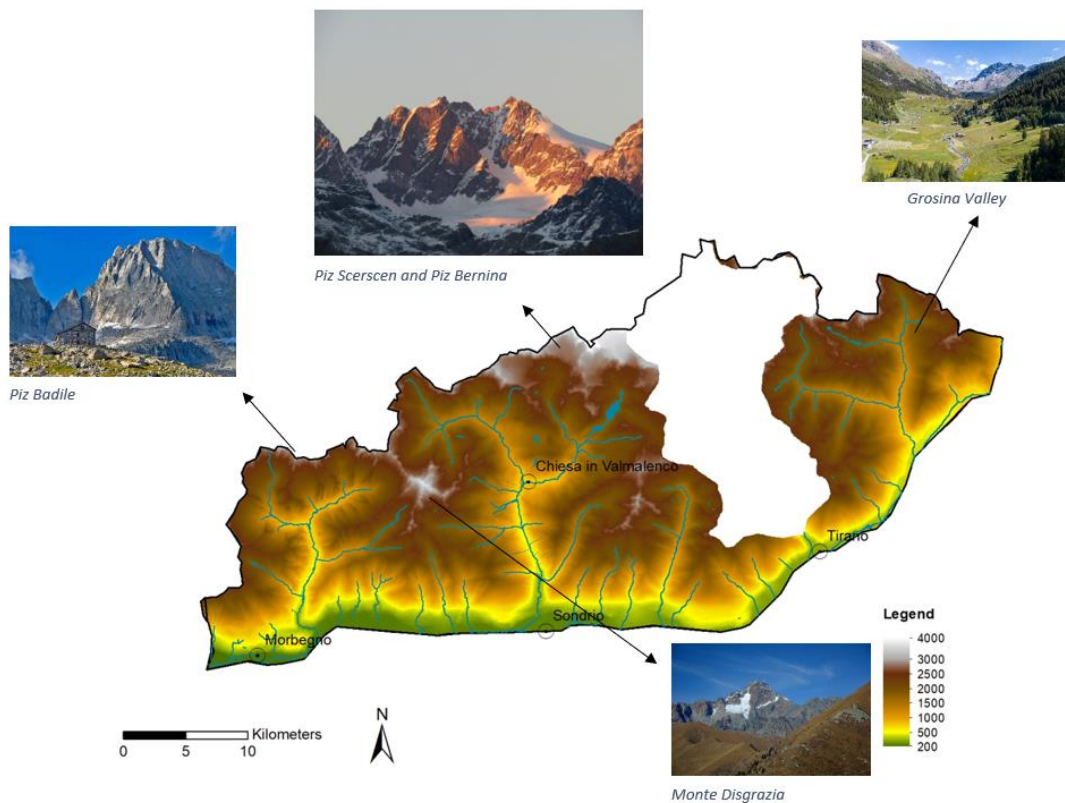
4.3.3 Retiche Occidentali:

This area corresponds to the portion of Western Rhaetian Alps occupying the right hydrographic side of the low and medium Valtellina, including numerous lateral valleys such as Val Masino, Val Malenco, Val Poschiavo (CH) and Val Grosina, appreciated for hiking, mountaineering and winter activities (especially in Val Malenco where an important ski area exist).

In this part of the territory rise the highest Lombard relief, culminating with the Piz Bernina (4049 m) and divided mainly into the two supergroups Masino-Bregaglia and Bernina, in turn divided into the groups of Cima di Castello (3379 m), Monte Disgrazia (3672 m), Bernina and Pizzo Scalino (3323 m). Other mountains worth mentioning are Pizzo Badile (3308 m), Piz Roseg (3937 m) and Piz Palü (3900 m). The ice cover is particularly important in Valmalenco where the presence of glacier such as Scerscen Superiore (4.78 km², 2007) and Fellaria Ovest (4.32 km², 2007) or rockglaciers is widespread. (G. Smiraglia, 2015).

The average altitude is 1850 m asl, with slope mainly faced South and annual precipitations of 1000 – 1200 mm/y.

Notice that, although Val Grosina is politically associated with the upper Valtellina, it has all the main characteristics (as in example slope aspect, geomorphology or average annual precipitation) of the nearby Rhaetian valleys, and is therefore annexed to this area.



4.3.4 Alta Valtellina:

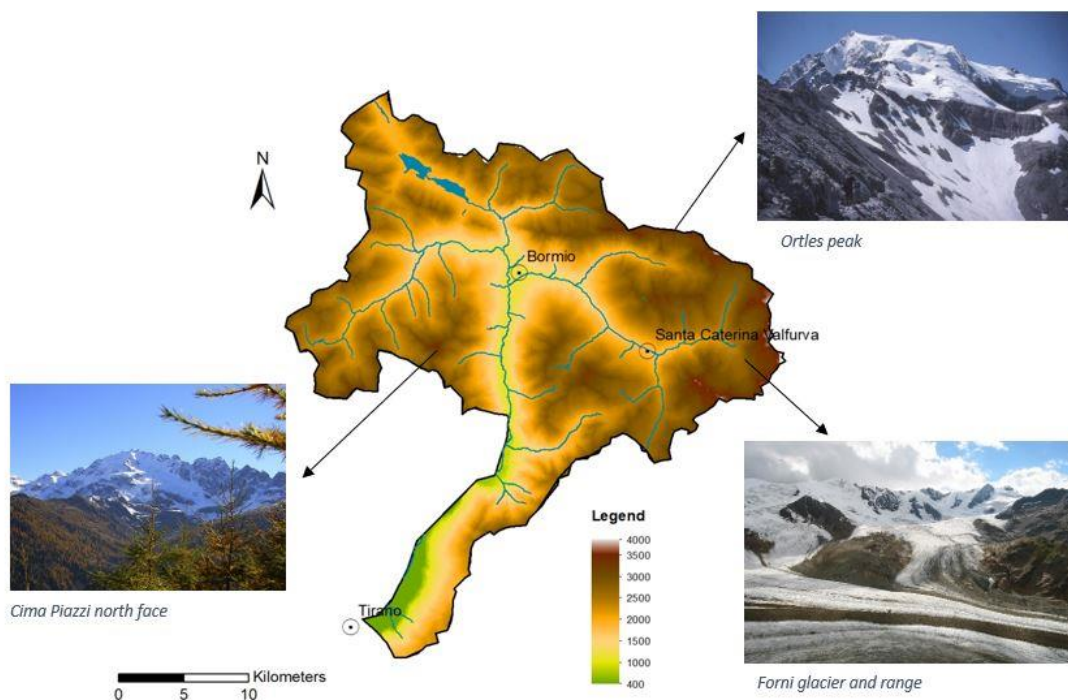
This territory corresponds in general to the upper portion of Valtellina, in which some lateral valleys are inserted (such as Valfurva, Valle del Braulio and Val Viola) near the town of Bormio.

The area is bordered by a crown of mountains with heights over 3000 m, all part of the western Rhaetian Alps, which lowers near important alpine passes (i.e. Stelvio Pass, Gavia Pass, Foscagno Pass). This morphological conformation confers on the valley floor strongly continental climatic characteristics, due to the barrier against the disturbed flows imposed by the mountains, also confirmed by an average annual precipitation of 800-1000 mm/y.

Among the main reliefs stand out the group of Cima Piazzzi (3439 m) to the West, and the whole group Ortles - Cevedale to the East, from which we can mention the Ortles (3905 m), the Gran Zebrù (3857 m) and the Pizzo Tresero (3602 m).

Given the main exposure of the slopes to the North-West and the high average altitude of the area (2250 m als), the glacial cover is still important, evidenced by the presence of the largest Italian valley glacier (Forni glacier, 11.34 km² in 2007). (G. Smiraglia, 2015)

The area is heavily frequented for mountaineering and winter tourism.



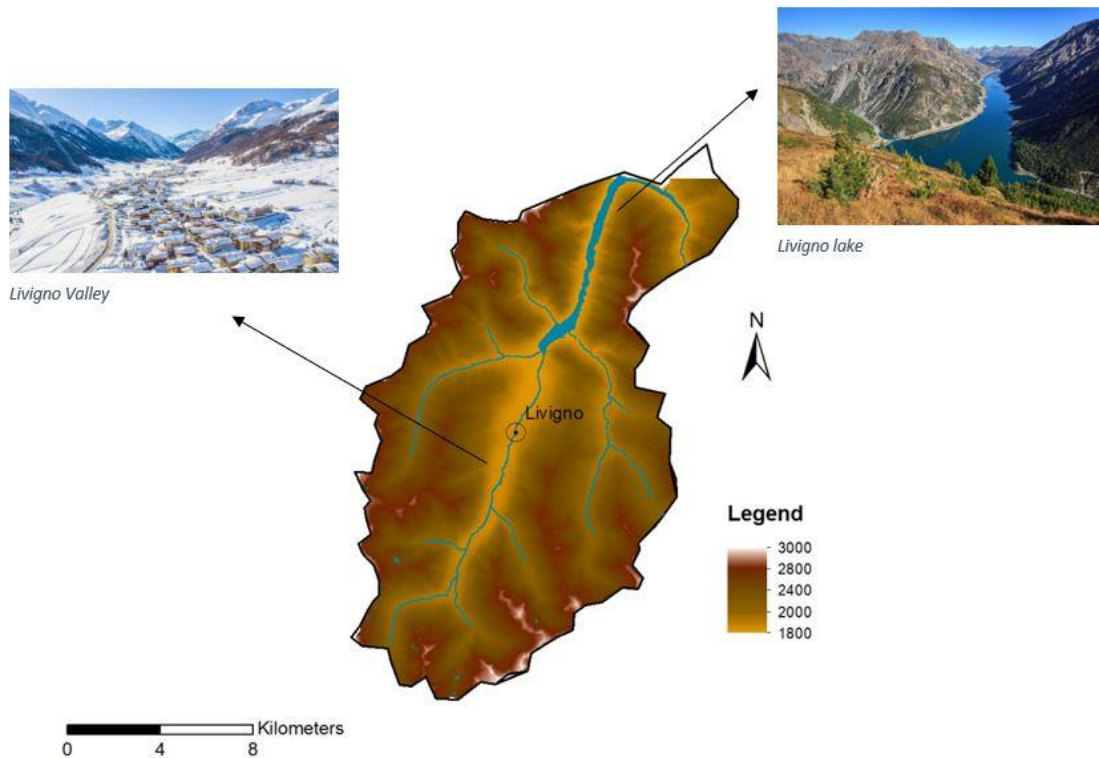
4.3.5 Livigno:

With this area is meant the territory of the so-called plateau of Livigno, which morphologically includes the upper portion of the valley of the river Spohl. This territory is not in the Mediterranean catchment area, as the river Spohl is a tributary of the Inn River and then the Danube, which in turn flows into the Black Sea.

This characteristic gives the area, located at a high average height (2400 m asl), special microclimatic characteristics with a strong continental average annual precipitation regime (600-800 mm/y) and often extreme temperatures in the winter months.

The territory, enclosed in the group of the Livigno Alps (Western Rhaetian Alps), is connected to the national territory only by the Foscagno Pass, near which stands the town of Trepalle, second in Europe by elevation. To the west, where the connection with the nearby Engadine (CH) is guaranteed by a tunnel (Munt la Schera), there is a modest artificial lake, whose waters are derived in Switzerland for hydroelectric purposes.

The high snowfall of the area is typical of the continental alpine sector (factor that makes Livigno one of the largest European ski and tourist resorts), and for the reason stated the separation of this territory from the others is considered of crucial importance.



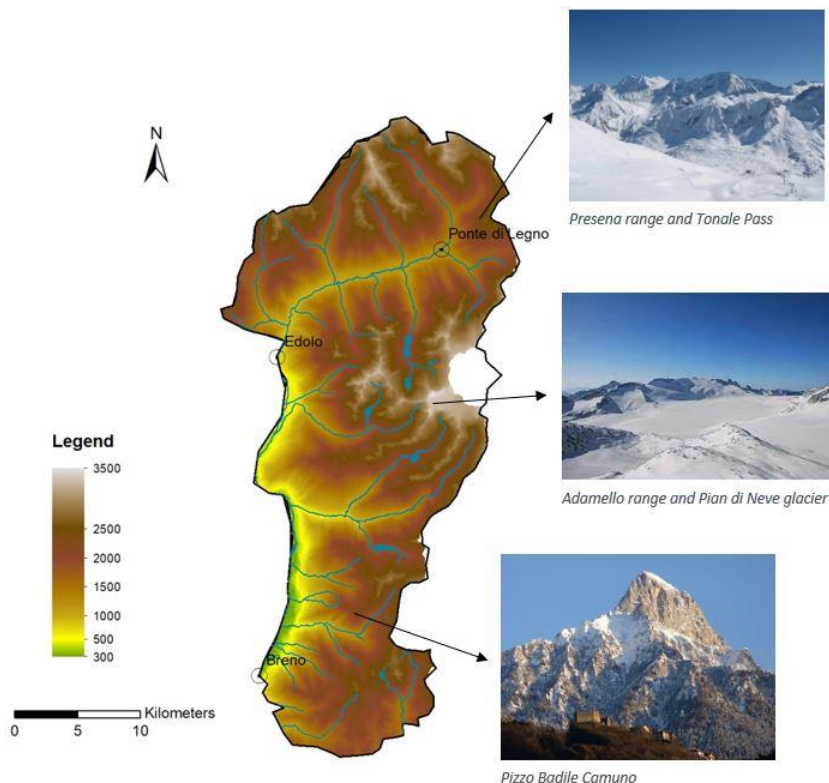
4.3.6 Adamello:

This area corresponds to the left hydrographic side of the middle and high Val Camonica, the valley with glacial origins modelled by the river Oglio. The name comes from the Adamello supergroup, that is the massif belonging to the Southern Rhaetian Alps which includes all the mountain of the area.

This massif, together with that of Presanella, is developed between Lombardy and Trentino Alto Adige and has a very complex orography well isolated from the nearby mountain groups through deep valleys. In addition to the Val Camonica, which has in the middle a North-South orientation and in the upper East-West orientation, worthy of note are the Val di Savio, Val Paghera and Val Malga.

The Adamello is among the massifs of the Alps with the largest glaciers. Pian di Neve (18 km²) is a flat glacier, which occupies the acropolis among the main peaks of the Lombard side, from the Lobbia Alta (3196 m asl) to the Adamello, at an altitude between 3100 and 3400 meters; together with the adjacent glacier of Mandrone is the largest glacier in the Italian Alps. The highest peak is the Mount Adamello (3539 m asl).

The average elevation is 1520 m and the main aspect is West. The average annual precipitation varies from 800 – 1000 mm/y in the northern side (characterized by a more continental climate) to the 1400-1600 mm/y of the southern part (closer to the great lake and the Padana plane).



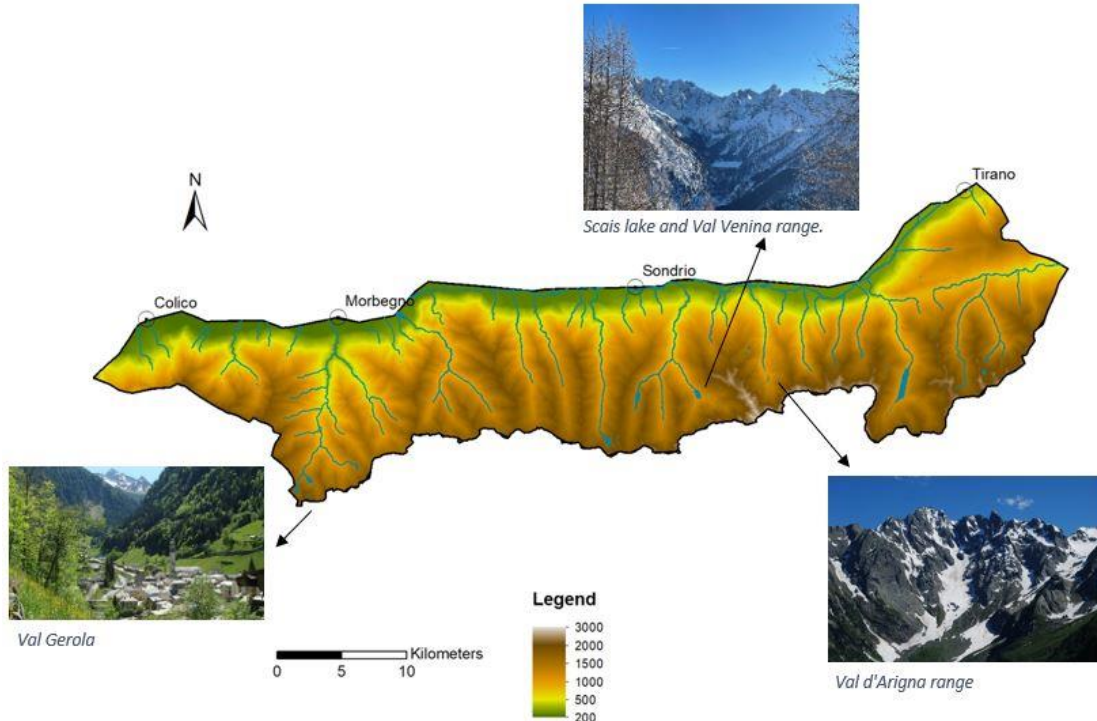
4.3.7 Orobic Nord:

This area represents the northern side of the Orobic Alps, located on the hydrographic left of the Valtellina, separating the provinces of Sondrio and Bergamo.

Looking at the previously described subdivision of the territory in altitude belts it is possible to appreciate the different starting heights of the bands in the two opposite sides of a generic relief and so the separation between the north and south faces is considered of utmost importance. The portion of the mountain range considered, in fact, even if it does not reach the heights of the opposing Rhaetian Alps, is prominent enough to act as a climatic watershed, both because of the different conditions of sunshine between the North and South sides, either because of the significant barrier effect imposed on disturbances.

The northern slope of the mountain chain is carved into precipitous but short valleys, often wild as the morphologically complex Val Venina, Val d'Arigna or Val Coronella (appreciated by ski mountaineers for the steep slopes and the snow that is often kept dusty for long periods) or permanently inhabited only in the western portion (i.e. Val Gerola, Val Tartano).

The highest peaks rise in the middle, like for example Pizzo Coca (3050 m), Pizzo di Scais (3038 m) and Pizzo Redorta (3038 m), the average elevation is 1450 m asl and the average annual precipitation are about 1400 – 1600 mm/y.



4.3.8 Orobie Sud :

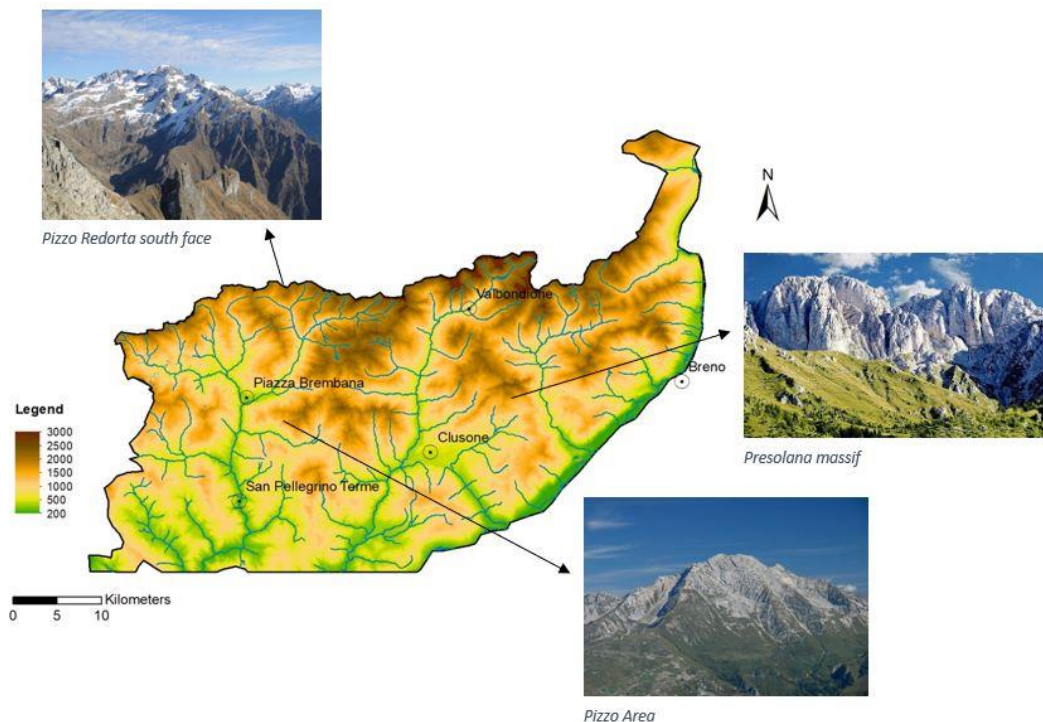
This last described mountainous area correspond on the Southern slope of the Orobie Alps together with the Bergamasque Pre-Alps, here joined in a single area because of the compatibility of the parameters considered for the subdivision.

The latter, also called Orobie Pre-Alps, are separated from the homonymous Alps in the north by some side valleys of the main Val Brembana, Valle Imagna, Val Seriana and Val Camonica. The Val Camonica then separates this area, which characterizes its right hydrographic side from the Adamello area.

From a climatic point of view, the continentality is less marked than the north orobic side, being the prealpine side directly exposed to the south-western perturbed flows. The average annual precipitation is among the highest of the entire region, especially close to the orobic chain due to the barrier effect (1800 – 2200 mm/y).

The main peaks are Pizzo Coca (3050 m) and the others border relief already mentioned for Orobie Nord, the Concarena (2549 m), Presolana (2521 m) and Pizzo Arera (2512 m).

The average elevation is 1230 m asl and the main aspect South.



5. DATASET AND DATASOURCE OVERVIEW

To adequately characterize the current and future snowy conditions over an area a considerable amount of data is required. The goodness of the database, mainly defined by the quality and the number of observations is therefore fundamental for the success of the work. The available sample, composed by the observations, must be as representative as possible of the population, to best describe the variables on which the calculations are carried out (Kottedoga T., 2008).

Unfortunately, in Italy, there is often a lack of records in snow matters compared to other countries in the Alps. The automatic measuring stations were positioned by the authorities in charge only from the early 90's, in substitutions of the manual measuring stations, already present since the beginning of the last century especially at the manned hydroelectric power plants. Historical data from manual measuring stations are, however, more difficult to validate and present lacks data.

5.1 Data sources and variables involved:

The acquisition of the dataset used in this project is performed by using the open data portal for ARPA measurement stations (ARPA Lombardia, 2021) and by directly contact the data provider for AINEVA ones (AINEVA, 2020). The variables on which the trend analysis is applied are mainly of three types:

- Snow variables (*SV*)
- Temperature variables
- Total precipitation

The formers are those on which the trend assessment is focused, instead, the temperature and precipitation ones are created with the aim of adequately understand the possible causes of snow variability in the area and to complement the study.

All the snow variables are computed from the daily snowpack height (*HS*) observed by the AINEVA and ARPA automatic snow gauges. These instruments can detect HS by measuring the distance between an ultrasonic emitter and the reflective surface of the snowpack. In general, the sensors are installed on a metal rod and is connected to the data acquisition and transmission stations by mean of a multipolar cable. The snowpack height is acquired with daily temporal resolution.

The computed snow variables, summarized in Table 5.1, are considered good descriptors of the main features regarding the snowiness:

STUDIED VARIABLES						
Name	Unit of measure	Category	Formulation	Description	Subvariables	Subvariable description
HS_av	cm	Snow Variable (SV)	$HS_{av} = mean_y (HS_{day})$	Snow cover annual average depth.	-	-
SCD(n)	number of days	Snow Variable (SV)	$SCD = count(days\ per\ year\ with\ HS > n\ with\ n = threshold)$	Days per year with HS > threshold (Snow Cover Duration)	SCD5	Threshold = 5 cm
					SCD1	Threshold = 1 cm
					SCD20	Threshold = 20 cm
					SCD50	Threshold = 50 cm
SD	number of days	Snow Variable (SV)	$SD = count(days\ per\ year\ with\ HN > 5\ cm)$	Snowy days in a year.	-	-
H(n)D	cm	Snow Variable (SV)	$HnD = max_y [HS(day\ n+1) - HS(day\ 1)]$	Maximum fresh snow accumulation on the ground in N days.	H3D	N = 3 days
					H2D	N = 2 days
					HN	N = 1 days
HN_av	cm	Snow Variable (SV)	$HN_{av} = mean_y [HS(day\ 2) - HS(day\ 1)]$	Average daily snow accumulation	-	-

Table 5.1: List of calculated snow variables

It is specified that the H(n)D variables are just an approximation of the solid precipitation useful for the present analysis. The fresh snow precipitation would be manually measurable as the snowy accumulation over a plane on which an operator takes care of removing the snow after each measurement. Historical series of such variable are unfortunately not available and therefore the snowy accumulation is assumed equal to the positive variation of the snowpack height (ΔHS), which includes for example also the eventual accumulations due to wind deposition. Since the ARPA and AINEVA stations are strategically located to limit the phenomenon of wind transport this approximation is considered correct for the purpose of this work.

The temperature variables are created starting from the hourly temperature registered at the ARPA stations thanks to an air thermometer. This instrument consists in a plastic body with an inserted PT100 sensor and an external finned protection (ventilated configuration) which allows the measurements to be carried out in a homogeneous temperature space.

The computed temperature variables are summarized in the following table:

STUDIED VARIABLES						
Tmean	°C	Temperature	$Tmean_y = mean_y (T_{day})$	Average yearly temperature	-	-
Tmax	°C	Temperature	$Tmax = max_y (T_{day})$	Maximum annual temperature	-	-
Tmin	°C	Temperature	$Tmin = min_y (T_{day})$	Minimum annual temperature	-	-

Table 5.2: List of calculated temperature variable.

The precipitation variable, representing by the total annual precipitation (P_{tot}), is calculated starting from the liquid precipitations measured by ARPA pluviometers and solid precipitation obtained from the HS variable. The pluviometers sensor consists in a metal collection cone with an inlet area of 1000 cm² and a double blow action frame connected to an impulse counter. For this variable, data with daily temporal resolution are used.

The total annual precipitation can be described as the total amount of water that reach the soil in one year, and so, it is composed of both the solid and liquid phases of the atmospheric precipitation (Eq. 4).

$$P_{tot} = P_{liquid} + SWE_{HN} \quad (4)$$

Where HN represents the daily precipitated fresh snow and P_{liquid} the daily average liquid precipitation measured by the ARPA pluviometers.

For measure the SWE with the best possible accuracy level, a heated rain gauges should be used. These instruments can melt the snowfall instantly thanks to an electrical resistance and register the equivalent in water of the fresh snow, but unfortunately, have been installed by ARPA agency only in the last few years, preventing their use for the historical series analysis.

With the sole purpose of the trend assessment the SWE is estimated in the following way (Eq. 5):

$$SWE = HN * \frac{\rho_{HN}}{\rho_w} \quad (5)$$

Where ρ_{HN} represent the density of the fresh snow, and ρ_w the density of the water (1000 kg/m³).

The density of the snow depends on physical and climatic parameters and would require specifics measurements conducted on the fields after each snowfall. In this work, the parameter is estimated based on the results reported in (Valt M, 2018), where is demonstrated that the average air temperature of the 24 hours containing the snowfall event (T_{air}) is the best predictor of the ρ_{HN} in the Italian Alps, with a 31% of uncertainty, considered valid for the aim of this processing.

In the mentioned study, the following linear model is proposed (Eq. 6):

$$\rho_{HN} = 4,05 * T_{air} + 127,2 \quad (6)$$

When the average daily temperature is positive, the total precipitation is considered composed only by the liquid phase, and so, the calculation of the daily total precipitation (P_{day}) can be summarized as (Eq. 7):

$$P_{day} = SWE_{HN} = HN * \frac{\rho_{HN}}{\rho_w} = HN * \frac{4,05T_{air} + 127,2}{\rho_w} / 100 \quad \text{if } T_{air} < 0^\circ C$$

$$P_{day} = P_{liquid} + SWE_{HN} \quad \text{if } T_{air} > 0^\circ C$$

(7)

5.2 Used measurement stations:

5.2.1 Snow gauges:

The ARPA and AINEVA automatic snow gauges network consist in a total number of 56 point, distributed in all the Lombard Alps at different altitudes and developed since the early '90s. The recent nature of this automatic sensors, unfortunately, allows only a trend assessment of the last 3 decades of HS historical series, based exclusively on the first positioned automatic stations.

After plotting the data in possession and checking their completeness in the life periods of the stations with a careful visual analysis the choice of the most suitable stations for the dataset used in this work is done. This choice is mainly based on the number of consecutive recording years (Y_i).

Whereas the first stations were positioned in Valmalenco during 1990 (at the arrival of the cableway serving the local ski area and at the Campo Moro hydroelectric power plant), the use of stations with at least $Y_i = 25$ y is proposed, because shorter historical series could lead to the assessment of short-term trends which would be unable to describe the realistic behavior of the variables in question.

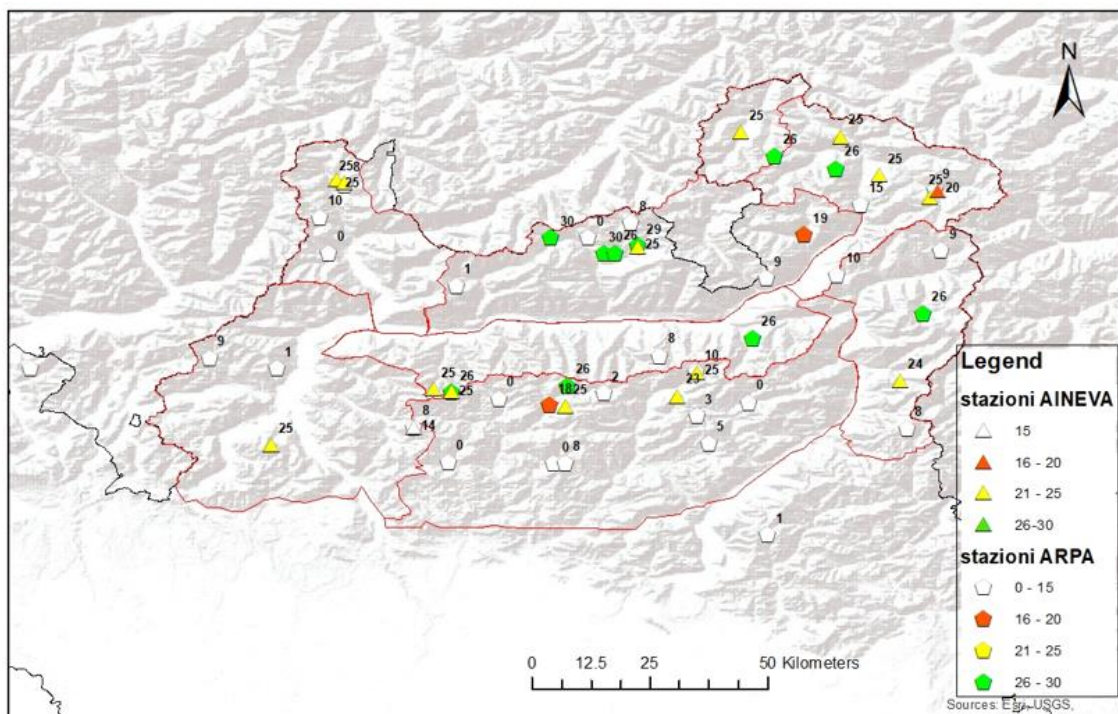


Figure 5.1: Spatial framework of the available measurement stations with the available measurements years.

As one can see in the images these stations are not able, on their own, to guarantee adequate spatial coverage (especially in the pre-Alpine areas and at lower altitudes). To overcome this problem, it is decided to expand the dataset with 5

other stations characterized by a shorter recording period, and respecting the conditions $Y_i > 15$ y.

Using this last condition, a sample of daily HS records, coming from 28 automatic ARPA and AINEVA snow gauges, is acquired as input for the elaborations described in the following chapters. The used stations are the colored ones in Figure 5.1: Spatial framework of the available measurement stations with the available measurements years.

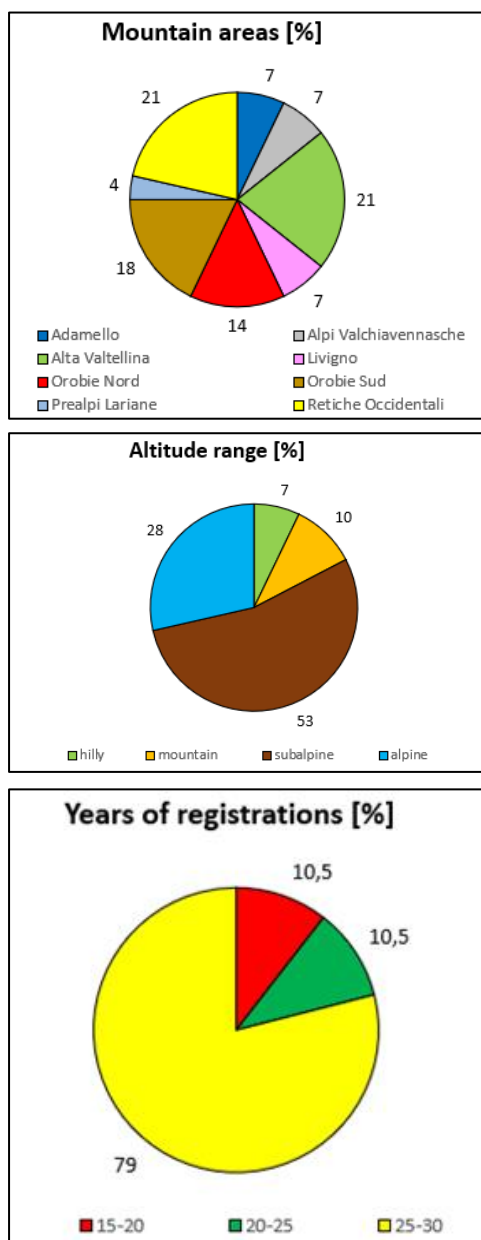


Figure 5.2: Some statistics feature of the available measurements stations.

As one can see from the images on the side the use of this 28 snow gauges dataset has a good spatial resolution and can adequately cover the entire Lombard mountainous region. The Prealpi Lariane region is the less represented ones, on the opposite Retiche Occidentali and Alta Valtellina are the most covered. As regards the distribution of the snow gauges in the vertical axis, one can see that all the altitude range are covered.

The greater number of snow measurements stations are positioned in subalpine environments, instead only the 7 % of the measurements comes from the hilly range and only the 10 % are in the Alpine ones. Notice that the choice of adding 5 stations with $Y_i > 15$ y is a compromise between spatial and temporal coverage. Despite this, given the maximum temporal duration of 30 years, it is believed that the dataset is sufficiently representative of the history of the variables in the last three decades. The 79 % of the measurement stations used has $25 < Y_i < 30$ y.

In addition, a quick homogeneity test of the chosen areas is performed calculating the average snow depth (HS_av) of the entire available station's historical series by applying an altitude correction to obtain HS values at 2000 m asl.

In (D. Bocchiola, 2007) a snow depth increase of 5 cm with 100 m in altitude is proposed. Considering that the correction on average snow depth transfer the stations at a plane with altitude of 2000 m asl, the Thiessen Polygon can be used.

As one can observe in the Figure 5.3 despite the little number of observations, the proposed subdivision based on geomorphological and climatic differences is also reflected by the distribution of the average snow depth at a generic altitude of 2000 m. This map is only indicative since the procedure is sensitive to the number of station in a certain area, more data point can lead to better results but however, it is possible to perceive a certain homogeneity of the variable HS_2000 with respect to the subdivision carried out.

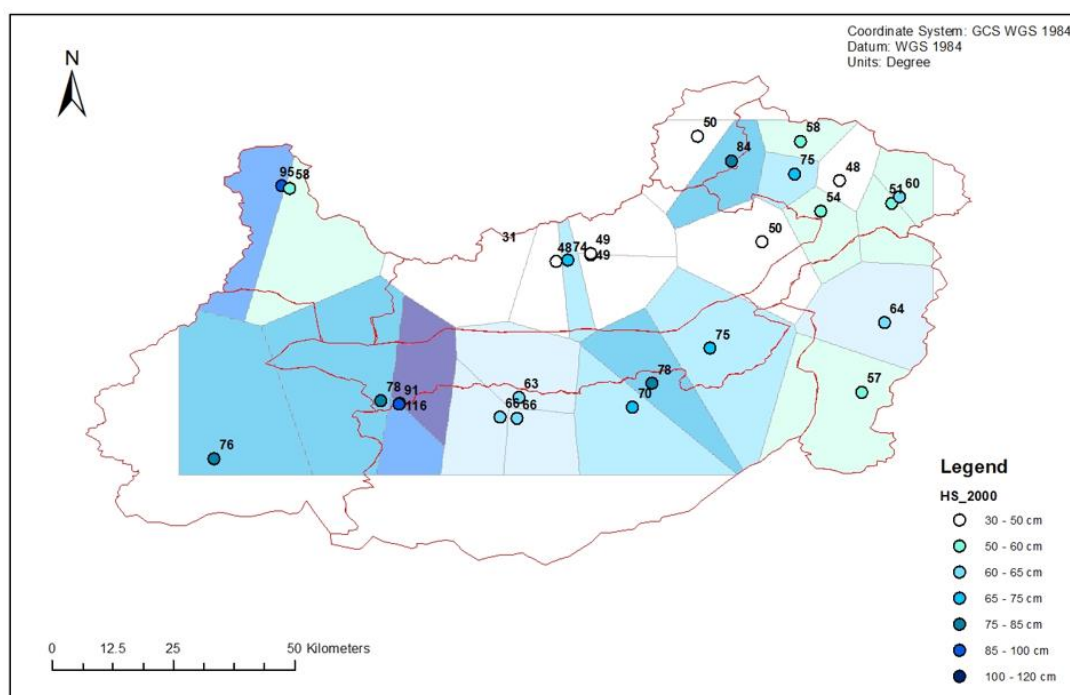


Figure 5.3: Thiessen polygons of HS at 2000 m asl.

In the Table 5.3 all the used stations for measuring HS are reported, together with the relative homogenous group characteristics.

5.2.2 Temperature and precipitation gauges:

The measuring stations from which the time series of liquid precipitation (used to calculate the total precipitation) and temperature are derived form a subset of the 28 stations described above. This choice is dictated by the fact that unfortunately not all stations equipped with nivometric sensor have a thermometer and a pluviometer with a series of measurements that can cover the period chosen for the trend assessments.

Nevertheless, the analysis of temperature and total precipitation trends is intended as a corollary to the analysis of snow variables trends and can characterize the general behavior of snow variables for the entire study area.

In the following Table 5.4 all the stations used for measuring the total precipitation and the temperature variables are reported, together with the consecutive registration years (Y_i) and the elevation at which are located.

N	COD	Name	Y_i	Elevation [m asl]	Altitude range	Mountain areas	Aspect
1	BRACC	Branzi Caserma Carabinieri	18	830	hilly 	Orobie Sud OS	SE
2	CARCA	Carona Carisole	26	1954	subalpine 	Orobie Sud OS	W
3	EDOPA	Edolo Pantano d' Avio	26	2108	alpine 	Adamello Ad	N
4	APR	Aprica	26	1950	subalpine 	Orobie Nord ON	N
5	CIVAO	Chiesa in Valmalenco Alpe dell' Oro	30	2040	alpine 	Retiche Occidentali RO	S
6	CIVFB	Chiesa in Valmalenco Funivia Bernina	30	2014	alpine 	Retiche Occidentali RO	W
7	GEAPE	Gerola Alta Pescegallo	26	1875	subalpine 	Orobie Nord ON	NW
8	GRODF	Grosio Diga Fusino	19	1220	mountain 	Retiche Occidentali RO	E
9	LANCM	Lanzada Campo Moro	29	1970	subalpine 	Retiche Occidentali RO	NW
10	LANPA	Lanzada Palù	26	2151	alpine 	Retiche Occidentali RO	NE
11	LIVLV	Livigno La Vallaccia	26	2660	alpine 	Livigno Li	N
12	VDSAR	Valdisotto Arginone	15	1050	mountain 	Alta Valtellina AV	NE
13	VDSOC	Valdisotto Oga S. Colombano	26	2300	alpine 	Alta Valtellina AV	NW
14	VBOBA	Valbondione Barbellino	25	1850	subalpine 	Orobie Sud OS	W
15	BORBO	Bormio 2000	25	2010	alpine 	Alta Valtellina AV	NW
16	LANCM	Lanzada Campo Moro	25	1970	subalpine 	Retiche Occidentali RO	SE
17	VDDCA	Valdidentro Cancano	25	1950	subalpine 	Alta Valtellina AV	NE
18	CAR	Carona	25	1840	subalpine 	Orobie Sud OS	S
19	CEVLA	Cevo Lago d'Arno	24	1830	subalpine 	Adamello Ad	W
20	LIVSR	Livigno S. Rocco	25	1875	subalpine 	Livigno Li	SE
21	VBOLI	Valbondione Lizzola	23	1490	mountain 	Orobie Sud OS	NE
22	MAD	Madesimo	25	1530	subalpine 	Alpi Valchiavennasch Va	E
23	MADMA	Madesimo Mater	25	1860	subalpine 	Alpi Valchiavennasch Va	NW
24	BELSP	Bellaggio San Primo	25	1070	hilly 	Prealpi Lariane PL	W
25	VFUPL	Valfurva Plaghera	25	2240	alpine 	Alta Valtellina AV	N
26	VFUCA	Valfurva S. Caterina 2	20	1735	subalpine 	Alta Valtellina AV	NW
27	GEATR	Gerola AltaTrona	25	1810	subalpine 	Orobie Nord ON	NW
28	GEAVG	Gerola Alta Valgerola	25	1840	subalpine 	Orobie Nord ON	N

Table 5.3: Snow gauges investigated

TEMPERATURE MEASUREMENTS STATIONS:				PRECIPITATION MEASUREMENTS STATIONS:			
N	Name	Elev. [m asl]	Yi	N	Name	Yi	Elev. [m asl]
1	Branzi Caserma carabinieri	830	18	1	Branzi Caserma Carabinieri	18	830
2	Edolo Pantano d'Avio	2108	26	2	Edolo Pantano d'Avio	26	2108
3	Aprica	1950	26	3	Aprica	26	1950
4	Chiesa in Valmalenco Funivia al Bernina	2014	17	4	Chiesa in Valmalenco Funivia Bernina	30	2014
5	Gerola Alta Pescegallo	1875	25	5	Gerola Alta Pescegallo	26	1875
6	Grosio diga Fusino	1220	19	6	Grosio Diga Fusino	19	1220
7	Lanzada Palu'	2151	20	7	Livigno La Vallaccia	26	2660
8	Livigno la Vallaccia	2660	25	8	Valfurva S. Caterina 2	20	1735
9	Valdisotto Arignone	1050	13	9	Valbondione Barbellino	25	1850
10	Valdisotto Oga	2300	25	10	Madesimo	25	1530
11	Bormio ponte sul Frodolfo	1250	19	11	Valdisotto Oga S. Colombano	26	2300
12	Foppolo	1682	16				
14	Cavargna	1100	16				
15	Valfurva Santa Caterina	1735	19				
16	Valmasino San Martino	943	16				
17	Cevo	1128	17				

Table 5.4: Temperature and precipitation gauges investigated.

6. PROPOSED TECHNIQUE FOR THE TREND ANALYSIS:

After the acquisition of the useful dataset and the computation of the investigated variables as described in the previous chapter, the presence of trend in the historical series is executed thanks to the software Matlab (The MathWorks Inc., 2018), which allows to quickly process great amount of data. In Matlab environments, a function able to perform the following statistical techniques (Bocchiola D, 2007) is created:

- Linear regression vs time.
- Moving window average vs long term average.
- Mann – Kendall statistic test.

This function, to detect the presence of trend and the relative significance level, is applied at the historical series of the assessed snow variables in the following way:

- Single sites annual analysis
- Homogeneous group annual analysis
- Seasonal analysis

These three different approaches allow not only to investigate the non-stationarity of the snow variables historical series, but also to investigate the presence of any possible behaviors that can be re-deducted to a certain factor like the elevation, the location, or the seasonality.

6.1 Statistical tools for trend assessment:

In this project, the linear regression with its significance value, the Moving window average compared to the long-term average and the statistics Mann – Kendall test with its significance value is used to evaluate the behavior of the studied snow variables in the last three decades, as well as the evolutionary behavior of the temperature and the total precipitations in the mentioned time period.

The use of these statistics techniques as effective tools for trend analysis of climatological variables is documented in scientific articles like (Matiu M, 2021). In (Bocchiola D, 2007), these techniques have been successfully applied to the historical series of HS and SCD for the Adamello glacierized area, located inside the case study area of this project.

6.1.1 Linear regression vs time:

The linear regression is the simplest methods for data interpolation, and consists in the use of a 1st order function as (Eq. 8):

$$y = mx + b \quad (8)$$

Where m is the angular coefficient of the regression and is representative of the linear trend.

Significance of the regression is given using P -value with a level of $\alpha = 5\%$ (Bocchiola D, 2007).

Notice that multiple trends could be detected in time series analysis, however, here focus is cast upon evaluation of the general trend, also in view of the relative shortness of the series, and therefore single regression analysis is carried out.

6.1.2 Moving window average vs long term average:

A moving window average (MW) over a 10-year period is calculated (Bocchiola D, 2007), in view of the discrete temporal duration of the available series. Applying the window at a sub-sample of 10-years data, the resulting value corresponds to the last year of the window and all the data have the same weight.

This technique should be called “nowcast moving average” and allows comparison with the results of Mann-Kendall test, taking all the previous data available at a given time. The MW average is then compared with the long-term average (LT), which is the average conducted on the whole sample (considering the entire registration period of the stations).

The MW average allows to smooth out short-term variability to identify better the overall behavior of the data samples. The fluctuations of the MW are then compared with the confidence interval of the LT , with a significance level $\alpha = 5\%$. The confidence interval is taken under the hypothesis of stationarity.

The results of the MW and LT average, together with the relative confidence limits on LT , are plotted and interpreted visually, considering that fluctuations of MW within the confidence interval should be charge to the year-to-year sampling variability. In case the MW settles outside the confidence limits, the series may be affected by a non-stationarity, either monotonic or periodic.

The confidence interval is defined as (Eq. 9):

$$\mu - z_{\alpha/2} * \frac{\sigma}{\sqrt{n}} \leq X \leq \mu + z_{\alpha/2} * \frac{\sigma}{\sqrt{n}} \quad (9)$$

With μ and σ LT average and standard deviation from the whole sample and n moving window size (10 year). X is the MW average and $z_{\alpha/2}$ is the quantile of the normal standard distribution with probability: $1 - \alpha/2$.

6.1.3 Mann-Kendall statistical test:

Mann–Kendall statistic test (MK) is widely adopted to assess significant trends in hydrometeorological time series (Matiu M, 2021). This is a non-parametric test, thus being less sensitive to extreme sample values and independent from hypothesis about the nature of the trend, either linear or not. For this reason, the

test can be considered somewhat complementary to the linear regression test, as also confirmed by the obtained results.

The MK test is based on the acceptance or rejections of the following null hypothesis:

Ho = absence of significative trend in the assessed series.

Let consider a sample of a random variable:

$$HS_y; y = 1,2 \dots, Y$$

With Y length of the series in years.

Let p_y denote the number of elements in the sample with $j > y$ and $HS_j < HS_y$, while τ indicates (Eq. 10):

$$\tau = \sum_{y=1}^Y p_y \quad (10)$$

One can show that τ is asymptotically normally distributed with the mean and standard deviation (Eq. 11):

$$\mu(\tau) = \sqrt{Y(Y-1)(2y+5)/72} \quad (11)$$

The normalized variable $\mu(\tau)$ has a standard normal distribution, so one can build the associated confidence interval.

The MK test verifies the H_0 null hypothesis of the time series by ensuring that the normalized variable $\mu(\tau)$ is included within the confidence interval, for a given significance level here taken at $\alpha = 5\%$.

6.2 Single sites analysis vs homogeneous group analysis:

To understand the influence that some geomorphological parameters could have on the SV variability and detect common path between individual stations the trend assessment techniques are applied to the SV historical series of:

- Single stations
- Stations grouped based in the homogeneous group defined in the chapter 4.3.

The single stations analysis consists in the trend assessments of the single site historical series. The obtained results lead to considerations about the general behavior of the assessed SV by looking at the trend of each gauge.

To group the time series based on the geomorphological characteristics of the measuring stations, first, the individual SV annual observations are normalized for a descriptive index value of the series.

In (Daniele Bocchiola, 2006) the sample average is proposed as a valid index value for the regionalization of H3D observations, testing its effectiveness for an area that coincides with that of the present work. Using the sample average is possible to pass from the SV to standard variables X_{SV} (Eq. 12), comparable to each other and independent from the single site.

$$X_{SV} = \frac{x_i}{\mu} \quad (12)$$

Where x_i are the individual observation and μ the sample average $\mu = \frac{\sum_{i=1}^{Y_i} X_i}{Y_i}$; with Y_i years of registrations.

Once the X_{SV} historical series are obtained the individual annual values of stations belonging to the same group have been averaged, obtaining X_{SV} series for each homogeneous group.

It is important to notice that the trend assessment applied on stations grouped basing on the aspect, did not lead to consistent results. This is probably due to the difference in elevation, that is considered a predominant factor, among stations of each aspect homogeneous group. Based on this evidence, the presentations of the results of this group will be omitted.

Another important observation concerns homogeneous groups based on altitudes. The analysis of these is carried out in a combined way, considering the contour bands (hilly and alpine) individually and the other combined. In this way it is possible to have a larger number of stations for each band and to overcome the problem that net boundaries do not fit well with the analysis carried out in this work.

It is possible to summarize the homogeneous groups of stations based on the altitude belts as follow:

- Hilly
- Hilly + Mountain
- Mountain + Subalpine
- Subalpine + Alpine
- Alpine

6.3 Annual vs seasonal analysis:

For the computation of the annual SV, the snow year starting on the August 1st, ending on the July 31st and named through the calendar year in which it begins.

Usually by snow year is meant the period of 365 days (or 366 if they affect a leap civil year) that begins with the first snowfall after the hot summer period, a definition that allows a certain freedom of interpretation, depending on each location. The choice of this period is due to the desire of consider a general snow year for the entire study area, which has stations at high altitudes (i.e., Livigno La

Vallaccia, 2660 m) in which the first snowfall of the season can take place already at the end of August.

The use of annual SV, however, does not allow to appreciate the presence of any paths of variability common to a given season, which is considered here an additional parameter potentially influencing the temporal evolution of the considered variables.

Since there is a significantly low number of snowfalls in the summer season, which do not constitute a permanent snow supply to the ground and affect only the highest altitudes, this season is omitted from the analysis, extending the period of autumn and spring to take account of late or early snowfall.

Based on this claim, the trend assessment is carried out also on the most representative SV computed seasonally, considering the following period:

- Autumn: September 1st – November 30th
- Winter: December 1st – February 28/29th
- Spring: March 1st – June 31st

Finally, the linear regression angular coefficients for each station in each season are visually compared in a scatter plot.

6.4 Correlation between SV and NAO winter index:

Based on the statements reported in the chapter 3.3 concerning the effects of the NAO teleconnection fluctuation on the case study area snowiness conditions it is considered interesting to verify the correlation and the relative linear regression between the NAO winter index and the historical series of some SV, grouped by altitude belts with the technique described above.

The monthly NAO index historical series comes from (National-weather-service, 2018). This service obtain the teleconnection patterns with an RCPA technique applied to monthly standardized 500 mb height anomalies obtained from the CDAS in the analysis region 20° N – 90°N. The monthly NAO indices were then averaged annually in December and February, as proposed in (Yoojin Kim, 2012), obtaining the winter NAO index.

The correlation is verified by Spearman's R correlation index (ρ_s), which describes the goodness of description by a monotonous function of the relationship between two variables. The significance of the correlation, as well as the significance of the linear regression are verified through the P value with threshold level at 95%.

7. PAST YEAR TREND ASSESSMENT:

In the present section the results of the trend analysis are reported without interpretations, both for the single sites analysis and the homogeneous group ones, starting from the SV and ending with the trend assessment on temperature variables and precipitation.

Once the statistical techniques presented in the previous chapter have been applied, the results have been plotted and reported in summary tables. These tables are omitted from this presentation for brevity, but may be displayed in the following annex:

- Annex 1: Past year trend assessment results.

Note that a trend is considered statistically significant if linear regression or the Mann-kendall test result is significant. In any case it has been noted that the results of the MK test and the P-value of the linear regression agree in almost all cases.

Regarding the analysis by homogeneous groups, the results are presented also in sketch, For their interpretation reference can be made to the following legend.

LEGEND:	
Sketchs:	
Positive trend	yellow
Positive significant trend	orange
Negative trend	light blue
Negative significant trend	blue
No data	white

Figure 7.1: Legend for the homogeneous group results:

It is possible to note that the analysis by altitude bands was performed in a combined way (as described in the previous chapter), and therefore the different colors do not correspond to the boundaries of the bands.

A personal interpretation of the results has been performed only on the MW vs LT average, for which it is necessary to visualize one by one the graphs obtained and verify the eventual leakage of the moving average from the confidence limits on the long-term average, indicative of the non-stationary nature of the data.

7.1 Snow variable results:

7.1.1 HS average:

The single stations analysis shows 17 positive trends of which 7 statistically significant and 11 negatives, of which only one (Bellagio San Primo) significant. The increase of this SV is often more pronounced since the early 2000s with a clearly under average period in the 90s, as evidenced for example by the MW average of some station (as for example Aprica). It is important to note that no negative trend is significant.

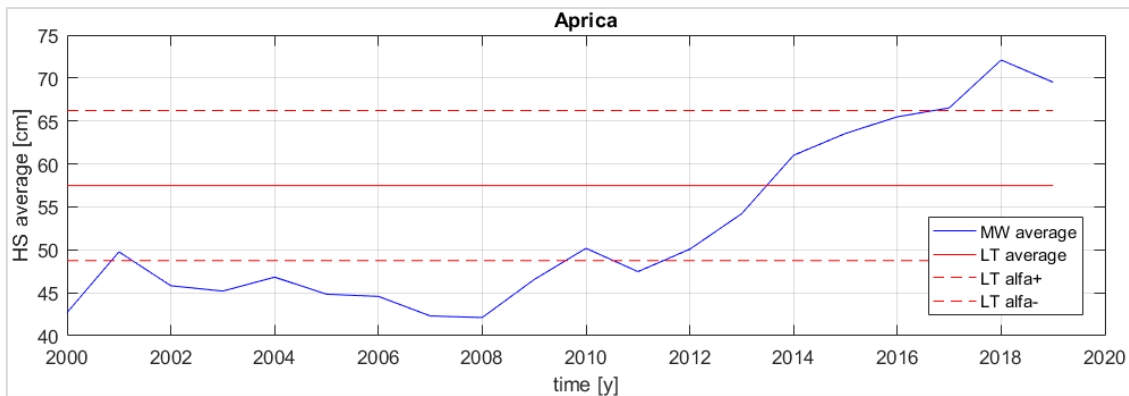


Figure 7.2: Example of a station with positive significant trend.

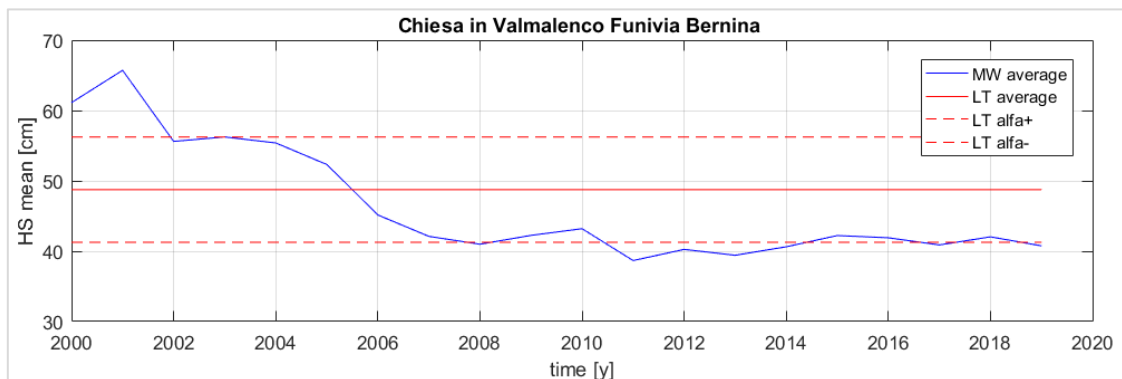


Figure 7.3: Example of a station with negative trend (non-significant).

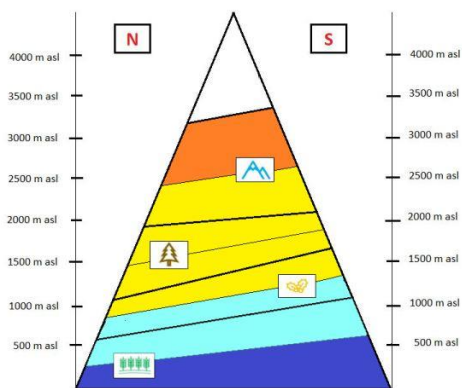


Figure 7.4: HS_av altitude belts results.

As regards the analysis based on homogeneous groups there are significant negative trend in the lower belts (Hilly) and significant positive trend in the upper ones (Alpine). In the middle belts there is no significance, but the trend is negative in hilly + mountain belt and positive in the upper ones.

The variable significantly decreases only in Prealpi Lariane. In the others mountain areas a negative non-significant trend is shown in Valchiavenna and Orobie Sud, and a non significant positive trend in the remaining.

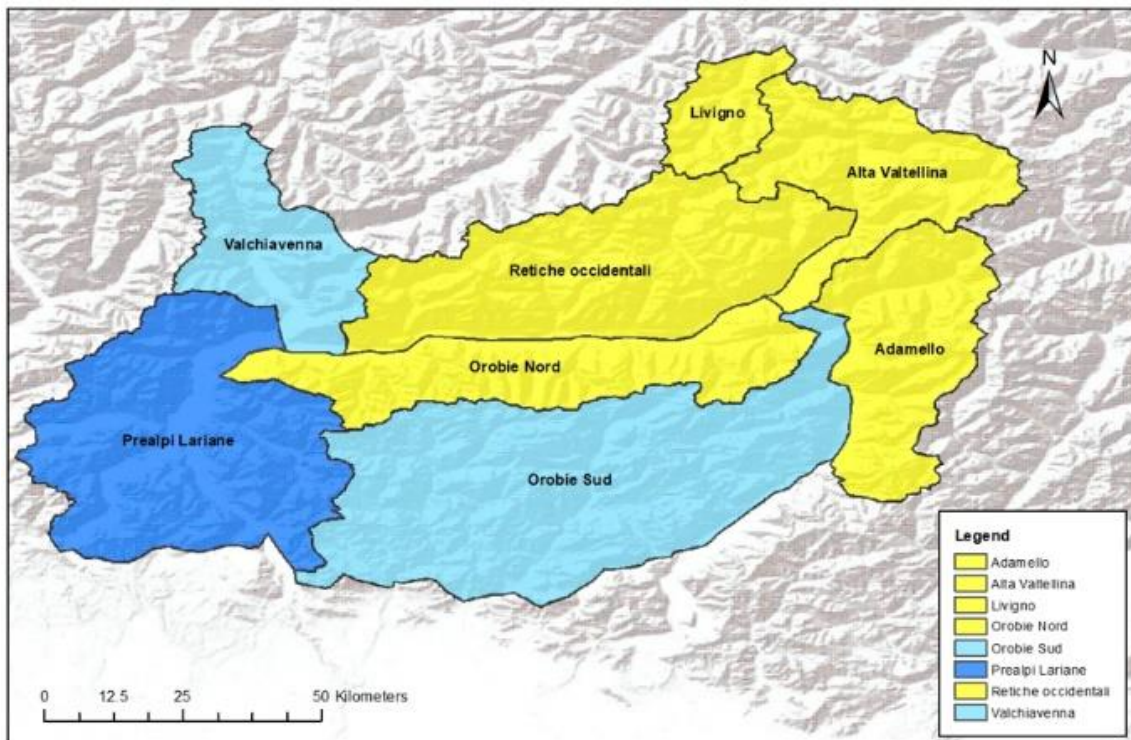


Figure 7.5: *Hs_av* mountain areas result.

The seasonal analysis shows in Autumn and Winter more positive trends than the annual variable, while in spring there are more negative trends. The statistical significance is little present, but it is possible to notice visually that there is a more marked reduction of snowpack average depth in the spring period, evidenced also by some stations for which the variable increases in Autumn and Winter times.

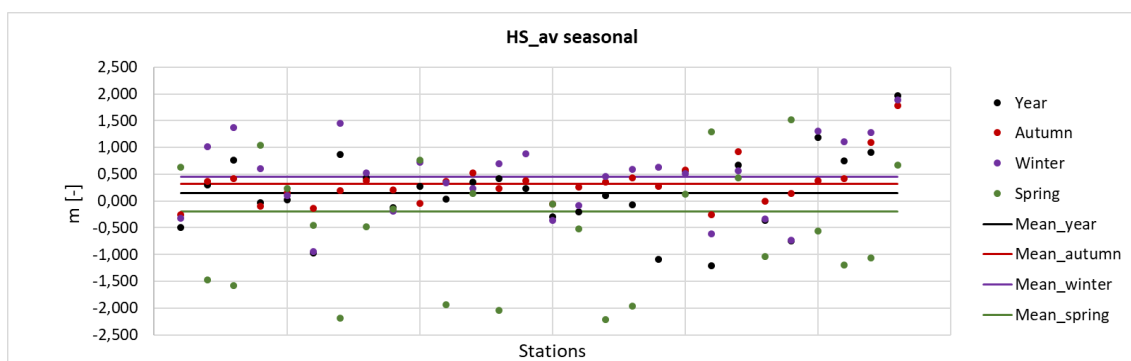


Figure 7.6: Annual vs seasonal analysis.

7.1.2 SCD(n):

This general acronym is here used meaning the annual snow cover durations in days computed with different thresholds value of the snowpack depth HS. The days with $HS > 5$ cm (SCD₅) is considered the standard variables so as is more representative (Bocchiola D, 2007), nevertheless the analysis is also carried out on the same variable computed with threshold HS value of 1 cm, 20 cm and 50 cm.

For SCD₅ the single stations analysis shows 18 negative trends and 10 positives, of which 4 statistically significant both negative.

The analysis carried out on SCD₁, SCD₂₀ and SCD₅₀ allows to confirm the results of SCD₅, with majority of negative trends and significance only on them.

Looking at the results you can observe that the use of $HS = 1$ cm as threshold value for the SCD computations leads to some disturbances for some stations, highlighted by the presence of snow days at low altitude in the summer period. This is probably due to external interferences such as grass growth. It is also important to note that $HS = 1$ cm is a too sensitive value since would be enough frost formation on the ground to record snow cover.

The number of stations with a positive trend is lower for SCD₅₀, exemplifying the fact that in several stations there is an increase in snow cover duration but with a shallower snowpack.

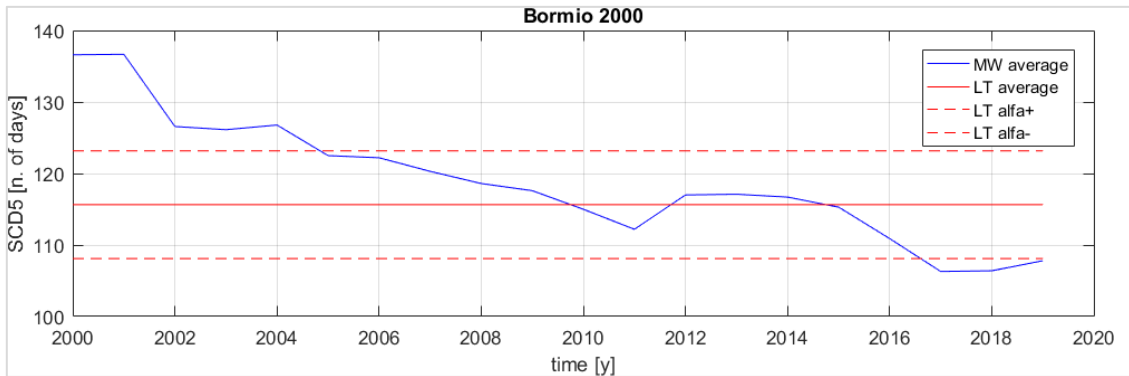


Figure 7.7: Example of a station with negative significant trend.

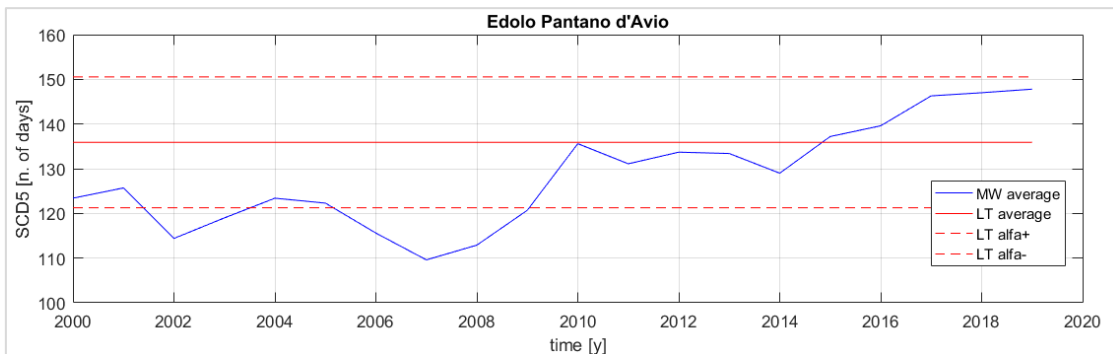


Figure 7.8: Example of station with positive non-significant trend.

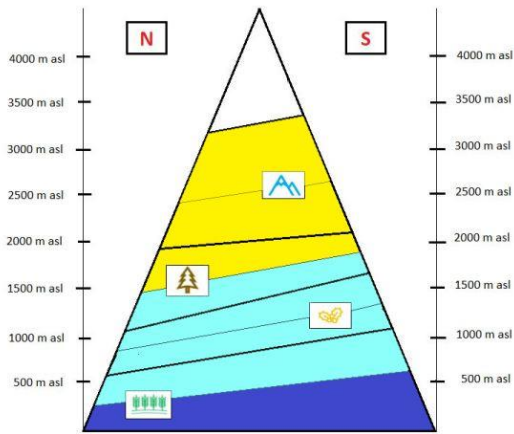


Figure 7.9: SCD5 altitude belts results

With regards to the analysis for homogeneous groups there is a statistically significant decrease in the lowest belt (Hilly) and non-significant in Hilly + Mountain and Mountain + Subalpine, whereas in the upper bands there is a non-significant increase. Snow cover duration significantly decrease in Adamello and Prealpi Lariane.

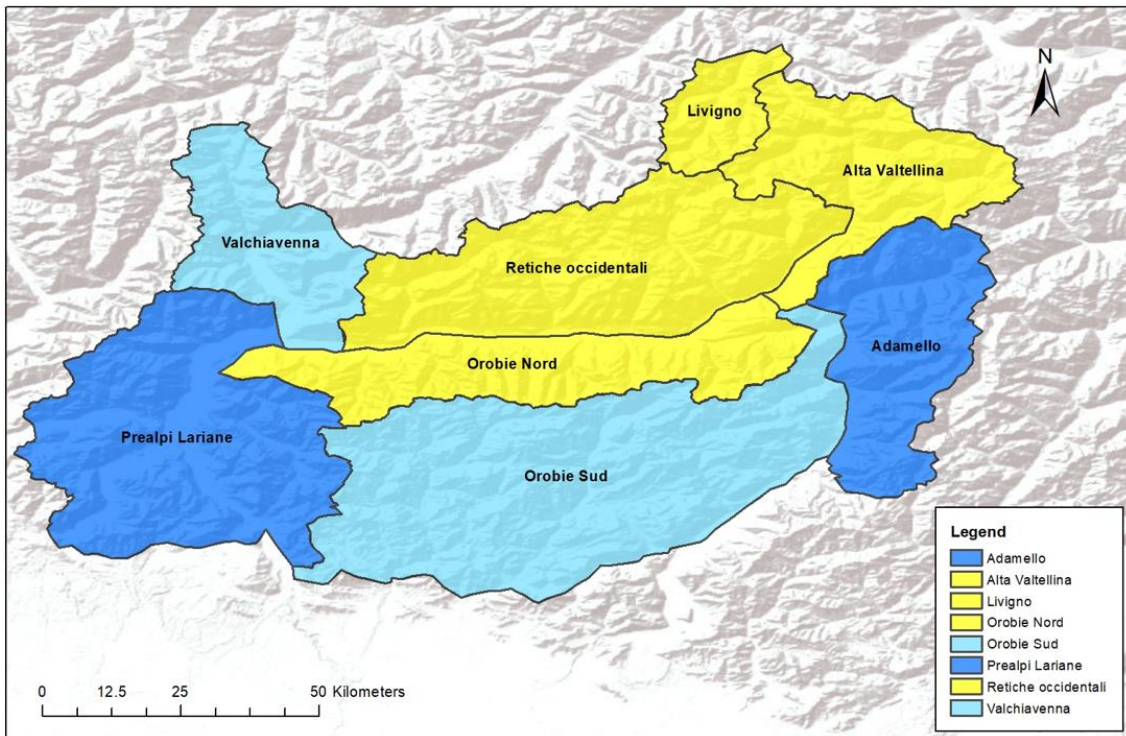


Figure 7.10: SCD5 mountain areas results.

7.1.3 SD:

This variable represent the number of days in the year with snowfall, approximated from HN (1 day snowfall) with a threshold value of 5 cm.

The single stations analysis do not show a particular prevailing nature of the trends (12 positives and 16 negatives, without significance).

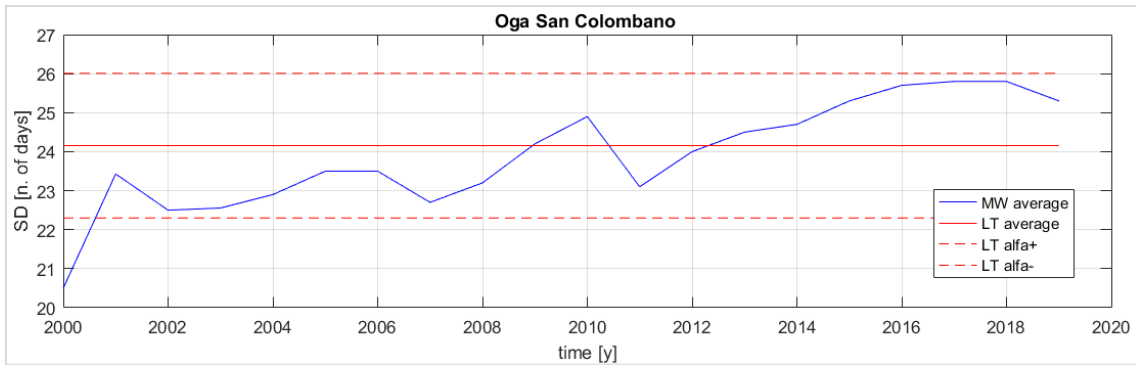


Figure 7.11: Example of a station with positive trend.

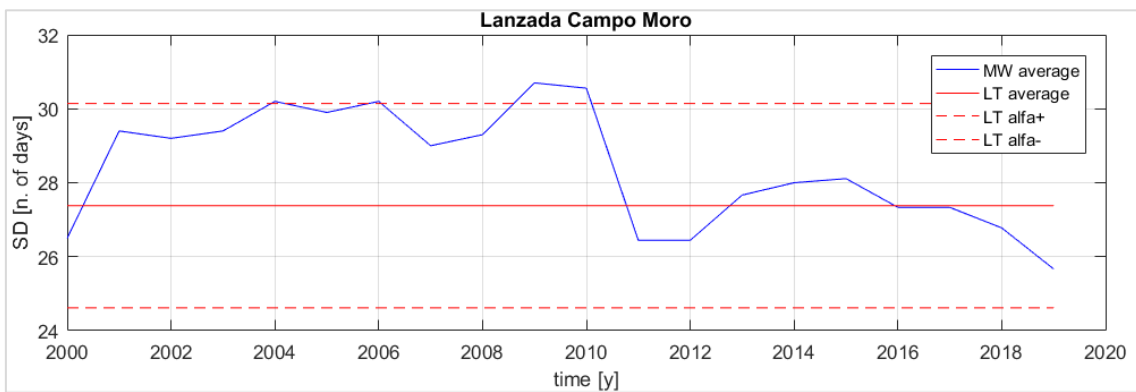


Figure 7.12: Example of a station with negative trend.

The results of the seasonal analysis seems to be more interesting since a clear decrease in the snowy days in the autumn season is detected, compensated by moderate growth in winter and spring.

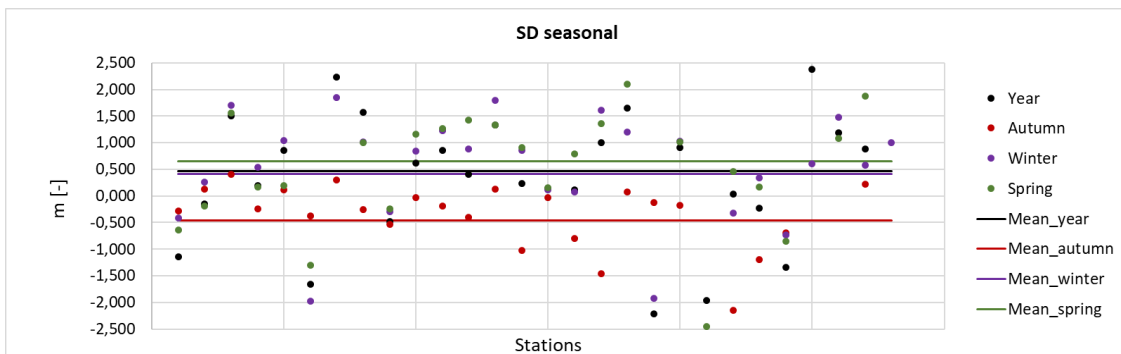
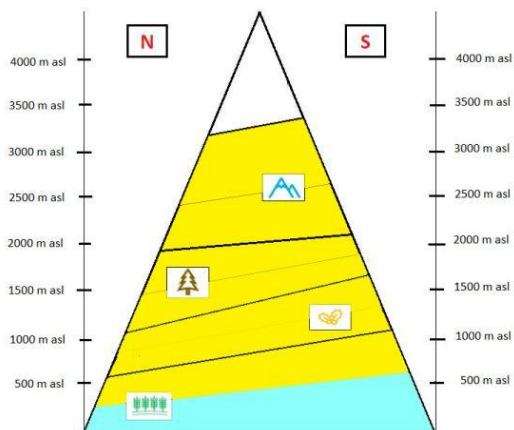


Figure 7.13: SD seasonal analysis.



As you can see in Figure 7.14 and Figure 7.15 even the analysis based on homogeneous groups doesn't lead to clear results since no significance is detected on the trends.

Figure 7.14: SD altitude belt results.

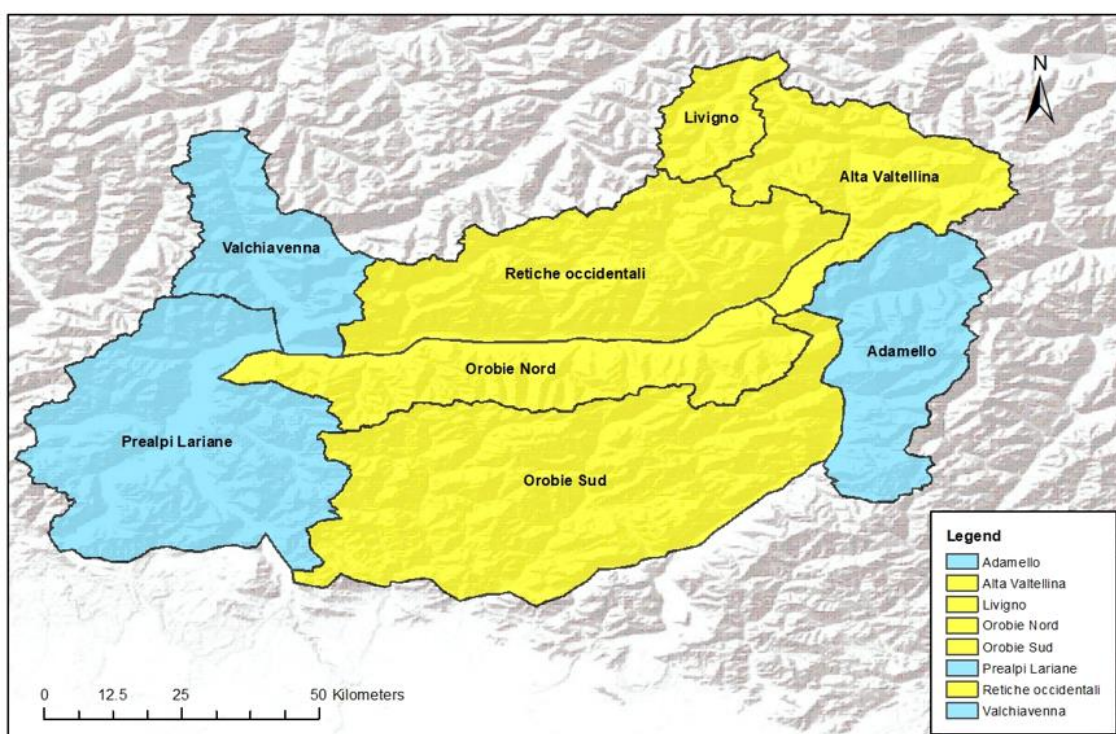


Figure 7.15: SD mountain areas results.

7.1.4 H(n)D:

With this acronym is intended the maximum annual n – days snowfall, approximated from the HS data as 1 day, 2 days and 3 days snow depth variations.

First, looking at Figure 7.16, it is possible to notice that the nature of the trends of these three variables is similar as well as the value of the trends. This allows to affirm that there aren't preferential behaviors of one of the three variables, and that in example, stations that shows a decrease of HN also shows a decrease of H2D and H3D, with similar value.

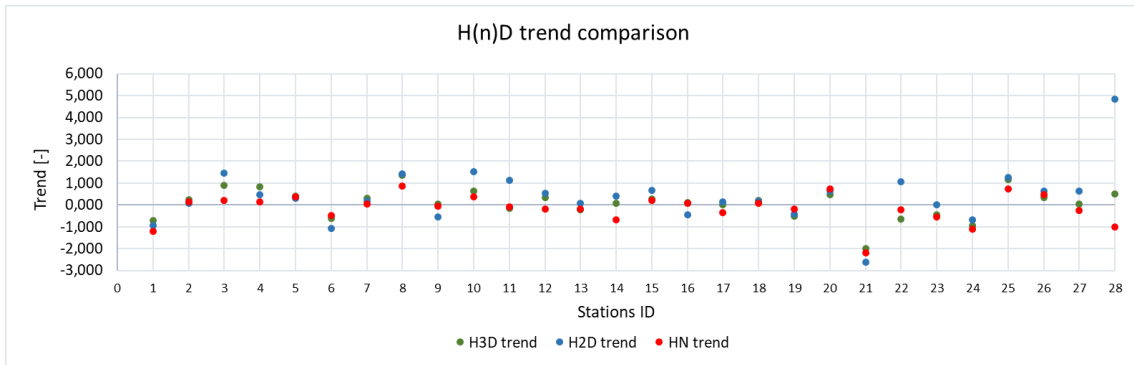


Figure 7.16: Comparison among $H(n)D$ trend [with $n=1,2,3$]

The trend significance is present only on few stations (the same for H2D and H3D) on two positive trends while for HN significance is detected for one positive and one negative trend.

In general, most of the trends are positive but not significant for the first two variables (18 for H3D and 20 for H2D) while for maximum daily precipitation the non-significant trends are 14 positive and 12 negative.

The low presence of significant results is typical of the maximum values, such as those of these variables, which are rather unstable.

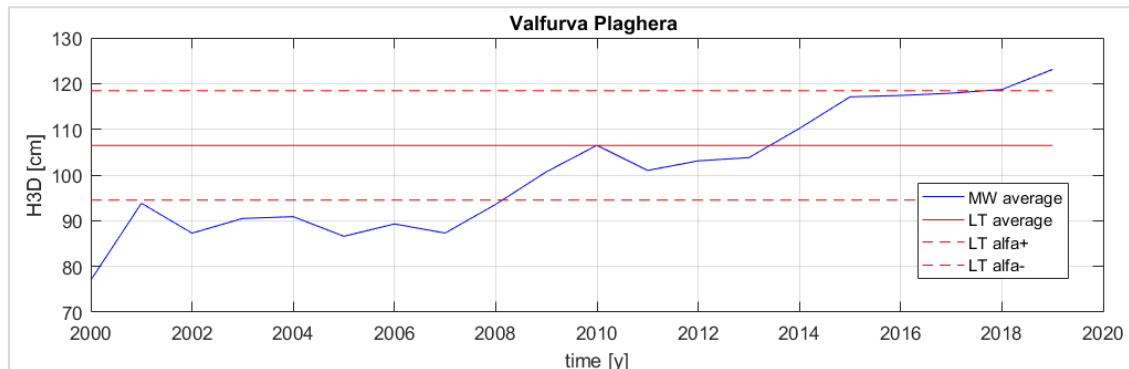


Figure 7.17: Example of a station with positive significative trend.

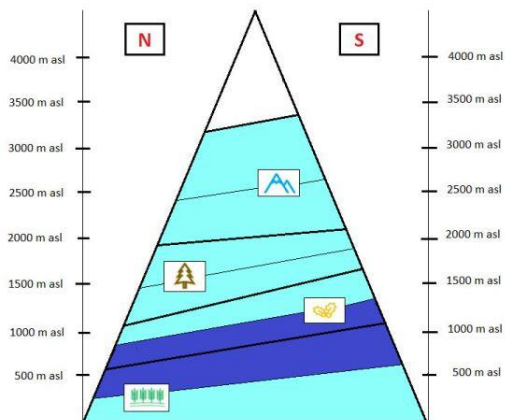


Figure 7.18: HN mountain areas results.

As regard the homogenous group analysis the only significant result is a negative trend in the hilly + mountain belt for HN variable, with negative and non-significant trends in the others elevation ranges. The analysis based on homogeneous mountain areas and the ones based on altitude belts for H2D and H3D (which sketches are not reported for brevity) show no significant results.

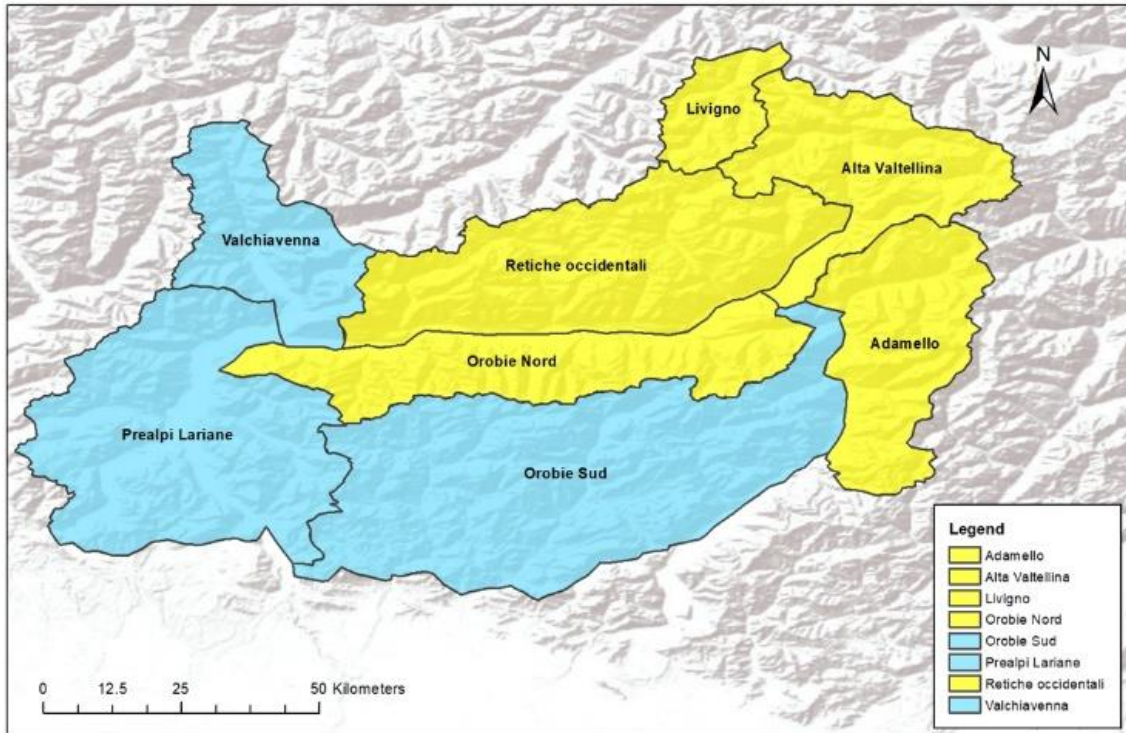


Figure 7.19: H3D and HN homogeneous areas results.

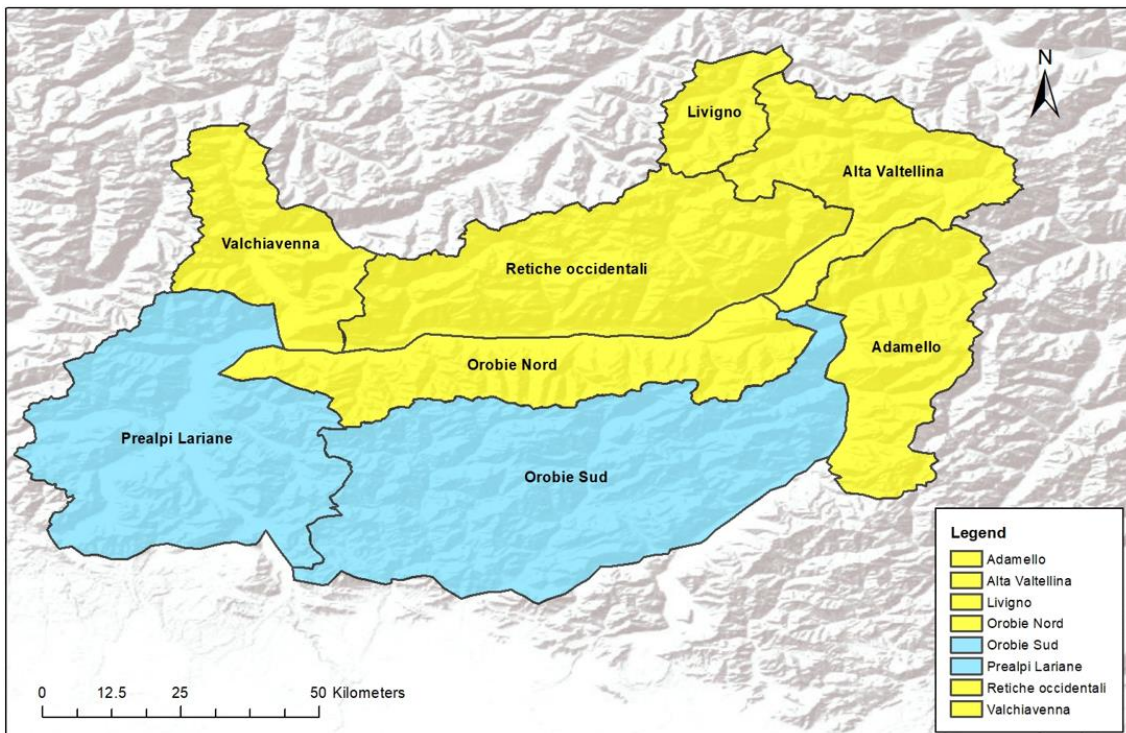


Figure 7.20: H2D homogeneous areas results.

It is important to note that despite the analysis for individual stations showed many positive trends the analysis on the same grouped in altitude belts leads to negative trends on all bands. This result, apparently contradictory, is due to the non-significance of the trends, which does not allow to affirm with certainty the behavior of the historical series.

Even the results of the seasonal analysis can be considered homogenous for all the three variables in question. In autumn time the trends are mostly negative, in opposition with the annual behavior and with a net decrease especially in the last years, as evidenced in the Figure 7.22. In winter and spring seasons the trends are in line with the annual ones, with more significance in spring.

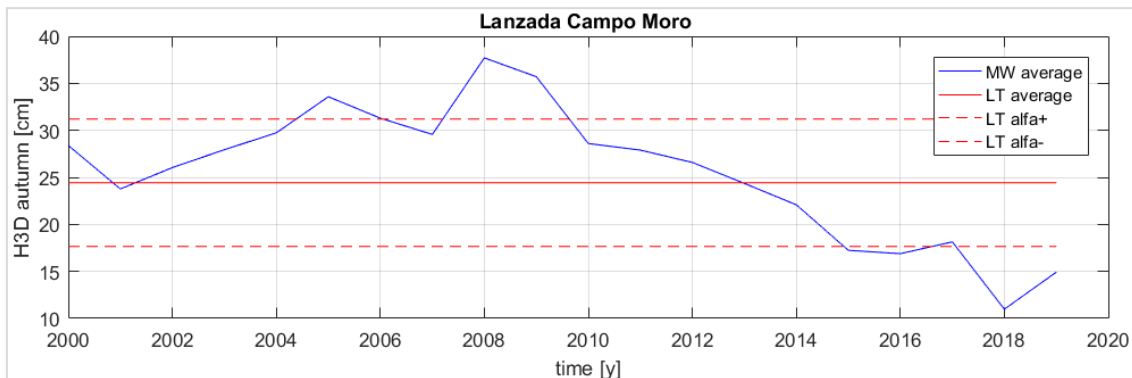


Figure 7.21: Example of a station with significant negative trend in autumn.

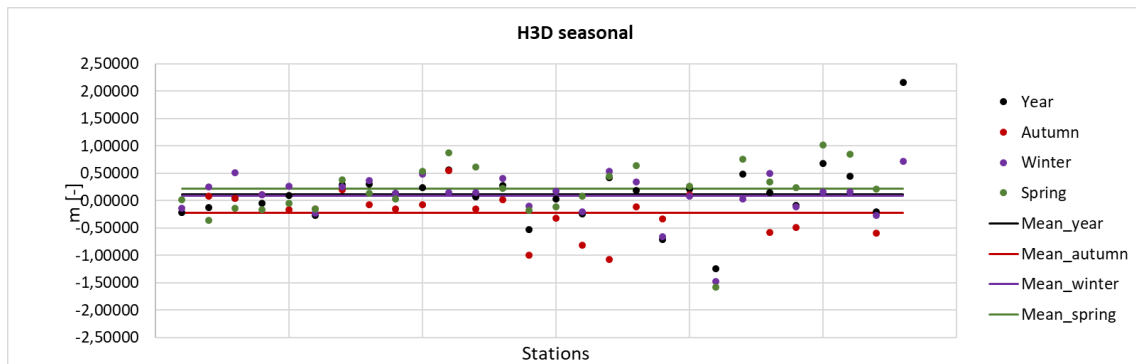


Figure 7.22: H3D seasonal analysis

7.1.5 HN average

This variable is the average annual 1-day snowfall computed from HS measurement.

The single site analysis shows only 1 significant negative trend (Valbondione Lizzola), visible in Figure 7.23. The others trend are 9 negatives and 18 positives but with no significance.

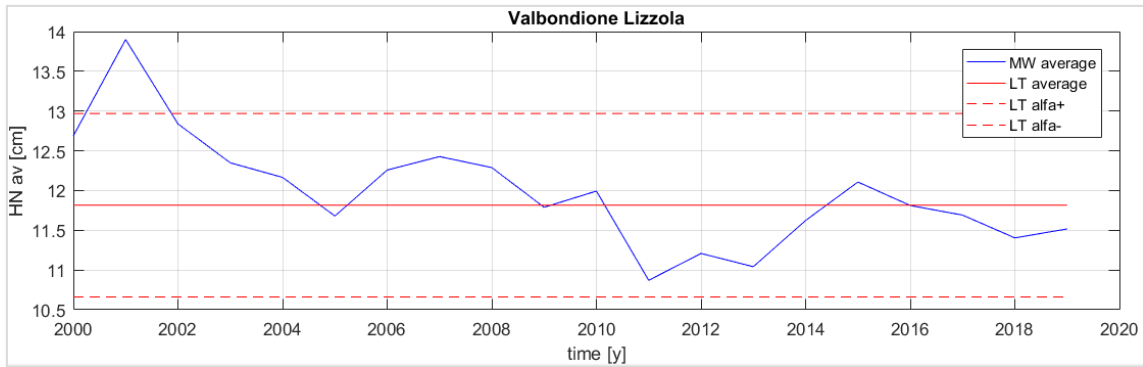


Figure 7.23: Station with significant negative trend.

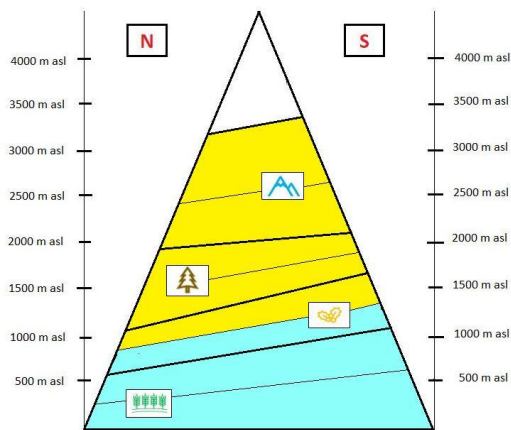


Figure 7.24: HN_av altitude belts results.

As you can see in Figure 7.24 and in Figure 7.25 the analysis based on homogeneous group of stations lead to non-significant results.

Negatives trends are detected in the lower altitude belts (Hilly and Hilly + Mountain) and in Prealpi Lariane, Valchiavenna and Orobie Sud.

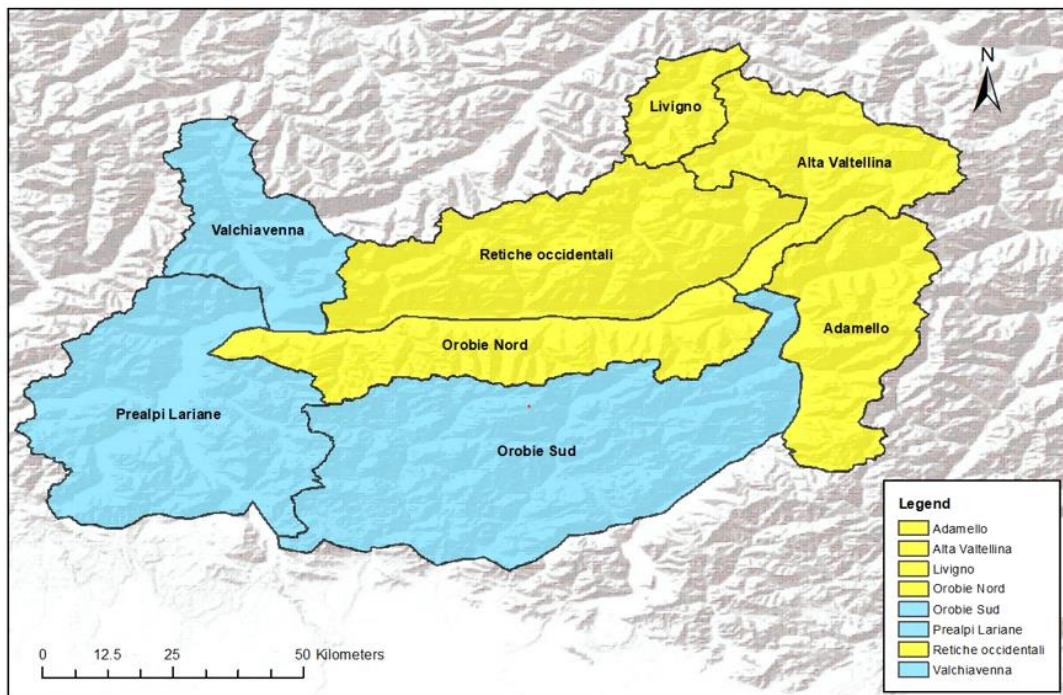


Figure 7.25: HN_av homogeneous areas results.

The seasonal analysis shows a greater decrease of the average daily snowfall in autumn, while in winter and spring there are trends in line with the annual ones (Figure 7.26).

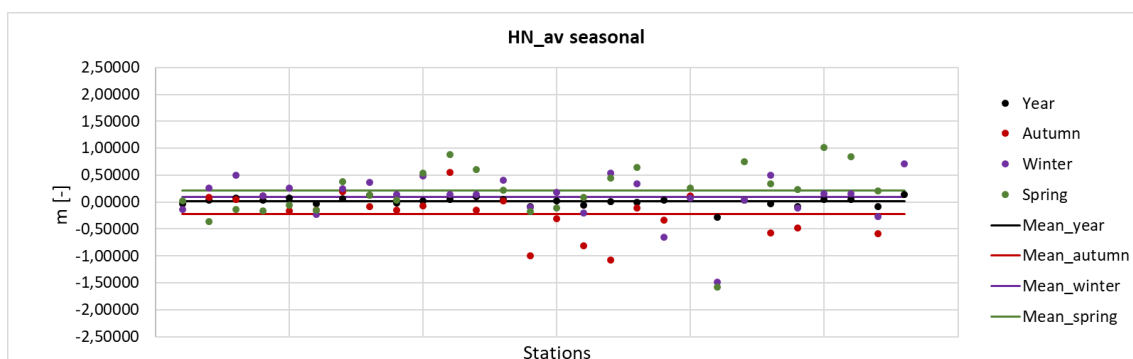


Figure 7.26: HN_av seasonal analysis results.

7.2 Precipitation and temperature results:

As already specified, the trend assessment on total precipitation and temperatures refers to a subset of the 28 stations used for the analysis of trends on snow variables.

For the sake of brevity, the summary tables of the results for each station are not given. For consultation, reference can be made to the previously mentioned “annex 1”.

Regarding temperature analysis, over the last 30 years the average annual temperature has increased. This is shown by the 87,5 % of the considered measurement stations, with significant trends on 62,5 % of these. A similar result is found on the maximum temperatures, which show a significant increase in 47 % of cases, while the minimum temperatures behave less clearly with majority of no significant positive trends and significance only for one negative trend, in Chiesa Valmalenco Funiva Bernina station.

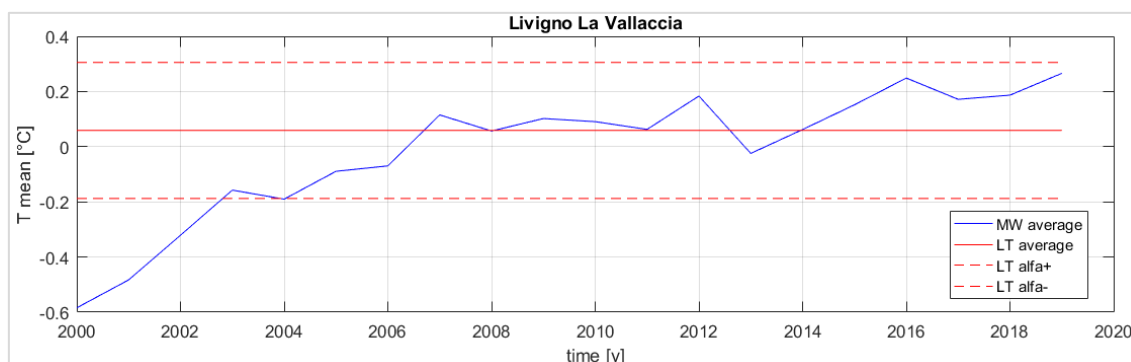


Figure 7.27: Positive significant T mean trend in Livigno la Vallaccia.

Due to the significance of the results on the annual average temperature it is possible to estimate the value of the trend, which lead to an average increase of 1,5 °C in the last 30 years.

The analysis on total precipitation shows a significant increase of this variable for 4 stations (36% of the sample of investigated stations). For the others stations the trend is non-significant, positive for 5 stations and negative for 2.

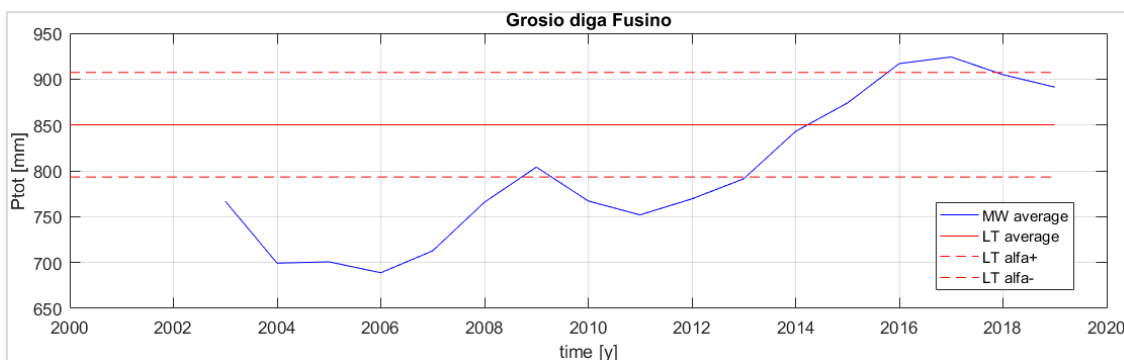


Figure 7.28: Example of station with positive significant trend on Ptot.

7.3 Correlation between SV and NAO index:

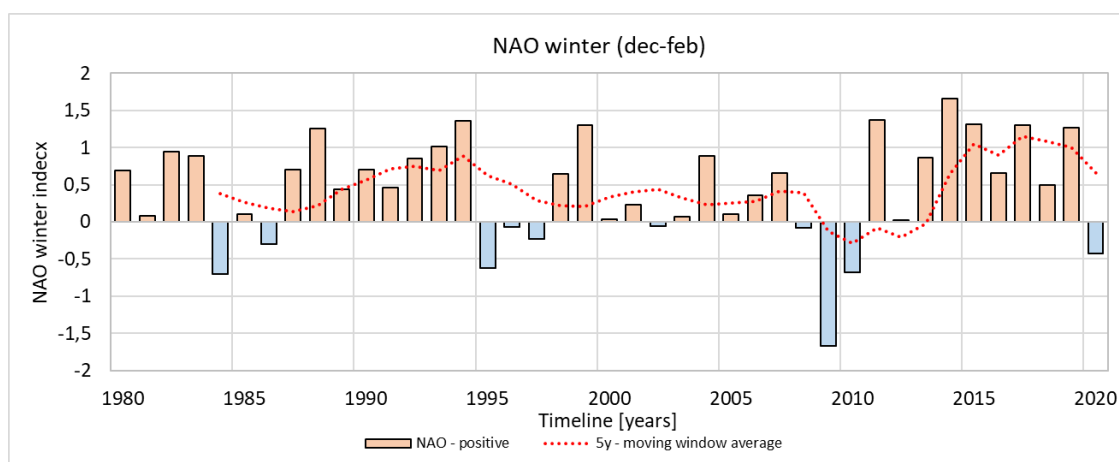


Figure 7.29: Variability of the NAO winter index since 1980.

Observing the trend of the NAO teleconnection index in winter during the period under study, it is possible to observe its high variability, unbalanced towards the NAO+ phases that we know bring stable weather conditions to the Lombard Alps (see Chapter 3.3.1). Looking at the graphic it is possible to highlight two negative peaks, one more marked in 2008 – 2011 and one less marked in 1995 – 1997.

It is important to mark that all the linear regressions executed on the analyzed variables and NAO winter shows a negative angular coefficient, which determines an inverse relationship (the higher the NAO winter index and the lower the annual value of the variables studied). For the sake of brevity, in addition to the

summary table of the results, only the regression graph of the general snow variable is reported, that is the variable X_{sv} obtained normalizing the SV for the index value and averaging annually between all the stations considered. This variable is considered representative for the whole area under study.

7.3.1 HS average:

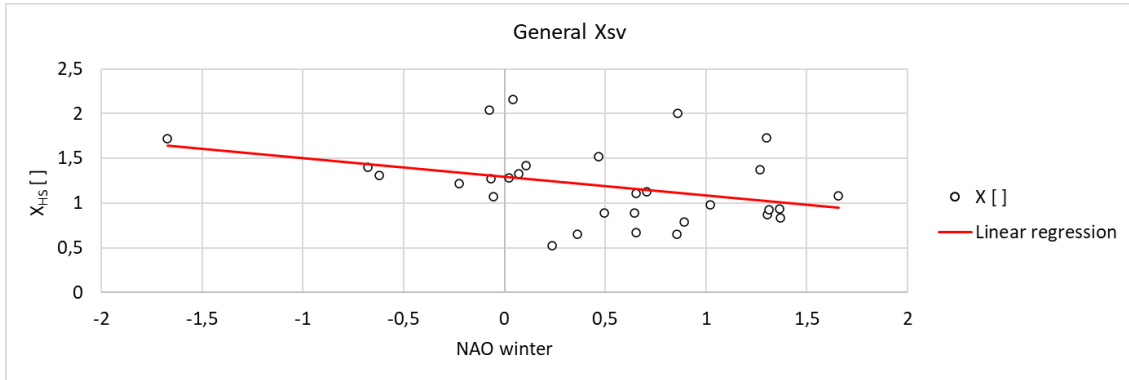


Figure 7.30: Linear regression between HS average and NAO winter.

		Correlation					
		General	Hilly	Hilly-Mountain	Mountain-Subalpine	Subalpine-Alpine	Alpine
ρ_s		-0,3607	-0,2533	-0,1576	-0,3765	-0,3330	-0,3585
P value		✓ 0,050	✗ 0,311	✗ 0,452	✓ 0,040	✗ 0,072	✓ 0,052
		Linear regression					
		General	Hilly	Hilly-Mountain	Mountain-Subalpine	Subalpine-Alpine	Alpine
P value		✓ 0,050	✗ 0,311	✗ 0,452	✓ 0,040	✗ 0,072	✓ 0,052

Table 7.1: Summary of the HS average – NAO results for altitude belts.

As one can see both the correlation and the linear regressions are statistically significant for the entire station's dataset. The analysis for single altitude belts shows how the significance is good in the upper belts, particularly in the Mountain - Subalpine (approximately between 1000 and 2000 m asl). In the lower belts there is no significance.

7.3.2 SCD5:

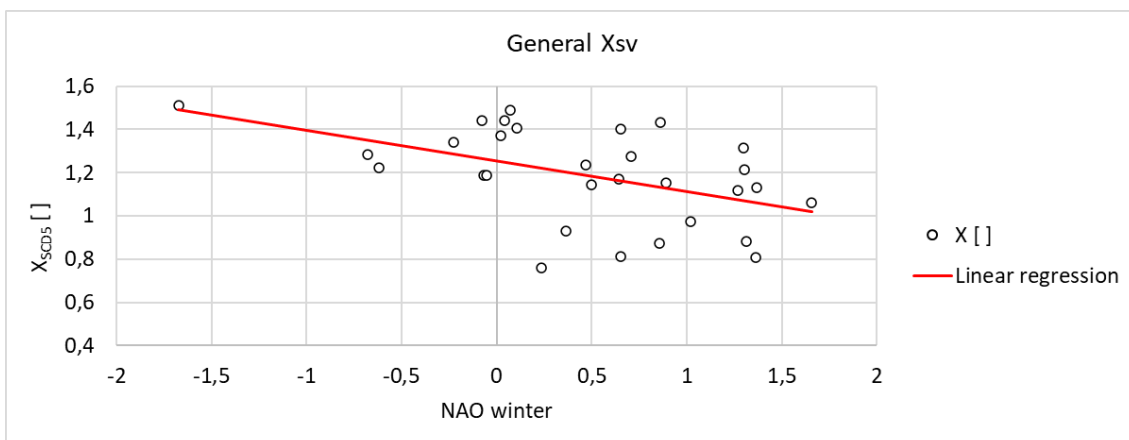


Figure 7.31: Linear regression between SCD5 and NAO winter index.

		Correlation					
		General	Hilly	Hilly-Mountain	Mountain-Subalpine	Subalpine-Alpine	Alpine
ρ_s		-0,4822	-0,2023	-0,2982	-0,4869	-0,5056	-0,4331
P value		✓ 0,007	✗ 0,421	✗ 0,148	✓ 0,006	✓ 0,004	✓ 0,017
		Linear regression					
		General	Hilly	Hilly-Mountain	Mountain-Subalpine	Subalpine-Alpine	Alpine
P value		✓ 0,050	✗ 0,311	✗ 0,452	✓ 0,040	✗ 0,072	✓ 0,052

Table 7.2: Summary of the SCD5 - NAO results for altitude belts.

Both the correlation and the linear regression are significant for the dataset considered entirely. In particular, it is possible to appreciate how the significance is present at the higher altitude belts and not in the lower ones.

7.3.3 SD:

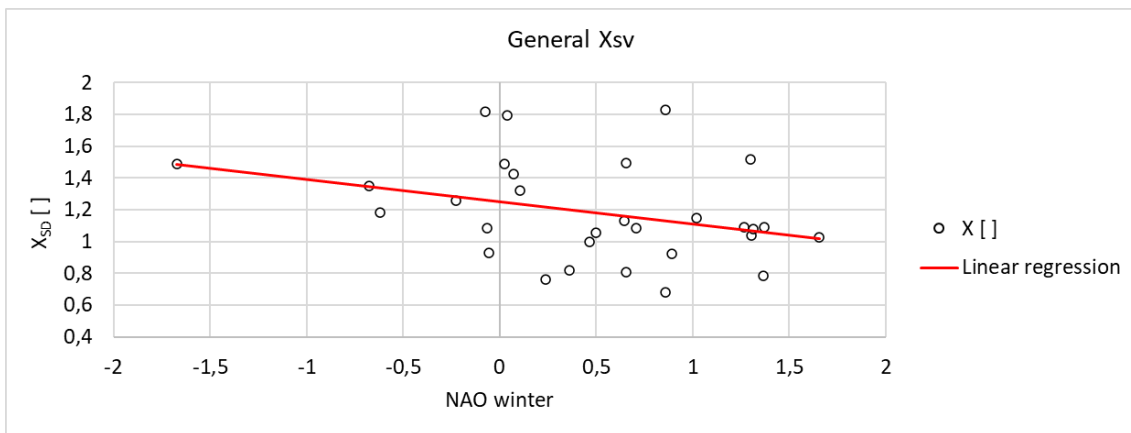


Figure 7.32: Linear regression between SD and NAO winter index.

		Correlation					
		General	Hilly	Hilly-Mountain	Mountain-Subalpine	Subalpine-Alpine	Alpine
ρ_s		-0,3297	-0,3091	-0,1731	-0,3560	-0,3267	-0,3196
P value		✗ 0,075	✗ 0,227	✗ 0,408	✓ 0,054	✗ 0,078	✗ 0,085
		Linear regression					
		General	Hilly	Hilly-Mountain	Mountain-Subalpine	Subalpine-Alpine	Alpine
P value		✓ 0,050	✗ 0,311	✗ 0,452	✓ 0,040	✗ 0,072	✓ 0,052

Table 7.3: Summary of the SD - NAO results for altitude belts.

For this variable only the linear regression is significant in general, but one can notice that the correlation P value is just above the threshold. The analysis carried out for altitude belts results in a significant linear regression for the Mountain + Subalpine belt.

7.3.4 HN average:

As one can see in Table 7.4 for this variable there is no significant correlation with the NAO winter index. The regression, instead, present some significant value, both in general and in the upper altitude belt (Mountain + subalpine).

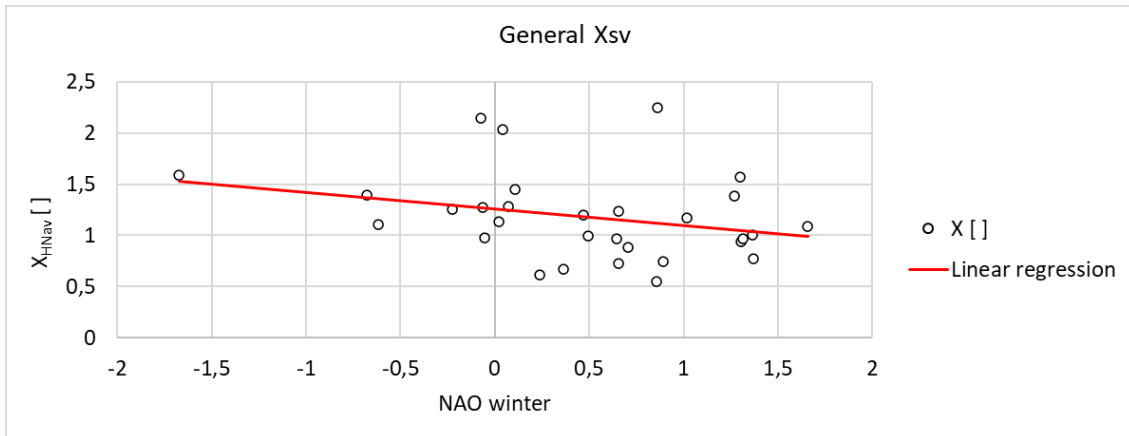


Figure 7.33: Linear regression between HN average and NAO winter index.

		Correlation					
		General	Hilly	Hilly-Mountain	Mountain-Subalpine	Subalpine-Alpine	Alpine
ρ_s		-0,2851	-0,1857	-0,1326	-0,2901	-0,2505	-0,3122
	P value	× 0,127	× 0,461	× 0,527	× 0,120	× 0,182	× 0,093
		Linear regression					
		General	Hilly	Hilly-Mountain	Mountain-Subalpine	Subalpine-Alpine	Alpine
P value		✓ 0,012	× 0,081	× 0,151	✓ 0,010	✓ 0,016	✓ 0,009

Table 7.4: Summary of the HN average - NAO results for altitude belts.

7.3.5 H3D:

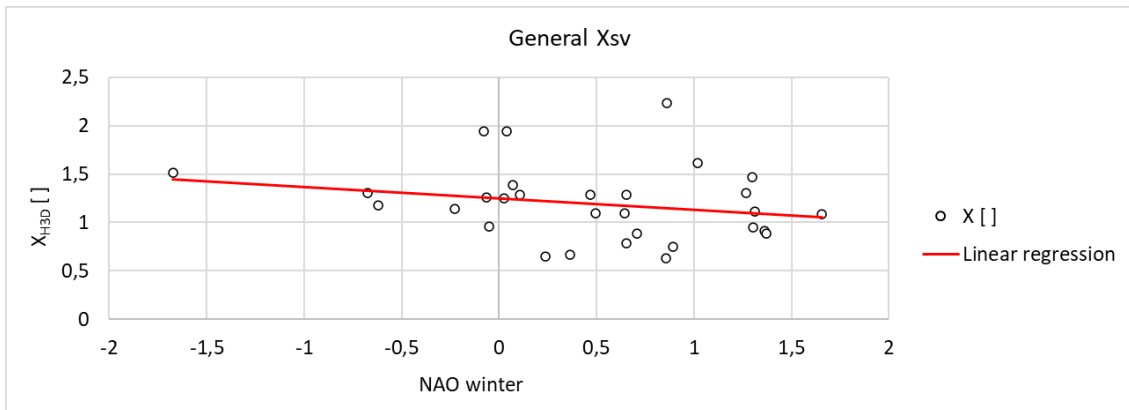


Figure 7.34: Linear regression between H3D and NAO winter index.

		Correlation					
		General	Hilly	Hilly-Mountain	Mountain-Subalpine	Subalpine-Alpine	Alpine
ρ_s		-0,2260	-0,1794	-0,1796	-0,2225	-0,2274	-0,1811
	P value	× 0,230	× 0,476	× 0,390	× 0,237	× 0,227	× 0,338
		Linear regression					
		General	Hilly	Hilly-Mountain	Mountain-Subalpine	Subalpine-Alpine	Alpine
P value		✓ 0,050	× 0,311	× 0,452	✓ 0,040	× 0,072	✓ 0,050

Table 7.5: Summary of the H3D - NAO results for altitude belts.

The results of the analysis on H3D are like the ones on HN average. The correlation with NAO winter index is non-significant but the linear regressions show significance in general and in some, upper altitude belts.

7.4 Comments of the results:

Once the outputs are listed, it's important, given the complexity of the studied phenomenon and climate change in general, to organize the results. In doing so, given the high heterogeneity, it is easy to fall back into subjective or influenced interpretations and therefore the concept of statistical significance is fundamental, being the only parameter able to validate or not the presence of a non-stationarity external to the year-by-year variability.

7.4.1 Temperature and total precipitation:

The temperature variables are the ones for which the trend analysis gives greater significance. For the average annual temperature the 87,5 % of the considered stations shows positive trend, with significance on the 62,5 % of the results. This allow to affirm that temperatures are clearly increased in the whole area of the Lombard Alps, with an average increment of +0,055 °C/y (+1,6 °C in 30 years).

The maximum and minimum temperatures have less clear behavior, especially the latter, for which it cannot be said that there has been a change.

Even the trend of total precipitation does not have a unique behavior, with 81 % of positive trends but significance for just 4 stations (36 % of the total). Given these results it is possible to say that precipitation is significantly increased in some single sites (Branzi, Grosio, Valbondione and Madesimo) and certainly no significant decrease is identified.

7.4.2 Snowiness:

In general, it is possible to divide the Snow Variables considered in two categories, those related to the characteristics of the snowpack (HS average, SCD5) and those related to solid precipitations (SD, HN average, H(n)D). As one can see from the obtained results, the behavior of variables belonging to the same category is similar, probably since the external forcing (able to influence their variability path) are similar. Some of these forcing are common to both the categories but it is fair to note that parameters such as solar radiation or temperature are more influential on the characteristics of the snowpack rather than snowfall regime.

The average annual snowpack depth (HS average) is decreased significantly at lower altitudes (in the hilly belt) with an average trend of -0,39 cm/y and is significantly increased at higher altitude (more or less starting from the 2000 m asl of the Alpine belt) with an average trend of +0,89 cm/y. There is no significance to intermediate altitudes, where probably there is a locally diversified

situation. Where this variable is decreasing, the decrease is greater in spring. The analysis for homogeneous mountain areas gives significant results only for the Prealpi Lariane, where a negative trend is detected. This agrees with the fact that the variable in question reports a significant decrease to lower elevations, which characterize more the territory of this area.

Even the snow cover duration has significantly decreased at lower altitudes with an average trend of -1,3 days/y, but no increase or decrease can be ascertained for it in the other elevations. The areas where this variable has decreased significantly are Prealpi Lariane and Adamello.

The increase of HS at the high altitudes could be justifiable by reflecting on the average temperatures recovered for the various altitude belts and represented in Table 7.6.

Altitude range	year	autumn	winter	spring	autumn+winter+spring
hilly	5,05	5,55	-2,64	5,86	0,09
mountain	7,80	8,21	-0,23	8,91	2,58
subalpine	4,31	4,93	-3,37	5,15	-0,61
alpine	2,31	2,82	-4,78	2,53	-2,25

Table 7.6: Annual and seasonal average temperature for altitude belts.

It can be noted that the average temperature of the upper ranges in the cold season is negative, and therefore it can be assumed that the estimated increase of +1,6 °C of the average annual temperatures in the last 30 years does not have an effect yet visible at these altitudes, as it still allows temperatures to be potentially fertile for solid-phase precipitation.

However, at lower altitudes, where the climate is milder, it is reasonable to think that the significant increase in temperatures has had a greater influence on the snowiness, leading to negative and significant trends.

In support of these claims there is the local significant increase in precipitation, which are influential on both SCD and HS average, as evidenced by the general significant correlation with the NAO winter index, and therefore with perturbed Atlantic flows.

The correlation with NAO winter index is significant at the intermediate altitudes, with P_values under threshold for the Mountain and Subalpine belt. In the Alpine belt, probably, it is more difficult to observe a significant correlation between NAO winter index and SV due to the influence on them by other phenomena, such as the strong wind that could affect the high land. At low altitudes, however, the non-significance of the correlation could be explained by the fact that a NAO-phase consist in more perturbed winters in the study area with milder conditions, resulting in a general rise in the frost level, with liquid precipitation in these belt.

For what concern the snow variables related to precipitations (SD, H(n)D, HN average) the behavior is less clear. The significance on the trend indicates a local increase of the maximum n-days precipitations (evidenced by some scattered stations), with a significant decrement only for one station on the HN variable. Most stations have a positive trend, but it is not statistically significant, preventing the detection with certainty of a trend common to the whole area.

In the hilly and mountain altitude belts a significant decrease of the average daily snow precipitation (HN average) is detected (average trend of -0,61 cm/y).

The seasonal analysis shows how all these variables decrease more in Autumn than in other seasons.

The correlation between these SV and the NAO winter index is never significant, despite this the linear regression is, suggesting that even for them the behavior is in line with that of HS average and SCD, with a decrease of the same in correspondence of NAO+ phases and vice versa.

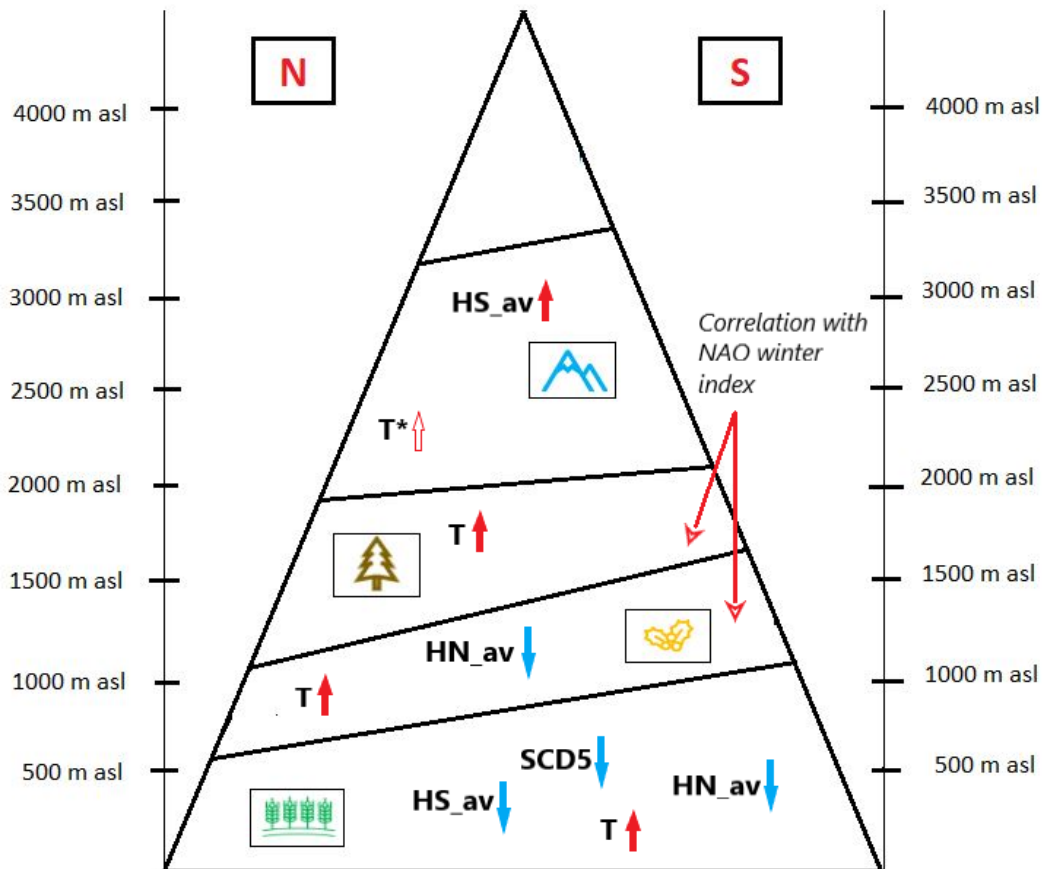


Figure 7.35: Main results obtained from the analysis by altitude belts.

The division of the territory of the Lombard Alps into altitude belts leads to more significant results, so that we can consider the altitude of the stations as the main parameter that influences the behavior of the historical series. No significance is detected in the analysis carried out for the stations grouped by slope aspects (not

reported), instead, for what concern the analysis for mountain areas the significance agrees with the average elevations of the area.

Looking at the Figure 7.35 is possible to see a schematic summary of the results obtained.

The average annual temperature is generally increased at all the elevations but without leading to average annual negative temperature in the upper belt (Alpine), represented in Figure 7.35 by an empty arrow and an asterisk. This probably led to the increasing of the average snowpack depth (HS_av) at this elevation, considering that the precipitations show a significant local increase for some stations and no significant decrease in the period.

The biggest changes are detected in the lower altitude belts, probably more sensitive to the temperature increase. At these elevations (especially in the Hilly belt) significant decreasing of the annual average snowpack depth (HS_av), annual snow cover duration (SCD5) and average annual 1-day snowfall (HN_av) are detected. HN_av has significantly decreased also in the Mountain belt.

The NAO winter index is significantly correlated to some snow variable (particularly HS_av and SCD5) at the intermediate elevation, particularly the Mountain and the Subalpine belts, for the reason previously explained.

In conclusion, the evidence of a stronger decreasing in Fall for the SV related to precipitations may be related to the stronger decrease of HS_av and SCD5 in Spring. This indicates that less snow on the ground in the last part of the season could be related to less solid precipitations at the beginnings.

8. METHODS AND MODELS TO PROJECT CLIMATE CHANGE

Climate change is studied by research groups all around the world, and scientific discoveries are being collected, reviewed and used by the IPCC (Intergovernmental Panel on Climate Change) to produce periodic reports, on which the socio-economic strategies and policies of the countries are based. Through its assessments, the IPCC determines the state of knowledge on climate change. It defines where there is agreement in the scientific community on topics related to this phenomena, and where further research is needed (IPCC, 2020).

As described in the thesis introduction climate change is a very complex phenomena, which involves an infinite number of components of the earth system that constantly change for natural or anthropic causes. Modeling the climate is a delicate and complex work, which requires the use of a big amount of data. One of the most widely used methodologies is the definition of climate change scenarios, which are plausible assumptions about the evolution of human society, and the use of complex climate models, which seek to reproduce the climate of our planet. To project the hydrogeological impact on climate change, these instruments are widely used, providing the climatic input for medium to long term impact analysis on water resources (A. Soncini, 2011).

This chapter presents, from a theoretical point of view, the models and the climate change scenarios used in this work, specifying the main characteristics and the possibilities of use.

8.1 Shared Socioeconomic Pathways (SSPs)

Global climate change studies rely on numerous assumptions and factors related to policy options and societal developments. Shared Socioeconomic Pathways (SSPs) were developed over the last years as a joint community effort (by an international team of climate scientists, economists and energy systems modelers) to provide a toolkit for the climate change research community to carry out integrated, multi-disciplinary analysis. They describe plausible major global developments that together would lead in the future to different challenges for mitigation and adaptation to climate change. They have also been described as “stories that happened in the future”, aiming to explore how the future can evolve under a consistent set of assumptions (Keywhan Riahi, 2017).

In other words, the SSPs are logical descriptions of the possible future development of human society and they have been used to help produce the IPCC Sixth Assessment Report on climate change, published on 9 August 2021.

The scenarios are:

- SSP1: Sustainability (Taking the Green Road)

- SSP2: Middle of the Road
- SSP3: Regional Rivalry (A Rocky Road)
- SSP4: Inequality (A Road divided)
- SSP5: Fossil-fueled Development (Taking the Highway)

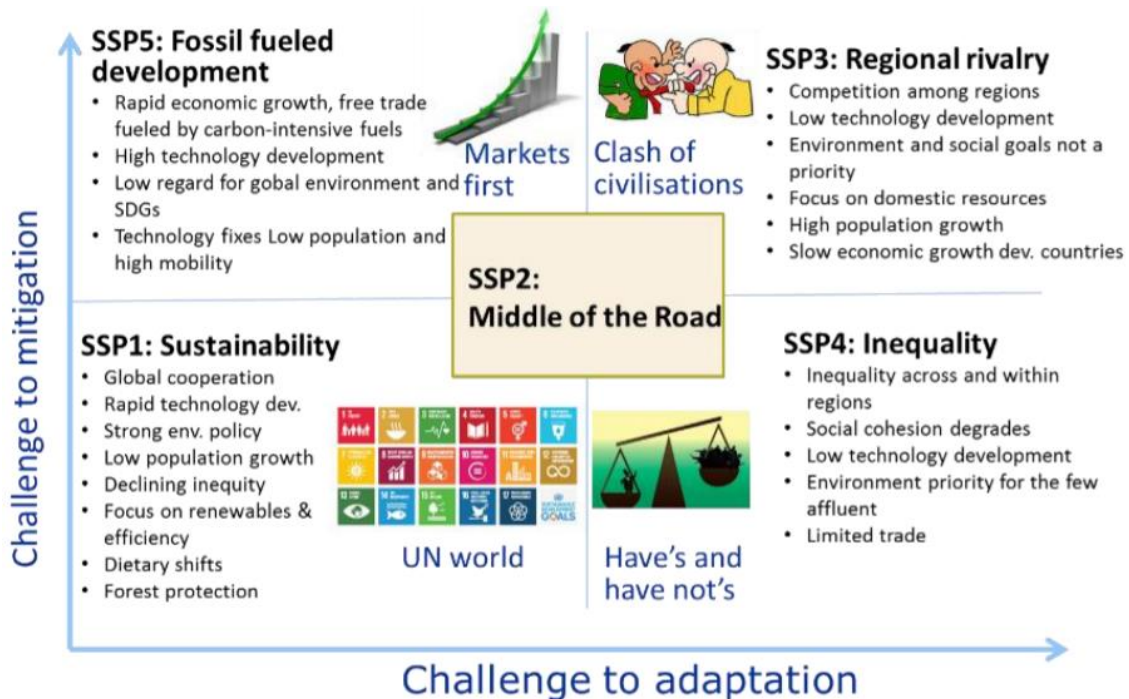


Figure 8.1: Framework of the Shared Socioeconomic Pathways scenarios.

As one can see in Figure 8.1 the SSPs are based on five narratives describing alternative socioeconomic developments.

8.1.1 SSP1 - Sustainability (taking the Green Road)

The world shifts gradually, but pervasively, toward a more sustainable path, emphasizing more inclusive development that respects perceived environmental boundaries. Management of the global commons slowly improves, educational and health investments accelerate the demographic transition, and the emphasis on economic growth shifts toward a broader emphasis on human well-being. Driven by an increasing commitment to achieving development goals, inequality is reduced both across and within countries. Consumption is oriented toward low material growth and lower resource and energy intensity.

8.1.2 SSP2 - Middle of the road:

The world follows a path in which social, economic, and technological trends do not shift markedly from historical patterns. Development and income growth proceeds unevenly, with some countries making relatively good progress while others fall short of expectations. Global and national institutions work toward but make slow progress in achieving sustainable development goals. Environmental systems experience degradation, although there are some improvements and

overall the intensity of resource and energy use declines. Global population growth is moderate and levels off in the second half of the century. Income inequality persists or improves only slowly and challenges to reducing vulnerability to societal and environmental changes remain.

8.1.3 SSP3 – Regional rivalry (A rocky road)

A resurgent nationalism, concerns about competitiveness and security, and regional conflicts push countries to increasingly focus on domestic or, at most, regional issues. Policies shift over time to become increasingly oriented toward national and regional security issues. Countries focus on achieving energy and food security goals within their own regions at the expense of broader-based development. Investments in education and technological development decline. Economic development is slow, consumption is material-intensive, and inequalities persist or worsen over time. Population growth is low in industrialized and high in developing countries. A low international priority for addressing environmental concerns leads to strong environmental degradation in some regions.

8.1.4 SSP4 – Inequality (A road divided)

Highly unequal investments in human capital, combined with increasing disparities in economic opportunity and political power, lead to increasing inequalities and stratification both across and within countries. Over time, a gap widens between an internationally connected society that contributes to knowledge and capital-intensive sectors of the global economy, and a fragmented collection of lower-income, poorly educated societies that work in a labor intensive, low-tech economy. Social cohesion degrades and conflict and unrest become increasingly common. Technology development is high in the high-tech economy and sectors. The globally connected energy sector diversifies, with investments in both carbon intensive fuels like coal and unconventional oil, but also low-carbon energy sources. Environmental policies focus on local issues around middle and high income areas.

8.1.5 SSP5 – Fossil fueled development (Taking the highway)

This world places increasing faith in competitive markets, innovation and participatory societies to produce rapid technological progress and development of human capital as the path to sustainable development. Global markets are increasingly integrated. There are also strong investments in health, education, and institutions to enhance human and social capital. At the same time, the push for economic and social development is coupled with the exploitation of abundant fossil fuel resources and the adoption of resource and energy intensive lifestyles around the world. All these factors lead to rapid growth of the global economy, while global population peaks and declines in the 21st century. Local environmental problems like air pollution are successfully managed. There is faith in the ability to effectively manage social and ecological systems, including by geo-engineering if necessary.

Among the various socio-economic parameters used for the definition of scenarios, population growth and per capita emissions play a key role, as can be seen in the Figure 8.2.

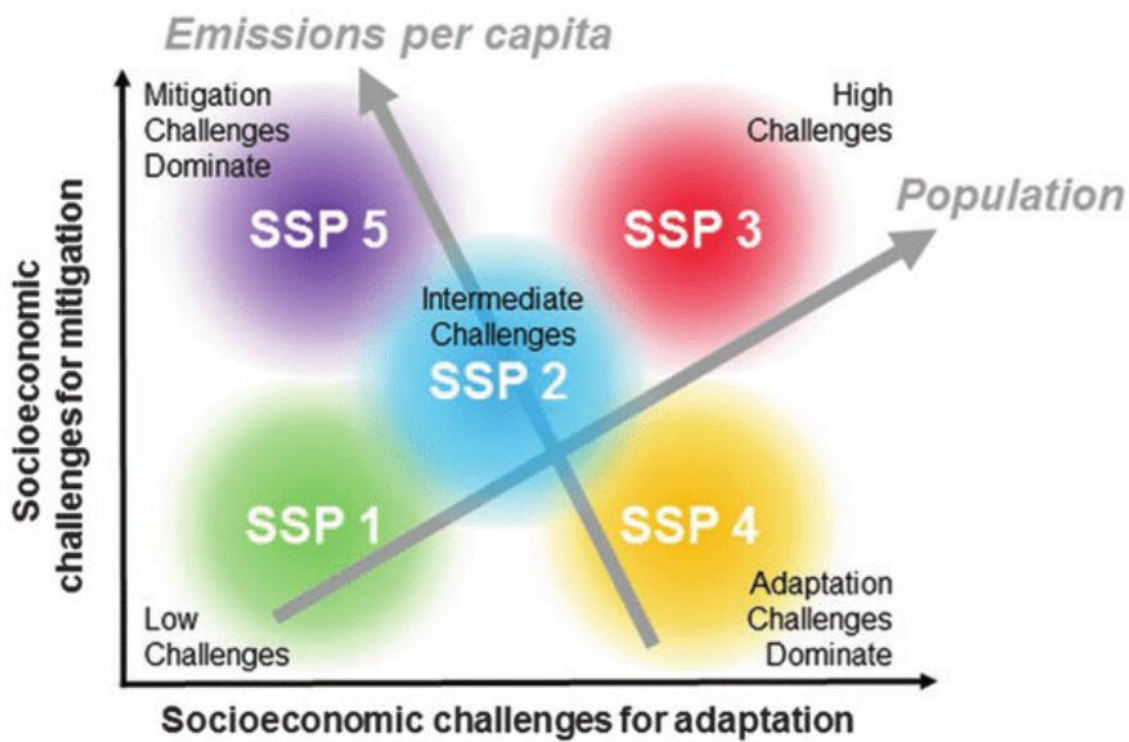


Figure 8.2: Approximate trends in population outcomes and emissions per capita outcomes superimposed to the SSPs conceptual map.

8.2 Effects of the SSPs scenarios on the earth climate:

The IPCC, in the latest published report, requires the use of a unique parameter for the choice of climate change scenarios to be used in future climate modelling. This parameter is the net balance of radiative forcing, that is the energy flow (measured in W/m^2) that describes the energy balance between incoming and outgoing energy in the earth-atmosphere system. Previously, the IPCC used RCP (Representative Concentration Pathways) scenarios, which represented trajectories of greenhouse gas concentration in the atmosphere.

The factors that can disturb the earth's energy balance are many (change in land use and therefore albedo effect, greenhouse gases etc.) and to each of them can be linked a radiative forcing value. The parameter currently used by the IPCC is the global radiative forcing achieved in 2100 (resulting from the sum of individual radiative forcing), which if positive results in an energy increase in the global climate system.

It is important to note that the concept of radiative forcing is linked to that of 'climatic sensitivity', which can be defined as the temperature increase reached at equilibrium following a unitary and constant increase of a radiative forcing.

8.2.1 The Integrated Assessment Modelling (IAM):

The IAMs are types of scientific models that tries to link main features of society and economy with biosphere and atmosphere into one modelling framework. The goal of Integrated Assessment Modelling is to accommodate informed policy – making, usually in the context of climate change though also in other areas of human and social development. While the detail and extent of integrated disciplines varies strongly per model, all IAM includes economic processes as well as processes producing greenhouse gases.

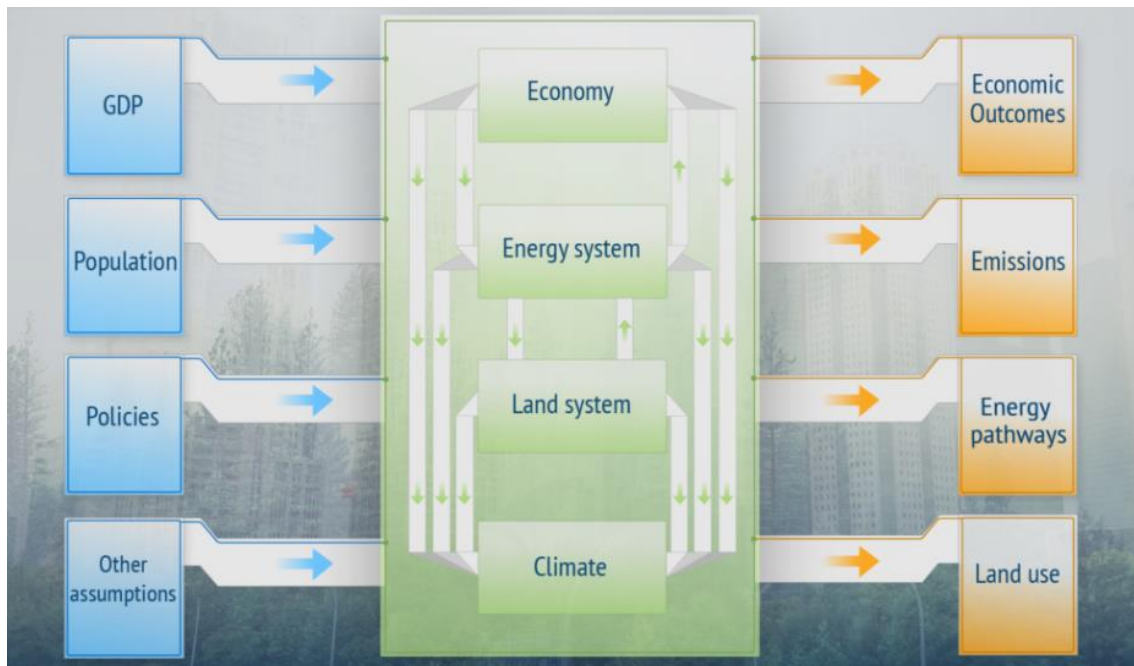


Figure 8.3: Flow chart concerning the functioning of IAMs models.

These models are combined with the SSPs scenarios to compute values of the radiative forcing, modelling the effect on climate of each Shared Socioeconomic Pathways.

8.2.2 The Scenario Model Intercomparison Project (Scenario MIP):

The Scenario Model Intercomparison Project (ScenarioMIP) is the primary activity within Phase 6 of the Coupled Model Intercomparison Project (CMIP6) that will provide multi-model climate projections based on alternative scenarios of future emissions and land use changes produced with integrated assessment models (Brian C. O'Neill, 2016).

The results of the ScenarioMIP experiments will provide new climate information for future scenarios that will facilitate integrated research across multiple communities. The mentioned working group proposed the use of four SSP scenarios, so that they are comparable with the RCP scenarios previously used by the IPCC, for which climate impacts have been calculated in terms of the radiative forcing that can be achieved at the end of the 21st century.

The scenarios are organized into two tiers and those used in this thesis work belong to Tier 1.

The following image represent the SSP-RCP scenario matrix illustrating ScenarioMIP simulations. Each cell in the matrix indicates a combination of Shared Socioeconomic Pathways and climate outcome based on a particular forcing pathway that IAM runs have shown to be feasible. Dark blue cells indicate scenarios that will serve as the basis for climate model projections in Tier 1.

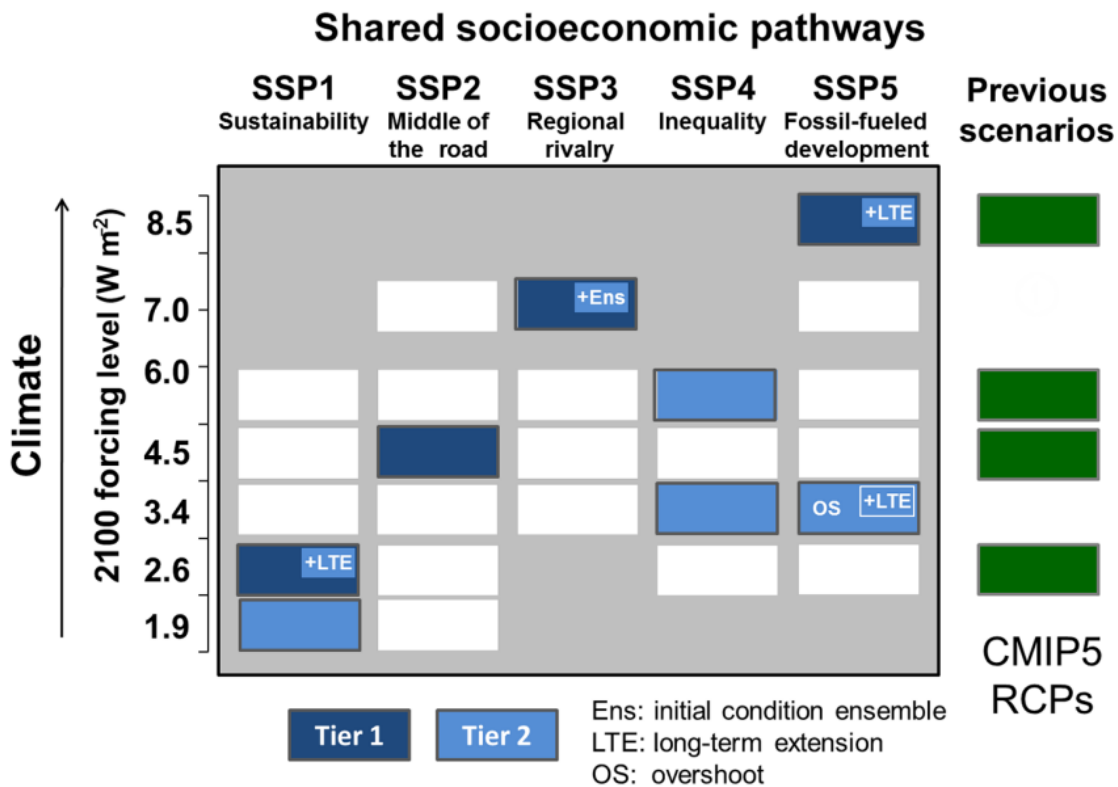


Figure 8.4: RCP - SSP scenario matrix illustrating the ScenarioMIP simulations.

8.3 Global circulation model

Once the projections of global climate forcing are obtained it is necessary to understand its effects throughout the globe, both in terms of temperature and precipitation projections. This can be done thanks to climatic models like the Global Circulation Model (GCM), which are mathematical representations of the physical laws that govern the Earth’s climate system, paying particular attention to the processes underlying the interactions between the atmosphere, oceans and land surface. The actual use of these tools to model future precipitation and temperature series in the field of hydrology is demonstrated in (A. Soncini, 2011).

The first mathematical model capable of realistically describing the monthly and seasonal trends of the troposphere was developed in 1956 by Norman Phillips.

Since then, several models have been developed, which have been gradually refined and enriched trying to simulate more and more elements and physical processes of the components involved.

There are two main categories of GCM: the Atmospheric General Circulation Model (AGCM) and the Ocean General Circulation Model (OGCM) which, when coupled, create a coupled circulation model atmosphere/ocean, called CGCM (Coupled GCM) or AOGCM (Atmospheric-Oceanic GCM).

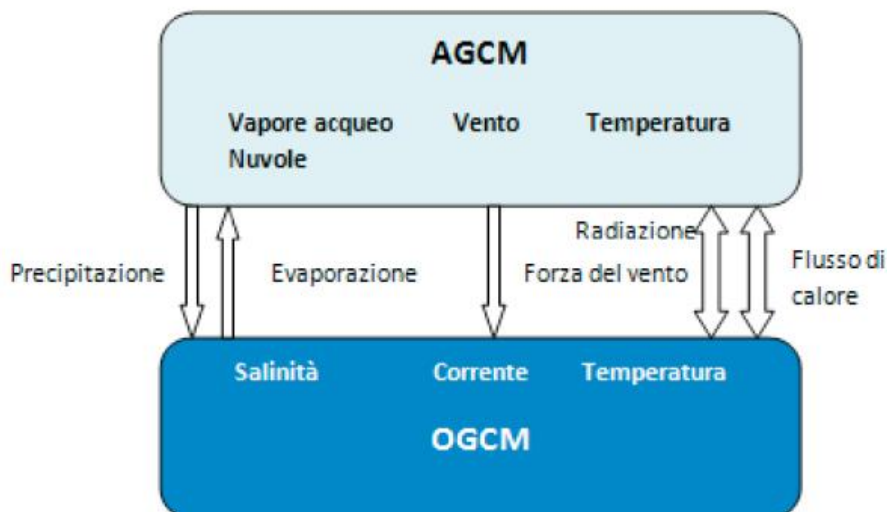


Figure 8.5: Exchange relations between OGCM and AGCM.

Temperature, precipitation, air humidity, atmospheric pressure, snow cover, soil humidity and solar radiation are the main variables reproduced by GCM. However, there are still several key components of the global climate system that GCMs cannot reproduce. For this reason, Earth System Models (ESM) are often used. These models derive from the combination of GCM with models capable of reproducing phenomena such as the carbon cycle, chemical processes in the atmosphere and in the soil, land use, vegetation dynamics and albedo changes.

These models provide, on the one hand, tools for the study of climate at a precise time in the past and, on the other hand, can be used for analyses and projections of future climate developments, both for long-term research and short-term weather forecasts.

The use of ESM assumes both temporal and spatial discretization according to grids with resolution dependent on the specific model. The spatial discretization of the earth is done with a big 3-D grid with planar cell size varying between 50 km and 200 km and layer height varying between 10 km in atmosphere and 30 km in the oceans. The time step varies from minute to day, although typically the daily scale is the most used.

The models provide values of the quantities of interest (temperature, precipitation, humidity etc.) for each time instant and for each 3D cell, assuming that this value can be considered constant for the entire cell.

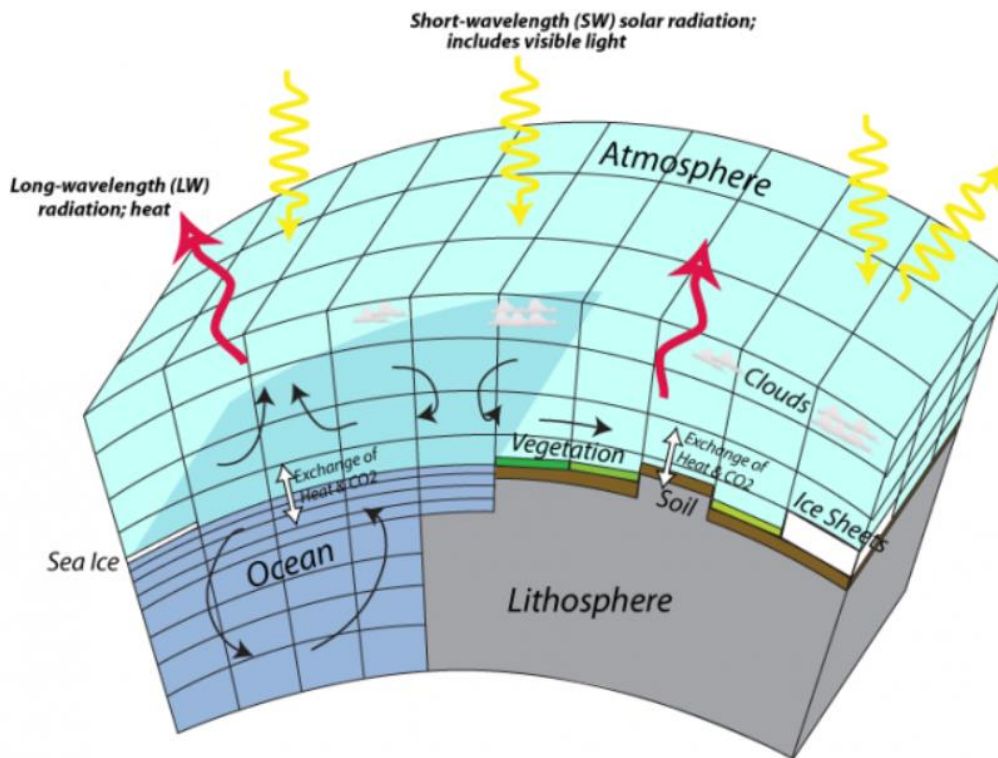


Figure 8.6: Schematic structure of a Global Circulation Model.

The more cells in a model, the closer it can approximate the real Earth, but too many cells would require more computing power.

8.3.1 GCM considered in this study:

In the present work 6 different climatic model present in the literature are considered, summarized in the following table:







Modello	Centro di ricerca	Nazione	Dimensione cella [°]	Strati	Numero celle
EC-EARTH3	Europe-wide-consortium	EU 	0.7° x 0.7°	91	512x256
MPI-ESM-ECHAM6.3	Max Planck Institute for Meteorology	D 	1.1° x 0.9°	95	384x192
CESM2	National Center for Atmosphere Research	USA 	1.25° x 0.9°	32	288x192
HadGEM3	Met Office Hadley Centre (MOHC)	UK 	1.875° x 1.25°	85	192x144
MIROC6	Japan-consortium	J 	1.4° x 1.4°	81	256x128
CMCC-CM2	Fondazione Centro Euro-Mediterraneo sui Cambiamenti Climatici (CMCC)	I 	1.25° x 0.9°	30	288x192

Table 8.1: Summary of the GCM used to project climate change.

- EC-EARTH3:

This is the ESM developed by the European Union, through a research team in which numerous universities and meteorological institutes participated. This model can be used at different resolutions and is divided in three main components: IFS for simulate the atmosphere and landmass, NEMO for the oceans and LIM2 for sea and glacier with also the Greenland ice sheet.

- MPI-ESM-ECHAM6.3:

This German model can be used at different resolution level and is developed in many versions. Every version incorporated a model top at 0.01 hPa (or about 80 km), a complete representation of physical process, and allows for coupling to an advanced representation of the terrestrial biosphere through the JSBACH sub model, as well as an advanced description of the atmospheric aerosol.

- CESM2:

This is an American model, created by the National Center for Atmosphere research, that provides state-of-the-art computer simulation of the earth past, present and future climate change. Many versions have been developed through the years; the ones used in this work dates to 2018.

- HadGEM3:

HadGEM3 is an English family of climatic models, developed by the MOHC institutions.

The HadGEM3 family of models comprises a range of specific model configurations incorporating different levels of complexity but with a common physical framework. The HadGEM3 family includes a coupled atmosphere-ocean configuration, with or without a vertical extension in the atmosphere to include a well-resolved stratosphere, and an Earth-System configuration which includes dynamic vegetation, ocean biology and atmospheric chemistry.

One of the main changes in the HadGEM3 family of models compared with previous versions is the inclusion of the NEMO ocean modelling framework, which is also used in the Met Office's Ocean forecasting system, and CICE the Los Alamos sea ice model. These are coupled to the atmospheric model through the OASIS coupler developed at CERFACS (Centre of basic and applied research) in France.

- MIROC6:

This family of model has been cooperatively developed by a Japanese modeling community. The versions used in this study is the 6th ones, released in 2018 with an improved simulation of the tropical climate system and midaltitude atmospheric circulations.

- CMCC-CM2:

This Italian model is a AOGCM which has been implemented and developed starting from the Scale Interaction Experiment SINTEX-G (SXG) model.

In CMCC-CM, the ocean component is the global ocean model OPA 8.2 (Madec et al. 1998), in its ORCA2 global configuration. The horizontal resolution is $2^\circ \times 2^\circ$ with a meridional refinement near the equator, approaching a minimum 0.5° grid spacing. The model has 31 vertical levels, 10 of which lie within the upper 100 m. The atmospheric model component is ECHAM5.

8.3.2 Limitations of the GCM:

Despite the important progress made in recent years in the development of GCMs, the uncertainties of the results obtained are still numerous. Such uncertainties are linked to the inability to reproduce phenomena that occur at scales lower than the model's own.

The resolution of the grids used by GCM is not sufficient for modelling atmospheric processes, which can undergo significant variations if one considers a spatial resolution far lower than that typical of the models themselves. The grid T63 ($1,875^\circ - 1,185^\circ$), used in many general circulation models, discretizes the entire Earth's surface in 96 latitude values and 192 longitude values, thus providing a representative value on a cell of average size equal to 200-300 km².

Since the projections reliability of the global models decreases at the smallest scales, it is necessary to derive from these values data at a higher spatial resolution, to better represent the local variability of the climatic quantities considered. Some techniques, such as regional climate models or downscaling methods (described in the next chapter) have been developed to study climate change at local and regional level.

Uncertainties are also associated with cloud representation and their response to climate change. Another limit in the predictive capacity of the model can be found in the non-linear behavior of the climate system which includes unstable dynamics and, therefore, in the fact that the climatic simulations depend strongly on the initial conditions that arise. Finally, there is considerable uncertainty in the reconstruction of the solar and volcanic forcing.

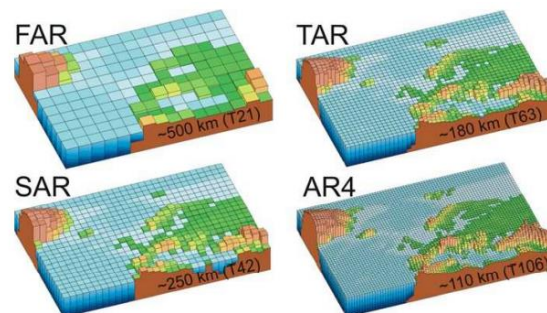


Table 8.2: Example of spatial resolution used by GCM developed in different eras: FAR (IPCC 1990), SAR (IPCC 1996), TAR (IPCC 2001), AR4 (IPCC 2007).

8.4 Downscaling procedure:

The downscaling procedure is a technique that allows to derive from the climatic model data at higher spatial resolution, to model local or regional climate. Because of their resolutions GCMs are not able to reproduce phenomena characterized by a spatial resolution smaller than cell sizes, which are fundamental to model the future climatology of a heterogeneous area such as the one under study. Despite this, GCMs represent the main physically based instrument that we have for climate projections and from these comes the necessity to use a downscaling procedure such as the ones presented here and provided several studies as (A. Soncini, 2011), (Groppelli B., 2011) and (Groppelli B., 2011).

In mountain basin the temperature and the topographic variability strongly affect the snowfall and the snow ground accumulation. Recently, rainfall simulation algorithms able to respect the “self-similarity” and “intermittence” properties in space and time have been developed. The algorithms are based on the random cascade theory. This model needs to be calibrated with total precipitation historical series of the involved stations in a reference period.

Spatial disaggregation on individual stations is made by the correction of the monthly bias present on the cumulative values of precipitation and intermittence (rainy days) for each station individually.

In particular, the used monthly bias are summarized as follows:

- *Bias P*: is the precipitation bias defined as the ratio of precipitation provided by the GCM models to observed precipitation, so $Bias P > 1$ means an overestimation of the precipitations by the model.
- *Bias T*: is the difference between the temperatures provided by the GCM and the ones measured by the stations.
- *Bias RD*: It is defined as the ratio between rainy days (RD) in the series modeled by GCM and the observed rainy days at the stations, so $Bias RD > 1$ means an overestimation of the rainy days by the model.

The values obtained for each station are used to correct the precipitations and temperature series provided by the GCM model in the reference period. The procedure for disaggregating the GCM results is reduced to the bias correction, or systematic daily error, defined as *Bias GAO* (Eq. 13).

Precipitation correction is made by calculating the monthly cumulative precipitation values observed at the stations: (R_{oss} for the reference period). The average monthly precipitation provided by climate models (R_{GCM}) is then corrected using a random multiplicative process that explicitly considers intermittence.

$$Bias_{GAO} = \frac{R_{oss}}{R_{GCM}} = B_{GAO} * B_0 * W_0 \quad (13)$$

In which are defined (Eq. 13):

$$\begin{cases} P(B_0 = 0) = 1 - p_0 \\ P(B_0 = p_0^{-1}) = p_0 \\ E[B_0] = p_0^{-1} \cdot p_0 + 0 \cdot (1 - p_0) = 1 \\ \begin{cases} W_0 = \exp w_0 - \sigma_{w_0}^2/2 \\ E[W_0] = 1 \end{cases} \end{cases} \quad (13)$$

Where B_{GAO} , B_0 , $\sigma_{w_0}^2$ are parameters typical of the model. In particular:

- B_{GAO} is a constant the forces the average monthly value of R_{oss} to make it equal to the relative observed average value.
- B_0 is the Beta type generator that represents the probability that the rainfall rate for a given day R_{GAO} is positive, conditioned by the positive R_{GCM} value modelled with a binomial distribution.
- w_0 is a strictly positive generator, used for adding a proper amount of variability to the precipitation during the identified rainfall periods.

Regarding temperature, the daily temperatures provided by the GCM models for the reference period are used and compared with the temperatures observed at the stations. The monthly average difference between the T observed and provided by the GCM is then evaluated and consequently the correct daily temperatures are given by (Eq. 14):

$$T_{corr,d} = T_{GCM,d} - \Delta T_i \quad (14)$$

Where:

- $T_{corr,d}$ is the corrected temperature provided by the GCM at the day d .
- $T_{GCM,d}$ is the temperature of the GCM model.
- ΔT_i is the difference between the observed monthly average and the ones from GCM in the month i .

At the end of the procedure series of precipitation and temperature systematically similar (at the monthly temporal scale) are obtained for each investigated station.

9. MODEL IMPLEMENTATION FOR HS PROJECTIONS

In Chapter 8, the methods and models used in this paper to obtain future projections of temperature, precipitation and snowfall were presented. These tools, recognized by the scientific community as effective tools for modeling climate change, are implemented in series, taking the outputs of one model and putting them as input to the next, leading to a cascade process that has as last step the trend analysis (as the one used for the historical series). Even in this case, the whole process is developed in Matlab environment.

In Figure 9.1 it's possible to appreciate how the various models are used in the cascade process. The final goal is the trend assessment.

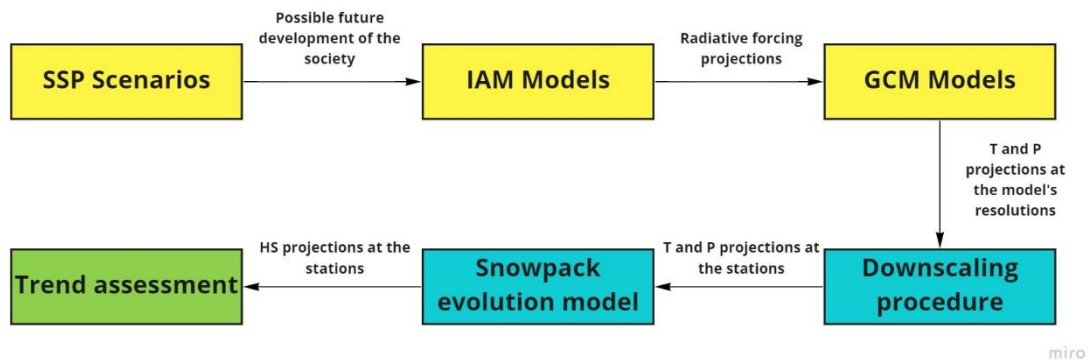


Figure 9.1: Flow chart representing the cascade process used for the analysis.

The yellow squares represent the step of the process executed by the data providers. In this work the output of the GCMs (future projections of temperature and precipitations at models' resolutions until the year 2100) are taken as input for the subsequent elaborations, as presented in the previous chapters. The GCM output data source is recoverable at: <https://esgf.llnl.gov/>.

The blue squares, instead, represents the models used in this works, which require calibration, as presented in the following chapters. The green square (i.e. the trend assessment) is the final goal of the process and the aim of this study.

For the theory behind the snowpack evolution model you can see the Chapter 2.4.

9.1 Database resizing:

In the chapter 5.2 the measurement stations used for trend assessment on historical series were presented. This chapter specifies the use of different stations samples according to the variable under study (Snow variables, temperature or precipitation), since not all the stations are equipped with all the three sensors.

In this part of the present study, to calibrate the used models, stations with available registrations of the three variables described are needed, and so the database must be resized.

From the 28 stations that have acceptable historical series of the HS variable, those without a rain gauge and thermometer are eliminated, obtaining a final dataset based on 11 stations.












N	COD	Name	Elevation [m asl]	Altitude range	Mountain areas	Aspect
1	BRACC	Branzi Caserma Carabinieri	830	hilly 	Orobie Sud	OS SE
2	EDOPA	Edolo Pantano d`Avio	2108	alpine 	Adamello	Ad N
3	APR	Aprica	1950	subalpine 	Orobie Nord	ON N
4	CIVFB	Chiesa in Valmalenco Funivia Bernina	2014	alpine 	Retiche Occidentali	RO W
5	GEAPE	Gerola Alta Pescegallo	1875	subalpine 	Orobie Nord	ON NW
6	GRODF	Grosio Diga Fusino	1220	mountain 	Retiche Occidentali	RO E
7	LIVLV	Livigno La Vallaccia	2660	alpine 	Livigno	Li N
8	VFUCA	Valfurva S. Caterina 2	1735	subalpine 	Alta Valtellina	AV NW
9	VBOBA	Valbondione Barbellino	1850	subalpine 	Orobie Sud	OS W
10	MAD	Madesimo	1530	mountain 	Alpi Valchiavennasch	Va SE
11	VDSOC	Valdisotto Oga S. Colombano	2300	alpine 	Alta Valtellina	AV NW

Figure 9.2: Stations used for the trend assessment on future climatic projections.

This is considered the best possible database obtainable with the available data sources (ARPA and AINEVA stations). Spatial and elevation coverage is no longer optimal but is considered acceptable due to the spatial uncertainty levels of the climate projections, which in any case prevents from an analysis for homogeneous group of station like the ones presented in the historical series analysis.

As one can see in Figure 9.3 no HS measuring stations with thermometer and pluviometer installed are available for the area of the Prealpi Lariane. This underscores the importance of continuously upgrading the measurement network to increase sensor redundancy on the territory.

A possibility to cope with the lack of data could be to find the temperature and rainfall data from the available stations closest to the nivometric station, correcting the values recorded by empirical relationships linking these variables to the difference in altitude between two points. This possibility is not carried out given the high variability imposed by the complex morphology of the territory and to avoid further approximations to a process that already presents errors intrinsic to the used models.

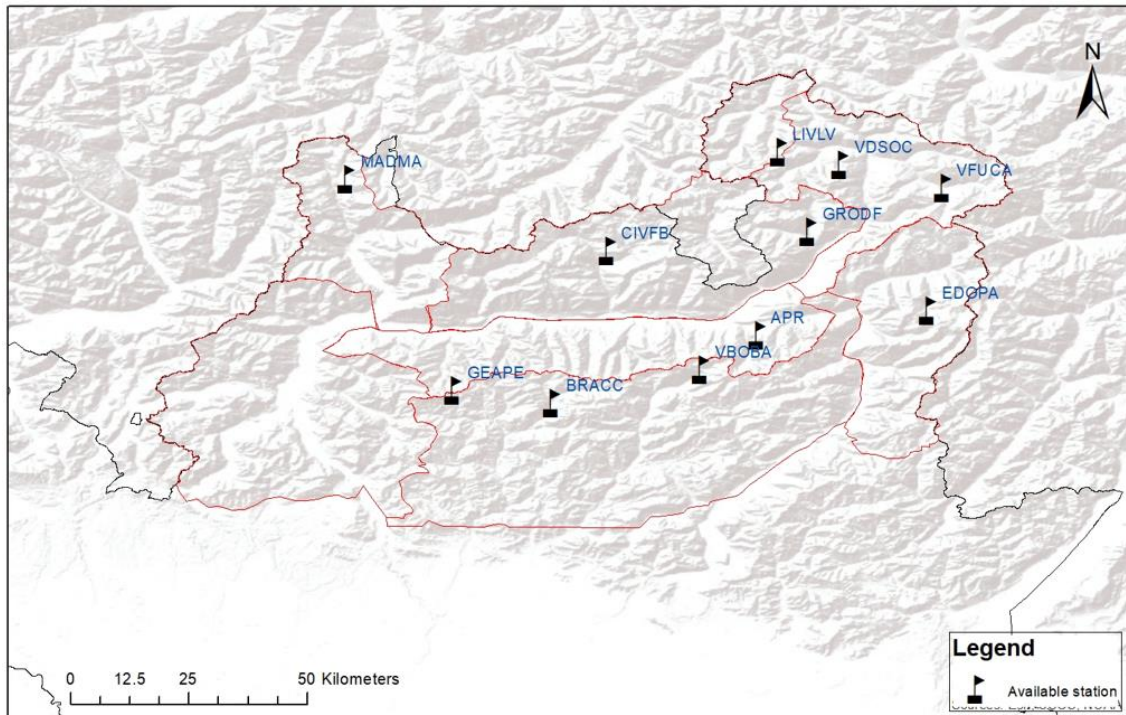


Figure 9.3: Spatial distribution of the stations used for the projections.

9.2 Models' calibration:

The models that need to be calibrated are the Downscaling model and the Snowpack evolution one. A correct calibration of these instrument result fundamental for obtain good results in the final projections used for the trend assessment.

9.2.1 Downscaling model calibration:

The downscaling model provided in (A. Soncini, 2011) requires as input the historical series of the stations, to compute the bias described in chapter 8.4. The bias are then used to downscale the output projections of the GCMs models, so as to switch from the scale of the model to that of the single station.

The information needed by the model are:

- Stations coordinates (Reference system: WGS84/UTM zone 32N)
- Start and end dates of the time series
- Measured daily historical series of total precipitation at the stations.
- Measured daily historical series of maximum, average and minimum temperature at the stations.

The model uses the coordinates entered to locate the stations in the resolution cells of the various GCM models and for each station calculates the bias used by the downscaling itself through the inserted historical series. For a correct functioning of the process, the model requires that a given day are present values

of the 4 input variables at the same time, and therefore it is necessary to filter the data by placing the error value (-999) for all variables whenever one of the two sensors (thermometer or pluviometer) provides an error value. In addition, the time series must have the same start and end date, and therefore the shortest series must be filled with the error values to obtain the time consistency.

The historical series used for the calibration are the ones used in the past year trend assessment for the previously described 11 stations. The control period is 1/08/1990 – 31/07/2021.

9.2.2 Snowpack evolution model calibration:

As described in the Chapter 2.4 the snowpack evolution model according to the Martinec method is composed by three main model. The calibration is needed for the settling and the melting model.

To assess the density of snow on the ground a relation, according to which the density of the new snow increases as a function of the days elapsed since the last snowfall and the Martinec parameter (m), is used. The former parameters need to calibrate at the studied sites, by computing the deviations between HS measured and modeled.

The calibration of the melting model, instead, is aimed at the estimation of degree day factors related to temperature and precipitation.

In general, the snowpack evolution models calibration requires as input the historical measured series of temperature and radiation. The control period is 1/1/1990 – 31/07/2021, as the ones used for the downscaling model calibration.

In addition, an input vector containing a range of parameters (on which to perform the calibration for each station) is required. Specifically, the following values have been inserted, taking as an example the values reported in (Giulia Arianna Premoli, 2014), where the model has been applied for an area climatically and geographically similar to that of the present study.

Parameter	Start	Step	End	Bibliographic reference
ρ neve [kg/m ³]	90	5	160	Cresta R., 2014
Albedo [-]	0,7	-	-	Cresta R., 2014
n [-]	-0,50	0,05	-0,10	Martinec J., 1991
TMF [mm d /°C]	1,0	0,1	7,0	Martinec J., 1991

Table 9.1: Calibration parameters range for the Snowpack evolution model

Branzi	Edolo	Aprica	CVM_funivia	Pescegallo	Grosio_Fusino	Livigno_Vallaccia	Santa_Caterina	Valbondione	Madesimo	Oga
135	125	160	95	95	145	130	110	100	100	115

Table 9.2: Calibrated snow density at the stations [kg/m³]. The values represent the average fresh snow density calibrated on the historical series.

Unfortunately, the stations available for this study do not have consistent solar radiation series. Pyranometers were in fact introduced by ARPA on a more limited number of stations and starting from more recent times than those necessary for the calibration. As a first attempt it is decided to exclude the incoming radiation from the model, assuming that the melting of the snowpack is exclusively due to air temperature.

After a careful visual evaluation of plotted model outputs, and based on the calculation of the NSE parameter, it was concluded that the approximation is good for the purposes of this paper, especially about the average annual values of HS for which there is an absolute maximum error of 25,98 % and an absolute mean error of 8,14 %.

The Nash–Sutcliffe efficiency (NSE) is calculated as one minus the ratio of the error variance of the modeled time-series divided by the variance of the observed time-series. In the situation of a perfect model with an estimation error variance equal to zero, the resulting Nash–Sutcliffe Efficiency equals 1 ($NSE = 1$). Conversely, a model that produces an estimation error variance equal to the variance of the observed time series results in a Nash–Sutcliffe Efficiency of 0.0 ($NSE = 0$). In the case of a modeled time series with an estimation error variance that is significantly larger than the variance of the observations, the NSE becomes negative. An efficiency less than zero ($NSE < 0$) occurs when the observed mean is a better predictor than the model.

As one can see in the Figure 9.4 the model works well in general, resulting less optimal for Aprica and Santa Caterina stations but without having predictive ability lower than the average value one.

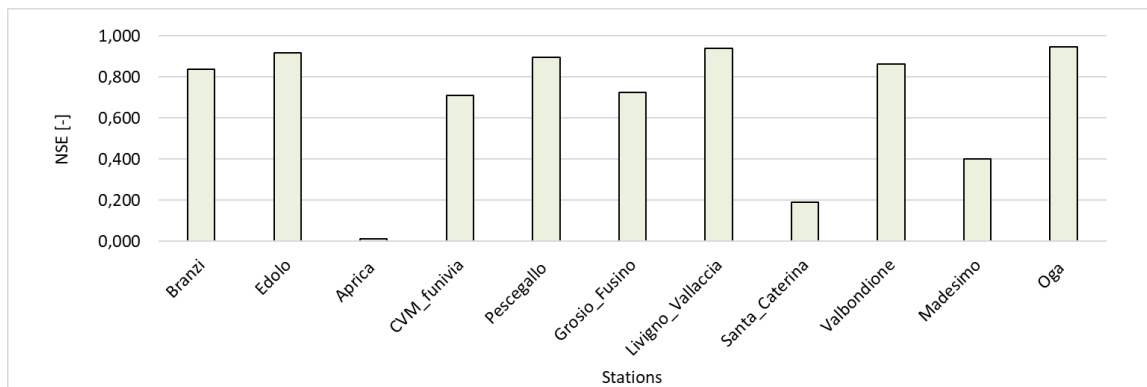


Figure 9.4: NSE index computed at the station.

10. FUTURE PROJECTIONS AND TREND ANALYSIS

The use of 6 different GCMs models projecting 4 different SSP scenarios (considering that the HadGEM3 model does not provides the *SSP3 7.0* scenario) leads to 23 different simulation outputs, containing the daily HS value from 1/08/2020 to 31/12/2099, as well as T and Ptot series.

For each of the 11 stations there will then be 23 projections of the daily snow depth, which constitute a huge number of data that need further processing to understand the series behavior.

Thanks to the use of the Matlab software, the SV presented in the chapter 5.1 are calculated from HS, and on them, some elaborations implemented.

10.1 Proposed elaborations

10.1.1 Trend analysis technique:

Given the huge amount of data, an in-depth analysis like that performed for the historical series is considered superfluous here, and a simplified trend analysis procedure is therefore proposed based on the calculation of the following parameters:

- Linear regression coefficient.
- Significance of the linear regression based on P-value (threshold significance level at 95 %).
- Mann-Kendall test coefficient (threshold significance level at 95 %).

The trend assessment is executed only for the annual variable. Differentiation for homogeneous areas and seasonal analysis aren't performed due to the moderate spatial coverage of the stations and the lower temporal resolution of such long projections. See chapter 6 for the theory relative to the trend assessment techniques.

As done for the past year trend assessment the results of the analysis are reported separately in:

- Annex 2: Future year trend assessment results.

10.1.2 Effects of different SSP scenarios on projections:

To show the results obtained in a clear and useful way, it is believed in the importance of focusing on the influence that the different SSP climate change scenarios have on the future developments of the snow variables. To do this, the annual values of the projections of each SV are normalized to an index value representative of the current situation. This index value is chosen as the average

value of the historical series, taking the representative period 1/08/2000 – 31/07/2020.

$$X_{SV} = \frac{x_i}{\mu}$$

Where x_i are the individual observation and μ the historical series average: $\mu = \frac{\sum_{i=1}^{Y_i} x_i}{Y_i}$; with Y_i years of registrations.

The X_{SV} are then averaged between the various stations and the various GCM annually, so as to obtain for each SV four general projections valid for the entire area of the Lombard Alps (one for each Shared Socioeconomic Pathway). The results are then plotted and discussed, showing the effects of the various SSP in terms of percentage changes in SV respect to today's values. These graphics allow to appreciate the possible behavior of the snowiness condition according to the social and environmental choices that human society will take during the XXI century.

10.1.3 Average values at mid-century and end of century:

This graphical product shows the average value forecasted in each station at the middle and at the end of XXI century, compared with today value. To do this, the mean of all the regression's coefficients is used, applying the regression at the mid-century (2060) and end of the century (2099). These graphs show a plausible value that the studied variables could reach in the two specified periods.

10.1.4 Extreme values at mid-century and end of century:

This graphical product shows the 'extreme' values forecasted in each station at the middle and at the end of XXI century, compared with today's values. To do this, the lower and higher value of the significant linear regression coefficients is used, applying the regression at the mid-century (2060) and end of the century (2099). These graphs not only show the uncertainty of the 23 scenarios provided, but also allow appreciating the worst and best scenarios that the Alpine society could face at the middle and at the end of the XXI century.

10.2 Snow variable results:

10.2.1 General evidence on the linear regression significance:

From the obtained results on the significance level related to the LR coefficients, as it is possible to verify in the attached *Annex 2*, for all the considered stations there is an increase in the statistical significance with the worsening of the SSP scenario. This behavior is visually common to all GCM models used, which show significant trends especially for the SSP3 7.0 and SSP5 8.5 scenarios, for which the trend values are more extreme. The behavior may be associated with the fact that worse socio-economic development scenarios lead to an extreme evolution of climate variables.

The significance on the Mann-Kendall test results and on the linear regression agree for all the variables and the scenarios considered in the study.

10.2.2 HS average

For most of the GCM considered the average annual snowpack depth decreases during the XXI century. The SSP1 2.6 scenario (Sustainability) leads to a decrease in the next few years, followed by a recovery after the mid-century that brings the values back to the current ones, highlighting a long-term change almost null. The most extreme condition is associated with the SSP5 8.5 scenario (Fossil-fueled development), which leads to an average HS reduction of 80% by the end of the century (Figure 10.1). Applying the average angular coefficient for each single site it is possible to confirm the described decrement, which seems to be more marked in some stations. The projections predict a null annual average snowpack depth in two stations at the end of the century (Figure 10.2). The variability in the various considered scenarios is high especially for some stations for which there is a considerable difference in the results between the worst and best scenario (Figure 10.3).

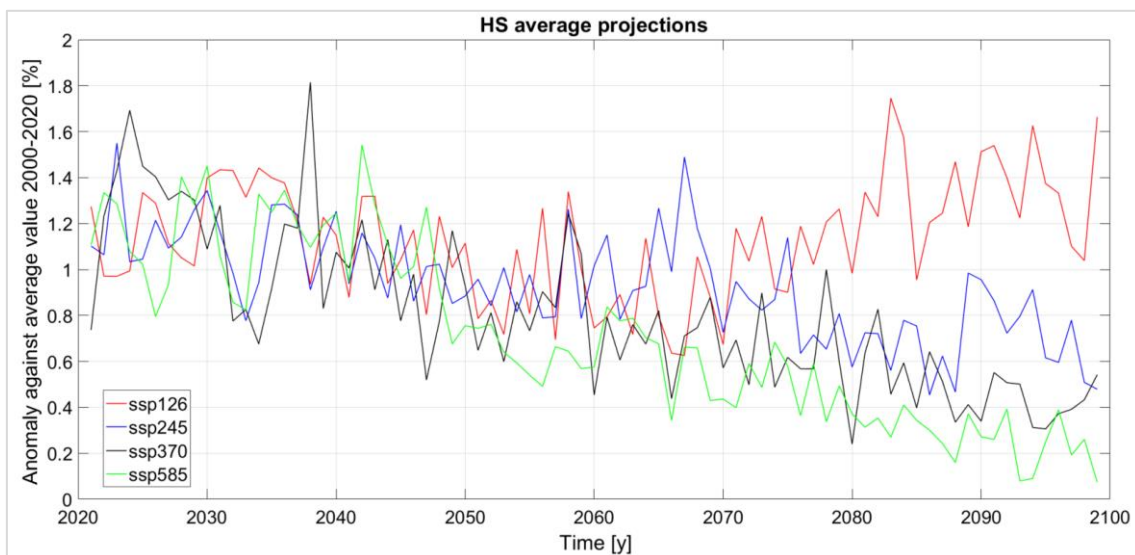


Figure 10.1: HS average XXI century projections for each SSP scenario.

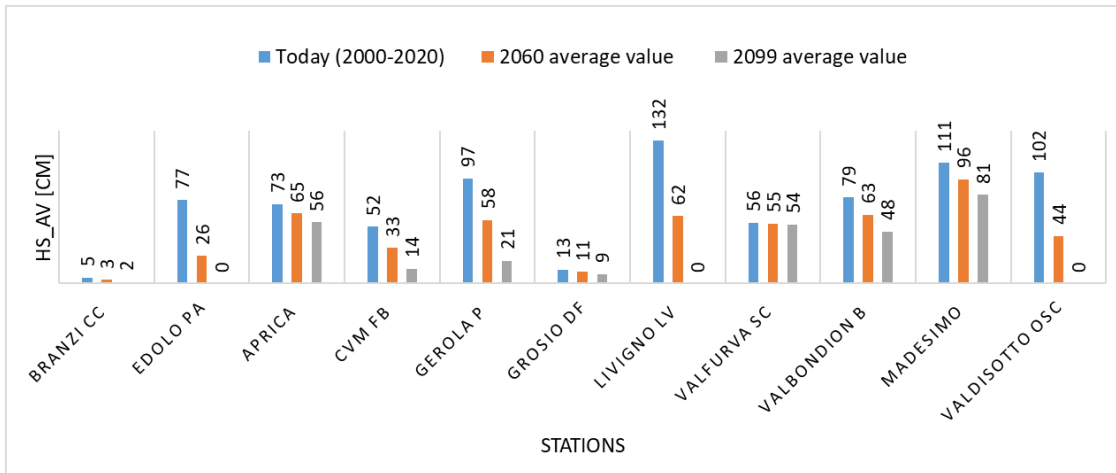


Figure 10.2: Average HS average value at mid-century and end of century

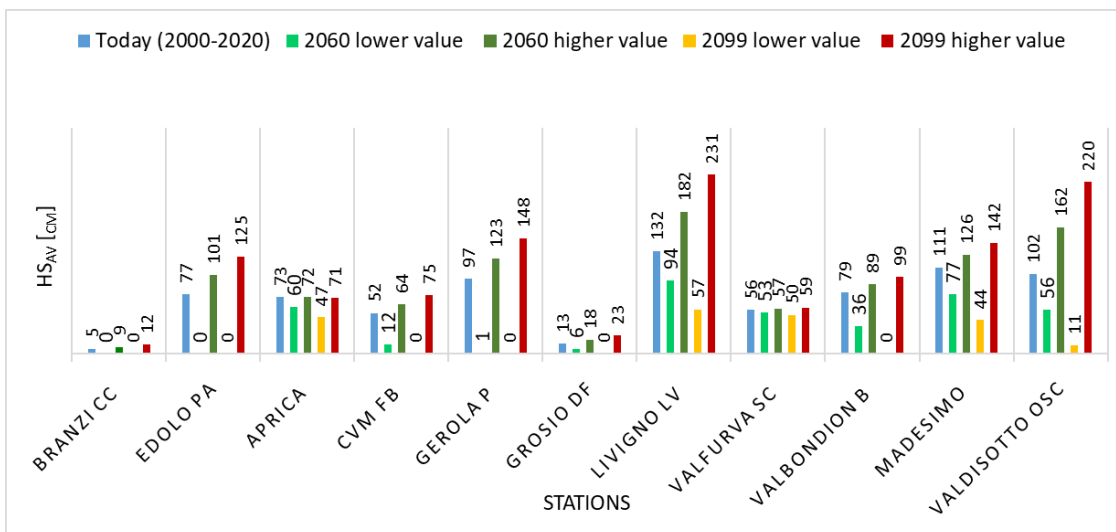


Figure 10.3: Extreme HS average value at mid-century and end of the century.

10.2.3 SCD₅:

For most of the GCM considered the average annual snow cover duration decreases during the XXI century. The behavior is evident looking at the different general projections for each SSP scenario. The results are similar to those of HS average, with a long-term change of SCD₅ almost null for the SSP1 2.6 scenario and an extreme reduction of the 70% at the end of the current century for the SSP5 8.5 scenario (Figure 10.4). The average decrement is evident for all the considered stations, which shows a similar average trend (Figure 10.5). As for HS average the variability in the different scenarios results is considerable (Figure 10.6).

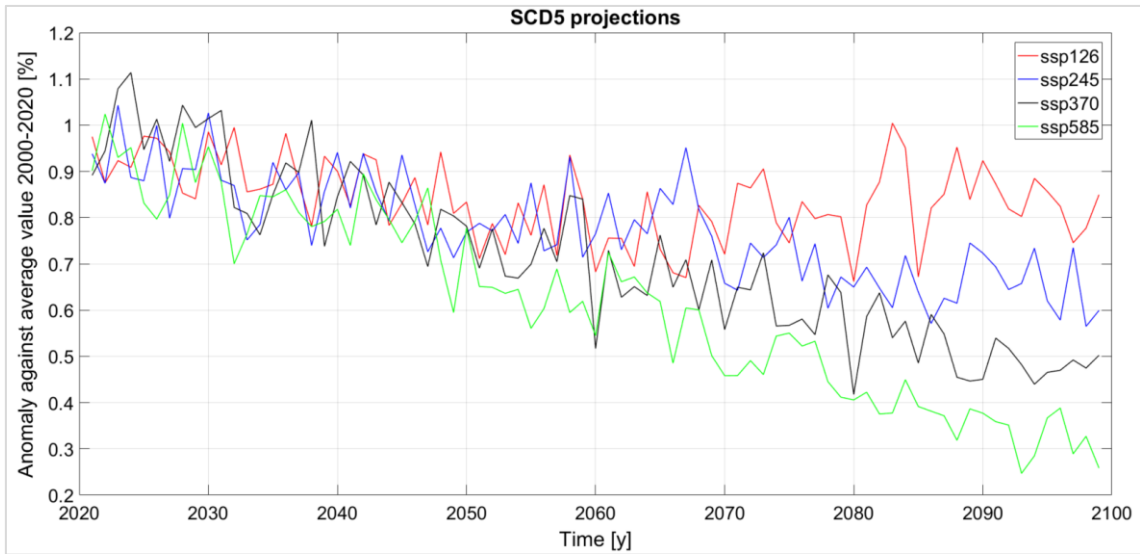


Figure 10.4: SCD5 XXI century projections for each SSP scenario.

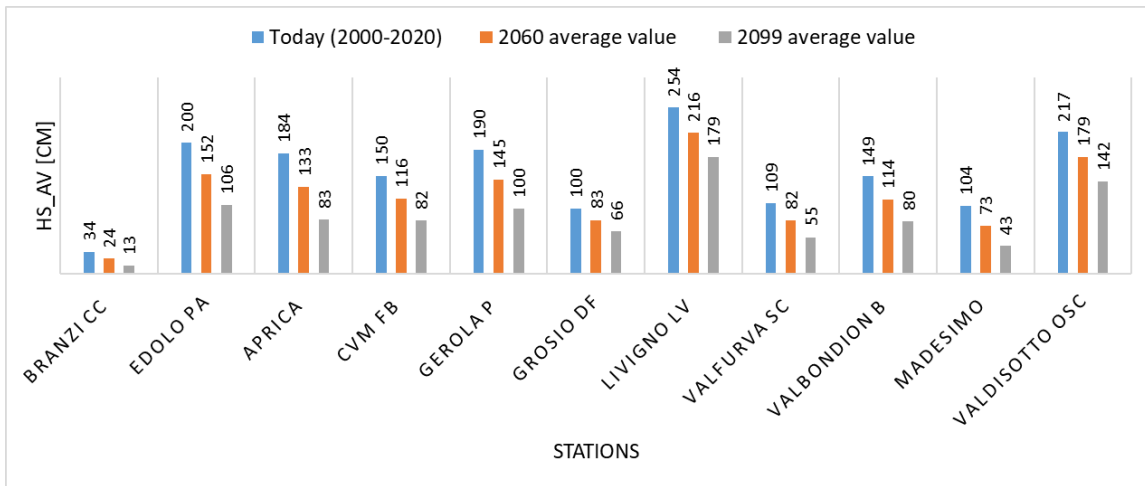


Figure 10.5: SCD5 average value at mid-century and end of century

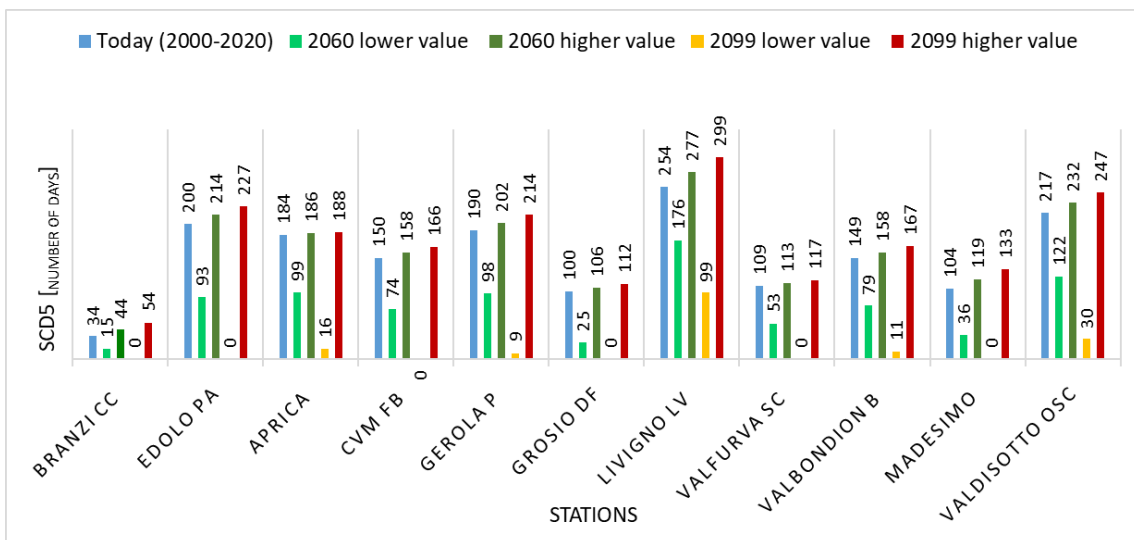


Figure 10.6: Extreme SCD5 average value at mid-century and end of the century.

10.2.4 SD:

The annual snow days also seems to decrease during the XXI century, with all the significant trends negative and positive trend without statistical significance. The effects of the various SSP scenarios detected for HS average and SCD₅ are confirmed for SD too, with a general reduction of the 100% at the end of the XXI century predicted by the SSP5 8.5 projections (Figure 10.7). The reduction is evident looking at the average value reached at mid-century and end of the century in the various stations, with 3 stations for which no one day with snow precipitations is predicted by 2099 (Figure 10.8). The variability between the various scenario is high, with the worst-case scenario predicting the achievement of null SD values even by mid-century for some stations (Figure 10.9).

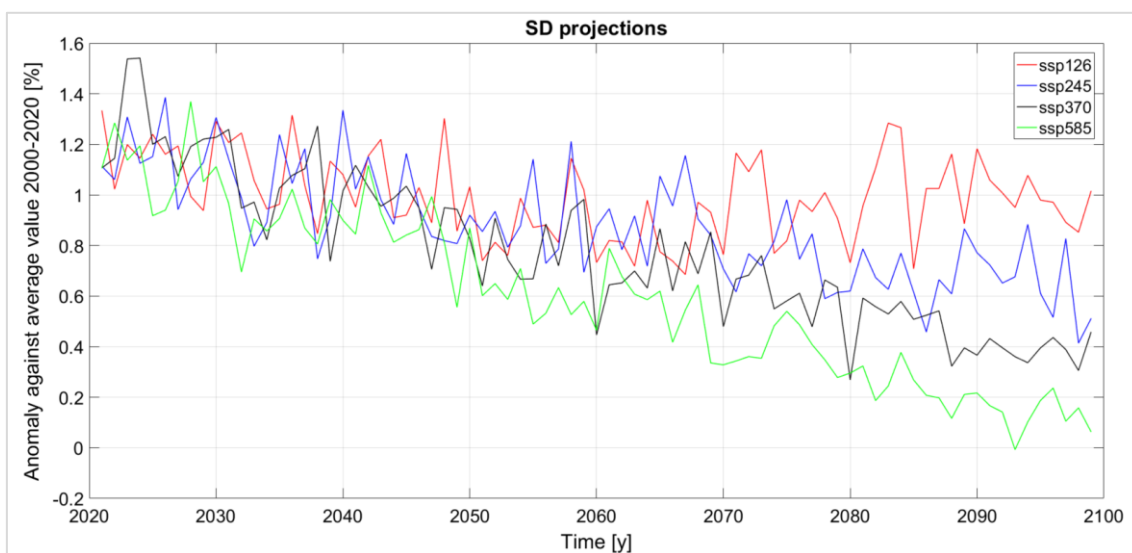


Figure 10.7: SD XXI century projections for each SSP scenario.

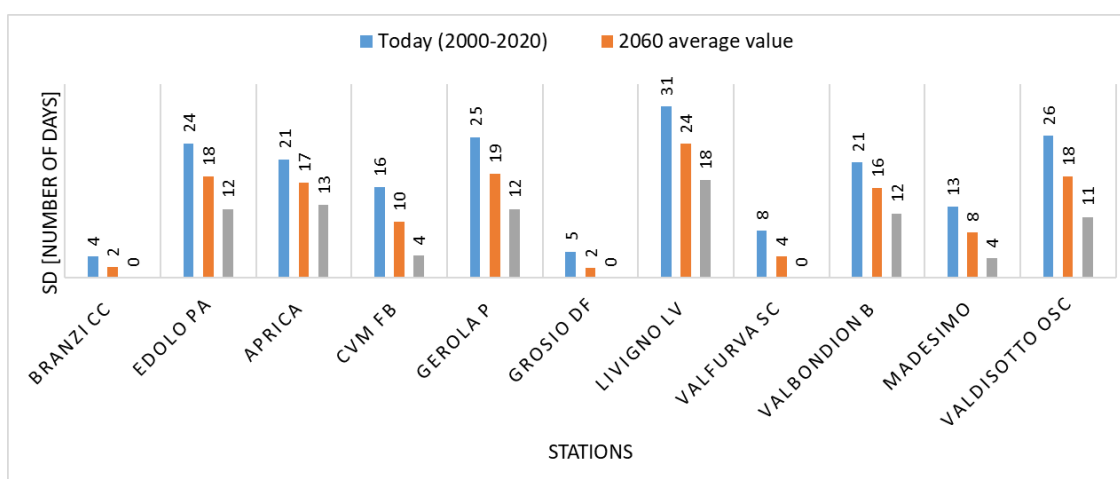


Figure 10.8: Average SD average value at mid-century and end of century

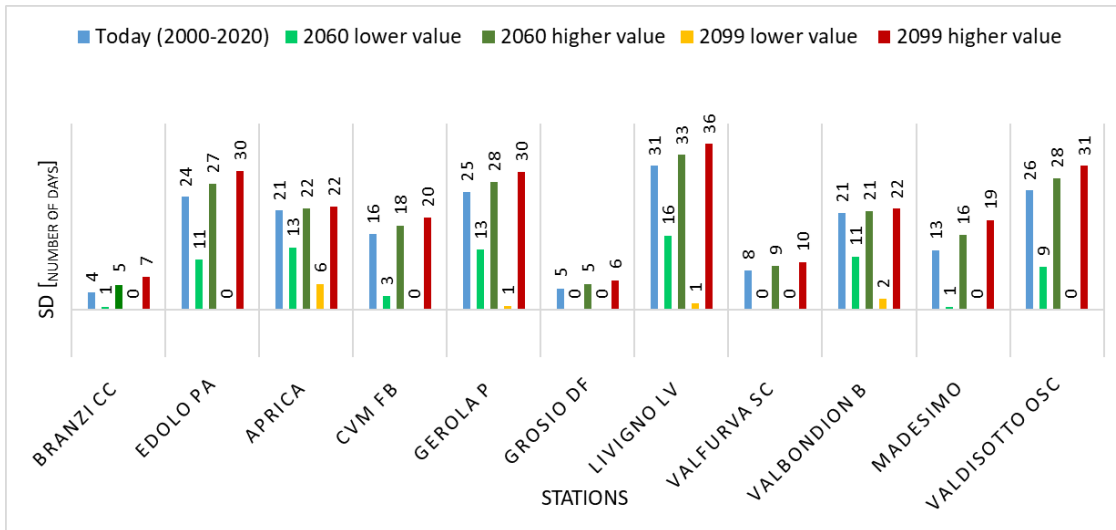


Figure 10.9: Extreme SD average value at mid-century and end of the century.

10.2.5 HN:

The maximum 1-day maximum annual snowfall decreases during XXI century. The behavior due to SSP scenarios considered is different, with no long-term change in the best scenario (SSP1 2.6) and a strong reduction for the worst-case scenario (SSP5 8.5). This reduction is forecasted to be around the 100% of the current values by the end of the century (Figure 10.10).

The average value reached at mid-century and end of the century in each station decreases in time, with three stations for which no snow precipitation are forecasted by 2099 (Figure 10.11). These stations are Edolo Pantano d'Avio, located at 2108 m asl in the Adamello area, Aprica, located at 1950 m asl in the Orobie Nord and Branzi Caserma Carabinieri, located at 830 m asl in Orobie Sud. The variability between the scenarios is consistent even in this case, especially for some stations (Figure 10.12).

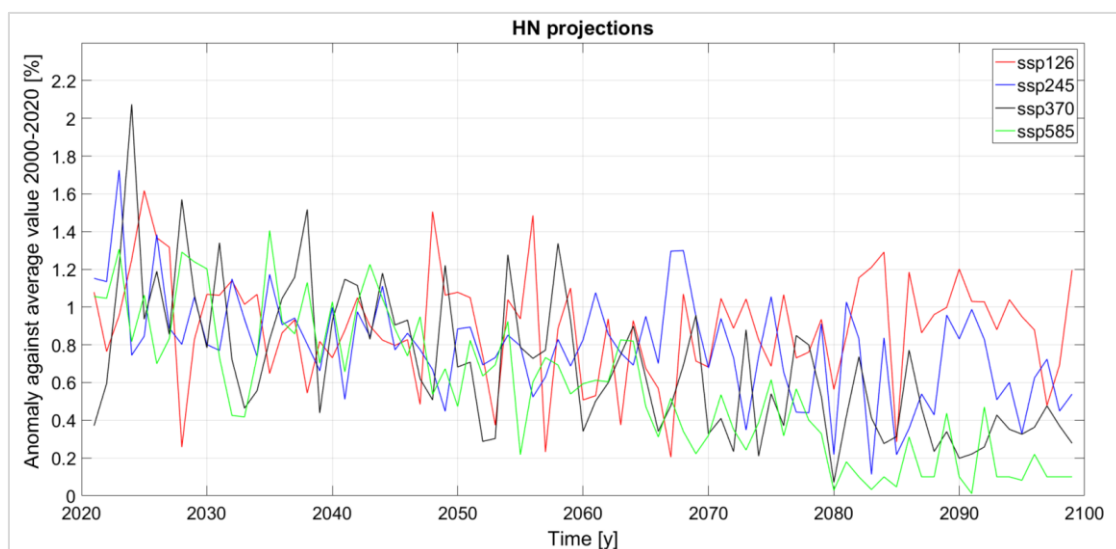


Figure 10.10: HN XXI century projections for each SSP scenario.

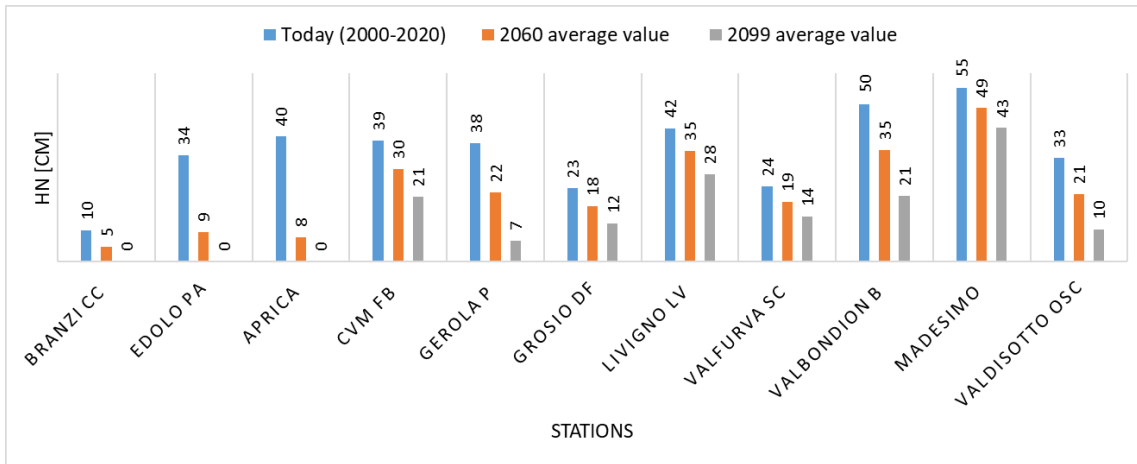


Figure 10.11: Average SD average value at mid-century and end of century.

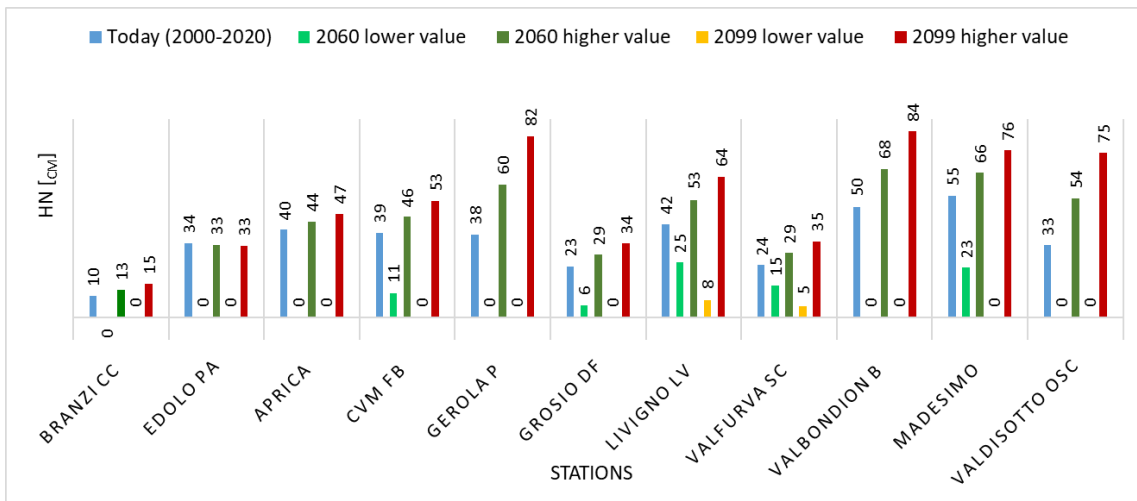


Figure 10.12: Extreme SD average value at mid-century and end of the century.

10.2.6 H2D:

The 2-day maximum annual snowfall seems to decrease during the current century too, with the statistical significance only on the negative trend. The SSP1 2.6 scenario show a certain stationarity of the variable in question, while the scenario SSP5 8.5 leads, after to values above average at the beginning of the century, to a decrease of 50% by 2099. However, this decrease is lower than the decrease foreseen for HN (Figure 10.13). The average value reached at mid-century and end of the century are smaller than the current ones, highlighting the decrease described (Figure 10.14). Even for this variable there is a strong variability between the results provided by the different scenarios, with null H2D value of H2D also in 2060 for the worst projection (Figure 10.15).

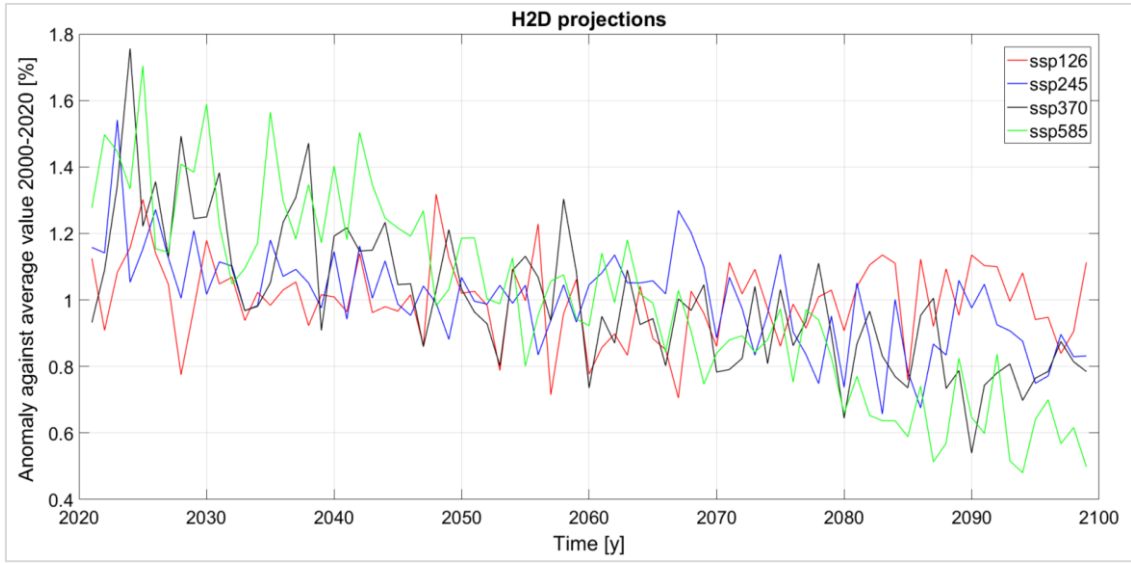


Figure 10.13: H2D XXI century projections for each SSP scenario.

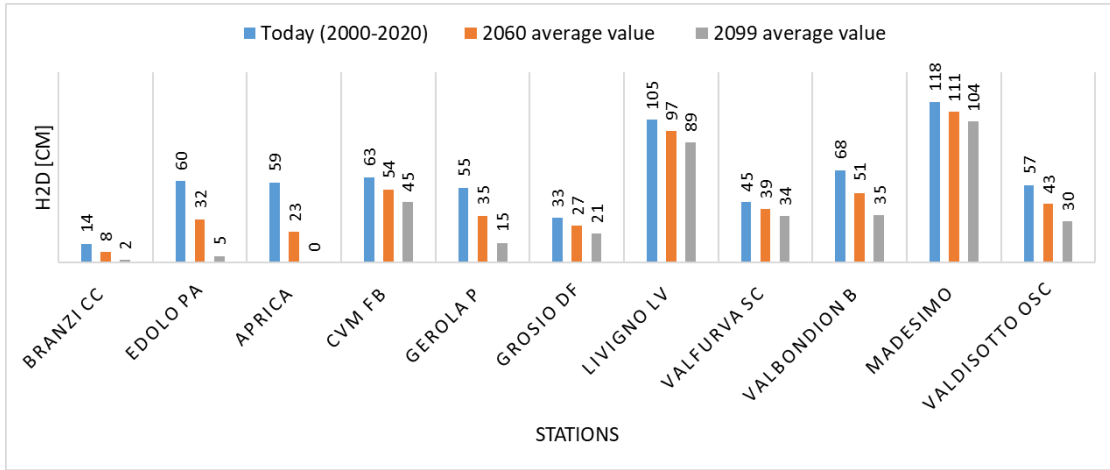


Figure 10.14: Average H2D average value at mid-century and end of century

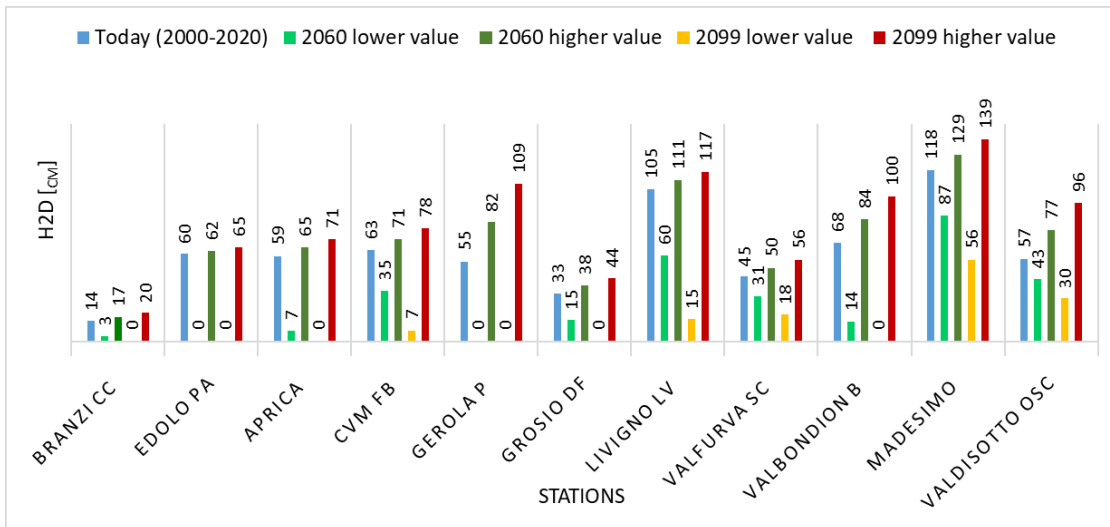


Figure 10.15: Extreme H2D average value at mid-century and end of the century.

10.2.7 H3D:

Even for the 3-day maximum annual snowfall a decrease during XXI century is detected, with the statistical significance only on the negative trend. The SSP1 2.6 scenario show a certain stationarity of the variable, while for the scenario SSP5 8.5 a reduction of about 80% of the current value is foreseen by 2099 (Figure 10.16). The reduction can be noticed also by looking at the average value at mid-century and end of the century, with one station for which a null value of H3D is foreseen by the end of the century (Figure 10.17). The variability is high again, with 7 stations for which the worst-case scenario detects null H3D value by the end of the XXI century and one stations for which the disappearance of precipitations, applying the trends deduced from the projections on this variable, is expected already by the mid-century Figure (Figure 10.18).

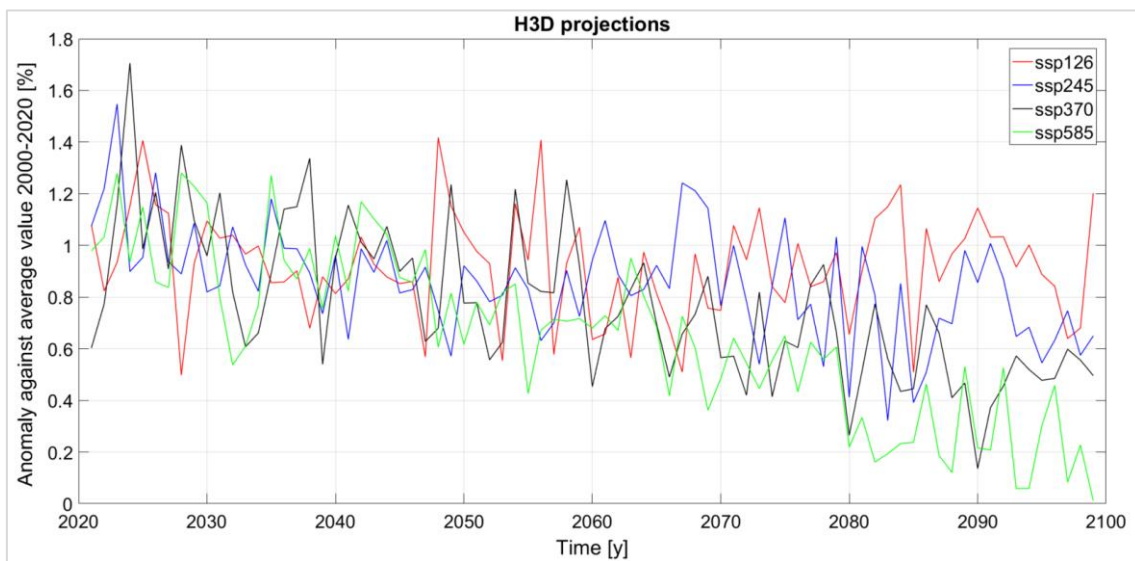


Figure 10.16: H3D XXI century projections for each SSP scenario.

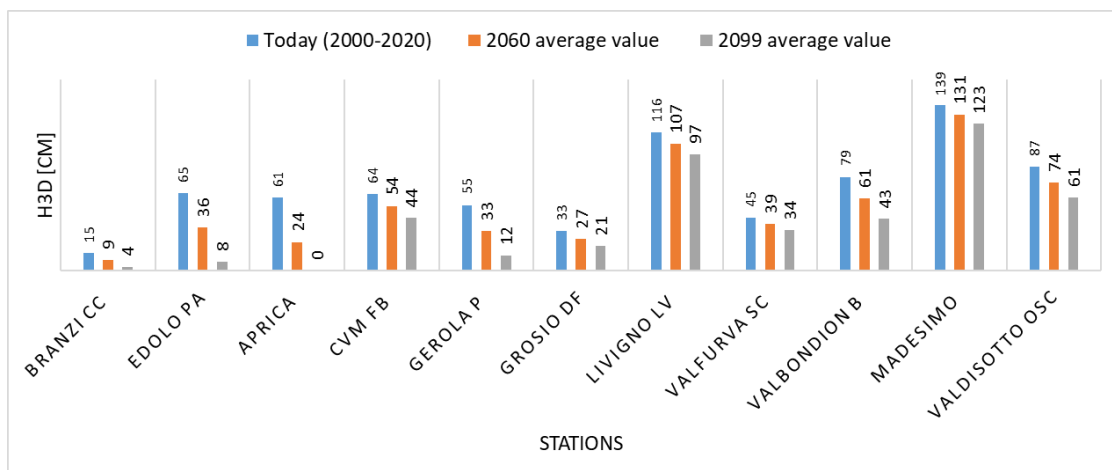


Figure 10.17: Average H3D average value at mid-century and end of century

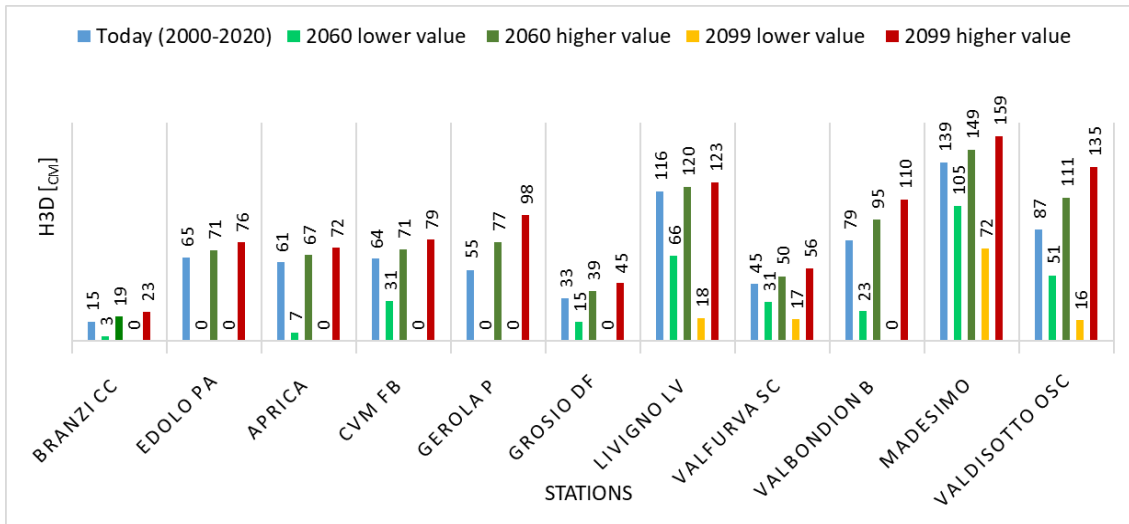


Figure 10.18: Extreme H3D average value at mid-century and end of the century.

10.2.8 HN average:

The 1-day average annual snowfall seems undergoes to a decreasing during XXI century less markedly than the others SV, with the statistical significance only on some negative trends in the worst SSP scenarios and few significant positive trends. The comparison between the various SSP scenarios projections shows a substantially long-term stationary trend, with a more marked decrease for SSP5 8.5 which leads to a reduction of 20 % by 2099, considered based on results little significant (Figure 10.19). This stationarity can be noticed also by looking at the average value at mid-century and end of the century, with a little increase foreseen for two stations (Figure 10.20). The variability between the various scenarios is high only for some stations, while for some stations there is a slight difference between the values of extreme trends, which confirms the more stationary behavior of this variable (Figure 10.21).

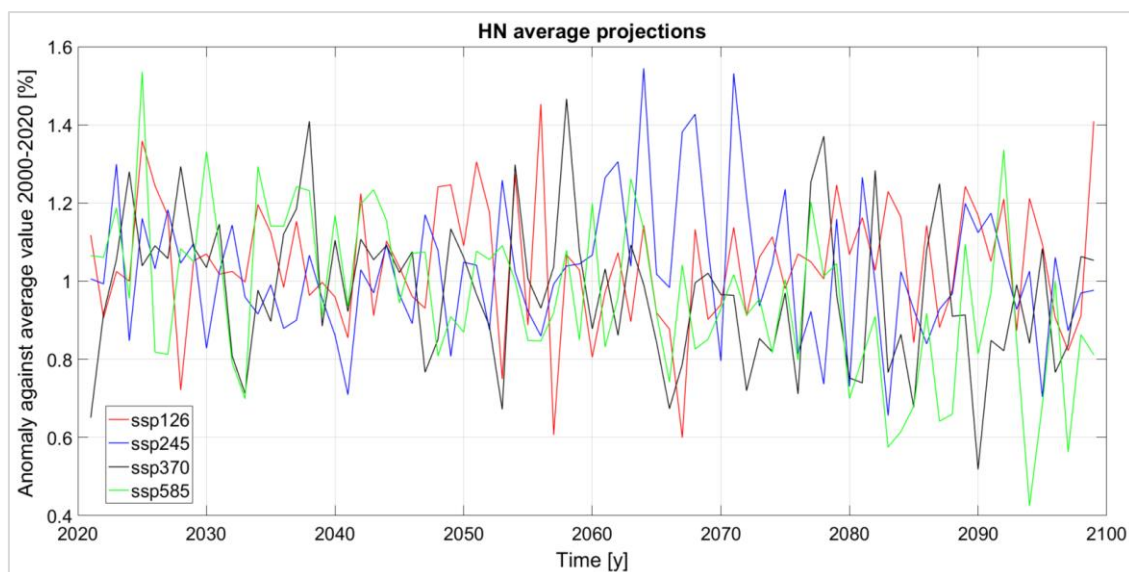


Figure 10.19: HN_av XXI century projections for each SSP scenario.

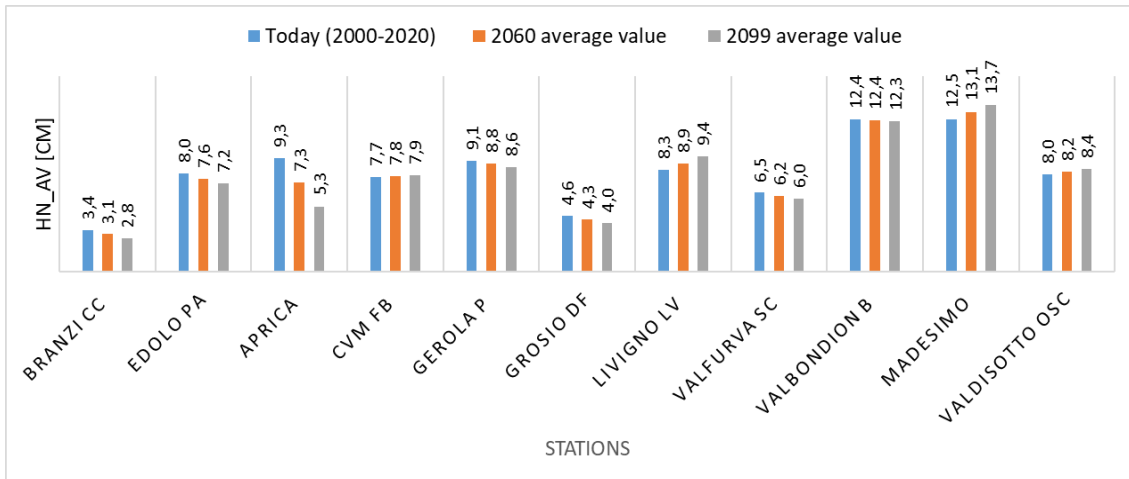


Figure 10.20: Average HN_av average value at mid-century and end of century

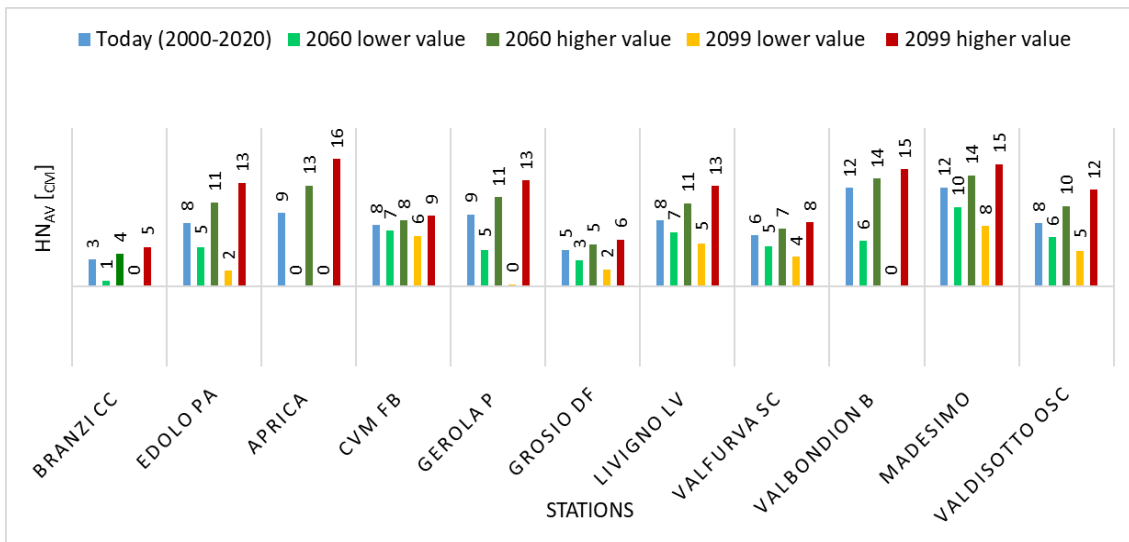


Figure 10.21: Extreme HN_av average value at mid-century and end of the century.

10.3 Temperature and precipitation results:

10.3.1 Average temperature:

The trend analysis on the annual average temperature shows agreed reused from all 23 investigated scenarios, with positive and significant trends except for the projections related to the SSP1 2.6 scenario for which the statistical significance is not present in all stations. The “XXI average projections for each SSP scenario” graphic is not provided here, as this technique is not adaptable to the temperature variable being not a volumetric quantity. The average single site temperatures foreseen at mid-century and end of the century are showed in (Figure 10.22). The variability between the various scenario is considerable (Figure 10.23), but all of them shows the same trend direction (i.e an increase of T_av during the XXI century). In Figure 10.23 the lower value and the higher value correspond respectively to the SSP1 2.6 and SSP5 8.5 scenario.

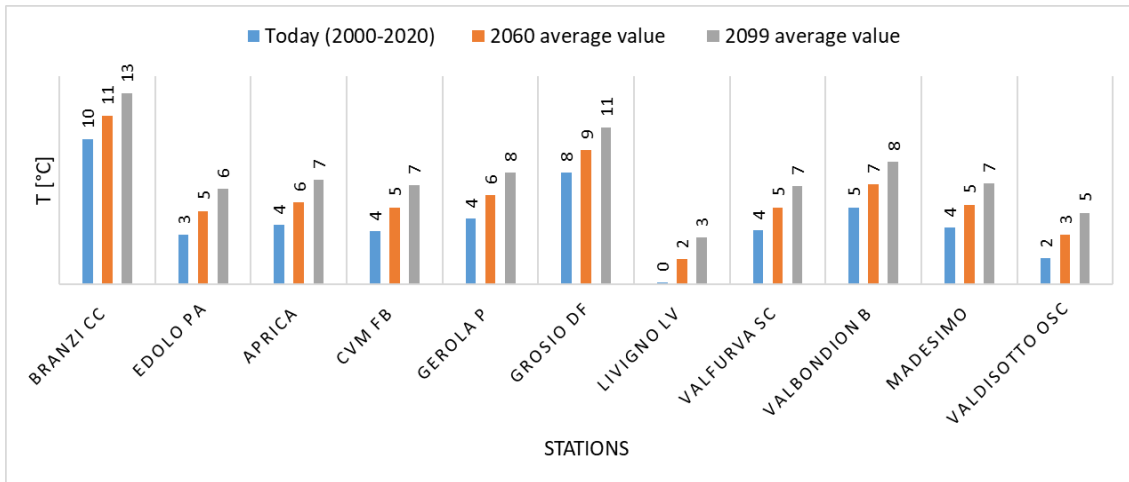


Figure 10.22: Average T_{av} value at mid-century and end of century

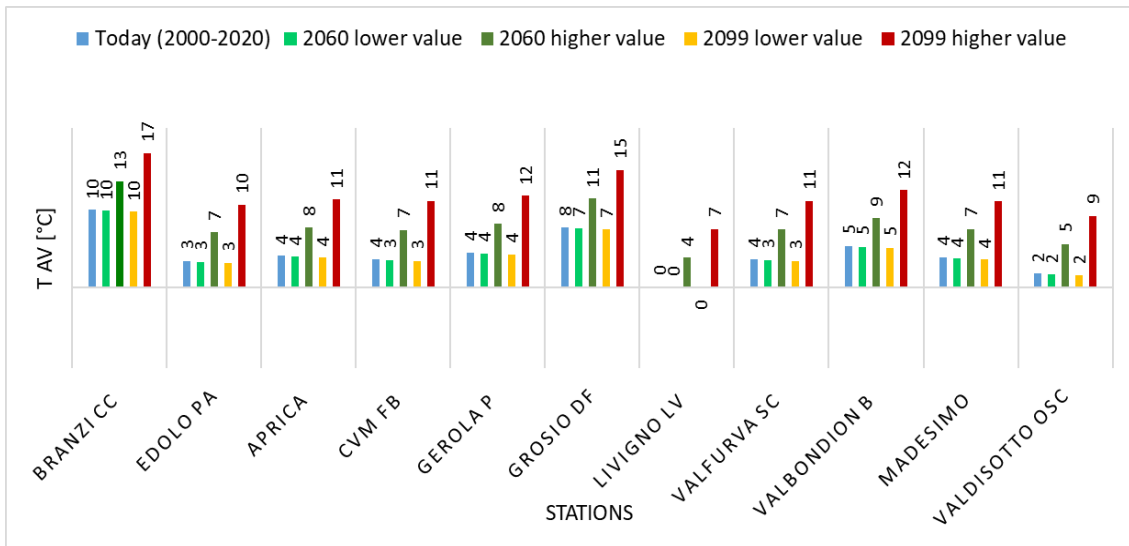


Figure 10.23: Extreme T_{av} average value at mid-century and end of the century.

10.3.2 Precipitation:

The trends are less marked than for the other investigated variables and statistical significance is present only in few cases, on both positive and negative trends. In general, as one can see in Figure 10.24, each SSP scenario projection seems to be stationary by the end of the century, showing a moderate local variability and a long-term stationarity.

The stationarity behavior of the precipitations is confirmed by the average value foreseen at mid-century and end of the century (Figure 10.25). Looking at (Figure 10.26) it is possible to appreciate the moderate variability between the various scenarios, with the two extreme scenarios forecasting a moderate reduction (for the lower trend) and a moderate increasing (for the higher trend). This is particularly valid for some stations (like Valgerola Pescegallo, one of the rainiest locations) and less significant for the others.

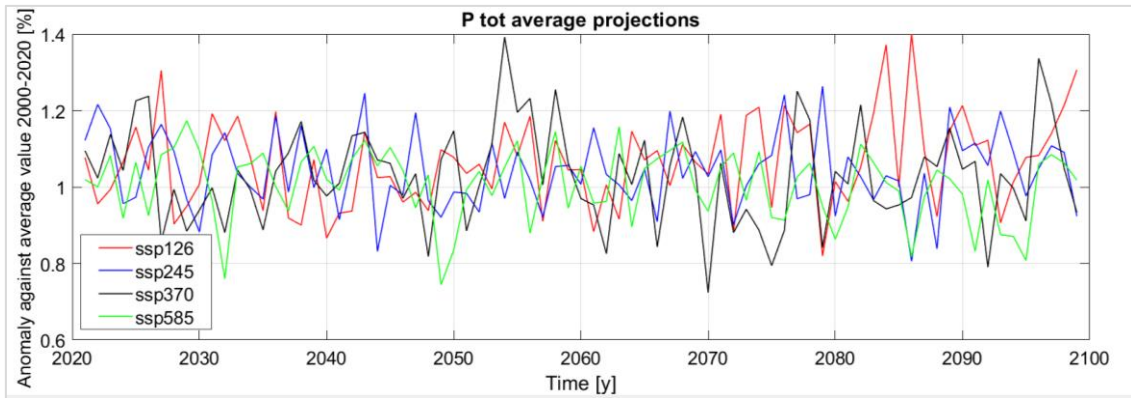


Figure 10.24: P_{tot} XXI century projections for each SSP scenario.

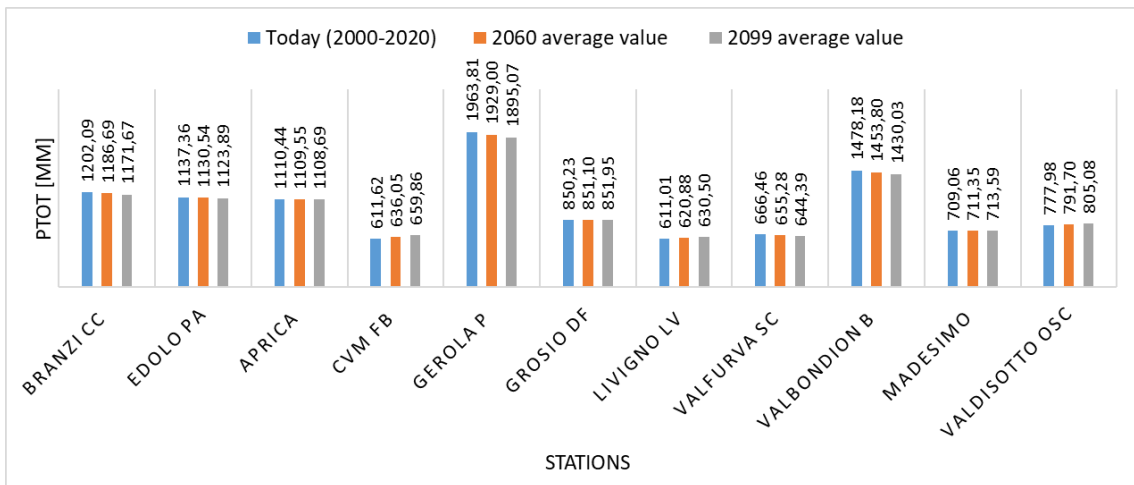


Figure 10.25: Average P_{tot} value at mid-century and end of century.

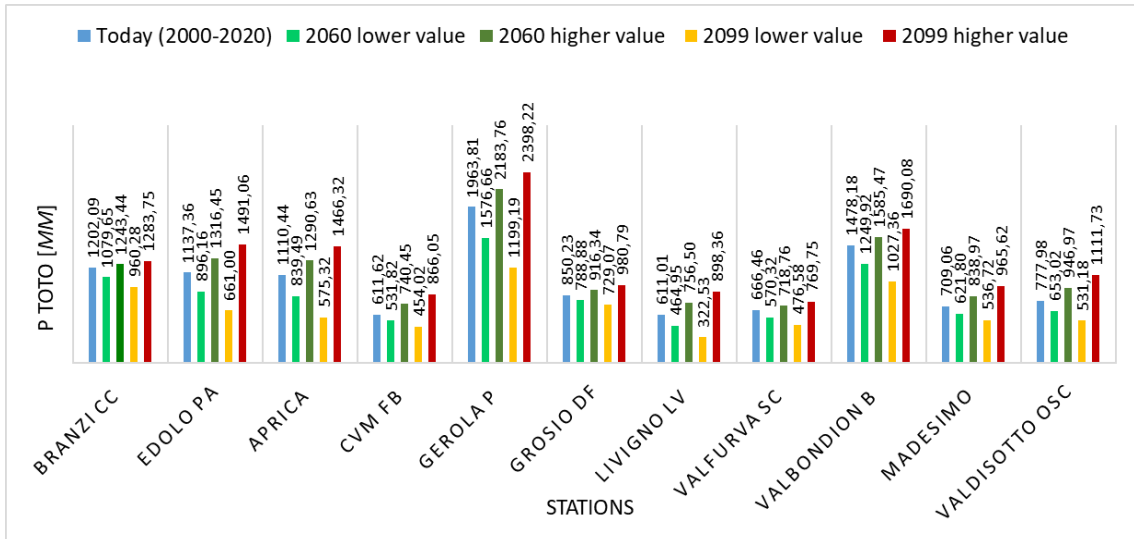


Figure 10.26: Extreme P_{tot} value at mid-century and end of the century.

10.4 Comments of the results

As done for the historical series analysis, once the outputs are listed the results must be discussed and interpreted. It's important to mark that, given the nature of the models used in this assessment, the described behavior must be taken only as a forecast, useful to understand the possible different scenarios that the alpine society might undergoes during the next years.

10.4.1 Temperature and total precipitation:

While all the investigated models seem to confirm a significant general increase of the temperature during the XXI century no trend can be foreseen for the total precipitation on the Lombard Alps area. The temperature increase can be quantified considering the average between the significant trends of the 23 scenarios in $+ 3/4$ °C by the end of the XXI century, so 0,04 °C/y. Considerable difference in the foreseen temperature value can be reached based on the different SSP scenarios, with basically a steady state for the SSP1 2.6 and an increment of 3 °C by mid-century and 7°C by the end of the century in the SSP5 8.5 scenario (Figure 10.23).

The average annual precipitations seem to be stationary whatever socioeconomical path the human society will take, as you can see in Figure 10.25. Some scenarios forecast increasing or decreasing for this variable but the statistical significance is rare, allowing to affirm that no certain behavior is forecasted for this variable.

10.4.2 Snow:

All the investigated SV, here considered representative of the snow conditions of the studied areas, seems to decrease during the XXI century with all the consequences associated described in chapter 1.1.

Despite the general evidence, the feasible scenarios seem to be very different, in terms of magnitude and severity of the phenomenon, based on the different SSP considered. The choices that human society will undertake over the next few years seem to be the main factor that drives the presented projections. Furthermore, the very concept of Shared Socioeconomic Patterns draws attention to the fact that the achievement of a more, or less serious scenario will not depend on local choices but on a common effort provided at global level.

The importance of concrete and immediate actions in response to climate change is extremely evident by observing the values reached by projecting the SV respect to the various SSPs. These results are summarized in Figure 10.27 and Figure 10.28, where the percentage residual value foreseen at mid-century and end of the century according to the various SSP scenarios are provided (the results are obtained averaging the GCM scenarios for each SSP scenario).

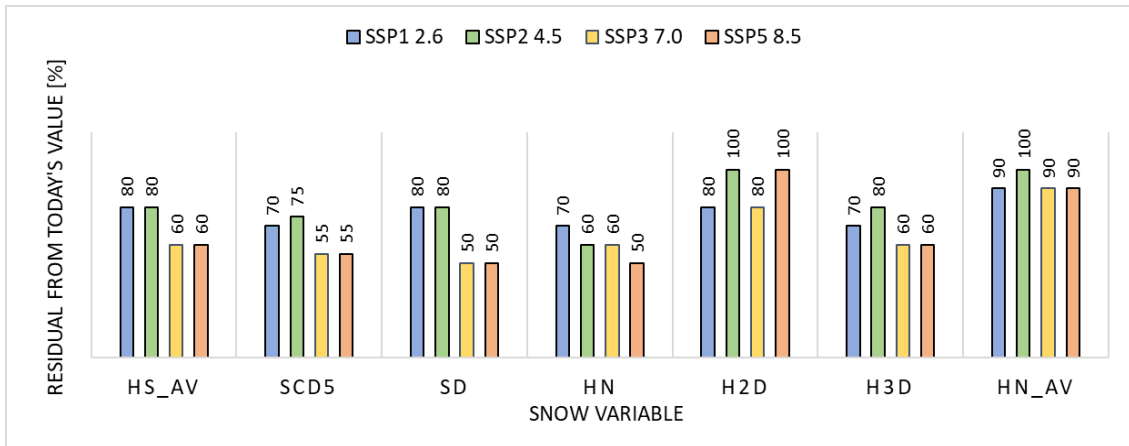


Figure 10.27: % residual reached at mid-century (2060) in the various SSP scenarios.

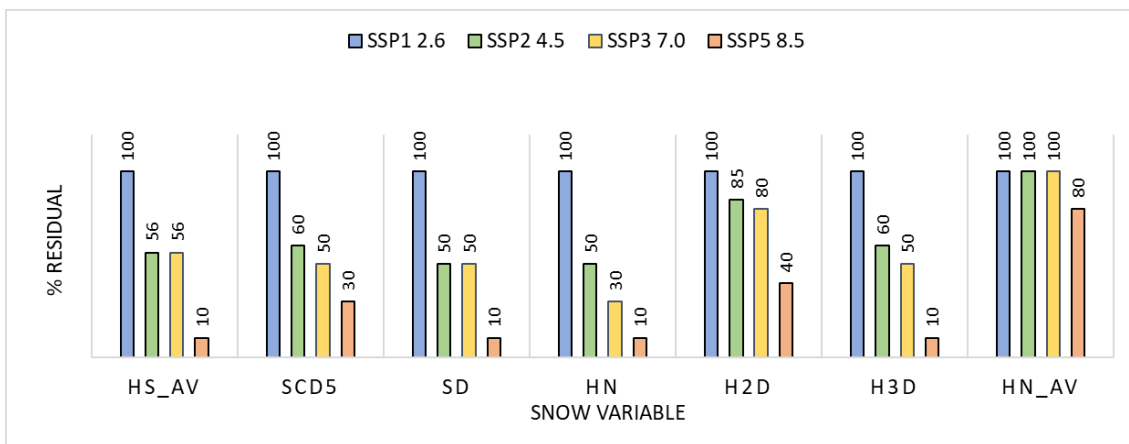


Figure 10.28: % residual reached at the end of the century (2099) in the various SSP scenarios.

The worst case is due to SSP5 8.5 scenario. If global society fossil fueled development occurs, ground snow cover (volume and durations) and snowfalls will be greatly compromised. Generally, you might have a reduction of the 90% in SCD5, HS average and maximum annual snowfalls. The average 1-day snowfall (HN average) is expected to decrease by only 20 %. Looking at average value reached at mid-century and end of the century (reported in the previous subchapter it's possible to hypothesize the snow disappearance for above 54 % of the stations investigated by 2099, while for above 18 % of them this condition could already be reached by 2060.

The response of the intermediate SSP scenarios (SSP2 4.5 and SSP3 7.0) is less catastrophic. If middle of the road scenario or regional rivalry ones occurs is expected a reduction by the end of the century of around 50 % for the SV investigated except for the HN average, for which long-term stationary is reported.

The SSP1 2.6 seems to be the only scenarios for which a significant reduction could be avoided. If sustainability development occurs the maintenance at the end of the century of values like those today seems to be feasible. It's also important to notice that according to this scenario there will be a general

reduction of the variables by mid-century (2060) but with a recovery in the following years until the re-establishment at the end of the century of today's values. This result is considered important, since means that with the SSP1 2.6 scenario it may be possible to cope the problem of climate change.

As already pointed out the results reported in figures are illustrative of the importance of Shared Socio-economic Pathways to which the society will undergoes, as a results of shared global choices.

In conclusion, the results obtained shall not be interpreted locally but as a general behavior which could likely applied at the entire Alpine chain, having this region characteristics like those of the portion under study.

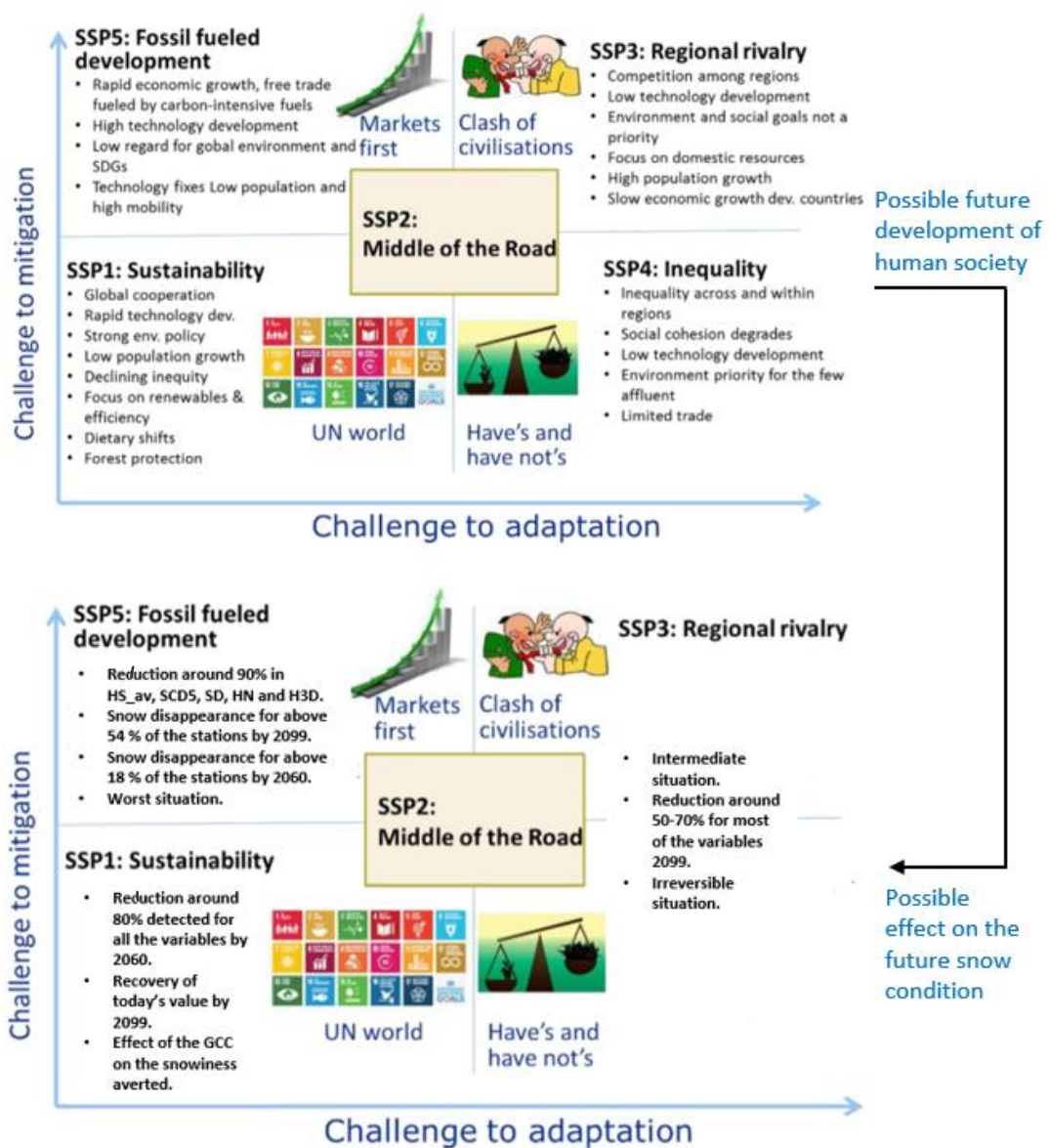


Figure 10.29: Summary of the SSP scenarios effect on the future snow conditions of the Lombard Alps.

11. ANALYSIS OF THE PRINCIPAL HAZARDS INVOLVED.

In the previous chapter the future snowiness regimes in the Lombard Alps have been investigated, giving a detailed description of the possible future scenarios concerning the different Snow Variables. The scenarios investigated seem to agree on a general decrease in the amount of snow on the ground in the area, the snow cover duration and the precipitation in solid phase. This phenomenon, associated with a general and significant increase in temperatures in all the stations, seem to occur with a substantial stationary behavior of the total precipitation.

As one can see in Chapter 1.1 (Snow is life), snow, with all the associated dynamics, is a source of life for human society and the environment, being extremely influential in the health, environmental and economic fields.

Starting from the information in Chapter 1.1, summarized in Figure 11.1. (here reported for convenience), and based on the results obtained in Chapter 10, the main practical effects on society and the environment are here analyzed.

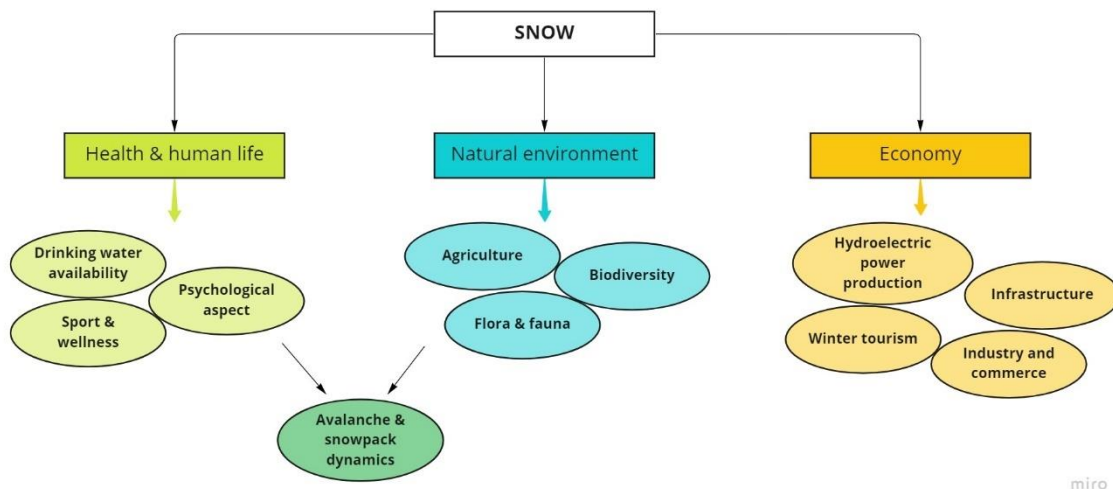


Figure 11.1: Factors affected by snow cover extent, duration, and dynamics.

In this chapter the main hazards chained to the general decrease in the snowiness are analyzed. These hazards are proposed based on the effect that snow has on various field together with the results obtained in the multi-scenario projections analysis and are seen as a new challenge that modern society must face during the current century.

11.1 Hydrological hazard

For more the 1/6 of the earth population seasonal snow cover constitutes a fundamental water reservoir, released gradually and when it's more needed by the people and the environment, irrigating the fields and responding to water demand.

In the studied area, this demand is particularly high in the most inhabited and cultivated areas of the valley floor. Downstream of the Lombard Alps is the Po Valley, which is one of the most inhabited, industrialized and cultivated areas of Italy, in which the water supply mainly depends on the streams that comes from the Alps.

The period of greatest water demand is the late spring and summer, in response to increased demand for drinking water but especially due to the flora and agriculture request, since plants are in the heart of the growing season.

11.1.1 The role of the snow in the hydrological cycle

To show how the winter snowfall on the Alpine compartment affects the availability of water released to the environment during melting the linear regression between the average annual snowpack height and the spring peak flow rate of two Lombard River is performed.

The rivers on which the analysis is carried out are the Adda and the Mallerio. These rivers are of different hierarchical order and respectively define a basin and a sub-basin of the same.

The discharge data are obtained from the water level measured with daily resolution by applying the stage-discharge relationship. The closure sections considered are in Sondrio for the river Mallerio and at the confluence in Lake Como for the river Adda (Fuentes), as you can see in Figure 11.2. The dataset is recovered in (ARPA Lombardia, 2021).

After plotting the discharge data, a 30-day moving window average is performed to see better the flow regime. The use of the moving average is considered to be a better approach for the detection of flow peaks than a static average, since the flow peak due to the snow melting are not sharp peak like those of the rain but more distributed over time. The moving window average allows to smooth the local peaks to identify those of greater temporal amplitude, in this case monthly.

In Figure 11.3 is possible to see a portion of the Adda historical discharge series in the Fuentes section. Thanks to the 30-days moving window average is possible to appreciate the presence of two peaks, one in late spring and one (less marked) in autumn, typical of a Pluvio-Nival river regime.

The same graphic is reported for the Mallerio in the Sondrio section (Figure 11.4). In this case it's possible to appreciate how the autumn peak isn't present in every season, indicating a more nival river regime.

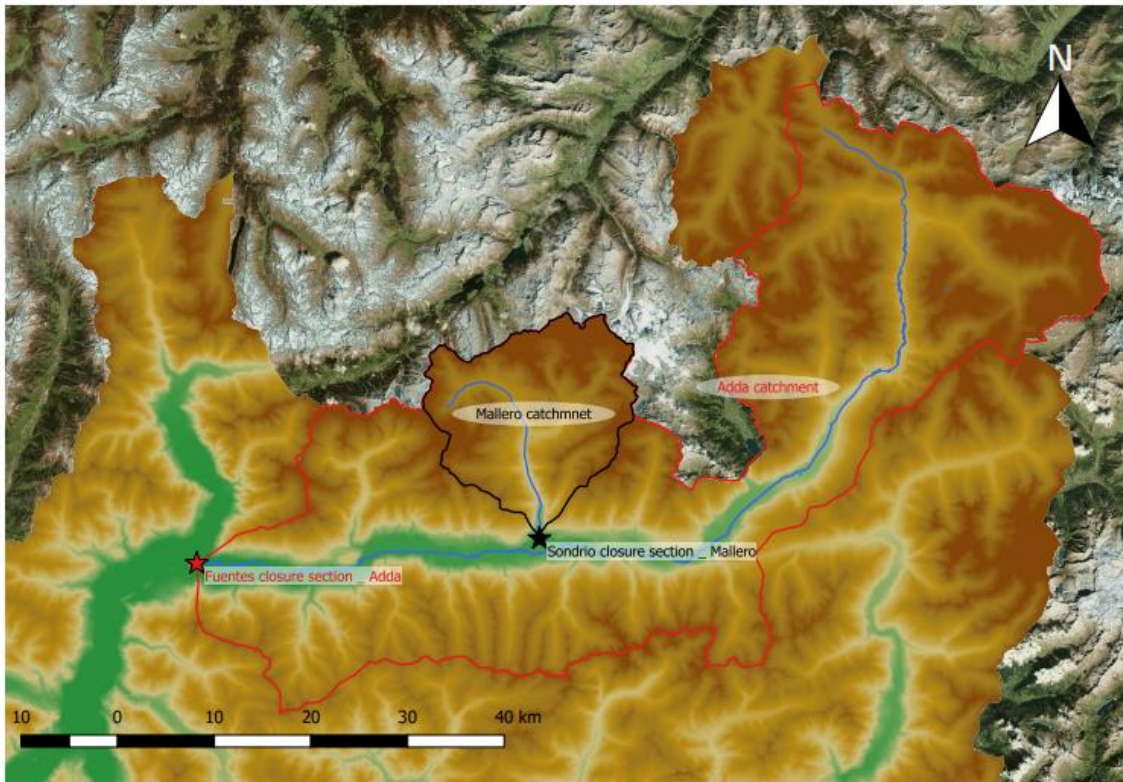


Figure 11.2: Spatial framework of the investigated river sections and relative catchments.

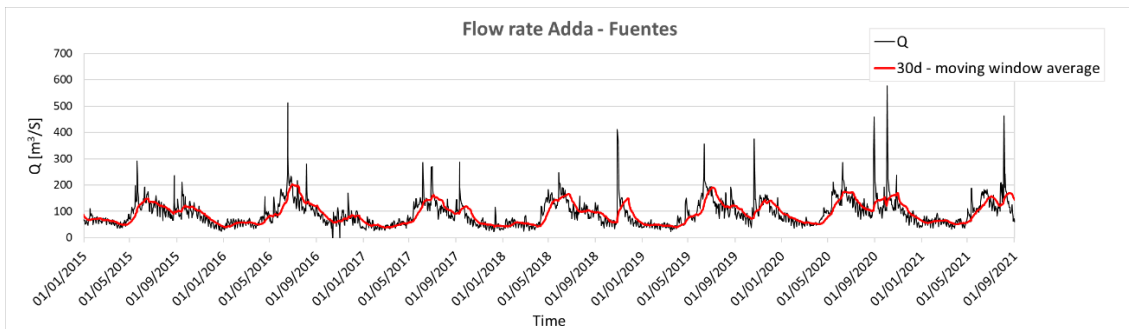


Figure 11.3: Portion of the historical flow rate of the Adda in the Fuentes section.

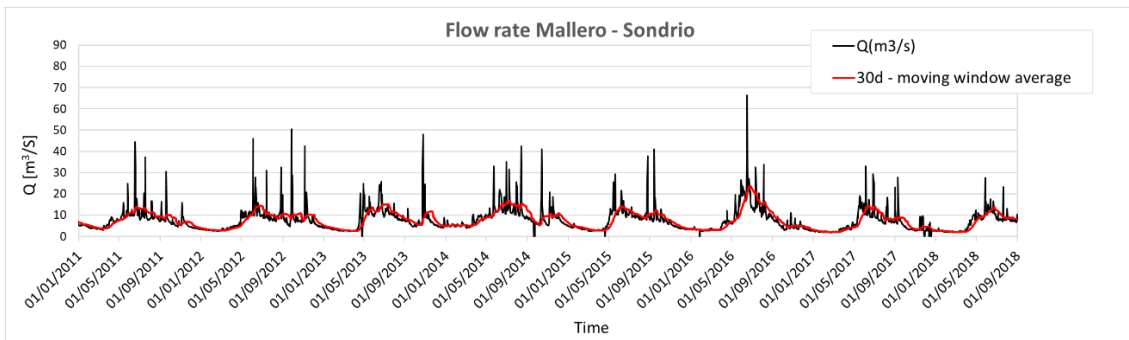


Figure 11.4: Portion of the historical flow rate of the Mallero in the Sondrio section.

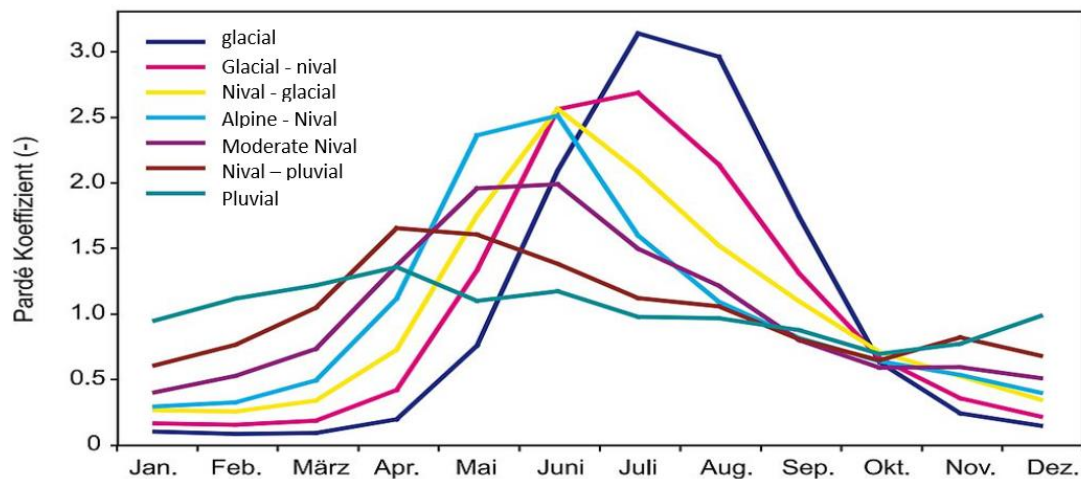


Figure 11.5: Relative runoff regime during the year for catchment zones at different altitudes. The Parde' coefficient is the quotient of the mean monthly runoff and the man annual runoff (WSL Institute for Snow and Avalanche Research SLF, 2022).

The linear regressions performed between the spring river peak flow rate and the average seasonal snowpack depth (HS_av) are showed in Figure 11.6 and Figure 11.7. The considered periods depend on the stage-flow relationship, unfortunately available only since 2002 for the Adda river section and since 2013 for the Mallero ones. HS_av is computed averaging the annual value of the measured stations inside the catchment defined by the considered closure sections.

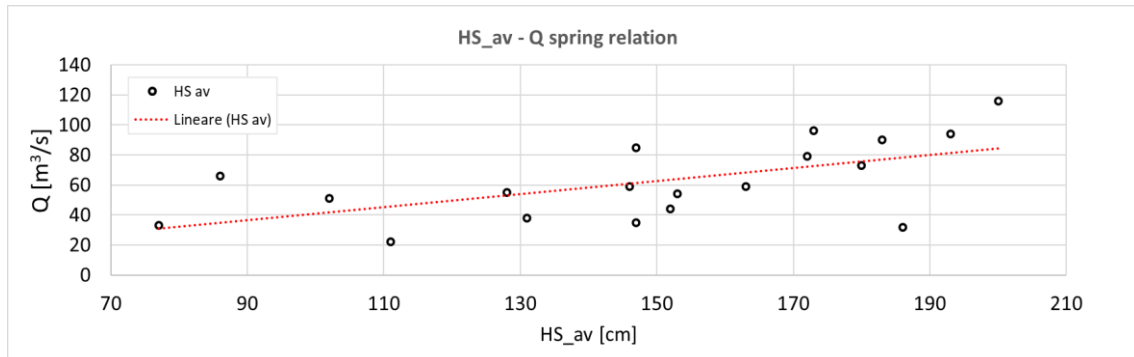


Figure 11.6: Linear regression between Adda spring peak flow rate and HS average.

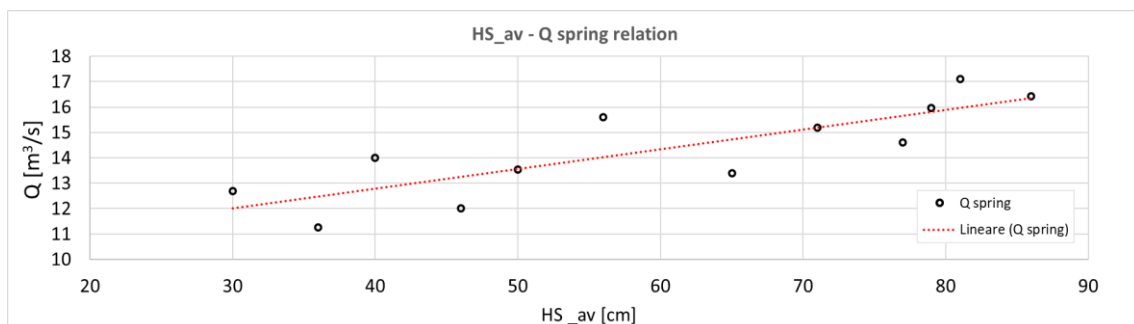


Figure 11.7: Linear regression between Adda spring peak flow rate and HS average.

The correlation, evaluated with the parameter ρ -spearman is significant, with P value = 0,043 for the Mallero river and P value = 0,023 for the Adda river. The regression is statistically significant both for the Adda river, P value = 0,0072, and for the Mallero river, P value = 0,00096. All these results consider the common significance threshold value of P value < 0,05.

In both cases the spring river peak runoff increase with the seasonal snow average depth, exemplifying for the study area the importance of the seasonal snow cover in the water availability during the melting period. Given the small number of the two samples, the entity of the trend is not reported.

11.1.2 Expected impact of climate change

In a warmer world, less winter precipitation falls as snow, and the melting of winter snow occurs earlier in spring. Even without any changes in precipitation intensity, both effects lead to a shift in peak river runoff to winter and early spring, away from summer and autumn when demand is highest. Where storage capacities are not sufficient, much of the winter runoff will immediately be lost to the oceans (Barnett T., 2005).

In the Lombard alps, a general decrease of the snowiness conditions (in particular the average annual snowpack depth, HS_av, and the seasonal snow cover duration, SCD5) are foreseen by the end of the XXI century, while the total precipitation regime is expected to be stationary (see chapter 10). This confirms the effect described above and focuses on a new potential hazard.

The stationarity of the total precipitation, which is remembered to be composed by the precipitation both in the liquid and solid phase, together with the general decrease in snow means that during the winter season snowfall will be increasingly replaced by rainfall, which water input (were not stored in the ground) will be lost instantaneously. During the late spring and summer season there will therefore be an increasing water shortage, to which modern society will have to cope with appropriate and urgent mitigation choices.

11.2 Avalanche hazard

Avalanches are one of the main hazards that interest the mountainous areas during the winter season. To understand the magnitude of the phenomenon, taking for example the season 2020/21, 130 people died in an avalanche accident throughout Europe. Figure 11.8 represents the historical course of the European avalanche fatalities, together with the 10-years moving window average (EAWS, 2022). The EAWS validates the data just from 1970.

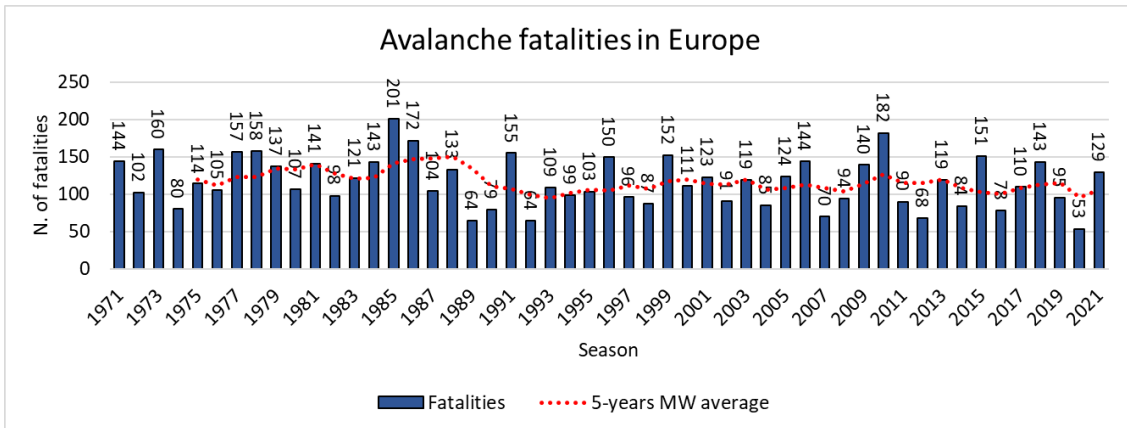


Figure 11.8: Historical series of the European avalanche fatalities.

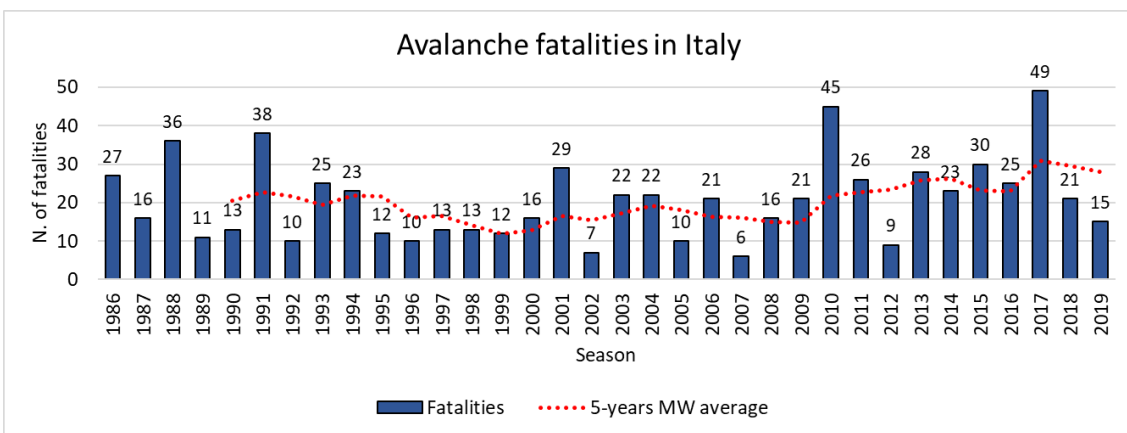


Figure 11.9: Historical series of Italian avalanche fatalities.

In this chapter is briefly discussed how the results presented in chapter 10 could affect this complex (and still not completely understood) phenomenon. Mainly, avalanche accidents involve people who frequents avalanche terrain for recreationist porpoises (i.e. hikers, skiers, snowmobilers, mountaineer...), nevertheless avalanche is an hazard that can involve infrastructure and villages.

11.2.1 Avalanche types and avalanche problems

Avalanches are subdivided based on their dynamics and main features in:

- Loose snow avalanches (wet or dry)
- Slab avalanches (wet or dry)
- Gliding avalanches

The slab avalanches are the most dangerous for people that travel in avalanche terrain, they can release naturally but in most of the cases are human triggered at any point within or even outside (in case of remotely triggered avalanches) the perimeter of the slab. These avalanches are responsible for more than 90 % of the deaths that occur in avalanches (WSL Institute for Snow and Avalanche Research SLF, 2022).

In addition, the EAWS defines the following avalanche problem, that basically describe typical situations, how they occur in the terrain and how they can support both avalanche forecasters and backcountry recreationists in their assessment of the avalanche danger (EAWS, 2022). The avalanche problems are the following.

- New snow
- Wind drifted snow
- Persistent weak layers
- Wet snow
- Gliding snow

The presence of one or more avalanche problem can lead to one of the different types of avalanches listed above. In example, the predisposing causes of a dry slab avalanche are the presence of a cohesive slab (soft in case of new snow deposit or hard in the case of wind drifted snow deposit) overlapped to a weak layer, that is a layer with lower cohesion and lower mechanical properties. The worst case is the presence of persistent weak layers that are composed of faceted crystals, embedded surface hoar or depth hoar. This avalanche problem is hard to detect if not by studying the history of the snowpack in the days leading up to the hike or making a stratigraphic profile. In aid to the difficult understanding of the snowpack safety conditions there is the avalanche bulletin, issued by the competent authorities in all developed countries affected by this type of hazard.

11.2.2 Expected impact of climate change

To better understand the concept proposed in this subchapter it's possible to refer to the theoretical hints in chapter 2.

According to (Strepazzon G., 2021), avalanche activity will decrease in spring and at lower elevations but increase at higher elevations in winter because of more favorable conditions for wet-snow avalanches earlier in the season. The future slab avalanches behavior is less clear, but it will probably grow as a result of the increasing of sudden thermal changes, especially in the winter season. Avalanches in general will involve more and more wet snow, that is heavier, increasing the danger in the case of burials and making Search and Rescue operations more complex.

The results obtained in this study shows a general decreasing of the snowiness in the studied areas, together with a significant increment of the temperature and a stationary total precipitation regime. The past year trend assessment allows to appreciate how much these changes are already underway, with a less clear behavior at higher altitudes, where an increase in the annual average snowpack depth in the past 30 years is observed.

With substantially stationary total precipitations and rising temperatures, wet snow avalanches (i.e., gliding avalanche, wet snow slab avalanche, loose snow wet avalanche) will become more and more frequent, especially in winter. These

avalanches cause only less than 10 % of avalanche victims, but can evolve into catastrophic avalanches, with high impact pressures (and therefore destructive power), high stopping distances and risk of infrastructure involvement. This type of avalanche, above the tree line, is currently common in spring while in winter it is almost exclusively associated with the sunniest aspect. Thermal changes can have a great impact on this aspect, making this type of avalanche increasingly frequent in the winter season and at all exposures.

The forecasted snow cover duration and average snowpack depth decreasing will certainly result in a long-term decrease in the number of large spontaneous avalanches, but no effect can be predicted with certainty about the danger to mountain dwellers and the number of accidents. As mentioned above, 90 % of avalanche victims are due to slab avalanches, which result from the complex snowpack structure as well as the complex interaction between snowpack and weather.



Figure 11.10: Dry snow soft slab avalanche observed and studied personally in Sisimiut - Greenland west coast (15-03-2022).

The release dynamics of the slab avalanches involves the presence of a cohesive slab overlapped to a weak layer, in which the collapse can be induced by an overload (natural or artificial). As presented in chapter 2.3.2, the formation of persistent weak layers results mainly from a type of metamorphism driven by the thermal gradient inside the snowpack. A thinner snowpack can lead to higher

gradients, and it is therefore not possible to predict a decrease of this hazard because of a general snowiness decrease in an area.

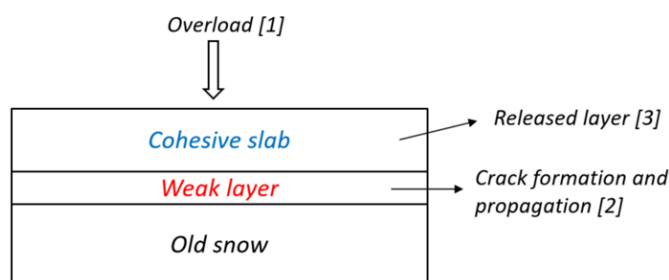


Figure 11.11: Sketch representing slab avalanche dynamics.

To demonstrate that there is no correlation between the annual average snowpack depth (indicative of the snowiness of a season) and the number of avalanche accidents in the Lombard Alps, a linear regression between these two variables is performed. The avalanche accidents data refer to all avalanche accidents recorded within the Lombard Alps area (AINEVA, 2020).

The linear regression, showed in Figure 11.13, is not significant (P value = 0,095), and no correlation is identified between the two variables (P value on ρ -spearman $> 0,05$).

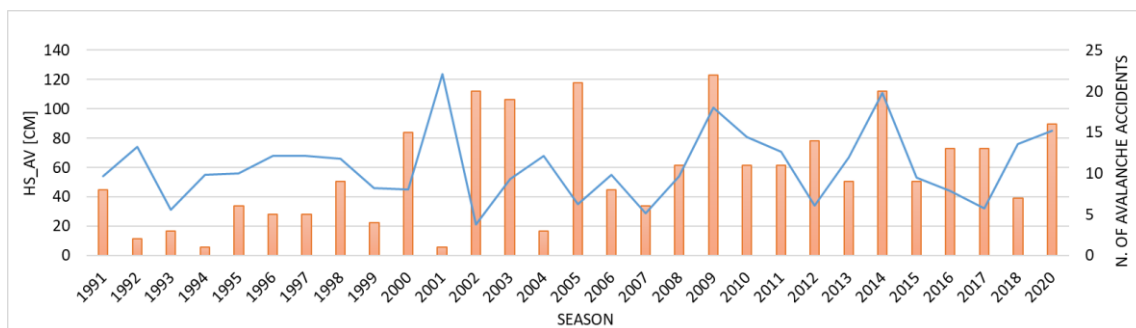


Figure 11.12: Avalanche accidents recorded in the Lombard alps and average annual snowpack depth.

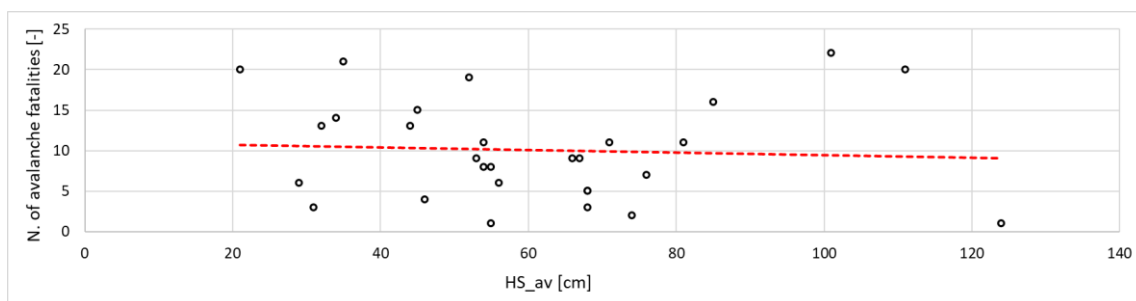


Figure 11.13: Linear regression between the N. of avalanche fatalities and HS_av in the Lombard alps.

In several studies, the annual maximum 3-day snow fall depth H_{3D} is often adopted as an input for avalanche hazard mapping procedure (Daniele Bocchiola,

2006). However, 90% of avalanche fatalities are due to human triggered slab avalanches and there is no scientific evidence about the correlation of these and H3D, strongly related to other types of avalanches, triggered by the new snow.

Most of the considered scenario foreseen a decreasing of H3D during the following century, that will lead to a decreasing of the big new snow avalanche event. Despite this, for some scenarios, an increasing is detected. In particular, using the *MPI-ESM-ECHAM6.3* GCM projecting the *SSP1 2.6* scenario a general average trend between all stations of +0,0525 cm/y is detected.

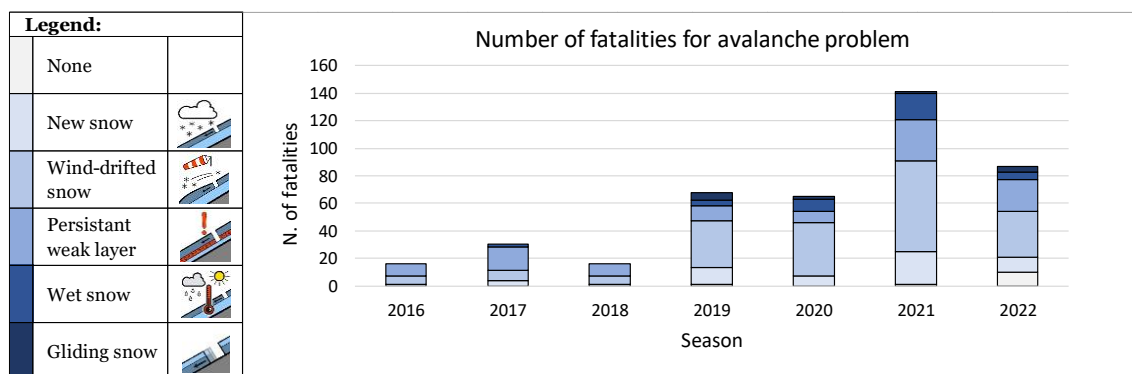


Figure 11.14: Avalanche fatalities per avalanche problem.

Figure 11.14 represents the number of avalanche fatalities for each avalanche problem, in the last 7 seasons (EAWS, 2022). As you can see the avalanche problem that led to the greater number of fatalities is 'Persistent weak layer' followed by 'Wind-drifted snow'. These are the two avalanche problems that mainly characterize the slab avalanches.

The avalanche problem 'New Snow', that is related to new snowfall, seems to be less dangerous, allowing to remark that there is no evidence that with a general decrease in the snow condition the number of avalanche fatalities will decrease.

11.2.3 Effect of the surface warming on slab avalanche release

In the article (Reuter B., 2012) is demonstrated that the snow surface warming increases the instability of a snowpack predisposed to slab avalanche release.

This phenomenon has been personally observed on several occasions during the study of the snowpack evolution in Sisimiut - Greenland to develop a local avalanche forecasting system. In Greenland, several slab releases (natural and human triggered) were registered after abrupt temperature increases from very low to near zero temperature. As well as the avalanche evidence, thanks to daily stability test on the arctic snowpack a worsening of the stability indexes with warmer conditions were documented.

The idea is that the surface warming (which can be of thermal or radiative origin) heats up the eventual wind cohesive slab, which change its mechanical properties (strongly related to temperature). As an example in Figure 11.15 is reported a the results obtained in (Mc Clung D.M., 1999), for which the temperature of the slab

involves a change in the theoretical stress distribution under a skier, explaining the frequent slab avalanches releases in warming surface condition also from a physical point of view.

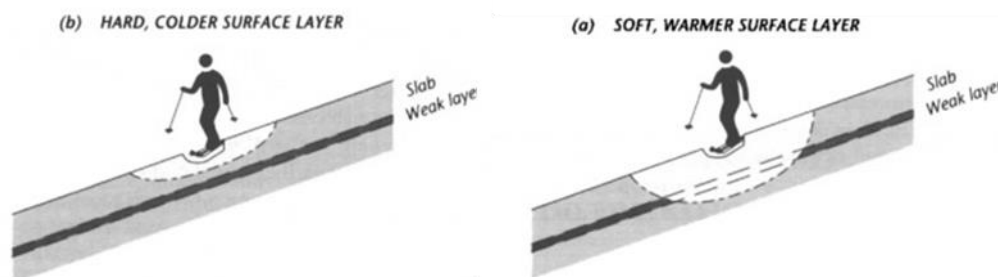


Figure 11.15: Theoretical stress distribution under a skier in warmer and colder slab.

This predisposing factor for slab avalanche release is also present in the Alps (Reuter B., 2012). In a warmer world, with the temperatures foreseen in the proposed possible scenarios, abrupt thermal change will be more frequent (especially during the cold season and at ever higher altitudes). This justifies the need of better understanding of this behavior, and possibly quantify the increasing danger.

12. CONCLUSIONS

12.1 Main results obtained in the study

Both the past and the future years trend assessments confirm a general decrease in the snow conditions of the Lombard Alps areas, together with a significant increase of the temperature and substantially steady total precipitation.

The current situation is highlighted by the past year trend assessment. Due to the significance of the results obtained in the analysis carried out for altitude belts, the elevation is considered the main morphological parameters that affect the variables behavior. In the last 30 years the temperatures have increased everywhere, but without leading to positive annual average value in the Alpine belt (about from 2000 m asl). Since for the total precipitation no significant negative trend is detected, this effect is believed to be responsible to the significant increase in the average annual snowpack depth (HS_av) in this altitude belt. Significant decreasing in HS_av, together with a significant decrease in the snow cover duration (SCD5) and daily average snowfall (HN_av) are detected at the lower elevations (Hilly belt, about up to 700-1100 m asl). HN_av is significantly decreased also in the Mountain belt (about up to 1200 – 1600 m asl). The snow variable behavior of the intermediate belts (Mountain and Subalpine) is generally non-significant, with certain behavior just for some single sites. Despite this, a significant correlation between some snow variables and the NAO teleconnection winter index is highlighted in these belts, confirming a general snow decrease related to winter with NAO+ phases. Regarding the seasonal analysis, the snow variables related to the snow on the ground (HS_av and SCD5) have decreased more in spring, while the ones related to precipitation (HnD, SD, HN_av) have decreased more in fall.

The future years trend analysis allow to understand the possible future development of the Lombard Alps snow conditions with respect to the forecasted climate change. Of particular interest, among the obtained results, is the difference in the expected effect based on the various Shared Socioeconomical Pathways scenario (SSPs). The SSP1 2.5 (Sustainability) will lead to a temperature increasing and snow decreasing until 2060, with a subsequent restoration of the current conditions by the end of the XXI century (2099). This means that if the world shifts gradually, but pervasively, toward a more sustainable path, emphasizing more inclusive development that respects perceived environmental boundaries, the effect of the GCC on the snow conditions of the areas under study will be managed. The SSP5 8.5 scenario (Fossil fueled development) is the worst ones and will lead to a reduction of about 90% in HS_av, SCD5, SD, HN and H3D by 2099. If the world places increasing faith in competitive markets, innovation and participatory societies to produce rapid technological progress and development of human capital as the path to sustainable development snow disappearance will be observed for 18% of the

investigated stations by 2060 and 54% by 2099. The change will be irreversible also for the two intermediate SSPs scenarios (SSP3:Regional rivalry and SSP4:Inequality). In general, with SSP2 4.5 and SSP3 7.0 a reduction around 50-70% for most of the investigated snow variables will be observed by 2099. As regards the total precipitation no significant change is detected in the area with this multi-scenarios analysis.

To better understand the results obtained, please refer to the two sketches made for the past year trend assessment (Figure 7.35) and future year trend assessment (Figure 10.29).

The effect of the detected change in the snow conditions of a mountain area such the Lombard Alps on the natural environment will be severe. The importance of seasonal snow accumulation as a water reservoir for the downstream environment as well as the effects on avalanche hazard are discussed. A general snow reduction, together with a substantial steady precipitation regime will lead to a shift in peak river runoff to winter and early spring, away from summer and autumn when demand is highest. Where storage capacities are not sufficient, much of the winter runoff will immediately be lost to the oceans. The effect on the avalanche are more difficult to predict, and since above 90% of avalanche fatalities are due to slab avalanches, less reliant on big snowfall and great snow amount, no decreasing of this complex phenomenon can be ascertained. Wet snow and gliding avalanche are expected to increase especially in the winter/early spring period, due to temperature increase that will lead to an increasing in the snow threshold altitude. The slab avalanche behavior is then discussed based on literature scientific pepper and the experience acquired during 5 months of snow monitoring in Greenland west coast. Recent evidence demonstrate how the slab avalanche release is influenced by the snow surface warming, which is expected to increase.

12.2 Main limitation encountered in the study

The main difficulties encountered in the study are due to the lack of data. Snow automatic measurements stations are present in the Lombard Alps area since early '90s, and even if the measuring network has been improved in the years there are still not equally distributed on the territory. In particular, the data deficit is greater at lower and higher altitude (Hilly and Perennial Snow belt) and in the Prealpi Lariane mountain region. Maintaining measurement stations at high altitudes is certainly not easy and it should be said that the measurement network has been greatly expanded in recent years. This means that more data will be available in future.

Always regarding the lack of data is difficult to reconstruct the historical river discharge since the stage-discharge relationship are available just for few periods and in few river sections.

It is believed that many of the problems encountered will be solved in the years to come, also due to the continuous sophistications of the available models.

12.3 Possible future development of the study

The study carried out in this thesis work can be updated in the future years and easily extended to others alpine regions, given the similarity of the climatic and morphologic parameters of the area.

The future updating of the work is fundamental given the climate change velocity; for this reason the calculations are implemented in Matlab environment. This point is fundamental for the progress in the present research, as the updating of the database with future new recordings together with the availability of new stations will lead to greater accuracy both in the historical analysis and in the climatic projections.

With regard to future projections, it can be noted that the quality of the results depends both on the GCM models used, for which a continuous evolution and precision of calculation is expected, and on the downscaling procedure, whose accuracy strongly depends on the size of the input database, composed from the historical recordings. The presence of new data will then improve the calibration of the snowpack evolution model.

In conclusion, the improvement of the general circulation models, together with the continuous increase of the historical measurements sample will lead to the improvement of the results quality, which will allow confirming or correcting the current route.

12.4 A warning from the season 2021-2022

As an example of how a snow reduction during the cold season, together with a strongly anticipated melting, can affect the hydrological cycle and the water availability, is emblematic to look at the current season.

The 2021-2022 winter season was one of the worst since the beginning of the recordings in the whole alpine chain, with very little snow precipitations, over average temperature and continuous dry period. To this very negative predisposing situation, in the Southern Alps is adding an extremely hot and dry spring, creating a perfect storm for water resources.

As reported by (Servizio Glaciologico Lombardo: SGL, 2022) the snow melting took place 1 month earlier, more or less in the entire Lombard Alps territory. As an example, in Figure 12.1 one can see HS and SCD series in the 2021-2022 season compared with the value of the previous nine seasons.

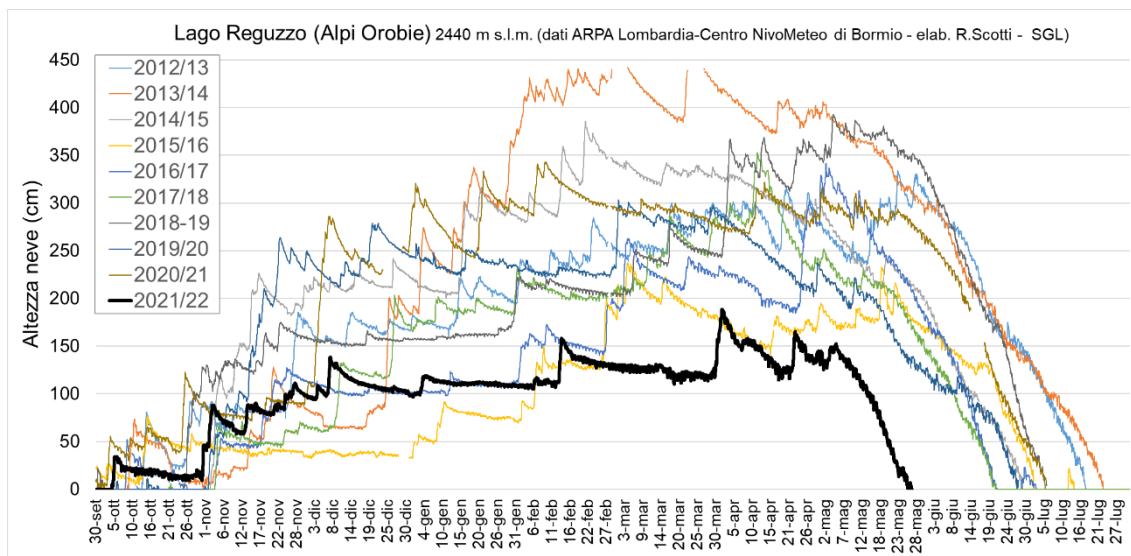


Figure 12.1: Historical series 2013 - 2022 Lago Reguzzo (Servizio Glaciologico Lombardo: SGL, 2022).

The effect of this anticipated melting, aggravated by almost null late-spring precipitation are visible in the entire mountain environment, with the alpine lakes at their historic lows, early and extreme glacial melting, disappearance of springs and consequently water scarcity.

So, while in some Alpine villages of Valtellina fountains are closed to save water resources, the regions of northern Italy demand the state of emergency for the damage that drought is causing to agriculture. A worrying situation that serves as a warning, stressing the importance of a global change in society and the need for adaptation measures to mitigate the damage.



Figure 12.2: The same alpine lake (Lago di Colina) in June 2013 (left) and June 2022 (right).

13. Bibliography

A. Soncini, D. B., 2011. Assessment of future snowfall regimes within the Italian Alps using general circulation models. *Cold regions science and technology* , Volume 68.

AINEVA, 2010. Neve e Valanghe - n.63. Neve e Valanghe (63).

AINEVA, 2020. *www.AINEVA.it*. [Online].

ARPA Lombardia, 2021. *ARPA Lombardia - Servizio Meteorologico Regionale*. [Online].

Barnett T., A. J. D., 2005. Potential impacts of a warming climate on water availability in snow-dominated regions.. *Nature*, Volume 438.

Bartelt P., L. M., 2002. A physical SNOWPACK model for the Swiss avalanche warning. *Cold regions science and technology* .

Beniston M., 2006. Mountain Weather and Climate: A General Overview and a Focus on Climatic Change in the Alps. *Hydrobiologia*, Issue 562.

Bocchiola D, D. G., 2007. *Evidence of climate change within the Adamello Glacier of Italy*, s.l.: s.n.

Bolin B., 2007. *A history of the science and politics of climate change: the role of the Intergovernmental Panel on Climate Change*, United States : OSTI.gov.

Bosello B., M. L. P., 2008. *Le alpi italiane e il cambiamento climatico: elementi di vulnerabilità ambientale ed ecologica e possibili strategie di adattamento.*, s.l.: s.n.

Brian C. O'Neill, C. T. D. P. v. V., 2016. The Scenario Model Intercomparison Project (ScenarioMIP) for CMIP6. *Geoscientific model development*.

Centro Meteorologico Lombardo, 2018. *Clima delle Lombardia*. [Online].

Craig F. Boren, 1979. *Snowpack albedo and snow density*, s.l.: ELSEVIER.

Cresta R., 2014. *Neve - Compendio di nivologia*. Collana Specialist ed. s.l.:Mulatiero Editore.

D. Bocchiola, R. R., 2007. Application of a regional approach for hazard mapping at an avalanche site in northern Italy.

Daniele Bocchiola, M. M. R. R., 2006. Regional snow depth frequency curves for avalanche hazard mapping in central Italian Alps.

EAWS, E. A. W. S., 2022. *www.avalanche.org*. [Online] Available at: <https://www.avalanches.org/fatalities/fatalities-20/> [Accessed 1 May 2022].

- ESRI, 2019. *Arcmap 10.7.1*, s.l.: s.n.
- European avalanche warning service, 2021. *EAWS - European avalanche warning services*. [Online] [Accessed 2022].
- Freppaz M., G. D. F. G. M. M., 2010. Soil Erosion Caused by Snow Avalanches: a Case Study in the Aosta Valley (NW Italy). *Artic, Antartic and Alpine research*, Volume 42.
- G. Smiraglia, G. D., 2015. *Nuovo catasto dei ghiacciai italiani*, s.l.: UNIMI.
- Giulia Arianna Premoli, 2014. *Modellazione monodimensionale dello Snow Gliding: Il caso di Mont de la Saxe (AO)*, Milano : Politecnico di Milano .
- Groppelli B., B. D. R. R., 2011. Spatial downscaling of precipitation from GCMs for climate change projections using random cascates: A case study in Italy.. *Water resources Research*, Volume 47.
- Groppelli B., S. A. B. D. R. R., 2011. Evaluation of future hydrological cycle under climate change scenarios in a mesoscale Alpine watershed of Italy. *Natural Hazards and Earth System Science* , 11(6), pp. 1769-1785.
- IPCC, 2020. <https://www.ipcc.ch/>. [Online].
- Keywhan Riahi, E. K. R. D., 2017. The Shared Socioeconomic Pathways and their energy, land use, and greenhouse gas emissions implications: An overview. *Global environmental change*.
- Kottedoga T., R. R., 2008. *Applied statistics for civil and environmental engineers*. 2 ed. s.l.:Blackwell.
- Marazzi, S., 2002. La Suddivisione Orografica Internazionale Unificata del Sistema Alpino (SOIUSA).
- Martinec J., 1991. Indirect evaluation of snow cover reserves in mountain basin. *Snow, hydrology and forests in High Alpine areas* .
- Martinec J., 2004. Runoff modelling, effect of climate change. . *Remote sensing in snow hydrology*.
- Matiu M, C. A. B. G. e. a., 2021. *Observed snow depth trends in the European Alps: 1971 to 2019*, s.l.: s.n.
- Mc Clung D.M., S. J., 1999. Skier triggering, snow temperatures and the stability index for dry-slab avalanche initiation. *Journal of Glaciology*, 45(150).
- McClung D., S. P., 2006. *The avalanche handbook*. 3 ed. s.l.:The mounatineers book.
- National-weather-service, 2018. *Climate prediction center - NOAA*. [Online].
- Pignatti, S., 1979. I piani di vegetazione in Italia. *Giornale botanico italiano*(113).

- Regione Lombardia, 2014. *Geoportale della Regione Lombardia*. [Online].
- Reuter B., S. J., 2012. The effect of surface warming on slab stiffness and the fracture behavior of snow. *Cold regions science and technology*.
- Servizio Glaciologico Lombardo: SGL, 2022. *Servizioglaciologicolombardo*. [Online]
Available at: www.servizioglaciologicolombardo.it
[Accessed 24 June 2022].
- Strepazzon G., S. J. C. I. Z. K., 2021. Effect of climate change on avalanche accidents and survival. *Frontiers in Physiology* .
- Stretton J., 2020. How climate change is affecting the Alps.. *Run the Alps* .
- The MathWorks Inc., 2018. *MATLAB. (2018). 9.7.0.1190202 (R2019b)*., Natick, Massachusetts: s.n.
- Valt M, G. L. S. F. e. a., 2018. Predicting new snow density in the Italian Alps: A variability analysis based on 10 years of measurements. *Hydrological Processes*, 32(20).
- WSL Institute for Snow and Avalanche Research SLF, 2022. *www.slf.ch*. [Online] [Accessed 2022].
- Yoojin Kim, K.-Y. K. B.-M. K., 2012. Physical mechanisms of European winter snow cover variability and its relationship to the NAO.
- Zhang X., C. L., 2006. Effect of the Ice-Snow Sports Travels on the National Economy and Social Development.

ANNEX 1: Past year trend assessment results

In the following pages the numeric results of the past year trend assessment are reported in tables.

For the understanding, you can refer to the following legend.

LEGEND:							
m	Linear regression coefficient	↓	Negative trend	↑	Positive trend		
L_signif.	Linear regression significance (P value < 0,05)	✓	Satisfied	✗	Not satisfied		
MW vs LT	Moving window average vs long term average result	↓	Negative behavior	↑	Positive behavior	-	Stationary behavior
MK	Mann-Kendall test result	✓	Satisfied	✗	Not satisfied		

Single stations annual analysis:

STATIONS	HS_average					SCD5					SD				
	m	L_signif.	MW	MK		m	L_signif.	MW	MK	m	L_signif.	MW	MK		
BRACC	-0.519	↓	✗ 0.187	↓	✗	-2.406	↓	✗ 0.079	↓	✗	-0.004	↓	✗ 0.974	-	✗
CARCA	1.627	↑	✓ 0.026	↑	✗	0.024	↑	✗ 0.974	-	✗	0.217	↑	✗ 0.236	↑	✗
EDOPA	2.189	↑	✓ 0.001	↑	✓	0.713	↑	✗ 0.242	↑	✗	0.191	↑	✗ 0.285	↑	✗
APR	1.681	↑	✓ 0.017	-	✓	0.125	↑	✗ 0.849	-	✗	-0.064	↓	✗ 0.731	-	✗
CIVAO	0.064	↑	✗ 0.914	-	✗	0.997	↑	✗ 0.316	-	✗	0.205	↑	✗ 0.180	↑	✗
CIVFB	-1.142	↓	✗ 0.073	↓	✗	-0.403	↓	✗ 0.556	↓	✗	-0.163	↓	✗ 0.182	↓	✗
GEAPE	2.929	↑	✓ 0.005	↑	✓	0.145	↑	✗ 0.843	-	✗	0.287	↑	✗ 0.116	↑	✗
GRODF	0.495	↑	✗ 0.114	↑	✗	3.290	↑	✗ 0.152	↑	✗	0.074	↑	✗ 0.573	-	✗
LANCM	-0.149	↓	✗ 0.754	-	✗	-0.618	↓	✗ 0.344	↓	✗	-0.043	↓	✗ 0.747	-	✗
LANPA	2.164	↑	✓ 0.005	↑	✓	0.712	↑	✗ 0.239	↑	✗	0.077	↑	✗ 0.650	↑	✗
LIVLV	1.806	↑	✗ 0.105	-	✗	0.178	↑	✗ 0.813	-	✗	0.179	↑	✗ 0.346	↑	✗
VDSAR	0.350	↑	✗ 0.407	↓	✗	-2.125	↓	✗ 0.363	-	✗	-0.374	↓	✓ 0.042	↓	✗
VDSOC	2.615	↑	✓ 0.002	↑	✓	0.697	↑	✗ 0.246	-	✗	0.241	↑	✗ 0.118	↑	✓
VBOBA	-0.720	↓	✗ 0.618	-	✗	-0.728	↓	✗ 0.397	-	✗	0.028	↑	✗ 0.875	-	✗
BORBO	-0.248	↓	✗ 0.731	-	✗	-1.296	↓	✓ 0.032	↓	✓	-0.060	↓	✗ 0.648	↑	✗
LANCM	-0.604	↓	✗ 0.448	-	✗	-0.207	↓	✗ 0.769	-	✗	0.181	↑	✗ 0.210	-	✗
VDDCA	0.650	↑	✗ 0.468	-	✗	-0.509	↓	✗ 0.410	↓	✗	-0.002	↓	✗ 0.990	-	✗
CAR	-0.280	↓	✗ 0.787	-	✗	-0.458	↓	✗ 0.568	↓	✗	-0.054	↓	✗ 0.789	-	✗
CEVLA	-1.470	↓	✗ 0.165	↓	✗	-2.892	↓	✓ 0.010	-	✓	-0.167	↓	✗ 0.371	-	✗
LIVSR	0.715	↑	✗ 0.222	-	✗	-0.034	↓	✗ 0.970	-	✗	0.118	↑	✗ 0.490	-	✗
VBOLI	-2.600	↓	✗ 0.071	↓	✗	-0.048	↓	✗ 0.945	↓	✗	0.074	↑	✗ 0.601	-	✗
MAD	0.913	↑	✗ 0.480	-	✗	-1.850	↓	✓ 0.007	↓	✓	-0.233	↓	✗ 0.185	-	✗
MADMA	-0.470	↓	✗ 0.440	-	✗	-0.418	↓	✗ 0.640	-	✗	-0.008	↓	✗ 0.960	-	✗
BELSP	-0.382	↓	✗ 0.188	↓	✗	-1.972	↓	✗ 0.050	↑	✗	-0.122	↓	✗ 0.362	-	✗
VFUPL	1.848	↑	✓ 0.035	↑	✓	-0.778	↓	✗ 0.219	↑	✗	-0.024	↓	✗ 0.869	-	✗
VFUCA	0.908	↑	✗ 0.255	-	✗	0.006	↑	✗ 0.994	-	✗	-0.010	↓	✗ 0.941	-	✗
GEATR	0.018	↑	✗ 0.990	-	✗	-0.449	↓	✗ 0.560	-	✗	-0.158	↓	✗ 0.378	↓	✗
GEAVG	2.626	↑	✗ 0.157	↑	✗	-1.497	↓	✓ 0.011	↓	✓	-0.203	↓	✗ 0.167	-	✗

STATIONS	HN				H2D				H3D				HN_average							
	N	m	L_signif.	MW	MK	m	L_signif.	MW	MK	m	L_signif.	MW	MK	m	L_signif.	MW	MK			
BRACC	-1.203	↓	✓ 0.039	↓	X	-0.957	↓	X 0.077	↓	X	-0.701	↓	X 0.177	↓	X	-0.03760	↓	X 0.556	↓	X
CARCA	0.145	↑	X 0.634	-	X	0.091	↑	X 0.812	-	X	0.239	↑	X 0.562	-	X	0.03316	↑	X 0.478	-	X
EDOPA	0.224	↑	X 0.362	↑	X	1.453	↑	✓ 0.010	↑	✓	0.890	↑	✓ 0.018	-	X	0.06859	↑	X 0.070	-	X
APR	0.158	↑	X 0.600	-	X	0.474	↑	X 0.220	-	X	0.836	↑	X 0.087	-	X	0.03788	↑	X 0.493	-	X
CIVAO	0.369	↑	X 0.248	↑	X	0.320	↑	X 0.754	↑	X	0.396	↑	X 0.389	↑	X	0.06892	↑	X 0.113	-	X
CIVFB	-0.496	↓	X 0.159	↓	X	-1.056	↓	X 0.260	-	X	-0.615	↓	X 0.204	↓	X	-0.03744	↓	X 0.304	↓	X
GEAPE	0.046	↑	X 0.851	↑	X	0.189	↑	X 0.598	↑	X	0.323	↑	X 0.400	↑	X	0.05770	↑	X 0.289	-	X
GRODF	0.853	↑	✓ 0.031	↑	✓	1.413	↑	✓ 0.012	↑	✓	1.348	↑	✓ 0.014	↑	✓	0.12292	↑	X 0.065	↑	X
LANCM	-0.044	↓	X 0.880	-	X	-0.548	↓	X 0.418	-	X	0.050	↑	X 0.890	-	X	-0.01902	↓	X 0.533	-	X
LANPA	0.377	↑	X 0.250	↑	X	1.508	↑	X 0.070	-	X	0.641	↑	X 0.149	-	X	0.01596	↑	X 0.638	↑	X
LIVLV	-0.086	↓	X 0.812	-	X	1.130	↑	X 0.528	-	X	-0.150	↓	X 0.831	-	X	0.04355	↑	X 0.203	↑	X
VDSAR	-0.173	↓	X 0.739	-	X	0.541	↑	X 0.522	-	X	0.330	↑	X 0.581	↑	X	0.09529	↑	X 0.320	-	X
VDSOC	-0.178	↓	X 0.479	-	X	0.090	↑	X 0.934	-	X	-0.214	↓	X 0.513	-	X	0.04491	↑	X 0.130	↑	✓
VBOBA	-0.669	↓	X 0.163	-	X	0.412	↑	X 0.578	-	X	0.082	↑	X 0.886	-	X	-0.08622	↓	X 0.356	-	X
BORBO	0.196	↑	X 0.527	-	X	0.669	↑	X 0.301	-	X	0.288	↑	X 0.433	-	X	0.02610	↑	X 0.601	-	X
LANCM	0.073	↑	X 0.835	↑	X	-0.448	↓	X 0.595	↓	X	0.122	↑	X 0.800	-	X	-0.05628	↓	X 0.338	-	X
VDDCA	-0.335	↓	X 0.731	-	X	0.131	↑	X 0.904	↑	X	0.014	↑	X 0.989	-	X	0.00481	↑	X 0.964	-	X
CAR	0.062	↑	X 0.877	↑	X	0.165	↑	X 0.844	↑	X	0.217	↑	X 0.711	↑	X	-0.00054	↓	X 0.995	↑	X
CEVLA	-0.194	↓	X 0.479	↓	X	-0.413	↓	X 0.417	↓	X	-0.525	↓	X 0.324	-	X	0.03107	↑	X 0.716	-	X
LIVSR	0.732	↑	X 0.219	↑	X	0.632	↑	X 0.320	↑	X	0.459	↑	X 0.428	↑	X	0.08845	↑	X 0.208	-	X
VBOLI	-2.172	↓	X 0.052	↓	X	-2.601	↓	X 0.207	↓	X	-1.995	↓	X 0.054	-	X	-0.28178	↓	✓ 0.020	↓	✓
MAD	-0.234	↓	X 0.816	-	X	1.072	↑	X 0.531	-	X	-0.660	↓	X 0.525	-	X	0.04096	↑	X 0.714	-	X
MADMA	-0.532	↓	X 0.602	-	X	0.008	↑	X 0.993	-	X	-0.464	↓	X 0.655	-	X	-0.03735	↓	X 0.720	-	X
BELSP	-1.114	↓	X 0.174	-	X	-0.665	↓	X 0.469	-	X	-0.952	↓	X 0.242	-	X	-0.08736	↓	X 0.435	↓	X
VFUPL	0.723	↑	X 0.056	↑	✓	1.255	↑	X 0.219	↑	X	1.152	↑	✓ 0.037	↑	✓	0.04621	↑	X 0.380	↑	X
VFUCA	0.474	↑	X 0.207	-	X	0.644	↑	X 0.402	↑	X	0.344	↑	X 0.417	↑	X	0.04697	↑	X 0.562	-	X
GEATR	-0.247	↓	X 0.802	-	X	0.641	↑	X 0.670	-	X	0.036	↑	X 0.970	-	X	-0.08712	↓	X 0.482	-	X
GEAVG	-1.005	↓	X 0.560	-	X	4.829	↑	X 0.068	-	X	0.505	↑	X 0.827	↑	X	0.14324	↑	X 0.413	↑	X

Single stations seasonal analysis:

As regards the seasonal analysis on single stations, the MK test and MW vs LT average results agree with the linear regression significance (P value < 0,05). Based on this evidence, given the amount of data, for brevity only the significance on linear regression is reported.

STATIONS	HS_autumn		HS_winter		HS_spring		SCD5_autumn		SCD5_winter		SCD5_spring		HN_autumn		HN_winter		HN_spring											
	N	L_signif.	m	L_signif.	m	L_signif.	m	L_signif.	m	L_signif.	m	L_signif.	m	L_signif.	m	L_signif.	m	L_signif.										
BRACC	-0.261	↓	X 0.291	-0.316	↓	X 0.407	0.635	↑	X 0.388	0.023	↑	X 0.963	-1.094	↓	X 0.247	-0.457	↓	X 0.346					-0.141	↓	X 0.465	0.016	↑	X 0.953
CARCA	0.361	↑	X 0.511	1.011	↑	X 0.321	-1.472	↓	X 0.329	-0.372	↓	X 0.376	-0.012	↓	X 0.939	-0.148	↓	X 0.640	0.083	↑	X 0.519	0.255	↑	X 0.482	-0.363	↓	X 0.457	
EDOPA	0.420	↑	X 0.408	1.373	↑	X 0.088	-1.577	↓	X 0.294	0.242	↑	X 0.526	0.032	↑	X 0.427	0.150	↑	X 0.588	0.047	↑	X 0.804	0.504	↑	X 0.226	-0.137	↓	X 0.773	
APR	-0.095	↓	X 0.868	0.601	↑	X 0.536	1.044	↑	X 0.500	-0.202	↓	X 0.624	0.004	↑	X 0.941	-0.284	↓	X 0.339	0.113	↑	X 0.573	0.113	↑	X 0.758	-0.170	↓	X 0.730	
CIVAO	0.159	↑	X 0.697	1.03	↑	X 0.883	0.233	↑	X 0.815	0.419	↑	X 0.286	0.693	↑	X 0.179	0.122	↑	X 0.672	-0.168	↓	X 0.470	0.266	↑	X 0.361	-0.054	↓	X 0.846	
CIVFB	-0.134	↓	X 0.740	-0.943	↓	X 0.188	-0.459	↓	X 0.641	0.137	↑	X 0.724	-0.114	↓	X 0.732	-0.384	↓	X 0.151	-0.156	↓	X 0.237	-0.225	↓	X 0.389	-0.153	↓	X 0.751	
GEAPE	0.196	↑	X 0.767	1.445	↑	X 0.257	-2.182	↓	X 0.309	-0.533	↓	X 0.198	-0.164	↓	✓ 0.029	0.259	↑	X 0.430	0.200	↑	X 0.286	0.253	↑	X 0.553	0.385	↑	X 0.571	
GRODF	0.380	↑	X 0.211	0.531	↑	X 0.115	-0.481	↓	X 0.341	0.106	↑	X 0.897	1.471	↑	X 0.208	0.507	↑	X 0.430	-0.080	↓	X 0.560	0.360	↑	✓ 0.040	0.128	↑	X 0.625	
LANCM	0.211	↑	X 0.559	-0.188	↓	X 0.727	-0.150	↓	X 0.885	-0.400	↓	X 0.325	-0.141	↓	X 0.700	-0.379	↓	X 0.166	-0.154	↓	X 0.066	0.135	↑	X 0.653	0.034	↑	X 0.928	
LANPA	-0.038	↓	X 0.951	0.723	↑	X 0.514	0.756	↑	X 0.654	0.185	↑	X 0.588	0.059	↑	X 0.202	-0.018	↓	X 0.955	-0.070	↓	X 0.749	0.480	↑	X 0.152	0.540	↑	X 0.220	
LIVLV	0.367	↑	X 0.682	0.333	↑	X 0.816	-1.940	↓	X 0.311	-0.074	↓	X 0.854	-0.103	↓	X 0.654	-0.069	↓	X 0.815	0.545	↑	X 0.173	0.147	↑	X 0.791	0.876	↑	X 0.203	
VDSAR	0.530	↑	X 0.194	0.239	↑	X 0.700	0.135	↑	X 0.838	0.278	↑	X 0.646	0.454	↑	X 0.753	0.011	↑	X 0.707	-0.148	↓	X 0.245	0.142	↑	X 0.658	0.610	↑	X 0.080	
VDSOC	0.238	↑	X 0.688	0.697	↑	X 0.388	-2.049	↓	X 0.147	0.079	↑	X 0.825	-0.086	↓	X 0.418	0.259	↑	X 0.390	0.019	↑	X 0.923	0.408	↑	X 0.330	0.220	↑	X 0.722	
VBOBA	0.380	↑	X 0.632	0.882	↑	X 0.480	2.688	↑	X 0.177	-0.239	↓	X 0.554	-0.139	↓	X 0.587	-0.298	↓	X 0.468	-0.994	↓	X 0.252	-0.096	↓	X 0.892	-0.182	↓	X 0.862	
BORBO	-0.057	↓	X 0.916	-0.358	↓	X 0.469	-0.061	↓	X 0.947	-0.288	↓	X 0.204	-0.989	↓	✓ 0.023	-0.697	↓	✓ 0.002	-0.316	↓	X 0.476	0.176	↑	X 0.656	-0.115	↓	X 0.814	
LANCM	0.264	↑	X 0.597	-0.081	↓	X 0.910	-0.515	↓	X 0.693	0.066	↑	X 0.865	0.102	↑	X 0.729	-0.209	↓	X 0.510	-0.813	↓	X 0.117	-0.205	↓	X 0.617	0.085	↑	X 0.881	
VDDCA	0.352	↑	X 0.571	0.462	↑	X 0.533	-2.211	↓	X 0.114	-0.384	↓	X 0.187	0.112	↑	X 0.603	-0.053	↓	X 0.846	-1.075	↓	X 0.086	0.538	↑	X 0.324	0.445	↑	X 0.453	
CAR	0.431	↑	X 0.516	0.586	↑	X 0.530	-1.966	↓	X 0.294	-0.497	↓	X 0.197	-0.207	↓	X 0.315	-0.087	↓	X 0.798	-0.110	↓	X 0.733	0.344	↑	X 0.575	0.640	↑	X 0.433	
CEVLA	0.268	↑	X 0.596	0.636	↑	X 0.504	3.876	↑	✓ 0.026	-0.406	↓	X 0.259	-2.607	↓	✓ 0.001	-0.813	↓	✓ 0.042	-0.335	↓	X 0.477	-0.654	↓	X 0.240	-2.677	↓	✓ 0.030	
LIVSR	0.581	↑	X 0.256	0.514	↑	X 0.478	0.123	↑	X 0.905	-0.188	↓	X 0.681	0.342	↑	X 0.254	0.071	↑	X 0.789	0.113	↑	X 0.659	0.077	↑	X 0.863	0.258	↑	X 0.579	
VBOLI	-0.255	↓	X 0.712	-0.612	↓	X 0.401	1.291	↑	X 0.501	0.260	↑	X 0.379	-1.328	↓	✓ 0.044	-0.224	↓	X 0.227										
MAD	0.917	↑	X 0.274	0.561	↑	X 0.517	0.431	↑	X 0.765	-0.730	↓	✓ 0.023	-1.322	↓	✓ 0.006	-0.672	↓	✓ 0.001				0.036	↑	X 0.959	0.754	↑	X 0.418	
MADMA	-0.003	↓	X 0.996	-0.336	↓	X 0.710	-1.043	↓	X 0.550	-0.494	↓	X 0.237	-0.256	↓	X 0.392	-0.104	↓	X 0.774	-0.574	↓	X 0.104	0.500	↑	X 0.478	0.335	↑	X 0.674	
BELSP	0.144	↑	X 0.692	-0.732	↓	X 0.098	1.523	↑	X 0.062	-0.365	↓	X 0.286	-1.177	↓	X 0.066	-0.239	↓	X 0.116	-0.483	↓	X 0.061	-0.110	↓	X 0.703	0.234	↑	X 0.545	
VFUPL	0.376	↑	X 0.561	1.309	↑	X 0.088	-0.555	↓	X 0.712	-0.285	↓	X 0.404	-1.011	↓	✓ 0.037	-0.168	↓	X 0.417				0.156	↑	X 0.744	1.012	↑	✓ 0.030	
VFUCA	0.416	↑	X 0.585	1.103	↑	X 0.096	-1.201	↓	X 0.379	-0.184	↓	X 0.681	0.421	↑	X 0.322	-0.108	↓	X 0.751				0.158	↑	X 0.684	0.847	↑	X 0.058	
GEATR	1.090	↑	X 0.179	1.274	↑	X 0.240	-1.061	↓	X 0.558	-0.417	↓	X 0.239	-0.371	↓	X 0.106	0.157	↑	X 0.649	-0.587	↓	X 0.483	-0.274	↓	X 0.724	0.207	↑	X 0.843	
GEAVG	1.788	↑	X 0.216	1.885	↑	X 0.214	0.673	↑	X 0.823	-0.405	↓	X 0.053	-1.156	↓	✓ 0.017	-0.794	↓	✓ 0.000				0.713	↑	X 0.416	3.956	↑	✓ 0.030	

STATIONS	H3D_autumn		H3D_winter		H3D_spring		SD_autumn		SD_winter		SD_spring		HN_autumn		HN_winter		HN_spring																	
	m	L signif.	m	L signif.	m	L signif.	m	L signif.	m	L signif.	m	L signif.	m	L signif.	m	L signif.	m	L signif.																
BRACC	-0.284	↓	×	0.272	-0.412	↓	0.451	↓	0.308	-0.225	↓	0.342	-0.480	↓	0.38917	0.635	↑	0.387599				-0.141	↓	×	0.465	0.016	↑	×	0.953					
CARCA	0.127	↑	×	0.870	0.254	↑	0.829	-0.192	↓	0.865	-0.016	↓	0.989	0.673	↑	0.632562	-1.472	↓	0.329437	0.083	↑	×	0.519	0.255	↑	×	0.482	-0.363	↓	×	0.457			
EDOPA	0.401	↑	×	0.659	1.701	↑	0.097	1.553	↑	0.159	0.721	↑	0.480	2.658	↑	0.091319	-1.577	↓	0.294413	0.047	↑	×	0.804	0.504	↑	×	0.226	-0.137	↓	×	0.773			
APR	-0.239	↓	×	0.790	0.544	↑	0.628	0.162	↑	0.885	-0.210	↓	0.858	0.733	↑	0.63457	1.044	↑	0.498995	0.113	↑	×	0.573	0.113	↑	×	0.758	-0.170	↓	×	0.730			
CIVAO	0.111	↑	×	0.884	1.044	↑	0.373	0.189	↑	0.807	0.769	↑	0.257	0.854	↑	0.322662	0.233	↑	0.815423	-0.168	↓	×	0.470	0.266	↑	×	0.361	-0.054	↓	×	0.846			
CIVFB	-0.374	↓	×	0.501	-1.976	↓	0.061	-1.299	↓	0.163	-0.757	↓	0.280	0.892	↑	0.205491	-0.459	↓	0.641012	-0.156	↓	×	0.237	-0.225	↓	×	0.389	-0.153	↓	×	0.751			
GEAPE	0.294	↑	×	0.757	1.852	↑	0.231	2.505	↑	0.149	-0.831	↓	0.528	0.892	↑	0.669457	-2.182	↓	0.308552	0.200	↑	×	0.286	0.253	↑	×	0.553	0.385	↑	×	0.571			
GRODF	-0.258	↓	×	0.413	1.021	↑	0.128	1.000	↑	0.156	-0.693	↓	0.187	0.555	↑	0.18447	-0.481	↓	0.341299	-0.080	↓	×	0.560	0.360	↑	×	0.040	0.128	↑	×	0.625			
LANCM	-0.536	↓	×	0.242	-0.300	↓	0.712	-0.241	↓	0.768	-0.191	↓	0.653	0.532	↑	0.593484	-0.150	↓	0.884856	-0.154	↓	×	0.066	0.135	↑	×	0.653	0.034	↑	×	0.928			
LANPA	-0.034	↓	×	0.974	0.840	↑	0.421	1.154	↑	0.308	-0.834	↓	0.517	-2.112	↓	0.046505	0.756	↑	0.653511	-0.070	↓	×	0.749	0.480	↑	×	0.152	0.540	↑	×	0.220			
LIVLV	-0.196	↓	×	0.903	1.223	↑	0.450	1.266	↑	0.303	-0.671	↓	0.706	0.032	↑	0.98857	-1.940	↓	0.311111	0.545	↑	×	0.173	0.147	↑	×	0.791	0.876	↑	×	0.203			
VDSAR	-0.398	↓	×	0.396	0.878	↑	0.276	1.419	↑	0.007	-0.610	↓	0.297	0.460	↑	0.439124	0.135	↑	0.838291	-0.148	↓	×	0.245	0.142	↑	×	0.658	0.610	↑	×	0.080			
VDSOC	0.130	↑	×	0.889	1.795	↑	0.080	1.326	↑	0.249	-0.734	↓	0.557	0.110	↑	0.940508	-2.049	↓	0.14727	0.019	↑	×	0.923	0.408	↑	×	0.330	0.220	↑	×	0.722			
VBOBA	-1.025	↓	×	0.330	0.856	↑	0.624	0.910	↑	0.652	-2.044	↓	0.021	-1.125	↓	0.614629	2.688	↑	0.176901	-0.994	↓	×	0.252	-0.096	↓	×	0.892	-0.182	↓	×	0.862			
BORBO	-0.027	↓	×	0.980	0.114	↑	0.885	0.154	↑	0.852	-0.290	↓	0.408	-1.515	↓	0.13547	-0.061	↓	0.946858	-0.316	↓	×	0.476	0.176	↑	×	0.656	-0.115	↓	×	0.814			
LANCM	-0.798	↓	×	0.307	0.077	↑	0.937	0.792	↑	0.469	-0.612	↓	0.451	0.090	↑	0.949058	-0.515	↓	0.693411	-0.813	↓	×	0.117	-0.205	↓	×	0.617	0.085	↑	×	0.881			
VDDCA	-1.458	↓	×	0.099	1.605	↑	0.112	1.359	↑	0.209	-1.607	↓	0.093	1.359	↑	0.300484	-2.211	↓	0.114096	-1.075	↓	×	0.086	0.538	↑	×	0.324	0.445	↑	×	0.453			
CAR	0.079	↑	×	0.938	1.200	↑	0.475	2.105	↑	0.153	-0.860	↓	0.286	1.149	↑	0.487581	-1.966	↓	0.294416	-0.110	↓	×	0.733	0.344	↑	×	0.575	0.640	↑	×	0.433			
CEVLA	-0.123	↓	×	0.862	-1.930	↓	0.157	-4.085	↓	0.008	-0.130	↓	0.866	-2.096	↓	0.114089	3.876	↑	0.0234	-0.335	↓	×	0.477	-0.654	↓	×	0.240	-2.677	↓	×	0.030			
LIVSR	-0.174	↓	×	0.856	1.027	↑	0.339	1.020	↑	0.318	0.198	↑	0.814	0.027	↑	0.984405	0.123	↑	0.905051	0.113	↑	×	0.659	0.077	↑	×	0.863	0.258	↑	×	0.579			
VBOBI																0.631445	1.291	↑	0.500839									↓	×	0.019	-1.582	↓	×	0.088
MAD	-2.146	↓	×	0.274	-0.326	↓	0.852	0.465	↑	0.794	-3.546	↓	0.003	3.130	↑	0.134168	0.431	↑	0.765145							↑	×	0.959	0.754	↑	×	0.418		
MADMA	-1.195	↓	×	0.166	0.338	↑	0.812	0.162	↑	0.920	-0.888	↓	0.064	-0.471	↓	0.758236	-1.043	↓	0.550183	-0.574	↓	×	0.104	0.500	↑	×	0.478	0.335	↑	×	0.674			
BELSP	-0.697	↓	×	0.228	-0.728	↓	0.448	-0.852	↓	0.391	-0.953	↓	0.179	-2.052	↓	0.020552	1.523	↑	0.061848	-0.483	↓	×	0.061	-0.110	↓	×	0.703	0.234	↑	×	0.545			
VFUPL	-2.911	↓	×	0.022	0.600	↑	0.582	2.883	↑	0.003	-3.964	↓	0.017	-0.140	↓	0.906635	-0.555	↓	0.711847								↑	×	0.744	1.012	↑	×	0.030	
VFUCA																0.745034	-1.201	↓	0.379253								↑	×	0.684	0.847	↑	×	0.058	
GEATR	0.223	↑	×	0.875	0.573	↑	0.756	1.870	↑	0.360	-1.266	↓	0.243	0.335	↑	0.880796	-1.061	↓	0.558342	-0.587	↓	×	0.483	-0.274	↓	×	0.724	0.207	↑	×	0.843			
GEAVG																0.223093	0.673	↑	0.823256							↑	×	0.416	3.956	↑	×	0.030		

Homogeneous groups analysis:

GROUP	HS_av [cm]						SCD5 [number of days]							
	Index value	m	trend	P_value	MW vs LT	MK_test	Index value	m	trend	P_value	MW vs LT	MK_test		
hilly (*)	13.2	-0.086	↓	√ 0.033	-	×	44	-0.07	↓	√ 0.045	-	×		
hilly + mountain	13.85	-0.004	↓	×	0.858	-	×	45	-0.005	↓	×	0.770	-	×
mountain + subalpine	43.36	0.011	↑	×	0.267	↑	×	101	-0.001	↓	×	0.839	-	×
subalpine + alpine	53.73	0.013	↑	×	0.266	-	×	127	0.002	↑	×	0.726	-	×
alpine	59.59	0.012	↑	√ 0.042	-	×	150	0.002	↑	×	0.541	-	×	
Prealpi Lariane	22.11	-0.028	↓	√ 0.019	↓	√	67	-0.025	↓	√ 0.040	-	×		
Valchiavenna	50.86	-0.003	↓	×	0.858	-	×	98	-0.011	↓	×	0.104	-	×
Orobie Sud	37.74	-0.004	↓	×	0.841	-	×	94	-0.002	↓	×	0.844	-	×
Orobie Nord	62.59	0.028	↑	×	0.062	↑	×	145	0.001	↑	×	0.887	-	×
Adamello	46.32	0.010	↑	×	0.474	-	×	115	-0.014	↓	√ 0.049	-	×	
Alta Valtellina	41.07	0.029	↑	×	0.060	↑	×	97	0.008	↑	×	0.289	↑	×
Livigno	66.97	0.020	↑	×	0.153	-	×	162	0.002	↑	×	0.695	-	×
Retiche Occidentali	40.36	0.007	↑	×	0.500	-	×	124	0.002	↑	×	0.676	-	×
N (NE,N,NW)	54.44	0.018	↑	×	0.081	↑	×	123	0.004	↑	×	0.290	-	×
E (NE,E,SE)	32.98	0.014	↑	×	0.387	↑	×	85	0.003	↑	×	0.679	-	×
W (NW,W,SW)	47.54	0.003	↑	×	0.738	-	×	118	-0.001	↓	×	0.848	-	×
S (SE,S,SW)	31.01	0.011	↑	×	0.403	-	×	98	0.005	↑	×	0.433	-	×

GROUP	SD [number of days]					HN [cm]					H2D [cm]							
	m	trend	L_signif.	MW vs LT	H_MK	m	trend	P_value	MW vs LT	MK_test	m	trend	P_value	MW vs LT	MK_test			
hilly (*)	-0,021	↓	×	0,650	-	×	-0,040	↓	×	0,093	↓	×	-0,0309	↓	×	0,181	↓	×
hilly + mountain	0,018	↑	×	0,350	-	×	-0,030	↓	√ 0,026	-	×	-0,013	↓	×	0,233	-	×	
mountain + subalpine	0,007	↑	×	0,308	↑	×	-0,005	↓	×	0,374	-	×	-0,002	↓	×	0,764	↑	×
subalpine + alpine	0,013	↑	×	0,141	↑	×	-0,006	↓	×	0,249	-	×	-0,007	↓	×	0,447	-	×
alpine	0,006	↑	×	0,334	-	×	-0,003	↓	×	0,648	-	×	0,002	↑	×	0,790	↑	×
Prealpi Lariane	-0,016	↓	×	0,362	-	×	-0,030	↓	×	0,174	-	×	-0,014	↓	×	0,469	-	×
Valchiavenna	-0,010	↓	×	0,430	-	×	-0,006	↓	×	0,701	-	×	0,004	↑	×	0,728	-	×
Orobie Sud	0,013	↑	×	0,316	↑	×	-0,013	↓	×	0,112	-	×	-0,005	↓	×	0,574	-	×
Orobie Nord	0,002	↑	×	0,782	-	×	0,001	↑	×	0,862	-	×	0,006	↑	×	0,344	-	×
Adamello	-0,001	↓	×	0,920	-	×	0,003	↑	×	0,678	-	×	0,012	↑	×	0,053	-	×
Alta Valtellina	0,013	↑	×	0,308	↑	×	0,002	↑	×	0,816	↑	×	0,009	↑	×	0,345	↑	×
Livigno	0,010	↑	×	0,291	-	×	0,007	↑	×	0,462	↑	×	0,012	↑	×	0,330	-	×
Retiche Occidentali	0,011	↑	×	0,144	↑	×	0,000	↑	×	0,987	↑	×	-0,002	↓	×	0,804	↑	×
N (NE,N,NW)	0,012	↑	×	0,123	↑	×	-0,005	↓	×	0,344	↑	×	-0,004	↓	×	0,651	↑	×
E (NE,E,SE)	0,015	↑	×	0,231	-	×	-0,003	↓	×	0,737	-	×	0,002	↑	×	0,812	↑	×
W (NW,W,SW)	0,006	↑	×	0,422	-	×	-0,010	↓	√ 0,036	-	√	-0,010	↓	×	0,			

GROUP	H3D [cm]					HN_average [cm]					
	m	trend	P_value	MW vs LT	MK_test	Index value	m	trend	P_value	MW vs LT	MK_test
hilly (*)	-0,029	↓	× 0,192	↓	×	10	-0,0049	↓	× 0,737	-	×
hilly + mountain	-0,017	↓	× 0,139	-	×	13	-0,0088	↓	× 0,268	-	×
mountain + subalpine	-0,003	↓	× 0,609	↑	×	32	0,0021	↑	× 0,562	-	×
subalpine + alpine	-0,003	↓	× 0,650	-	×	30	0,0004	↑	× 0,915	↑	×
alpine	-0,002	↓	× 0,749	↑	×	29	0,0033	↑	× 0,308	↑	×
Prealpi Lariane	-0,021	↓	× 0,242	-	×	17	-0,0094	↓	× 0,435	-	×
Valchiavenna	-0,007	↓	× 0,581	-	×	39	0,0000	↓	× 1,000	-	×
Orobie Sud	-0,004	↓	× 0,584	-	×	28	-0,0041	↓	× 0,467	-	×
Orobie Nord	0,008	↑	× 0,236	-	×	38	0,0026	↑	× 0,649	-	×
Adamello	0,007	↑	× 0,295	-	×	27	0,0072	↑	× 0,110	-	×
Alta Valtellina	0,006	↑	× 0,448	↑	×	23	0,0049	↑	× 0,365	↑	×
Livigno	0,004	↑	× 0,603	↑	×	33	0,0081	↑	× 0,146	-	×
Retiche Occidentali	0,001	↑	× 0,908	↑	×	22	0,0011	↑	× 0,747	-	×
N (NE,N,NW)	-0,001	↓	× 0,838	↑	×	32	0,0012	↑	× 0,756	↑	×
E (NE,E,SE)	0,001	↑	× 0,888	↑	×	23	-0,0009	↓	× 0,863	-	×
W (NW,W,SW)	-0,007	↓	× 0,175	-	×	29	-0,0007	↓	× 0,844	-	×
S (SE,S,SW)	-0,001	↓	× 0,926	↑	×	21	0,0050	↑	× 0,280	↑	×

ANNEX 2: Future years trend assessment results

Station	HS average		SCD5		SD		HN		H2D		H3D		HN average		
	n.	trend	Sign.	trend	Sign.	trend	Sign.	trend	Sign.	trend	Sign.	trend	Sign.	trend	Sign.
1	↓ 0.0504	×	×	↓ 0.0642	×	↑ 0.0058	×	↓ 0.0463	×	↓ 0.0525	×	↓ 0.0450	×	↓ 0.0153	×
2	↓ 0.3777	×	×	↓ 0.0909	×	↓ 0.0011	×	↓ 0.3143	×	↓ 0.4127	×	↓ 0.3822	×	↓ 0.0470	×
3	↓ 0.0215	×	×	↓ 0.2995	×	↓ 0.0204	×	↑ 0.0926	×	↑ 0.1545	×	↑ 0.1427	×	↓ 0.0176	×
4	↑ 0.1087	×	×	↑ 0.1072	×	↑ 0.0253	×	↓ 0.0664	×	↑ 0.0002	×	↑ 0.0334	×	↑ 0.0104	×
5	↓ 0.3017	×	×	↓ 0.1032	×	↓ 0.0176	×	↑ 0.0618	×	↓ 0.0400	×	↓ 0.0874	×	↓ 0.0268	×
6	↓ 0.0333	×	×	↓ 0.0410	×	↓ 0.0113	×	↑ 0.0059	×	↑ 0.0382	×	↑ 0.0422	×	↓ 0.0051	×
7	↓ 0.1901	×	×	↓ 0.2300	×	↓ 0.0091	×	↓ 0.4405	×	↓ 0.3791	×	↓ 0.3843	×	↓ 0.0155	×
8	↓ 0.0080	×	×	↓ 0.0025	×	↑ 0.0202	×	↓ 0.0343	×	↓ 0.0449	×	↓ 0.0578	×	↓ 0.0079	×
9	↓ 0.1209	×	×	↓ 0.1208	×	↓ 0.0019	×	↑ 0.4332	×	↑ 0.3923	×	↑ 0.2973	×	↑ 0.0110	×
10	↑ 0.0290	×	×	↑ 0.0062	×	↑ 0.0272	×	↑ 0.1785	×	↑ 0.2694	×	↑ 0.2499	×	↑ 0.0025	×
11	↑ 0.3665	×	×	↑ 0.0543	×	↓ 0.0120	×	↑ 0.5282	×	↑ 0.4909	×	↑ 0.6085	×	↑ 0.0533	×

CESM2_ssp1 2.6

Station	HS average		SCD5		SD		HN		H2D		H3D		HN average		
	n.	trend	Sign.	trend	Sign.	trend	Sign.	trend	Sign.	trend	Sign.	trend	Sign.	trend	Sign.
1	↓ 0.0114	×	×	↓ 0.1869	✓	↓ 0.0343	✓	↓ 0.1240	×	↓ 0.1387	×	↓ 0.1295	×	↑ 0.0118	×
2	↓ 0.5848	×	×	↓ 0.6938	✓	↓ 0.1752	✓	↑ 0.1655	×	↑ 0.2052	×	↑ 0.2513	×	↑ 0.0479	×
3	↓ 0.0144	×	×	↓ 0.7779	✓	↓ 0.0872	✓	↓ 0.3435	×	↓ 0.3249	×	↓ 0.3224	×	↑ 0.1178	×
4	↓ 0.3212	✓	✓	↓ 0.5182	✓	↓ 0.1056	✓	↑ 0.1952	×	↑ 0.1438	×	↑ 0.2106	×	↑ 0.0124	×
5	↓ 0.7043	×	×	↓ 0.8104	✓	↓ 0.1285	✓	↓ 0.1069	×	↓ 0.0731	×	↑ 0.0003	×	↓ 0.0068	×
6	↓ 0.0194	×	×	↓ 0.1996	×	↓ 0.0348	×	↓ 0.0809	×	↓ 0.0724	×	↓ 0.0761	×	↓ 0.0070	×
7	↓ 0.8690	×	×	↓ 0.5838	✓	↓ 0.0945	✓	↑ 0.0694	×	↑ 0.1902	×	↑ 0.1385	×	↑ 0.0141	×
8	↓ 0.0026	×	×	↓ 0.4943	✓	↓ 0.0934	✓	↓ 0.0264	×	↓ 0.0210	×	↓ 0.0225	✓	↑ 0.0042	×
9	↓ 0.1671	×	×	↓ 0.5348	✓	↓ 0.0945	✓	↓ 0.0864	×	↓ 0.0319	×	↑ 0.0135	×	↑ 0.0105	×
10	↓ 0.1269	×	×	↓ 0.4041	✓	↓ 0.0695	✓	↓ 0.0049	×	↑ 0.0335	×	↓ 0.0184	×	↑ 0.0651	×
11	↓ 0.6860	×	×	↓ 0.4563	✓	↓ 0.1175	✓	↑ 0.2212	×	↑ 0.1397	×	↑ 0.2084	×	↑ 0.0342	×

CESM2_ssp2 4.5

Station	HS average		SCD5		SD		HN		H2D		H3D		HN average		
	n.	trend	Sign.	trend	Sign.	trend	Sign.	trend	Sign.	trend	Sign.	trend	Sign.	trend	Sign.
1	↓ 0.0639	×	×	↓ 0.4742	✓	↓ 0.0868	✓	↓ 0.2895	✓	↓ 0.3042	✓	↓ 0.3071	✓	↓ 0.0115	×
2	↓ 1.6775	✓	✓	↓ 1.2111	✓	↓ 0.1846	✓	↓ 0.8722	✓	↓ 1.0967	✓	↓ 1.1578	✓	↓ 0.0542	×
3	↓ 0.3239	✓	✓	↓ 1.3678	✓	↓ 0.1138	✓	↓ 0.9397	✓	↓ 1.1412	✓	↓ 1.2286	✓	↓ 0.0712	✓
4	↓ 0.7244	✓	✓	↓ 1.0115	✓	↓ 0.1549	✓	↓ 0.4692	✓	↓ 0.4956	✓	↓ 0.4437	✓	↓ 0.0252	✓
5	↓ 1.3289	✓	✓	↓ 1.4820	✓	↓ 0.2076	✓	↓ 0.6028	✓	↓ 0.8717	✓	↓ 0.9379	✓	↓ 0.0460	✓
6	↓ 0.0935	✓	✓	↓ 0.5604	✓	↓ 0.0947	✓	↓ 0.1949	✓	↓ 0.2114	✓	↓ 0.2169	✓	↓ 0.0237	✓
7	↓ 1.0971	×	×	↓ 0.8374	✓	↓ 0.1397	✓	↑ 0.2014	×	↑ 0.3806	×	↑ 0.3924	×	↑ 0.0349	×
8	↓ 0.0125	×	×	↓ 0.6191	✓	↓ 0.1016	✓	↓ 0.0949	×	↓ 0.0932	×	↓ 0.0902	×	↓ 0.0027	×
9	↓ 0.5416	✓	✓	↓ 1.1849	✓	↓ 0.1414	✓	↓ 0.5580	✓	↓ 0.6180	✓	↓ 0.6702	✓	↓ 0.0738	✓
10	↓ 0.7041	✓	✓	↓ 0.8981	✓	↓ 0.1175	✓	↓ 0.3978	×	↓ 0.4412	×	↓ 0.4500	✓	↓ 0.0339	×
11	↓ 1.9872	✓	✓	↓ 0.8114	✓	↓ 0.1772	✓	↓ 0.2970	×	↓ 0.4058	×	↓ 0.4494	×	↓ 0.0088	×

CESM2_ssp3 7.0

Station	HS average		SCD5		SD		HN		H2D		H3D		HN average		
	n.	trend	Sign.	trend	Sign.	trend	Sign.	trend	Sign.	trend	Sign.	trend	Sign.	trend	Sign.
1	↓ 0.0825	×	×	↓ 0.3126	✓	↓ 0.0533	✓	↓ 0.2287	×	↓ 0.2517	×	↓ 0.2570	×	↑ 0.0192	×
2	↓ 1.7960	✓	✓	↓ 1.6843	✓	↓ 0.2113	✓	↓ 0.5402	×	↓ 0.6621	×	↓ 0.6483	×	↓ 0.0395	×
3	↓ 0.2044	✓	✓	↓ 0.6973	✓	↓ 0.0650	✓	↓ 0.9869	✓	↓ 1.0240	✓	↓ 1.0368	✓	↓ 0.5278	✓
4	↓ 0.5513	✓	✓	↓ 1.2226	✓	↓ 0.2024	✓	↑ 0.0004	×	↓ 0.0059	×	↑ 0.0198	×	↑ 0.0277	×
5	↓ 1.1721	✓	✓	↓ 1.4866	✓	↓ 0.2098	✓	↓ 0.5540	×	↓ 0.8279	×	↓ 0.9172	×	↑ 0.0087	×
6	↑ 0.0014	×	×	↓ 0.3718	✓	↓ 0.0707	✓	↓ 0.0799	×	↓ 0.0584	×	↓ 0.0640	×	↑ 0.0143	×
7	↓ 2.1490	✓	✓	↓ 1.0978	✓	↓ 0.1573	✓	↓ 0.4195	×	↓ 0.3790	×	↓ 0.2748	×	↑ 0.0240	×
8	↓ 0.0309	✓	✓	↓ 0.7285	✓	↓ 0.1250	✓	↓ 0.1389	✓	↓ 0.1595	✓	↓ 0.1567	✓	↓ 0.0072	×
9	↓ 0.1258	×	×	↓ 1.0022	✓	↓ 0.1226	✓	↓ 0.1925	×	↓ 0.2637	×	↓ 0.3027	×	↑ 0.0270	×
10	↓ 0.8474	✓	✓	↓ 1.0667	✓	↓ 0.0925	✓	↓ 0.6963	✓	↓ 0.7342	✓	↓ 0.7373	✓	↓ 0.0612	×
11	↓ 2.2223	✓	✓	↓ 1.1674	✓	↓ 0.2086	✓	↓ 0.1245	×	↓ 0.3192	×	↓ 0.3794	×	↑ 0.0085	×

CESM2_ssp5 8.5

Station	HS average		SCD5		SD		HN		H2D		H3D		HN average	
	trend	Sign.	trend	Sign.	trend	Sign.	trend	Sign.	trend	Sign.	trend	Sign.	trend	Sign.
1	↑ 0.0148	×	↓ 0.1909	✓	↓ 0.0334	✓	↓ 0.0337	×	↓ 0.0497	×	↓ 0.0435	×	↓ 0.0003	×
2	↓ 1.4578	✓	↓ 0.9312	✓	↓ 0.1413	✓	↓ 0.7971	×	↓ 0.7607	×	↓ 0.7426	×	↓ 0.0128	×
3	↓ 0.3211	✓	↓ 1.8907	✓	↓ 0.1446	✓	↓ 1.1275	✓	↓ 1.2834	✓	↓ 1.3242	✓	↓ 0.0989	✓
4	↓ 0.2510	×	↓ 0.5186	✓	↓ 0.1130	✓	↑ 0.0106	×	↓ 0.0088	×	↓ 0.0129	×	↑ 0.0096	×
5	↓ 1.4937	✓	↓ 0.9350	✓	↓ 0.1140	✓	↓ 0.5375	×	↓ 0.8553	✓	↓ 0.7422	×	↓ 0.0797	✓
6	↑ 0.0063	×	↓ 0.3874	✓	↓ 0.0771	✓	↑ 0.0062	×	↑ 0.0068	×	↓ 0.0115	×	↑ 0.0136	×
7	↓ 1.1550	×	↓ 0.8824	✓	↓ 0.1697	✓	↓ 0.2081	×	↓ 0.3517	×	↓ 0.3351	×	↓ 0.0070	×
8	↓ 0.0313	×	↓ 0.6878	✓	↓ 0.1429	✓	↓ 0.1494	✓	↓ 0.1526	✓	↓ 0.1526	✓	↓ 0.0107	×
9	↓ 0.6855	×	↓ 0.6781	✓	↓ 0.1115	✓	↓ 0.1689	×	↓ 0.2999	×	↓ 0.2862	×	↓ 0.0013	×
10	↓ 0.1422	×	↓ 0.4758	✓	↓ 0.0990	✓	↑ 0.2612	×	↑ 0.1843	×	↑ 0.2585	×	↑ 0.0376	×
11	↓ 1.0267	✓	↓ 0.6862	✓	↓ 0.2000	✓	↓ 0.2141	×	↓ 0.3193	×	↓ 0.3604	×	↑ 0.0062	×

CMCC_CM2_SR5_ssp1 2.6

Station	HS average		SCD5		SD		HN		H2D		H3D		HN average	
	trend	Sign.	trend	Sign.	trend	Sign.	trend	Sign.	trend	Sign.	trend	Sign.	trend	Sign.
1	↓ 0.0389	×	↓ 0.2421	✓	↓ 0.0466	✓	↓ 0.0924	×	↓ 0.1121	✓	↓ 0.1101	✓	↓ 0.0088	×
2	↓ 1.3526	✓	↓ 1.1049	✓	↓ 0.1494	✓	↓ 0.3946	×	↓ 0.8255	×	↓ 0.8014	×	↓ 0.0197	×
3	↓ 0.3376	✓	↓ 2.2170	✓	↓ 0.1724	✓	↓ 1.2248	✓	↓ 1.4107	✓	↓ 1.3930	✓	↓ 0.0952	✓
4	↓ 0.4160	✓	↓ 0.7727	✓	↓ 0.1865	✓	↓ 0.1965	×	↓ 0.1661	×	↓ 0.1516	×	↓ 0.0237	×
5	↓ 1.2482	✓	↓ 1.2751	✓	↓ 0.2227	✓	↓ 0.6261	✓	↓ 0.6841	✓	↓ 0.6850	✓	↑ 0.0062	×
6	↓ 0.1108	×	↓ 0.5832	✓	↓ 0.0840	✓	↓ 0.2380	✓	↓ 0.2060	×	↓ 0.2208	✓	↓ 0.0291	×
7	↓ 1.0493	✓	↓ 1.1173	✓	↓ 0.2222	✓	↓ 0.2424	×	↓ 0.1780	×	↓ 0.1991	×	↑ 0.0122	×
8	↓ 0.0539	✓	↓ 1.1122	✓	↓ 0.1941	✓	↓ 0.2061	✓	↓ 0.2515	✓	↓ 0.2499	✓	↓ 0.0074	×
9	↓ 0.7393	✓	↓ 1.1454	✓	↓ 0.1449	✓	↓ 0.7297	✓	↓ 1.1687	✓	↓ 1.1907	✓	↓ 0.0440	×
10	↓ 0.3327	✓	↓ 0.8439	✓	↓ 0.1329	✓	↓ 0.4263	✓	↓ 0.5937	✓	↓ 0.5575	✓	↑ 0.0055	×
11	↓ 1.5008	✓	↓ 0.9249	✓	↓ 0.2625	✓	↓ 0.0024	×	↓ 0.1378	×	↓ 0.1682	×	↑ 0.0083	×

CMCC_CM2_SR5_ssp2 4.5

Station	HS average		SCD5		SD		HN		H2D		H3D		HN average	
	trend	Sign.	trend	Sign.	trend	Sign.	trend	Sign.	trend	Sign.	trend	Sign.	trend	Sign.
1	↓ 0.0085	×	↓ 0.3276	✓	↓ 0.0598	✓	↓ 0.0935	×	↓ 0.0996	×	↓ 0.0896	×	↓ 0.0005	×
2	↓ 2.8613	✓	↓ 1.7485	✓	↓ 0.2171	✓	↓ 1.3161	✓	↓ 1.4213	✓	↓ 1.4858	✓	↓ 0.1389	✓
3	↓ 0.3941	✓	↓ 2.0310	✓	↓ 0.1677	✓	↓ 1.4070	✓	↓ 1.4306	✓	↓ 1.4167	✓	↓ 0.1293	✓
4	↓ 0.7168	✓	↓ 0.9682	✓	↓ 0.1760	✓	↓ 0.3187	×	↓ 0.3296	✓	↓ 0.3140	×	↓ 0.0088	×
5	↓ 2.0258	✓	↓ 1.5561	✓	↓ 0.2542	✓	↓ 0.4404	×	↓ 0.5736	×	↓ 0.7168	✓	↓ 0.0026	×
6	↓ 0.1149	✓	↓ 0.8418	✓	↓ 0.1288	✓	↓ 0.2851	✓	↓ 0.2898	✓	↓ 0.3032	✓	↑ 0.0078	×
7	↓ 1.8631	✓	↓ 1.2593	✓	↓ 0.2426	✓	↓ 0.8894	✓	↓ 0.9480	✓	↓ 1.0337	✓	↓ 0.0274	×
8	↓ 0.0166	×	↓ 0.9934	✓	↓ 0.1687	✓	↓ 0.1305	✓	↓ 0.1384	✓	↓ 0.1367	✓	↓ 0.0008	×
9	↓ 0.7047	✓	↓ 1.2847	✓	↓ 0.2105	✓	↓ 0.5589	×	↓ 0.5381	×	↓ 0.5548	✓	↑ 0.0441	×
10	↓ 0.7583	✓	↓ 1.1540	✓	↓ 0.1819	✓	↓ 0.3405	✓	↓ 0.4572	✓	↓ 0.4178	✓	↓ 0.0407	×
11	↓ 1.8632	✓	↓ 1.2070	✓	↓ 0.3037	✓	↓ 0.0325	×	↓ 0.0934	×	↓ 0.0181	×	↓ 0.0024	×

CMCC_CM2_SR5_ssp3 7.0

Station	HS average		SCD5		SD		HN		H2D		H3D		HN average	
	trend	Sign.	trend	Sign.	trend	Sign.	trend	Sign.	trend	Sign.	trend	Sign.	trend	Sign.
1	↓ 0.1211	✓	↓ 0.4679	✓	↓ 0.0749	✓	↓ 0.2068	✓	↓ 0.2081	✓	↓ 0.2139	✓	↓ 0.0677	×
2	↓ 2.8372	✓	↓ 2.4125	✓	↓ 0.2804	✓	↓ 1.3810	✓	↓ 1.7025	✓	↓ 1.7544	✓	↓ 0.0577	×
3	↓ 0.2518	✓	↓ 2.1311	✓	↓ 0.1997	✓	↓ 1.2692	✓	↓ 1.2885	✓	↓ 1.3247	✓	↓ 0.0456	✓
4	↓ 0.7640	✓	↓ 1.6714	✓	↓ 0.3207	✓	↓ 0.1580	×	↓ 0.1450	×	↓ 0.1271	×	↑ 0.0394	×
5	↓ 2.3918	✓	↓ 2.2964	✓	↓ 0.3106	✓	↓ 0.9647	✓	↓ 1.2653	✓	↓ 1.3764	✓	↓ 0.0648	×
6	↓ 0.1790	✓	↓ 0.7988	✓	↓ 0.1398	✓	↓ 0.4432	✓	↓ 0.4538	✓	↓ 0.4580	✓	↓ 0.0246	×
7	↓ 1.9642	✓	↓ 1.6058	✓	↓ 0.3733	✓	↑ 0.7222	×	↑ 0.6933	×	↑ 0.6048	×	↑ 0.1190	✓
8	↓ 0.0658	✓	↓ 1.3895	✓	↓ 0.2491	✓	↓ 0.3057	✓	↓ 0.3332	✓	↓ 0.3506	✓	↓ 0.0157	✓
9	↓ 0.6986	✓	↓ 1.7441	✓	↓ 0.2338	✓	↓ 0.4539	✓	↓ 0.5439	✓	↓ 0.5899	✓	↑ 0.1221	×
10	↓ 0.6081	✓	↓ 1.5660	✓	↓ 0.2576	✓	↓ 0.3218	×	↓ 0.2725	×	↓ 0.3398	×	↑ 0.0503	×
11	↓ 2.2414	✓	↓ 1.7294	✓	↓ 0.4093	✓	↓ 0.1940	×	↓ 0.2102	×	↓ 0.2129	×	↑ 0.0864	×

CMCC_CM2_SR5_ssp5 8.5

Station	HS average		SCD5		SD		HN		H2D		H3D		HN average	
	trend	Sign.	trend	Sign.	trend	Sign.	trend	Sign.	trend	Sign.	trend	Sign.	trend	Sign.
1	↑ 0,0492	×	↑ 0,2556	×	↑ 0,0426	×	↑ 0,0598	×	↑ 0,0502	×	↑ 0,0582	×	↑ 0,0193	×
2	↑ 0,5511	×	↑ 0,1090	×	↑ 0,0368	×	↓ 0,0855	×	↑ 0,0575	×	↑ 0,1453	×	↑ 0,0395	×
3	↓ 0,1078	×	↓ 0,3077	×	↓ 0,0000	×	↓ 0,4199	×	↓ 0,4274	×	↓ 0,4507	×	↓ 0,1431	×
4	↓ 0,0411	×	↓ 0,0363	×	↑ 0,0046	×	↓ 0,0551	×	↑ 0,1547	×	↑ 0,1294	×	↑ 0,0152	×
5	↑ 0,3265	×	↑ 0,0513	×	↓ 0,0070	×	↑ 0,5640	×	↑ 0,6798	×	↑ 0,5465	×	↑ 0,0460	×
6	↑ 0,1353	×	↑ 0,1466	×	↓ 0,0138	×	↑ 0,1322	×	↑ 0,1317	×	↑ 0,1475	×	↑ 0,0170	×
7	↑ 0,4429	×	↓ 0,0007	×	↓ 0,0256	×	↑ 0,2714	×	↑ 0,1135	×	↑ 0,0899	×	↑ 0,0550	×
8	↑ 0,0371	✓	↑ 0,0937	×	↓ 0,0194	×	↑ 0,0618	×	↑ 0,0714	×	↑ 0,0681	×	↑ 0,0205	✓
9	↑ 0,1863	×	↑ 0,0447	×	↑ 0,0114	×	↑ 0,0018	×	↑ 0,1114	×	↑ 0,1326	×	↓ 0,0055	×
10	↓ 0,0880	×	↓ 0,0012	×	↓ 0,0250	×	↑ 0,2070	×	↑ 0,2107	×	↑ 0,1690	×	↑ 0,0283	×
11	↓ 0,1292	×	↑ 0,0321	×	↑ 0,0241	×	↓ 0,1279	×	↓ 0,2055	×	↓ 0,1742	×	↓ 0,0104	×

EC_EARTH3_ssp1 2.6

Station	HS average		SCD5		SD		HN		H2D		H3D		HN average	
	trend	Sign.	trend	Sign.	trend	Sign.	trend	Sign.	trend	Sign.	trend	Sign.	trend	Sign.
1	↓ 0,1234	×	↓ 0,3585	✓	↓ 0,0784	✓	↓ 0,1101	×	↓ 0,1579	×	↓ 0,1664	×	↑ 0,0152	×
2	↓ 0,5464	×	↓ 0,5059	×	↓ 0,0708	×	↓ 0,4680	×	↓ 0,4735	×	↓ 0,4882	×	↑ 0,0486	×
3	↓ 0,2148	✓	↓ 1,3207	✓	↓ 0,0925	✓	↓ 1,1545	✓	↓ 1,1238	✓	↓ 1,2137	✓	↓ 0,0680	×
4	↓ 0,6351	×	↓ 0,4682	✓	↓ 0,0784	×	↓ 0,5078	×	↓ 0,4503	×	↓ 0,5635	✓	↓ 0,0183	×
5	↓ 0,7115	✓	↓ 0,7250	✓	↓ 0,1131	✓	↓ 0,5071	×	↓ 0,5459	×	↓ 0,6138	✓	↓ 0,0133	×
6	↓ 0,0483	×	↓ 0,3962	✓	↓ 0,0624	✓	↑ 0,0247	×	↓ 0,0009	×	↓ 0,0333	×	↑ 0,0171	×
7	↓ 1,0917	×	↓ 0,4399	✓	↓ 0,0770	✓	↓ 0,1556	×	↓ 0,3153	×	↓ 0,4344	×	↑ 0,0186	×
8	↓ 0,0219	×	↓ 0,4732	✓	↓ 0,0856	✓	↓ 0,1936	✓	↓ 0,2055	×	↓ 0,2047	×	↑ 0,0129	×
9	↓ 0,4519	✓	↓ 0,6170	✓	↓ 0,0671	✓	↓ 0,4587	✓	↓ 0,4988	✓	↓ 0,4998	✓	↓ 0,0528	✓
10	↓ 0,3907	×	↓ 0,2686	×	↓ 0,0682	✓	↓ 0,0284	×	↓ 0,0427	×	↓ 0,0486	×	↑ 0,0255	×
11	↓ 0,8685	✓	↓ 0,3419	×	↓ 0,0643	×	↑ 0,2807	×	↑ 0,2461	×	↑ 0,4434	×	↓ 0,0084	×

EC_EARTH3_ssp2 4.5

Station	HS average		SCD5		SD		HN		H2D		H3D		HN average	
	trend	Sign.	trend	Sign.	trend	Sign.	trend	Sign.	trend	Sign.	trend	Sign.	trend	Sign.
1	↓ 0,1648	✓	↓ 0,4609	✓	↓ 0,0768	✓	↓ 0,3087	✓	↓ 0,3058	✓	↓ 0,3028	✓	↓ 0,0306	✓
2	↓ 2,1661	✓	↓ 1,9660	✓	↓ 0,2518	✓	↓ 0,7749	×	↓ 1,1449	✓	↓ 1,2220	✓	↓ 0,0658	×
3	↓ 0,1078	×	↓ 1,4428	✓	↓ 0,1267	✓	↓ 0,6162	✓	↓ 0,7116	✓	↓ 0,8227	✓	↑ 0,1047	×
4	↓ 0,9777	✓	↓ 1,4231	✓	↓ 0,2414	✓	↓ 0,5230	×	↓ 0,6757	✓	↓ 0,8285	✓	↓ 0,0388	×
5	↓ 1,3920	✓	↓ 1,6105	✓	↓ 0,2480	✓	↓ 0,6535	✓	↓ 0,8622	✓	↓ 0,8862	✓	↑ 0,0070	×
6	↓ 0,1153	✓	↓ 0,7822	✓	↓ 0,1171	✓	↓ 0,2289	✓	↓ 0,2591	✓	↓ 0,2534	✓	↓ 0,0100	×
7	↓ 3,2009	✓	↓ 1,5819	✓	↓ 0,2549	✓	↓ 0,4306	×	↓ 0,5636	×	↓ 0,5726	×	↑ 0,0210	×
8	↓ 0,0517	✓	↓ 1,1188	✓	↓ 0,1787	✓	↓ 0,2061	✓	↓ 0,2103	✓	↓ 0,2157	✓	↓ 0,0168	✓
9	↓ 0,7093	✓	↓ 1,3384	✓	↓ 0,1647	✓	↓ 0,5553	✓	↓ 0,6311	✓	↓ 0,7226	✓	↑ 0,0323	×
10	↓ 0,5662	✓	↓ 1,1499	✓	↓ 0,1576	✓	↓ 0,5074	×	↓ 0,5076	×	↓ 0,5442	×	↑ 0,0075	×
11	↓ 2,5559	✓	↓ 1,6122	✓	↓ 0,2867	✓	↓ 0,4161	×	↓ 0,5524	×	↓ 0,5422	×	↑ 0,0351	×

EC_EARTH3_ssp3 7.0

Station	HS average		SCD5		SD		HN		H2D		H3D		HN average	
	trend	Sign.	trend	Sign.	trend	Sign.	trend	Sign.	trend	Sign.	trend	Sign.	trend	Sign.
1	↓ 0,0970	×	↓ 0,3863	✓	↓ 0,0717	✓	↓ 0,2016	×	↓ 0,2015	×	↓ 0,2091	×	↓ 0,0395	×
2	↓ 2,5333	✓	↓ 2,6954	✓	↓ 0,3368	✓	↓ 1,0609	✓	↓ 1,1871	✓	↓ 1,2880	✓	↑ 0,2446	×
3	↓ 0,2426	✓	↓ 1,2837	✓	↓ 0,1372	✓	↓ 0,7015	✓	↓ 0,7991	✓	↓ 0,8060	✓	↓ 0,1381	✓
4	↓ 0,9964	✓	↓ 1,9014	✓	↓ 0,3337	✓	↓ 0,6867	✓	↓ 0,7011	✓	↓ 0,8207	✓	↓ 0,0048	×
5	↓ 1,4959	✓	↓ 2,0630	✓	↓ 0,3097	✓	↓ 0,9338	✓	↓ 1,1015	✓	↓ 1,1425	✓	↑ 0,0274	×
6	↓ 0,1329	✓	↓ 0,8704	✓	↓ 0,1379	✓	↓ 0,4130	✓	↓ 0,4660	✓	↓ 0,4642	✓	↓ 0,0141	×
7	↓ 3,3380	✓	↓ 1,6506	✓	↓ 0,2847	✓	↓ 0,0633	×	↓ 0,1374	×	↓ 0,2013	×	↑ 0,0485	×
8	↓ 0,0802	✓	↓ 1,2167	✓	↓ 0,1933	✓	↓ 0,2782	✓	↓ 0,2911	✓	↓ 0,3008	✓	↓ 0,0343	✓
9	↓ 0,5534	✓	↓ 1,4916	✓	↓ 0,1925	✓	↓ 0,7284	✓	↓ 0,7695	✓	↓ 0,9586	✓	↑ 0,0124	×
10	↓ 0,6689	✓	↓ 1,5871	✓	↓ 0,2226	✓	↓ 0,8105	✓	↓ 0,7837	✓	↓ 0,8414	✓	↑ 0,0043	×
11	↓ 2,8892	✓	↓ 2,0116	✓	↓ 0,3632	✓	↓ 0,5969	×	↓ 0,6041	✓	↓ 0,5811	×	↑ 0,0515	×

EC_EARTH3_ssp5 8.5

Station	HS average		SCD5		SD		HN		H2D		H3D		HN average	
	trend	Sign.	trend	Sign.	trend	Sign.	trend	Sign.	trend	Sign.	trend	Sign.	trend	Sign.
1	↓ 0,0783	×	↓ 0,2140	✓	↓ 0,0359	×	↓ 0,2263	✓	↓ 0,2276	✓	↓ 0,2207	✓	↓ 0,0883	×
2	↓ 0,3309	×	↓ 0,7823	✓	↓ 0,1148	✓	↓ 0,0448	×	↓ 0,0855	×	↓ 0,1297	×	↑ 0,0640	×
3	↓ 0,2283	✓	↓ 1,4324	✓	↓ 0,1114	✓	↓ 0,6081	✓	↓ 0,8753	✓	↓ 0,8187	✓	↑ 0,0859	×
4	↓ 0,2647	×	↓ 0,6300	✓	↓ 0,1328	✓	↓ 0,0188	×	↑ 0,0003	×	↑ 0,0747	×	↑ 0,0097	×
5	↓ 0,2347	×	↓ 0,7590	✓	↓ 0,1276	✓	↓ 0,1127	×	↑ 0,0541	×	↑ 0,0743	×	↑ 0,0541	×
6	↓ 0,0293	×	↓ 0,2510	✓	↓ 0,0397	✓	↓ 0,1708	✓	↓ 0,1744	✓	↓ 0,1870	✓	↓ 0,0287	×
7	↓ 0,5628	×	↓ 0,5441	✓	↓ 0,1254	✓	↓ 0,1502	×	↓ 0,2844	×	↓ 0,1940	×	↑ 0,0202	×
8	↑ 0,0127	×	↓ 0,4933	✓	↓ 0,1045	✓	↓ 0,0114	×	↓ 0,0167	×	↓ 0,0207	×	↑ 0,0115	×
9	↓ 0,4569	×	↓ 0,6190	✓	↓ 0,0965	✓	↓ 0,5360	✓	↓ 0,4985	×	↓ 0,4914	×	↓ 0,0052	×
10	↓ 0,1841	×	↓ 0,5950	✓	↓ 0,0985	✓	↓ 0,1554	×	↓ 0,1708	×	↓ 0,2406	×	↓ 0,0064	×
11	↓ 1,0052	✓	↓ 0,7312	✓	↓ 0,1532	✓	↑ 0,0484	×	↑ 0,0026	×	↑ 0,0614	×	↓ 0,0029	×

HadGEM3_GC31_LL_ssp1 2.6

Station	HS average		SCD5		SD		HN		H2D		H3D		HN average	
	trend	Sign.	trend	Sign.	trend	Sign.	trend	Sign.	trend	Sign.	trend	Sign.	trend	Sign.
1	↓ 0,0160	×	↓ 0,2409	✓	↓ 0,0391	✓	↓ 0,0479	×	↓ 0,0612	×	↓ 0,0690	×	↑ 0,0354	×
2	↓ 0,8737	✓	↓ 1,1221	✓	↓ 0,1471	✓	↓ 0,4949	×	↓ 0,5063	×	↓ 0,4168	×	↓ 0,0337	×
3	↓ 0,1938	×	↓ 0,9843	✓	↓ 0,0783	✓	↓ 0,8743	✓	↓ 1,0334	✓	↓ 1,0307	✓	↓ 0,0324	×
4	↓ 0,3650	✓	↓ 0,9843	✓	↓ 0,1651	✓	↓ 0,1601	×	↓ 0,1047	×	↓ 0,0969	×	↑ 0,0007	×
5	↓ 0,3524	×	↓ 0,8217	✓	↓ 0,1591	✓	↑ 0,3606	×	↑ 0,2694	×	↑ 0,2866	×	↑ 0,1238	×
6	↑ 0,0175	×	↓ 0,3385	✓	↓ 0,0455	✓	↓ 0,0259	×	↓ 0,0330	×	↓ 0,0305	×	↓ 0,0079	×
7	↓ 1,1741	✓	↓ 0,9385	✓	↓ 0,1735	✓	↓ 0,2047	×	↓ 0,1583	×	↓ 0,1703	×	↑ 0,0011	×
8	↓ 0,0390	✓	↓ 0,6142	✓	↓ 0,1089	✓	↓ 0,1491	✓	↓ 0,1445	✓	↓ 0,1434	✓	↓ 0,0246	×
9	↓ 0,2075	×	↓ 0,9204	✓	↓ 0,1336	✓	↓ 0,0456	×	↓ 0,0345	×	↓ 0,0646	×	↑ 0,0489	×
10	↓ 0,1316	×	↓ 0,8097	✓	↓ 0,1243	✓	↓ 0,0329	×	↑ 0,0695	×	↑ 0,0737	×	↑ 0,0474	×
11	↓ 1,1425	✓	↓ 1,0506	✓	↓ 0,1278	✓	↓ 0,7020	✓	↓ 0,6238	✓	↓ 0,5901	✓	↓ 0,0416	×

HadGEM3_GC31_LL_ssp2 4.5

Station	HS average		SCD5		SD		HN		H2D		H3D		HN average	
	trend	Sign.	trend	Sign.	trend	Sign.	trend	Sign.	trend	Sign.	trend	Sign.	trend	Sign.
1	↓ 0,1455	×	↓ 0,4320	✓	↓ 0,0650	✓	↓ 0,2481	×	↓ 0,2629	×	↓ 0,2930	×	↓ 0,0220	×
2	↓ 2,2524	✓	↓ 2,4164	✓	↓ 0,2688	✓	↓ 1,0974	✓	↓ 1,2560	✓	↓ 1,4142	✓	↓ 0,0175	×
3	↓ 0,1805	×	↓ 1,2292	✓	↓ 0,1001	✓	↓ 0,8282	×	↓ 0,9013	×	↓ 0,8955	×	↑ 0,1430	×
4	↓ 0,8343	✓	↓ 1,7981	✓	↓ 0,3268	✓	↓ 0,5167	✓	↓ 0,6381	✓	↓ 0,6558	✓	↓ 0,0016	×
5	↓ 2,0709	✓	↓ 2,1758	✓	↓ 0,2710	✓	↓ 1,3532	✓	↓ 1,6807	✓	↓ 1,7806	✓	↓ 0,1115	✓
6	↓ 0,0813	✓	↓ 0,6755	✓	↓ 0,1146	✓	↓ 0,3250	✓	↓ 0,3429	✓	↓ 0,3660	✓	↓ 0,0307	×
7	↓ 3,5114	✓	↓ 1,9730	✓	↓ 0,3683	✓	↓ 0,8401	✓	↓ 0,8578	✓	↓ 0,8454	✓	↓ 0,0133	×
8	↓ 0,0144	×	↓ 0,9177	✓	↓ 0,1708	✓	↓ 0,0937	✓	↓ 0,1099	✓	↓ 0,1170	✓	↑ 0,0115	×
9	↓ 1,0862	×	↓ 1,6232	✓	↓ 0,1602	✓	↓ 1,3819	✓	↓ 1,3598	✓	↓ 1,3887	✓	↓ 0,1669	✓
10	↓ 0,8135	✓	↓ 1,6904	✓	↓ 0,3061	✓	↓ 0,4087	✓	↓ 0,4057	✓	↓ 0,4676	✓	↑ 0,0386	×
11	↓ 2,6691	✓	↓ 2,3624	✓	↓ 0,3972	✓	↓ 0,9719	✓	↓ 1,1292	✓	↓ 1,1533	✓	↓ 0,0051	×

HadGEM3_GC31_LL_ssp5 8.5

Station	HS average		SCD5		SD		HN		H2D		H3D		HN average	
	trend	Sign.	trend	Sign.	trend	Sign.	trend	Sign.	trend	Sign.	trend	Sign.	trend	Sign.
1	↑ 0,0807	×	↑ 0,0252	×	↑ 0,0127	×	↑ 0,0680	×	↑ 0,0716	×	↑ 0,0954	×	↑ 0,0160	×
2	↓ 0,1502	×	↓ 0,2192	×	↑ 0,0233	×	↓ 0,0151	×	↓ 0,0695	×	↓ 0,0269	×	↓ 0,0452	×
3	↓ 0,1154	×	↓ 0,4448	×	↓ 0,0133	×	↓ 0,4806	×	↓ 0,3851	×	↓ 0,3594	×	↓ 0,0780	×
4	↓ 0,2299	×	↓ 0,1470	×	↓ 0,0591	×	↓ 0,0166	×	↓ 0,0989	×	↓ 0,0807	×	↑ 0,0116	×
5	↑ 0,1098	×	↓ 0,1958	×	↑ 0,0202	×	↑ 0,0987	×	↑ 0,1651	×	↑ 0,1712	×	↑ 0,0059	×
6	↑ 0,0890	×	↓ 0,0256	×	↑ 0,0233	×	↑ 0,1226	×	↑ 0,1318	×	↑ 0,1366	×	↑ 0,0069	×
7	↓ 0,4578	×	↓ 0,2505	×	↓ 0,0884	✓	↓ 0,5510	×	↓ 0,6479	×	↓ 0,6179	×	↑ 0,0049	×
8	↓ 0,0152	×	↓ 0,1144	×	↓ 0,0223	×	↓ 0,0837	×	↓ 0,0917	×	↓ 0,0874	×	↓ 0,0092	×
9	↑ 0,1763	×	↓ 0,1073	×	↓ 0,0012	×	↑ 0,3740	×	↑ 0,4056	×	↑ 0,3999	×	↑ 0,0225	×
10	↓ 0,0202	×	↓ 0,0894	×	↑ 0,0201	×	↑ 0,2311	×	↑ 0,1674	×	↑ 0,1305	×	↓ 0,0001	×
11	↓ 0,1232	×	↓ 0,1372	×	↓ 0,0205	×	↓ 0,0953	×	↓ 0,0374	×	↓ 0,0454	×	↑ 0,0032	×

MIROC6_ssp1 2.6

Station	HS average		SCD5		SD		HN		H2D		H3D		HN average	
	trend	Sign.	trend	Sign.	trend	Sign.	trend	Sign.	trend	Sign.	trend	Sign.	trend	Sign.
1	↓ 0,0685	×	↓ 0,3288	✓	↓ 0,0563	✓	↓ 0,0333	×	↓ 0,0346	×	↓ 0,0184	×	↓ 0,0224	×
2	↓ 0,3550	×	↓ 0,4933	✓	↓ 0,0641	✓	↓ 0,0169	×	↓ 0,0686	×	↓ 0,1684	×	↑ 0,0019	×
3	↓ 0,1351	×	↓ 1,2699	✓	↓ 0,0997	✓	↓ 0,1308	×	↓ 0,2090	×	↓ 0,2824	×	↑ 0,0984	×
4	↓ 0,2014	×	↓ 0,3482	✓	↓ 0,0752	✓	↓ 0,0860	×	↓ 0,1023	×	↓ 0,1467	×	↓ 0,0068	×
5	↓ 0,5394	×	↓ 0,5284	✓	↓ 0,1139	✓	↑ 0,0113	×	↓ 0,0357	×	↓ 0,1238	×	↑ 0,0469	×
6	↓ 0,0885	×	↓ 0,4399	✓	↓ 0,0747	✓	↓ 0,2112	×	↓ 0,2105	×	↓ 0,2367	×	↓ 0,0048	×
7	↓ 0,2848	×	↓ 0,4307	✓	↓ 0,0931	✓	↓ 0,0233	×	↑ 0,0927	×	↑ 0,0338	×	↑ 0,0164	×
8	↓ 0,0232	×	↓ 0,4082	✓	↓ 0,0677	✓	↓ 0,0383	×	↓ 0,0551	×	↓ 0,0620	×	↑ 0,0008	×
9	↓ 0,2731	×	↓ 0,5480	✓	↓ 0,0667	✓	↓ 0,3300	×	↓ 0,4840	×	↓ 0,4203	×	↓ 0,0164	×
10	↓ 0,0605	×	↓ 0,3128	✓	↓ 0,0334	×	↑ 0,1200	×	↑ 0,1818	×	↑ 0,2085	×	↑ 0,0159	×
11	↓ 0,6100	×	↓ 0,4280	✓	↓ 0,0828	✓	↑ 0,0608	×	↑ 0,2146	×	↑ 0,2390	×	↑ 0,0013	×

MIROC6_ssp2 4.5

Station	HS average		SCD5		SD		HN		H2D		H3D		HN average	
	trend	Sign.	trend	Sign.	trend	Sign.	trend	Sign.	trend	Sign.	trend	Sign.	trend	Sign.
1	↓ 0,1371	×	↓ 0,4958	✓	↓ 0,0562	✓	↓ 0,2997	×	↓ 0,2566	×	↓ 0,2896	×	↓ 0,0268	×
2	↓ 1,0263	✓	↓ 1,0829	✓	↓ 0,1430	✓	↑ 0,1401	×	↑ 0,3060	×	↑ 0,3434	×	↑ 0,0526	×
3	↓ 0,1208	×	↓ 1,8162	✓	↓ 0,1426	✓	↓ 0,5039	×	↓ 0,5806	✓	↓ 0,6139	✓	↑ 0,0804	×
4	↓ 0,2927	✓	↓ 0,7244	✓	↓ 0,1576	✓	↑ 0,0178	×	↑ 0,0312	×	↑ 0,0960	×	↑ 0,0400	×
5	↓ 1,1958	✓	↓ 1,1155	✓	↓ 0,1712	✓	↓ 0,5626	✓	↓ 0,5864	✓	↓ 0,6452	✓	↑ 0,0095	×
6	↓ 0,1408	✓	↓ 0,6334	✓	↓ 0,0690	✓	↓ 0,3041	✓	↓ 0,2888	✓	↓ 0,2950	✓	↓ 0,0297	✓
7	↓ 1,6406	✓	↓ 0,7557	✓	↓ 0,1571	✓	↑ 0,4193	×	↑ 0,5875	×	↑ 0,4616	×	↑ 0,0290	×
8	↓ 0,0160	✓	↓ 0,8118	✓	↓ 0,1280	✓	↑ 0,0083	×	↑ 0,0216	×	↑ 0,0215	×	↓ 0,0025	×
9	↓ 0,6157	✓	↓ 0,9006	✓	↓ 0,1279	✓	↓ 0,5288	✓	↓ 0,5758	✓	↓ 0,6316	✓	↓ 0,0332	×
10	↓ 0,3070	✓	↓ 0,8079	✓	↓ 0,1276	✓	↑ 0,0520	×	↑ 0,0302	×	↑ 0,0345	×	↑ 0,0138	×
11	↓ 1,5834	✓	↓ 0,9198	✓	↓ 0,1825	✓	↓ 0,1621	×	↓ 0,1961	×	↓ 0,1719	×	↓ 0,0075	×

MIROC6_ssp3 7.0

Station	HS average		SCD5		SD		HN		H2D		H3D		HN average	
	trend	Sign.	trend	Sign.	trend	Sign.	trend	Sign.	trend	Sign.	trend	Sign.	trend	Sign.
1	↓ 0,0903	×	↓ 0,4173	✓	↓ 0,0767	✓	↓ 0,1294	×	↓ 0,1735	✓	↓ 0,1743	✓	↓ 0,0046	×
2	↓ 1,3401	✓	↓ 1,6444	✓	↓ 0,1617	✓	↓ 1,1444	✓	↓ 1,1696	✓	↓ 1,1480	✓	↓ 0,0766	✓
3	↓ 0,0710	✓	↓ 1,7237	✓	↓ 0,1477	✓	↓ 0,3886	✓	↓ 0,3909	✓	↓ 0,4285	✓	↑ 0,2451	×
4	↓ 0,2640	✓	↓ 0,8939	✓	↓ 0,1777	✓	↓ 0,2230	×	↓ 0,2972	×	↓ 0,2871	×	↑ 0,0187	×
5	↓ 1,2536	✓	↓ 1,4749	✓	↓ 0,1605	✓	↓ 0,8254	✓	↓ 1,0525	×	↓ 0,9866	✓	↑ 0,0859	✓
6	↓ 0,0535	×	↓ 0,5106	✓	↓ 0,0799	✓	↓ 0,1152	×	↓ 0,1013	×	↓ 0,1170	×	↑ 0,0068	×
7	↓ 1,9880	✓	↓ 1,2486	✓	↓ 0,2183	✓	↓ 0,5065	×	↓ 0,4079	×	↓ 0,4377	×	↓ 0,0255	×
8	↓ 0,0409	✓	↓ 0,8268	✓	↓ 0,1295	✓	↓ 0,1972	✓	↓ 0,1961	✓	↓ 0,1931	✓	↓ 0,0162	×
9	↓ 0,4242	✓	↓ 0,9428	✓	↓ 0,1304	✓	↓ 0,3641	×	↓ 0,4608	×	↓ 0,4824	×	↓ 0,0156	×
10	↓ 0,2650	✓	↓ 0,8578	✓	↓ 0,1368	✓	↓ 0,2534	×	↓ 0,3554	✓	↓ 0,3056	×	↓ 0,0121	×
11	↓ 1,3995	✓	↓ 1,1389	✓	↓ 0,2185	✓	↑ 0,0360	×	↑ 0,2081	×	↑ 0,1744	×	↑ 0,0294	×

MIROC6_ssp5 8.5

Station	HS average		SCD5		SD		HN		H2D		H3D		HN average	
	trend	Sign.	trend	Sign.	trend	Sign.	trend	Sign.	trend	Sign.	trend	Sign.	trend	Sign.
1	↑ 0,0271	×	↑ 0,0670	×	↑ 0,0286	×	↑ 0,0494	×	↑ 0,0479	×	↑ 0,0567	×	↓ 0,0091	×
2	↑ 0,6084	×	↑ 0,3349	×	↑ 0,0709	×	↓ 0,0540	×	↓ 0,0786	×	↓ 0,1761	×	↓ 0,0063	×
3	↓ 0,1239	×	↑ 0,0487	×	↑ 0,0118	×	↓ 0,2102	×	↓ 0,1637	×	↓ 0,1828	×	↓ 0,0644	×
4	↑ 0,2946	×	↑ 0,1981	×	↑ 0,0454	×	↑ 0,1807	×	↑ 0,1914	×	↑ 0,1865	×	↑ 0,0066	×
5	↑ 0,6499	✓	↑ 0,2973	×	↑ 0,0535	✓	↑ 0,2254	×	↑ 0,2062	×	↑ 0,2015	×	↑ 0,0317	×
6	↓ 0,0117	×	↑ 0,0017	×	↑ 0,0053	×	↑ 0,0933	×	↑ 0,0755	×	↑ 0,0606	×	↓ 0,0159	×
7	↑ 2,5934	✓	↑ 0,5585	✓	↑ 0,0595	×	↑ 0,0726	×	↑ 0,1474	×	↑ 0,0180	×	↑ 0,0282	×
8	↑ 0,0331	✓	↑ 0,1121	×	↑ 0,0238	×	↑ 0,1367	✓	↑ 0,1471	✓	↑ 0,1458	✓	↑ 0,0152	×
9	↑ 0,2445	×	↑ 0,2286	×	↓ 0,0021	×	↑ 0,0691	×	↑ 0,0579	×	↑ 0,1444	×	↑ 0,0296	×
10	↑ 0,3909	✓	↑ 0,3692	✓	↑ 0,0816	✓	↑ 0,1433	×	↑ 0,1740	×	↑ 0,2320	×	↑ 0,0269	×
11	↑ 1,4941	✓	↑ 0,3910	✓	↑ 0,0669	×	↓ 0,0167	×	↑ 0,1955	×	↑ 0,1431	×	↑ 0,0447	×

MPI_ESM_ssp1 2.6

Station	HS average		SCD5		SD		HN		H2D		H3D		HN average	
n.	trend	Sign.	trend	Sign.	trend	Sign.	trend	Sign.	trend	Sign.	trend	Sign.	trend	Sign.
1	↑ 0,0124	×	↓ 0,0529	×	↓ 0,0127	×	↑ 0,0186	×	↑ 0,0205	×	↑ 0,0308	×	↓ 0,0075	×
2	↓ 0,4120	×	↓ 0,2795	×	↓ 0,0245	×	↓ 0,5227	×	↓ 0,5018	×	↓ 0,4272	×	↓ 0,0205	×
3	↓ 0,1074	×	↓ 1,0340	✓	↓ 0,0962	✓	↓ 0,6034	✓	↓ 0,7174	✓	↓ 0,7168	✓	↑ 0,0386	×
4	↓ 0,3574	×	↓ 0,2323	×	↓ 0,0259	×	↓ 0,0986	×	↓ 0,1664	×	↓ 0,2896	×	↓ 0,0175	×
5	↓ 0,3079	×	↓ 0,3122	×	↓ 0,0389	×	↓ 0,0906	×	↓ 0,0420	×	↓ 0,0020	×	↓ 0,0116	×
6	↓ 0,1060	×	↓ 0,1698	×	↓ 0,0234	×	↓ 0,1846	×	↓ 0,1998	×	↓ 0,1867	×	↓ 0,0248	×
7	↓ 3,4955	✓	↓ 0,8216	✓	↓ 0,0429	×	↓ 0,5253	×	↓ 0,7572	×	↓ 0,6544	×	↓ 0,0689	✓
8	↓ 0,0205	×	↓ 0,2794	✓	↓ 0,0419	✓	↓ 0,1595	✓	↓ 0,1611	✓	↓ 0,1536	✓	↓ 0,0156	×
9	↓ 0,2397	×	↓ 0,1096	×	↓ 0,0433	×	↓ 0,1201	×	↓ 0,1442	×	↓ 0,2940	×	↓ 0,0016	×
10	↓ 0,1358	×	↓ 0,2223	×	↓ 0,0457	✓	↑ 0,3396	×	↑ 0,2914	×	↑ 0,1795	×	↑ 0,0527	×
11	↓ 0,6404	×	↓ 0,3233	✓	↓ 0,0673	×	↓ 0,7904	×	↓ 0,8837	✓	↓ 0,7311	×	↓ 0,0085	×

MPI_ESM_ssp2 4.5

Station	HS average		SCD5		SD		HN		H2D		H3D		HN average	
n.	trend	Sign.	trend	Sign.	trend	Sign.	trend	Sign.	trend	Sign.	trend	Sign.	trend	Sign.
1	↓ 0,0357	✓	↓ 0,4334	✓	↓ 0,0776	✓	↓ 0,2032	✓	↓ 0,2243	✓	↓ 0,2201	✓	↓ 0,0065	×
2	↓ 1,5869	✓	↓ 1,4081	✓	↓ 0,1691	✓	↓ 0,4120	×	↓ 0,4745	×	↓ 0,5463	×	↓ 0,0075	×
3	↓ 0,2944	✓	↓ 1,5974	✓	↓ 0,1223	✓	↓ 0,8232	✓	↓ 0,9089	✓	↓ 1,0074	✓	↓ 0,1317	✓
4	↓ 0,3436	✓	↓ 0,9795	✓	↓ 0,1470	✓	↓ 0,2585	×	↓ 0,2041	×	↓ 0,2534	×	↑ 0,0219	×
5	↓ 0,8491	✓	↓ 1,2398	✓	↓ 0,1827	✓	↓ 0,2501	×	↓ 0,3260	×	↓ 0,3513	×	↓ 0,0054	×
6	↓ 0,0492	×	↓ 0,5188	✓	↓ 0,0789	✓	↓ 0,0504	×	↓ 0,0549	×	↓ 0,0846	×	↑ 0,0075	×
7	↓ 2,9552	✓	↓ 1,1686	✓	↓ 0,1849	✓	↑ 0,6876	×	↑ 0,8466	×	↑ 0,6204	×	↑ 0,0298	×
8	↑ 0,0139	×	↓ 0,8435	✓	↓ 0,1428	✓	↓ 0,0204	×	↓ 0,0215	×	↓ 0,0250	×	↑ 0,0210	×
9	↓ 0,1417	×	↓ 0,8690	✓	↓ 0,1301	✓	↓ 0,0961	×	↓ 0,1098	×	↓ 0,0932	×	↑ 0,0925	×
10	↓ 0,2190	×	↓ 0,9273	✓	↓ 0,1392	✓	↑ 0,1822	×	↑ 0,1725	×	↑ 0,1645	×	↑ 0,0696	×
11	↓ 1,9067	✓	↓ 1,0580	✓	↓ 0,1762	✓	↓ 0,5758	×	↓ 0,7487	✓	↓ 0,7849	✓	↑ 0,0027	×

MPI_ESM_ssp3 7.0

Station	HS average		SCD5		SD		HN		H2D		H3D		HN average	
n.	trend	Sign.	trend	Sign.	trend	Sign.	trend	Sign.	trend	Sign.	trend	Sign.	trend	Sign.
1	↓ 0,0353	✓	↓ 0,2769	✓	↓ 0,0654	✓	↓ 0,1412	✓	↓ 0,1524	✓	↓ 0,1539	✓	↑ 0,0086	×
2	↓ 1,5220	✓	↓ 1,6108	✓	↓ 0,2051	✓	↓ 0,6079	×	↓ 0,5461	×	↓ 0,5566	×	↓ 0,0125	×
3	↓ 0,3253	✓	↓ 1,5780	✓	↓ 0,1272	✓	↓ 1,0169	✓	↓ 1,2332	✓	↓ 1,3563	✓	↓ 0,0968	✓
4	↓ 0,7612	✓	↓ 1,2167	✓	↓ 0,1997	✓	↓ 0,4552	×	↓ 0,3467	×	↓ 0,4824	×	↓ 0,0167	×
5	↓ 0,8356	✓	↓ 1,5086	✓	↓ 0,2197	✓	↓ 0,3666	×	↓ 0,4830	×	↓ 0,5168	✓	↑ 0,0204	×
6	↓ 0,0818	✓	↓ 0,4773	✓	↓ 0,0726	✓	↓ 0,3305	✓	↓ 0,3691	✓	↓ 0,3639	✓	↓ 0,0135	×
7	↓ 6,4740	✓	↓ 1,7949	✓	↓ 0,2238	✓	↓ 0,9255	×	↓ 1,1372	×	↓ 1,2414	×	↓ 0,0360	×
8	↓ 0,0460	✓	↓ 0,7855	✓	↓ 0,1272	✓	↓ 0,2338	✓	↓ 0,2468	✓	↓ 0,2546	✓	↓ 0,0259	✓
9	↓ 0,4469	✓	↓ 1,1864	✓	↓ 0,1528	✓	↓ 0,6239	✓	↓ 0,7206	✓	↓ 0,7779	✓	↓ 0,0439	×
10	↓ 0,4516	✓	↓ 1,0759	✓	↓ 0,1734	✓	↑ 0,1009	×	↑ 0,0895	×	↑ 0,0520	×	↑ 0,0379	×
11	↓ 3,3987	✓	↓ 1,6993	✓	↓ 0,2639	✓	↓ 1,1805	✓	↓ 1,2274	✓	↓ 1,2481	✓	↓ 0,1099	✓

MPI_ESM_ssp5 8.5

Station	T average		T min		T max		P tot	
n.	m.	sign.	m.	sign.	m.	sign.	m.	sign.
1	↑ 0,0072	✓	↑ 0,0209	×	↑ 0,0166	✓	↑ 0,5096	×
2	↑ 0,0072	✓	↑ 0,0194	×	↑ 0,0169	✓	↑ 1,3321	×
3	↑ 0,0072	✓	↑ 0,0031	×	↑ 0,0039	×	↑ 0,4895	×
4	↑ 0,0059	×	↑ 0,0151	×	↑ 0,0158	✓	↑ 0,6926	×
5	↑ 0,0072	✓	↑ 0,0183	×	↑ 0,0169	✓	↑ 1,7019	×
6	↑ 0,0059	×	↑ 0,0159	×	↑ 0,0155	✓	↓ 0,4237	×
7	↑ 0,0059	×	↑ 0,0131	×	↑ 0,0167	✓	↑ 0,0997	×
8	↑ 0,0059	×	↑ 0,0059	×	↑ 0,0138	×	↓ 0,2181	×
9	↑ 0,0072	✓	↑ 0,0196	×	↑ 0,0161	✓	↑ 1,3681	×
10	↑ 0,0052	×	↑ 0,0132	×	↑ 0,0162	✓	↓ 0,1271	×
11	↑ 0,0059	×	↑ 0,0141	×	↑ 0,0162	✓	↓ 0,1872	×

Station	T average		T min		T max		P tot	
n.	m.	sign.	m.	sign.	m.	sign.	m.	sign.
1	↑ 0,0245	✓	↑ 0,0192	×	↑ 0,0348	✓	↑ 0,2741	×
2	↑ 0,0245	✓	↑ 0,0243	×	↑ 0,0355	✓	↑ 1,2831	×
3	↑ 0,0244	✓	↑ 0,0237	✓	↑ 0,0092	×	↑ 3,2120	×
4	↑ 0,0227	✓	↑ 0,0270	×	↑ 0,0282	✓	↑ 0,9418	×
5	↑ 0,0245	✓	↑ 0,0241	×	↑ 0,0353	✓	↑ 0,8926	×
6	↑ 0,0227	✓	↑ 0,0268	×	↑ 0,0287	✓	↓ 0,6143	×
7	↑ 0,0227	✓	↑ 0,0295	×	↑ 0,0313	✓	↓ 0,2849	×
8	↑ 0,0227	✓	↑ 0,0317	×	↑ 0,0283	✓	↓ 0,5239	×
9	↑ 0,0245	✓	↑ 0,0233	×	↑ 0,0339	✓	↓ 1,2210	×
10	↑ 0,0212	✓	↑ 0,0269	×	↑ 0,0296	✓	↓ 0,6644	×
11	↑ 0,0227	✓	↑ 0,0285	×	↑ 0,0299	✓	↓ 1,0195	×

CESM2_ssp1 2.6

Station	T average		T min		T max		P tot	
n.	m.	sign.	m.	sign.	m.	sign.	m.	sign.
1	↑ 0,0487	✓	↑ 0,0531	✓	↑ 0,0688	✓	↓ 2,7402	✓
2	↑ 0,0487	✓	↑ 0,0503	✓	↑ 0,0702	✓	↓ 6,0299	✓
3	↑ 0,0487	✓	↑ 0,0377	✓	↑ 0,0491	✓	↓ 4,4484	✓
4	↑ 0,0472	✓	↑ 0,0864	✓	↑ 0,0712	✓	↓ 1,7312	×
5	↑ 0,0487	✓	↑ 0,0506	✓	↑ 0,0701	✓	↓ 9,6787	✓
6	↑ 0,0472	✓	↑ 0,0877	✓	↑ 0,0695	✓	↓ 1,5337	✓
7	↑ 0,0472	✓	↑ 0,0833	✓	↑ 0,0701	✓	↓ 1,7112	×
8	↑ 0,0472	✓	↑ 0,0752	✓	↑ 0,0717	✓	↓ 1,9089	✓
9	↑ 0,0487	✓	↑ 0,0525	✓	↑ 0,0691	✓	↓ 5,7067	✓
10	↑ 0,0454	✓	↑ 0,0912	✓	↑ 0,0746	✓	↓ 1,8956	×
11	↑ 0,0472	✓	↑ 0,0849	✓	↑ 0,0706	✓	↓ 1,3270	×

CESM2_ssp2 4.5

Station	T average		T min		T max		P tot	
n.	m.	sign.	m.	sign.	m.	sign.	m.	sign.
1	↑ 0,0642	✓	↑ 0,0368	✓	↑ 0,1073	✓	↓ 2,3411	×
2	↑ 0,0642	✓	↑ 0,0353	✓	↑ 0,1089	✓	↓ 4,5434	×
3	↑ 0,0642	✓	↑ 0,0500	✓	↑ 0,0765	✓	↓ 3,3081	×
4	↑ 0,0611	✓	↑ 0,0638	✓	↑ 0,0951	✓	↓ 0,2065	×
5	↑ 0,0642	✓	↑ 0,0345	✓	↑ 0,1089	✓	↓ 4,8899	×
6	↑ 0,0611	✓	↑ 0,0643	✓	↑ 0,0945	✓	↓ 1,3914	×
7	↑ 0,0611	✓	↑ 0,0633	✓	↑ 0,0951	✓	↓ 1,2613	×
8	↑ 0,0611	✓	↑ 0,0620	✓	↑ 0,0938	✓	↓ 2,2886	×
9	↑ 0,0642	✓	↑ 0,0349	✓	↑ 0,1073	✓	↓ 2,1156	×
10	↑ 0,0581	✓	↑ 0,0545	✓	↑ 0,0908	✓	↓ 1,8680	×
11	↑ 0,0611	✓	↑ 0,0633	✓	↑ 0,0952	✓	↓ 1,7386	×

CESM2_ssp3 7.0

CESM3_ssp5 8.5

Station	T average			T min			T max			P tot		
	n.	m.	sign.	m.	sign.	m.	sign.	m.	sign.	m.	sign.	
1	↑	0,0264	✓	↓	0,0035	×	↑	0,0196	✓	↑	1,0337	×
2	↑	0,0264	✓	↓	0,0031	×	↑	0,0193	✓	↑	2,7253	×
3	↑	0,0264	✓	↑	0,0196	✓	↑	0,0219	✓	↑	2,8351	×
4	↑	0,0278	✓	↓	0,0201	×	↑	0,0177	✓	↑	1,5777	×
5	↑	0,0264	✓	↓	0,0024	×	↑	0,0192	✓	↑	3,7033	×
6	↑	0,0278	✓	↑	0,0191	×	↑	0,0175	✓	↑	1,0721	×
7	↑	0,0278	✓	↑	0,0197	×	↑	0,0176	✓	↑	3,0886	×
8	↑	0,0278	✓	↑	0,0168	×	↑	0,0162	✓	↑	1,3075	✓
9	↑	0,0264	✓	↓	0,0031	×	↑	0,0189	✓	↑	2,2394	×
10	↑	0,0275	✓	↑	0,0281	×	↑	0,0172	✓	↑	2,0057	×
11	↑	0,0278	✓	↑	0,0197	×	↑	0,0172	✓	↑	1,4082	×

CMCC_CM2_SR5_ssp1 2.6

Station	T average			T min			T max			P tot		
	n.	m.	sign.	m.	sign.	m.	sign.	m.	sign.	m.	sign.	
1	↑	0,0548	✓	↑	0,0763	✓	↑	0,0658	✓	↓	0,1197	×
2	↑	0,0547	✓	↑	0,0745	✓	↑	0,0678	✓	↓	2,1843	×
3	↑	0,0547	✓	↑	0,0605	✓	↑	0,0505	✓	↑	0,0125	×
4	↑	0,0590	✓	↑	0,1056	✓	↑	0,0753	✓	↓	0,1700	×
5	↑	0,0547	✓	↑	0,0749	✓	↑	0,0680	✓	↑	1,6963	×
6	↑	0,0590	✓	↑	0,1044	✓	↑	0,0725	✓	↓	0,0352	×
7	↑	0,0590	✓	↑	0,1072	✓	↑	0,0751	✓	↓	0,1934	×
8	↑	0,0590	✓	↑	0,1048	✓	↑	0,0672	✓	↑	0,6319	×
9	↑	0,0547	✓	↑	0,0769	✓	↑	0,0689	✓	↓	1,1207	×
10	↑	0,0579	✓	↑	0,1058	✓	↑	0,0742	✓	↑	0,9450	×
11	↑	0,0590	✓	↑	0,1069	✓	↑	0,0757	✓	↓	0,9595	×

CMCC_CM2_SR5_ssp3 7.0

Station	T average			T min			T max			P tot		
	n.	m.	sign.	m.	sign.	m.	sign.	m.	sign.	m.	sign.	
1	↓	0,0004	×	↓	0,0107	×	↑	0,0014	×	↑	0,2408	×
2	↑	0,0011	×	↓	0,0073	×	↑	0,0031	×	↑	2,5267	×
3	↓	0,0004	×	↓	0,0037	×	↓	0,0002	×	↑	2,5219	×
4	↓	0,0004	×	↓	0,0109	×	↑	0,0010	×	↑	1,5756	×
5	↓	0,0004	×	↓	0,0123	×	↑	0,0006	×	↑	0,1508	×
6	↑	0,0003	×	↓	0,0239	×	↑	0,0055	×	↑	0,9053	✓
7	↓	0,0006	×	↓	0,0285	×	↑	0,0040	×	↑	1,7417	×
8	↑	0,0003	×	↓	0,0188	×	↑	0,0049	×	↑	0,0143	×
9	↓	0,0004	×	↓	0,0118	×	↑	0,0007	×	↑	0,9274	×
10	↓	0,0014	×	↓	0,0266	×	↑	0,0008	×	↓	0,3562	×
11	↑	0,0003	×	↓	0,0259	×	↑	0,0058	×	↑	1,4055	×

EC_EARTH3_ssp1 2.6

Station	T average			T min			T max			P tot		
	n.	m.	sign.	m.	sign.	m.	sign.	m.	sign.	m.	sign.	
1	↑	0,0626	✓	↑	0,0664	✓	↑	0,0906	✓	↓	0,3028	×
2	↑	0,0623	✓	↑	0,0578	✓	↑	0,0952	✓	↑	0,9819	×
3	↑	0,0626	✓	↑	0,0625	✓	↑	0,0707	✓	↑	0,0592	×
4	↑	0,0626	✓	↑	0,0638	✓	↑	0,0910	✓	↑	1,1115	×
5	↑	0,0626	✓	↑	0,0607	✓	↑	0,0926	✓	↑	0,8083	×
6	↑	0,0571	✓	↑	0,0454	✓	↑	0,0654	✓	↑	0,9846	✓
7	↑	0,0572	✓	↑	0,0469	✓	↑	0,0662	✓	↑	1,5737	×
8	↑	0,0571	✓	↑	0,0495	✓	↑	0,0653	✓	↑	1,0928	×
9	↑	0,0626	✓	↑	0,0625	✓	↑	0,0910	✓	↓	1,0118	×
10	↑	0,0559	✓	↑	0,0457	✓	↑	0,0644	✓	↑	0,4847	×
11	↑	0,0571	✓	↑	0,0448	✓	↑	0,0665	✓	↑	3,0726	✓

EC_EARTH_ssp3 7.0

Station	T average			T min			T max			P tot		
	n.	m.	sign.	m.	sign.	m.	sign.	m.	sign.	m.	sign.	
1	↑	0,0225	✓	↑	0,0244	×	↑	0,0265	✓	↓	0,0066	×
2	↑	0,0225	✓	↑	0,0288	×	↑	0,0278	✓	↑	0,9020	×
3	↑	0,0225	✓	↑	0,0290	✓	↑	0,0281	✓	↑	1,1037	×
4	↑	0,0238	✓	↑	0,0306	×	↑	0,0246	✓	↑	0,9064	×
5	↑	0,0225	✓	↑	0,0292	×	↑	0,0274	✓	↓	0,0627	×
6	↑	0,0238	✓	↑	0,0285	×	↑	0,0259	✓	↑	0,0413	×
7	↑	0,0237	✓	↑	0,0299	×	↑	0,0252	✓	↑	1,0205	×
8	↑	0,0238	✓	↑	0,0309	×	↑	0,0255	✓	↓	0,4890	×
9	↑	0,0225	✓	↑	0,0290	×	↑	0,0254	✓	↓	0,2168	×
10	↑	0,0238	✓	↑	0,0359	×	↑	0,0246	✓	↓	1,0036	×
11	↑	0,0237	✓	↑	0,0301	×	↑	0,0250	✓	↓	0,1342	×

HadGEM3_GC31_LL_ssp1 2.6

Station	T average			T min			T max			P tot		
	n.	m.	sign.	m.	sign.	m.	sign.	m.	sign.	m.	sign.	
1	↑	0,0371	✓	↑	0,0441	✓	↑	0,0397	✓	↑	0,9712	×
2	↑	0,0371	✓	↑	0,0446	✓	↑	0,0400	✓	↑	1,4725	×
3	↑	0,0371	✓	↑	0,0538	✓	↑	0,0272	✓	↑	0,8368	×
4	↑	0,0423	✓	↑	0,0638	✓	↑	0,0435	✓	↑	1,3811	×
5	↑	0,0371	✓	↑	0,0437	✓	↑	0,0400	✓	↓	0,1749	×
6	↑	0,0423	✓	↑	0,0644	✓	↑	0,0434	✓	↑	1,0573	×
7	↑	0,0423	✓	↑	0,0641	✓	↑	0,0433	✓	↑	2,1828	×
8	↑	0,0423	✓	↑	0,0671	✓	↑	0,0328	✓	↑	0,6138	×
9	↑	0,0371	✓	↑	0,0432	✓	↑	0,0405	✓	↑	0,4520	×
10	↑	0,0421	✓	↑	0,0676	✓	↑	0,0451	✓	↑	1,0465	×
11	↑	0,0423	✓	↑	0,0642	✓	↑	0,0427	✓	↑	0,5121	×

CMCC_CM2_SR5_ssp2 4.5

Station	T average			T min			T max			P tot		
	n.	m.	sign.	m.	sign.	m.	sign.	m.	sign.	m.	sign.	
1	↑	0,0798	✓	↑	0,0835	✓	↑	0,1091	✓	↑	0,9439	×
2	↑	0,0798	✓	↑	0,0860	✓	↑	0,1091	✓	↑	3,1463	×
3	↑	0,0798	✓	↑	0,0872	✓	↑	0,0877	✓	↑	3,1114	×
4	↑	0,0824	✓	↑	0,0956	✓	↑	0,1092	✓	↑	1,5444	×
5	↑	0,0798	✓	↑	0,0866	✓	↑	0,1091	✓	↑	5,4988	×
6	↑	0,0824	✓	↑	0,0958	✓	↑	0,1074	✓	↑	0,5836	×
7	↑	0,0824	✓	↑	0,0956	✓	↑	0,1086	✓	↑	1,2279	×
8	↑	0,0824	✓	↑	0,0953	✓	↑	0,1059	✓	↓	0,1752	×
9	↑	0,0798	✓	↑	0,0868	✓	↑	0,1098	✓	↑	2,0849	×
10	↑	0,0806	✓	↑	0,0883	✓	↑	0,1073	✓	↑	0,0631	×
11	↑	0,0824	✓	↑	0,0956	✓	↑	0,1074	✓	↑	1,8711	×

CMCC_CM2_SR5_ssp5 8.5

Station	T average			T min			T max			P tot		
	n.	m.	sign.	m.	sign.	m.	sign.	m.	sign.	m.	sign.	
1	↑	0,0265	✓	↑	0,0446	✓	↑	0,0420	✓	↓	1,9356	✓
2	↑	0,0260	✓	↑	0,0448	✓	↑	0,0434	✓	↓	1,1318	×
3	↑	0,0264	✓	↑	0,0450	✓	↑	0,0220	✓	↓	2,5232	×
4	↑	0,0265	✓	↑	0,0450	✓	↑	0,0418	✓	↓	1,0290	×
5	↑	0,0265	✓	↑	0,0469	✓	↑	0,0424	✓	↓	2,3455	×
6	↑	0,0226	✓	↑	0,0371	✓	↑	0,0303	✓	↓	0,3954	×
7	↑	0,0228	✓	↑	0,0431	✓	↑	0,0323	✓	↓	0,1480	×
8	↑	0,0226	✓	↑	0,0269	×	↑	0,0281	✓	↓	0,6924	×
9	↑	0,0265	✓	↑	0,0462	✓	↑	0,0424	✓	↓	2,4120	×
10	↑	0,0224	✓	↑	0,0454	✓	↑	0,0290	✓	↓	0,3410	×
11	↑	0,0226	✓	↑	0,0382	✓	↑	0,0301	✓	↑	1,2978	×

EC_EARTH3_ssp2 4.5

Station	T average			T min			T max			P tot		
	n.	m.	sign.	m.	sign.	m.	sign.	m.	sign.	m.	sign.	
1	↑	0,0779	✓	↑	0,0944	✓	↑	0,1222	✓	↑	0,1228	×
2	↑	0,0770	✓	↑	0,1042	✓	↑	0,1245	✓	↑	1,2261	×
3	↑	0,0779	✓	↑	0,0866	✓	↑	0,0808	✓	↑	0,5230	×
4	↑	0,0779	✓	↑	0,0963	✓	↑	0,1225	✓	↑	1,5250	×
5	↑	0,0779	✓	↑	0,0937	✓	↑	0,1232	✓	↑	0,7388	×
6	↑	0,0707	✓	↑	0,1022	✓	↑	0,0872	✓	↑	1,6526	✓
7	↑	0,0712	✓	↑	0,1004	✓	↑	0,0934	✓	↑	3,6373	✓
8	↑	0,0707	✓	↑	0,1064	✓	↑	0,0800	✓	↑	0,8768	×
9	↑	0,0779	✓	↑	0,0951	✓	↑	0,1226	✓	↓	0,5715	×
10	↑	0,0703	✓	↑	0,0975	✓	↑	0,0953	✓	↑	1,0639	×
11	↑	0,0707	✓	↑	0,1014	✓	↑	0,0886	✓	↑	3,7157	✓

EC_EARTH_ssp5 8.5

Station	T average			T min</		
---------	-----------	--	--	---------	--	--

Station	T average		T min		T max		P tot	
	m.	sign.	m.	sign.	m.	sign.	m.	sign.
1	↑ 0,0894	✓	↑ 0,1443	✓	↑ 0,1221	✓	↓ 3,0609	✓
2	↑ 0,0894	✓	↑ 0,1397	✓	↑ 0,1233	✓	↓ 5,3264	✓
3	↑ 0,0894	✓	↑ 0,1110	✓	↑ 0,0982	✓	↓ 6,7736	✓
4	↑ 0,0914	✓	↑ 0,1908	✓	↑ 0,1211	✓	↓ 1,9950	×
5	↑ 0,0894	✓	↑ 0,1374	✓	↑ 0,1234	✓	↓ 7,3178	✓
6	↑ 0,0914	✓	↑ 0,1923	✓	↑ 0,1209	✓	↓ 1,4838	✓
7	↑ 0,0914	✓	↑ 0,1863	✓	↑ 0,1231	✓	↓ 2,5204	×
8	↑ 0,0914	✓	↑ 0,1878	✓	↑ 0,1152	✓	↓ 2,4036	✓
9	↑ 0,0894	✓	↑ 0,1399	✓	↑ 0,1227	✓	↓ 4,9936	✓
10	↑ 0,0885	✓	↑ 0,1673	✓	↑ 0,1108	✓	↓ 2,1815	×
11	↑ 0,0914	✓	↑ 0,1870	✓	↑ 0,1231	✓	↓ 2,7457	×

Station	T average		T min		T max		P tot	
	m.	sign.	m.	sign.	m.	sign.	m.	sign.
1	↑ 0,0046	×	↑ 0,0095	×	↑ 0,0137	✓	↑ 0,0594	×
2	↑ 0,0046	×	↑ 0,0074	×	↑ 0,0155	✓	↑ 0,2188	×
3	↑ 0,0046	×	↑ 0,0028	×	↑ 0,0045	×	↑ 0,0565	×
4	↑ 0,0031	×	↑ 0,0131	×	↑ 0,0113	✓	↓ 0,0230	×
5	↑ 0,0046	×	↑ 0,0062	×	↑ 0,0156	✓	↓ 0,7655	×
6	↑ 0,0031	×	↑ 0,0152	×	↑ 0,0095	✓	↑ 0,0188	×
7	↑ 0,0031	×	↑ 0,0150	×	↑ 0,0135	✓	↑ 0,8069	×
8	↑ 0,0031	×	↑ 0,0217	×	↑ 0,0025	×	↑ 0,4443	×
9	↑ 0,0046	×	↑ 0,0055	×	↑ 0,0147	✓	↑ 1,2522	×
10	↑ 0,0031	×	↑ 0,0103	×	↑ 0,0121	✓	↑ 1,2278	×
11	↑ 0,0031	×	↑ 0,0156	×	↑ 0,0133	✓	↑ 0,9240	×

HadGEM3_GC31_LL_ssp5 8.5

Station	T average		T min		T max		P tot	
	m.	sign.	m.	sign.	m.	sign.	m.	sign.
1	↑ 0,0218	✓	↑ 0,0280	✓	↑ 0,0290	✓	↓ 0,8024	×
2	↑ 0,0218	✓	↑ 0,0289	✓	↑ 0,0250	✓	↓ 1,4037	×
3	↑ 0,0218	✓	↑ 0,0272	✓	↑ 0,0189	✓	↓ 1,1839	×
4	↑ 0,0195	✓	↑ 0,0352	✓	↑ 0,0226	✓	↑ 0,0880	×
5	↑ 0,0218	✓	↑ 0,0290	✓	↑ 0,0243	✓	↓ 2,4139	×
6	↑ 0,0195	✓	↑ 0,0340	✓	↑ 0,0239	✓	↓ 0,3103	×
7	↑ 0,0195	✓	↑ 0,0370	✓	↑ 0,0209	✓	↓ 1,8766	×
8	↑ 0,0195	✓	↑ 0,0416	✓	↑ 0,0289	✓	↓ 0,4759	×
9	↑ 0,0218	✓	↑ 0,0279	✓	↑ 0,0268	✓	↓ 1,2818	×
10	↑ 0,0195	✓	↑ 0,0331	✓	↑ 0,0225	✓	↑ 0,6158	×
11	↑ 0,0195	✓	↑ 0,0375	✓	↑ 0,0207	✓	↑ 0,4994	×

MIROC6_ssp1 2.6

Station	T average		T min		T max		P tot	
	m.	sign.	m.	sign.	m.	sign.	m.	sign.
1	↑ 0,0403	✓	↑ 0,0295	✓	↑ 0,0537	✓	↓ 0,8731	×
2	↑ 0,0403	✓	↑ 0,0295	✓	↑ 0,0546	✓	↓ 1,5425	×
3	↑ 0,0403	✓	↑ 0,0306	✓	↑ 0,0268	✓	↓ 1,0684	×
4	↑ 0,0374	✓	↑ 0,0437	✓	↑ 0,0423	✓	↑ 0,7388	×
5	↑ 0,0403	✓	↑ 0,0294	✓	↑ 0,0546	✓	↓ 0,4302	×
6	↑ 0,0374	✓	↑ 0,0426	✓	↑ 0,0431	✓	↓ 0,5290	×
7	↑ 0,0374	✓	↑ 0,0445	✓	↑ 0,0439	✓	↓ 0,1810	×
8	↑ 0,0374	✓	↑ 0,0442	✓	↑ 0,0413	✓	↓ 0,8742	×
9	↑ 0,0403	✓	↑ 0,0289	✓	↑ 0,0532	✓	↓ 2,4796	×
10	↑ 0,0374	✓	↑ 0,0417	✓	↑ 0,0434	✓	↑ 0,8495	×
11	↑ 0,0374	✓	↑ 0,0437	✓	↑ 0,0431	✓	↓ 0,2345	×

MIROC6_ssp2 4.5

Station	T average		T min		T max		P tot	
	m.	sign.	m.	sign.	m.	sign.	m.	sign.
1	↑ 0,0554	✓	↑ 0,0553	✓	↑ 0,0715	✓	↓ 1,3012	×
2	↑ 0,0554	✓	↑ 0,0553	✓	↑ 0,0723	✓	↓ 2,2456	×
3	↑ 0,0553	✓	↑ 0,0502	✓	↑ 0,0489	✓	↓ 2,2670	×
4	↑ 0,0496	✓	↑ 0,0671	✓	↑ 0,0439	✓	↓ 0,5428	×
5	↑ 0,0554	✓	↑ 0,0562	✓	↑ 0,0725	✓	↓ 4,8480	✓
6	↑ 0,0496	✓	↑ 0,0675	✓	↑ 0,0441	✓	↓ 0,4696	×
7	↑ 0,0496	✓	↑ 0,0657	✓	↑ 0,0453	✓	↓ 2,5778	×
8	↑ 0,0496	✓	↑ 0,0571	✓	↑ 0,0456	✓	↓ 0,7817	×
9	↑ 0,0554	✓	↑ 0,0595	✓	↑ 0,0715	✓	↓ 1,7189	×
10	↑ 0,0496	✓	↑ 0,0679	✓	↑ 0,0446	✓	↓ 1,6440	×
11	↑ 0,0496	✓	↑ 0,0657	✓	↑ 0,0448	✓	↓ 1,8013	×

MIROC6_ssp3 7.0

Station	T average		T min		T max		P tot	
	m.	sign.	m.	sign.	m.	sign.	m.	sign.
1	↓ 0,0031	×	↓ 0,0081	×	↓ 0,0006	×	↑ 0,2293	×
2	↓ 0,0029	×	↓ 0,0044	×	↑ 0,0022	×	↑ 4,4773	✓
3	↓ 0,0029	×	↑ 0,0001	×	↓ 0,0135	×	↑ 3,8553	✓
4	↓ 0,0029	×	↓ 0,0050	×	↑ 0,0024	×	↑ 2,7208	×
5	↓ 0,0031	×	↓ 0,0079	×	↓ 0,0001	×	↑ 2,7475	×
6	↓ 0,0029	×	↓ 0,0050	×	↑ 0,0023	×	↑ 0,9920	×
7	↓ 0,0029	×	↓ 0,0044	×	↑ 0,0018	×	↑ 3,2206	×
8	↓ 0,0029	×	↓ 0,0014	×	↓ 0,0012	×	↑ 0,3902	×
9	↓ 0,0029	×	↓ 0,0048	×	↑ 0,0022	×	↑ 1,8189	×
10	↓ 0,0031	×	↓ 0,0094	×	↓ 0,0007	×	↑ 3,2476	✓
11	↓ 0,0029	×	↓ 0,0043	×	↑ 0,0024	×	↑ 4,2246	✓

MIROC6_ssp5 8.5

Station	T average		T min		T max		P tot	
	m.	sign.	m.	sign.	m.	sign.	m.	sign.
1	↑ 0,0176	✓	↑ 0,0095	×	↑ 0,0290	✓	↓ 1,0692	×
2	↑ 0,0177	✓	↑ 0,0167	×	↑ 0,0276	✓	↓ 3,6242	×
3	↑ 0,0177	✓	↑ 0,0314	✓	↑ 0,0182	✓	↓ 3,2973	×
4	↑ 0,0177	✓	↑ 0,0153	×	↑ 0,0275	✓	↓ 1,2441	×
5	↑ 0,0176	✓	↑ 0,0128	×	↑ 0,0304	✓	↓ 2,8308	×
6	↑ 0,0177	✓	↑ 0,0157	×	↑ 0,0269	✓	↓ 0,9887	×
7	↑ 0,0177	✓	↑ 0,0169	×	↑ 0,0280	✓	↓ 3,6516	×
8	↑ 0,0177	✓	↑ 0,0167	×	↑ 0,0286	✓	↓ 0,9216	×
9	↑ 0,0177	✓	↑ 0,0182	×	↑ 0,0278	✓	↓ 2,6836	×
10	↑ 0,0176	✓	↑ 0,0142	×	↑ 0,0307	✓	↓ 0,6567	×
11	↑ 0,0177	✓	↑ 0,0166	×	↑ 0,0276	✓	↓ 3,1241	×

MP1_ESM_ssp1 2.6

Station	T average		T min		T max		P tot	
	m.	sign.	m.	sign.	m.	sign.	m.	sign.
1	↑ 0,0423	✓	↑ 0,0511	✓	↑ 0,0391	✓	↑ 0,7331	×
2	↑ 0,0430	✓	↑ 0,0554	✓	↑ 0,0394	✓	↑ 2,5205	×
3	↑ 0,0429	✓	↑ 0,0570	✓	↑ 0,0349	✓	↑ 4,5048	×
4	↑ 0,0430	✓	↑ 0,0555	✓	↑ 0,0394	✓	↑ 3,2206	✓
5	↑ 0,0423	✓	↑ 0,0516	✓	↑ 0,0394	✓	↑ 0,0058	×
6	↑ 0,0430	✓	↑ 0,0546	✓	↑ 0,0392	✓	↑ 1,0050	×
7	↑ 0,0430	✓	↑ 0,0559	✓	↑ 0,0394	✓	↑ 0,1598	×
8	↑ 0,0430	✓	↑ 0,0590	✓	↑ 0,0435	✓	↓ 0,3533	×
9	↑ 0,0430	✓	↑ 0,0551	✓	↑ 0,0394	✓	↑ 2,6822	×
10	↑ 0,0423	✓	↑ 0,0480	✓	↑ 0,0395	✓	↑ 0,3018	×
11	↑ 0,0430	✓	↑ 0,0559	✓	↑ 0,0397	✓	↑ 2,5463	×

MPI_ESM_ssp2 4.5

Station	T average		T min		T max		P tot	
	m.	sign.	m.	sign.	m.	sign.	m.	sign.
1	↑ 0,0557	✓	↑ 0,0671	✓	↑ 0,0706	✓	↓ 0,0504	×
2	↑ 0,0564	✓	↑ 0,0721	✓	↑ 0,0748	✓	↓ 0,4335	×
3	↑ 0,0564	✓	↑ 0,0579	✓	↑ 0,0420	✓	↓ 0,5690	×
4	↑ 0,0565	✓	↑ 0,0725	✓	↑ 0,0733	✓	↑ 0,7768	×
5	↑ 0,0556	✓	↑ 0,0660	✓	↑ 0,0721	✓	↓ 0,2911	×
6	↑ 0,0565	✓	↑ 0,0724	✓	↑ 0,0737	✓	↓ 0,4700	×
7	↑ 0,0564	✓	↑ 0,0711	✓	↑ 0,0758	✓	↓ 0,7042	×
8	↑ 0,0564	✓	↑ 0,0701	✓	↑ 0,0686	✓	↑ 0,0031	×
9	↑ 0,0565	✓	↑ 0,0731	✓	↑ 0,0741	✓	↑ 0,0708	×
10	↑ 0,0557	✓	↑ 0,0674	✓	↑ 0,0727	✓	↑ 0,8211	×
11	↑ 0,0564	✓	↑ 0,0715	✓	↑ 0,0748	✓	↓ 1,3647	×

MPI_ESM_ssp3 7.0

MPI_ESM_ssp5 8.5